Conformational changes in DNA and MutS during mismatch repair in *Escherichia coli*, analyzed by fluorescence spectroscopy

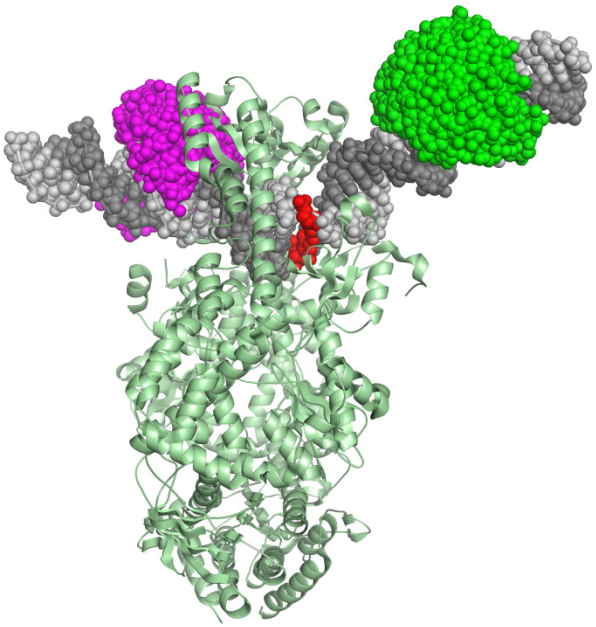

Inauguraldissertation

zur Erlangung des Grades
Doktor der Naturwissenschaften
Dr. rer. nat.
Des Fachbereiches Biologie und Chemie
der Justus-Liebig Universität

Vorgelegt von

M. Sc. Michele Cristóvão

Gießen, 2009

The present study has been carried out at the Institute of Biochemistry, Justus-Liebig University Giessen, between March 2006 and March 2009, under the supervision of Prof. Dr. Peter Friedhoff and Prof. Dr. Alfred Pingoud.

Dean	**Prof. Dr. P. Schreiner** Institut für Organische Chemie Justus-Liebig-Universität Heinrich-Buff-Ring 58 35392 Giessen
Advisor	**Prof. Dr. Peter Friedhoff** Institut für Biochemie Justus-Liebig-Universität Heinrich-Buff-Ring 58 35392 Giessen
Co-advisor	**Dr. Mark Szczelkun** Department of Biochemistry School of Medical Sciences University Walk Bristol BS8 1TD, UK

Acknowledgements

I would like to thank:

Prof. Dr. Alfred Pingoud, for giving me the opportunity to work in his lab, for the constructive critics and suggestions.

Prof. Dr, Peter Friedhoff, my supervisor, for his guidance, amazing patience, motivation, insightful discussions, interest and availability.

Dr. George Silva, G.---, thank you for all your help with my constant computer fights, for your motivation to do good science, for your love for science, time for discussions, patience and your friendship. Thanks for pushing me to do better.

Jasmina (Jazzy☺) for all you help, discussions and laughs. It wouldn't have been the same without you, specially our time in Düsseldorf.

Dr. Silke Silva, Silke, for your friendship and patience and interesting nights playing Guitar Hero☺.

Laura and Jada, pity you are not here anymore, but it was great having you around in the beginning of my life in Giessen, with all the gym time and even some nights out.

Lena and Daniel, thanks for the fun times playing wii. That was always great!

To all my friends, who I left in different places, but that have an important role in my life.

To tall the "Marie Curie people", specially Chris and Kara, for all the interesting meetings.

And of course to all the MMR group, for the interesting working environment.

I specially would like to thank my parents, Anne e Manuel Cristóvão, for their spirit of sacrifice, strength, example, love and support. Adelina, Amandio and Íris for always being there for me. A very special thanks to Heinz Abels, whose enormous curiosity was always very inspiring and motivating.

I would also like to thank the following collaboration partners:

Evangelos Sisamakis, Dr. Paul Rothwell and Prof. Claus Seidel, Institute of Molecular Physical Chemistry, Univerisity of Düsseldorf. In particular, I would like to thank Evangelos for his invaluable help and availability.

PD Dr. Ute Curth, Medizinische Hochschule, Hannover, Germany

I would like to thank the Marie Curie Research Training Network "DNA Enzymes" for funding my work.

Erklärungen

Hiermit versichere ich, die vorliegende Arbeit selbständig verfasst und keine andere als die angegebenen Hilfsmittel benutzt zu haben. Stellen, die ich anderen Arbeiten und Veröffentlichugen dem Wortlaut oder Sinn entsprechend entnommen habe, sind durch Quellenangaben gekenzeichnet.

Giessen, den 24. März 2009

Summary

Conformational changes both in DNA and MutS during the initial steps of DNA mismatch repair system and during the ATPase cycle were analyzed using state-of-the-art fluorescence techniques, down to the single molecule level. The work is presented in three chapter focusing on different aspects of the mismatch repair initiation process.

MutS binds mismatches with preferred orientations

MutS scans the DNA for base-base mismatches and small insertion-deletion loops. A hallmark of the mismatch recognition mechanism is DNA kinking by 45º-60º as observed in the co-crystal structure of MutS-DNA complexes from bacteria to man. The change in the distance of two positions in the DNA upon kinking was exploited by FRET (Fluorescence Resonance Energy Transfer). 16 different 42bp oligonucleotides containing all possible base-base combinations (four Watson-Crick and 12 mismatches) in a central position, with an acceptor fluorophore on the tope strand and a donor on the bottom strand, were tested for DNA binding and kinking by MutS using an in-solution FRET assay. In addition, selected base-base mismatches were analyzed for changes in fluorescence anisotropy of the donor and acceptor fluorophores to probe the binding orientation of MutS. Finally, single molecule Multiparameter Fluorescence Detection (smMFD) was used to analyze the binding and bending modes of MutS at highest resolution. The results demonstrate that MutS binds certain mismatches with a preferred orientation which can be analyzed by the asymmetry introduced via the fluorescence dyes attached to the DNA. These observation were corroborated by FRET analysis between fluorophore-labeled DNA and MutS labeled with fluorophores in the clamp or the connector domain. The preferential binding orientation may have important impact on the coupling of mismatch repair and replication, in particular on the mechanism involving directed loading of the heterodimeric MutSα by interaction with the replication factor PCNA.

Nucleotide influence of the DNA binding

MutS belongs to the ABC ATPase family (**A**TP-**B**inding **C**assette) whose ATPase activity is largely coupled to the dimerization of the ATPase domains. A crucial feature of these enzymes is the coupling of ATP-binding and hydrolysis to a substrate binding site, i.e. DNA in case of MutS.. The double labeled G:T oligonucleotide was used to determine the binding and bending kinetics of MutS to DNA in the presence of ADP, ATP and ADPnP. In addition, the influence of nucleotide on the MutS-induced DNA bending was analyzed using smMFD to determine the bent/kinked populations present with each nucleotide. The results showed that the association of MutS to DNA in the presence of ADP involves at least a two step mechanism, possible a fast

binding/bending step followed by a kinking at the mismatch. A quantitative analysis of the FRET population showed that the DNA with $MutS_{ADP}$ almost homogeneous forming mainly a kinked/bent complex. In contrast, complex formed in the absence of nucleotide or in the presence of ATP are more heterogenous involving at least two complexes, one of which is kinked/bent whereas other are either unbent or bound not at the mismatch. Pre-steady state kinetic analysis of MutS-DNA association in the presence of ATP and MutS-DNA dissociation in the presence of ATP, ADP or ADPnP revealed distinct phases depending on the nucleotide state of the starting complex. The data obtained by the smMFD and the fast kinetics of DNA binding and bending was inserted into a model for DNA/ATP binding by MutS.

Communication between ATPase domain and clamp domain

Several conformational changes that MutS undergoes during the DNA binding and ATPase cycle have been proposed, however, little experimental data is available proving these hypothesis. In the present work conformational changes in MutS were monitored using a FRET analysis employing single-cysteine variants of MutS. To simplify the data analysis a fully functional single-cysteine dimer variant of MutS ($MutS^{R449C/D835R}$) was generated thereby avoiding complication due to the formation of tetramers in case of wild type MutS. The work presented here shows that single-cysteine mutants of MutS could be fluorescently labeled with one or two fluorophores suitable for FRET analysis without affecting the function of the protein, e.g. in DNA binding, mismatch recognition and mismatch-provoked MutH activation.. Sedimentation velocity analysis and in-solution FRET measurements demonstrated that the fluorescently labeled $MutS^{R449C/D835R}$ forms stable dimers in the presence of DNA or nucleotide. Binding of the non-hydrolyzable ATP-analogue ADPnP resulted in a closed, compact form of MutS which is unable to bind to DNA. The dynamics of conformational changes in the clamp domain upon DNA and/or nucleotide binding were monitored using stopped-flow. Based on these data the clamp domain of MutS exists in at least four different states, i.e. flexible/open in the ADP-bound form, tight/closed in the ATP-bound form, wide/closed in the mismatch/ADP-bound form and tight/close in the DNA/ATP-bound form.

The data obtained from the fluorescence analysis using double labeled DNA, labeled DNA/labeled MutS and double labeled MutS were included in model for the DNA binding and ATPase cycle of MutS.

Zusammenfassung

In der vorliegende Arbeit wurden Konformationsänderungen in DNA und MutS, die in den initialen Schritten des DNA-Fehlerreparatursystems und des ATPase Zyklus von MutS vorkommen, mittels Fluoreszenztechniken bis auf Einzelmolekülebene untersucht. Die Arbeit ist in drei Kapitel unterteilt, die jeweils verschiedene Aspekte des Fehlerreparatursystems-Prozesses adressieren.

MutS bindet Basenfehlpaarungen mit bevorzugte Orientierungen

MutS untersucht die DNA auf Basenfehlpaarungen und Insertions/Deletionsschleifen (IDLs). Ein Kennzeichen des DNA-Reparatursystems ist das DNA biegen/knicken durch MutS, das zuerst in den Ko-Kristallstrukturen von bakteriellen und später auch humanes MutS in Komplex mit fehlgepaarter DNA beobachtet worden ist. DNA-Biegung führt zu Abstandsänderung zwischen zwei Punkten auf der DNA; solche Änderungen lassen sich mittels FRET (*Fluorescence Resonance Energy Transfer*) untersuchen. Hierzu wurden 16 verschiedene, doppelsträngige Oligonukleotide mit alle möglichen Basenpaarungen (4 Watson-Crick und 12 Fehlpaarungen) an einer zentralen Position und jeweils einem Akezeptor-Fluorophor im oberen und einem Donor-Fluorophor im unterem Strang hergestellt. Zur Untersuchung der MutS DNA-Bindung und DNA-Biegung wurden FRET-Experimente durchgeführt und in Ergänzung Änderungen in der Donor- und Akzeptorfluoreszenzanisotropie untersucht. Einzelmolekül-Experimente, die verschiedenste Eigenschaften der Fluorophore gleichzeitig detektieren (*single-molecule Multiparameter Fluorescence Detection, smMFD*), ermöglichten, Details zum Bindungs- und Biegungmodus der MutS-DNA-Komplexe klären. Die Ergebnisse zeigen, dass MutS bestimmte Basenfehlpaarungen mit eine bevorzugte Orientierung bindet. Diese Ergebnisse wurde durch FRET-Experiment mit Fluorophor-markierter DNA und Fluorophormarkierten MutS bestätigt. Die bevorzugte Orientierung von MutS hat Konsequenzen für die Geometrie und Orientierung des MutS-MutL-Komplexes, der die nachfolgenden Schritte der DNA-Reparatur koordiniert. Die Erkennung bestimmter Fehlpaarung in nur einer Orientierung hat wichtige Implikationen im Zusammenhang der Kopplung von Fehlpaarungsreparatur und Replikation im eukaryontischen System, insbesondere dem Aufladen von MutSα durch Interaktion mit dem Replikationsfaktor PCNA

Beeinträchtigung des Nukleotides auf die DNA-Bindung

MutS gehört zu der Familie der ABC-ATPasen, dessen ATPase-Aktivität mit der Dimerisierung der ATPase-Domäne gekoppelt ist. Eine besondere Eigenschaft dieser Enzyme ist die Kopplung der ATP-Bindung und Hydrolyse mit der Substrat-Bindung, DNA-Bindung im

Falle von MutS. Doppelt-Fluorophor-markierte doppelsträngige Oligonukleotide sind für die Bestimmung der Kinetik von DNA-Bindung und Biegung durch MutS in Ab- und Anwesenheit von ADP, ATP und ADPnP untersucht worden. Zusätzlich wurde der Einfluss verschiedener Nukleotide auf die MutS-induzierte DNA-Biegung in Enzelmolekülexperimenten untersucht, um Subpopulationen zu identifizieren. Die Ergebnisse zeigten, daß die Assoziation von DNA und MutS in der Anwesenheit von ADP mindestens in zwei Schritten erfolgt, die einem Bindung/Biegungsschritt und einem DNA-Knicken zugeordnet werden konnten. Die quantitative Analyse der FRET Populationen zeigte zudem, daß in der Anwesenheit von ADP, MutS einen weitgehend homogenen, spezifischen Komplex mit geknickter DNA bildet. Im Gegensatz hierzu sind die DNA/MutS Komplex in der Abwesenheit von Nukleotid oder in der Anwesenheit von ATP heterogener, u.a, unter Ausbildung zusätzlicher umgebogener Komplexe. Die kinetische Analyse der MutS/DNA Assoziation in der Anwesenheit von ATP und Dissoziation in der Anwesenheit von ADP, ATP oder ADPnP zeigten verschiedene Phasen, die abhängig von dem Nukleotid-Zustand des initialen DNA/MutS-Komplexes waren. Die Ergebnisse der smMFD-Experimente sowie der pre-steady-state Kinetiken wurden zu einem kinetischen Modell kombiniert.

Kommunikation zwischen die ATPase-Domäne und die *clamp* domäne

Es wurde postuliert, dass MutS während des DNA-Bindung und ATPase-Zyklus verschiedene Konformationen annimmt. Allerdings gibt es nur wenig direkte experimentelle Evidenz für die Kinetik und die Struktur der Konformationsumwandlungen, die vor allem in der *clamp* und der *mismatch*-Bindungsdomäne betreffen sollen. Die Konformationsumwandlung der *clamp*-Domäne wurden in der vorliegenden Arbeit mittels fluorophormarkierter Einzelcysteinvarianten und FRET untersucht. Zur Vereinfachung der Analyse wurde eine Einzelcysteinvariante erzeugt, die nur noch als Dimer vorliegt (z.B. $MutS^{R449C/D835R}$), um Komplikationen zu vermeiden, die bei der Verwendung der tetramerbildenden MutS-Wildtyp zu erwarten waren. Die vorliegende Arbeit zeigt, daß Einzelcysteinvarianten von MutS Varianten ohne Funktionsverlust (z.B. DNA Bindung, Fehlererkennung und fehlerinduzierte MutH-Aktivierung) fluorophormarkiert werden können. Sedimentationsgeschwindigkeitsanalyse und in-Lösung FRET Messugen zeigten, daß fluorophormarkiertes $MutS^{R449C/D835R}$ stabile Dimere in der Anwesenheit von DNA und Nukleotid. Bildet. Die Bindung des nicht-hydrolysierbaren ATP Analogs ADPnP überführt MutS in eine geschlossene, kompakte Form, die nicht mehr zur DNA-Bindung fähig ist. Die Dynamik der Komformationsumwandlugen in der *clamp*-Domäne von MutS nach DNA- und/oder Nukleotid-Bindung wurden durch schnelle Kinetiken untersucht. Aus den Ergebnissen lässt sich folgern, daß die MutS *clamp*-Domäne in mindestens vier verschiedene Zustände vorliegen kann, flexibel/offen in dem ADP-gebundenen Zustand, kompakt/geschlossen im ATP-gebundenen Zustand,

weit/geschlossen im dem mismatch/ADP-gebundenen Zustand und kompakt/geschlossen in einem DNA/ATP-gebundenen Zustand.

Die durch FRET-Experimente erhaltenen Ergebnisse mit doppeltmakierter DNA, markierter DNA/markiertem MutS und doppelmarkiertem MutS wurden in ein kinetisch/strukturelles Modell des MutS-DNA-Bindung und ATPasezyklus integriert.

Abbreviations

ABC	ATP binding cassette
ADP	Adenosine diphosphate
ATP	Adenosine triphosphate
ADPnP	5′-adenylyl-β,γ-imidodiphosphate
a.u.	arbitrary unit
bp	base pair
BSA	bovine serum albumin
DMSO	dimethylsulfoxide
DNA	deoxyribonucleic acid
dNTP	deoxyribonucleic triphosphate
DTT	1,4-dithiothreitol
EDTA	ethylene diamine tetraacetate
e.g.	*Exempli gratia*, "for example"
EMSA	electrophoretic mobility shift assay
EtBr	Ethidium bromide
FRET	Fluorescence Resonance Energy Transfer
g	gram
i. e.	*Id est*, "that is"
IPTG	isopropyl-β-D-1-thiogalactopyranoside
l	liter
LB	Luria-Bertani
m	milli
M	Molar
Mini-prep	plasmid DNA mini-preparation
min	minute
MLH	MutL homologue
MSH	MutS homologue
MMR	DNA Mismatch Repair
MW	molecular weight
n	nano
n.d.	not determined
OD	optical density
o/n	overnight
PAGE	polyacrylamide gel electrophoresis
PCR	polymerase chain reaction
PMSF	phenylmethanesulphonylfluoride
Rpm	rotations per minute
SDS	sodium dodecyl sulfate
sec	second
smMFD	single molecule Multiparameter Fluorescence Detection
SSB	single strand binding protein
TCEP	tris(2-carboxyethyl)phosphine
TPE	Tris-phosphate-EDTA buffer
u	unit
UV	ultraviolet
µ	micro
vs.	versus

Contents

I. Introduction

1.1 Maintenance of genomic stability

1.1.1 DNA damaging agents

The genetic information, stored in the DNA double helix, is continuously being targeted by exogenous as well as endogenous mutagenic agents. The damage induced can occur either before, during or after replication and needs to the repaired before the cells evolve to malignant tumors. Exogenous agents may arise from damage-induced radiation. Endogenous agents can derive from cellular metabolism, such as reactive oxygen species (ROS), arising from mitochondrial oxidative respiration or lipid peroxidation, from spontaneous disintegration of chemical bonds or from errors occurring during replication [5]. The damage or error in the DNA structure needs to be detected and repaired in order to prevent the onset of cell death.

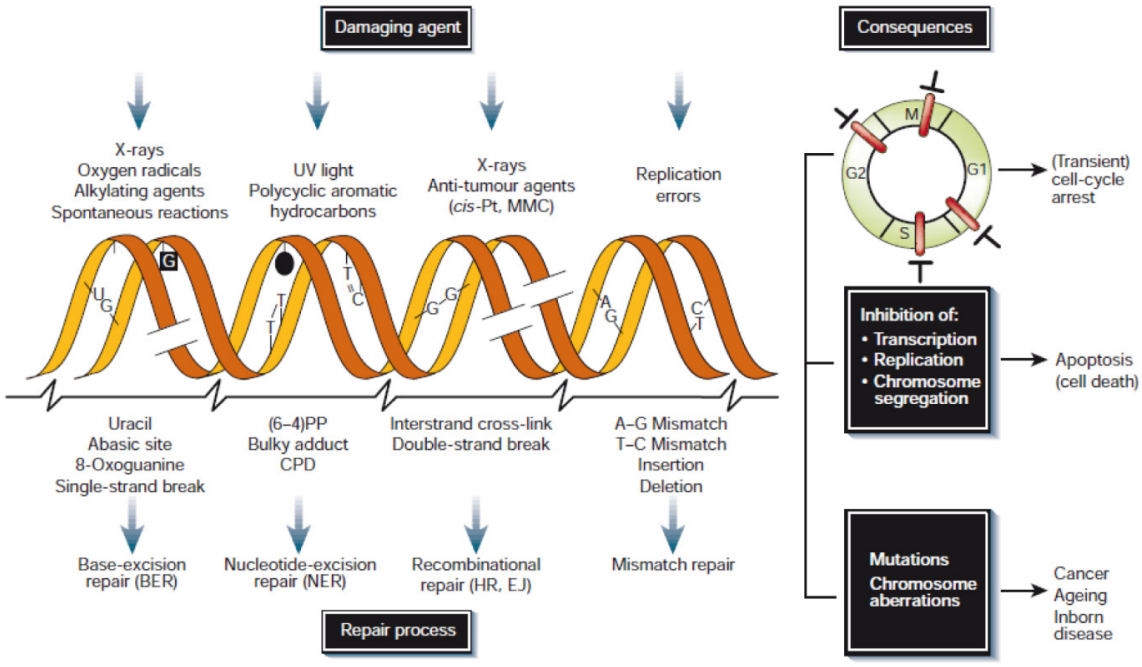

Fig. 1. 1: DNA damage. a) DNA damaging agent, consequent DNA damage and repair mechanism. b) Consequences of the DNA damage in the cell cycle and arrest points in the different phases, which can occur by inhibition of transcription, replication or chromosome segregation and ultimately lead to cell death. In the bottom are the long term consequences for DNA damage. Abreviations: cis-Pt, cisplatin and MMC, mytomycin C, are DNA crosslinking agents; (6-4)PP, (6-4) photoproducts, CPD, cyclobutane pyrimidine dimer; BER and NER, base excision and nucleotide excision repair; HR, homologous recombination; EJ, end joining[3].

1.1.2 DNA Repair

Several DNA repair systems are responsible for maintaining the integrity of the genome. If the damage is severe, the repair systems cause cell cycle arrest at specific checkpoints, to allow for repair. Cell cycle arrest can proceed through blocked transcription, replication or specific damage sensors. If cell damage is beyond repair, programmed-cell death is activated [3](Fig. 1. 1).

To cope with the different types of DNA damage, several repair systems have evolved that recognize and repair different type of lesions. Nucleotide excision repair (NER) deals with lesions that deform the helix structure. They are generally responsible for obstruction of replication and transcription originating from an exogenous agent. Base excision repair (BER) is responsible for correcting small chemical base alterations that may block transcription or replication. These are generally, although not always, caused by an endogenous agent. NER and BER only affect one of the strands and generate single-strand breaks that are quite easily repaired. Double strand breaks (DSB), however, impose a bigger challenge to the cell. DSB are addressed by one of two repair systems: homologous recombination or end-joining. In homologous recombination, the system requires a second identical DNA copy as template to correct the lesion. The template is available after replication and if not, end-joining will link both ends of a DSB, without a template. This makes end-joining more error prone.

Transition or transversion mutations are corrected by the mismatch repair system (MMR). When a mismatch arises, it is recognized and the repair system is activated, including several downstream proteins that ultimately lead to the removal of a larger stretch of single-strand DNA. After the lesion is removed, the gap is resynthesized [3] and sealed. As the mismatch repair system is the focus of this project, it will be discussed in more detail in the next section.

1.2 Mismatch repair system:

1.2.1 Overview and biological role

The mismatch repair system corrects errors that arise during replication and homologous recombination[6]. It recognizes and repairs base-base mismatches, caused by polymerase misincorporations, and insertion/deletion loops that arise from microsatellite instability (MSI)[7]. By recognizing these lesions, MMR reduces the spontaneous mutation rate that is associated with hereditary and sporadic human cancers [8]. Defects in the proteins that comprise the human mismatch repair system lead to high mutation rates, illegitimate recombination and resistance to chemotherapeutic agents. Complete inactivation of the repair

system is implicated in the onset of hereditary nonpolyposis colon cancer (HNPCC) and in the development of a subset of sporadic tumors[9].

In addition to mismatch recognition, MMR is involved in homologous recombination, meiotic chromosome pairing and segregation, theories of speciation and evolution, adaptative mutation and immunoglobulin class switching and hypermutation[6]. This way, MMR is crucial not only for maintaining genome integrity but also for promoting genome diversity. It is therefore understandable that this system is highly conserved from bacterial to mammalian cells. It was suggested that ancient horizontal gene transfer from bacteria originated the eukaryotic and archaeal mismatch repair system[10]. The study of the mismatch repair system in *E. coli* has greatly contributed to the understanding of the mechanism by which MMR recognizes and repairs post-replicative errors. However, the influence of MMR defects in the development of cancer can only be fully understood with the human system[7].

1.2.2 Mismatch Repair System in *E. coli*

The mismatch repair system can be characterized by three important main points, which are addressed in more detail below[8] (Fig. 1. 2):

1. Repair is strand specific and directed to the newly synthesized strand;

2. Repair is bidirectional: strand discrimination can be located either 3' or 5' from the mismatch;

3. MutS recognizes a wide variety of base-base mismatches, along with insertion/deletion loops with great specificity.

E. coli MutS is a homodimeric protein responsible for scanning the DNA in search of a mismatch (base-base mismatches and small nucleotide insertion-deletion mispairs). Upon finding an error in the DNA (step 2), MutS binds to it, induces a 60º kink in the DNA at the mismatch site [2], recruits a second homodimeric protein, MutL, also termed the molecular matchmaker. The formed ternary complex is able to activate the endonuclease activity of MutH (step 3). Both MutS and MutL are ATPase and this step is ATP dependent. The mismatch site and the strand discrimination site can be located up to 1000bp apart and the communication between both sites is still unclear.

After the DNA is nicked site specifically by MutH, 5' to the G of the unmethylated GATC site, UvrD is loaded onto the nick and starts to unwind the DNA (step 4), in a MutS and MutL dependent fashion[11, 12]. The unwinding direction seems to be biased by the MutS/MutL complex, so that it occurs in the direction of the mismatch[13]. The exonuclease responsible for the digestion of the unwound DNA strand depends on the orientation of the nick to the mismatch: ExoI or ExoX degrade in a 3' to 5' orientation; ExoVII or RecJ digest in a 5' to 3' orientation[9]. The single stranded DNA is stabilized by single strand binding

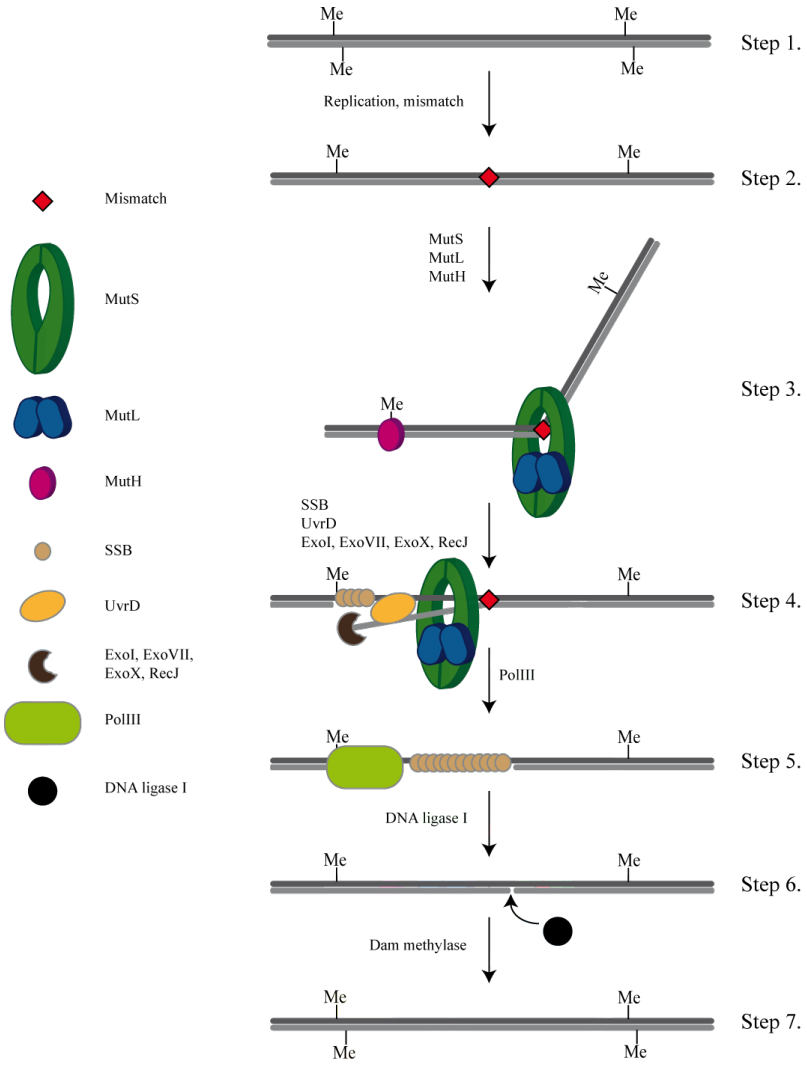

Fig. 1. 2: Repair pathway for the *E. coli* mismatch repair system.

protein (SSB) until DNA polymerase III holoenzyme (PolIII) repolymerises the gap (step 5) and the nick is sealed by DNA ligase I (step 6) [8, 9]. Dam methylase will then methylate the newly synthesized DNA strand (step 7).

Table 1. 1: Comparison between the E. coli and human repair proteins, and their function.

E. coli	Human	Function
$(MutS)_2$	hMutSα (MSH2-MSH6)[a]	DNA mismatch/damage recognition
	hMutSβ (MSH2-MSH3)	
$(MutL)_2$	hMutLα (MLH1-PMS2)[a]	Molecular matchmaker; endonuclease, termination of mismatch-provoked excision
	hMutLβ (MHL1-PMS1)	
	hMutLγ (MLH1-MLH3)	
MutH	?[b]	Strand discrimination
UvrD	?[b]	DNA helicase
ExoI, ExoVII, ExoX, RecJ	ExoI	DNA excision, mismatch excision
PolIII holoenzyme	Polδ	DNA-resynthesis
	PCNA	Initiation of MMR, DNA re-synthesis
SSB	RPA	ssDNA binding/protection, stimulating mismatch excision; termination of DNA excision; promoting DNA resynthesis
	HMGB1	Mismatch-provoked excision
	RFC	PCNA loading; 3' nick-directed repair; activation of MutLα endonuclease
DNA ligase	DNA ligase I	Nick ligation

[a]Major component in cells
[b]Not yet identified

Despite great effort from several groups over the years, the question of how the communication between the mismatch site and the strand discrimination site occurs, remains unanswered. Different models have been suggested, which can be classified has "stationary" or "moving" models[8]. The "stationary" model suggests that MutS remains bound to the mismatch, while the mismatch and the strand discrimination sites are brought in proximity through bending or looping of the DNA. The "moving" model, on the other hand, implies that MutS is triggered into forming a sliding clamp, either by ATP-hydrolysis dependent movement (translocation model) or by ATP binding. The latter model implies two conformational changes of MutS: the first occurs at mismatch-binding event, promoting the ADP to ATP exchange, and the second occurs when ATP binds, when MutS attains the sliding clamp conformation[8].

The crucial steps in MMR are: recognition of the mismatch, discrimination between the correct and the incorrect DNA strand, removal of the mismatch, repolimerisation of the gap and ligation of the corrected strand. Mechanistically, the similarity between human and *E. coli* MMR lies in the substrate specificity, in the nick directed strand specification and in the bidirectionality of the incorrect strand excision[8]. The main distinction between the human and the *E. coli* system resides in the correct and incorrect strand discrimination signal. In *E.*

coli DNA, the N6 position of Adenine in GATC sequences is methylated. Because methylation lags after DNA replication, the new DNA strand is transiently unmethylated, is thus recognized as the newly synthesized and incorrect strand and nicked by a endonuclease[7]. The human system lacks the methylation sites, but the strand discrimination is still thought to be nick directed, in which the system recognizes 5' or 3' termini of Okazaki fragments in the lagging strand or 3' terminus in the leading strand[7].

The mismatch repair system proteins were first identified in *E. coli* but several human proteins have been found to belong to the MMR based on their homology to the bacterial proteins. Table 1. 1 lists the *E. coli* proteins and known human homologs and their function[7, 8].

1.3 MutS: Mismatch recognition protein

E. coli MutS is a 853aa long homodimeric protein, which exist in solution as a mixture of dimers and tetramers. The *E. coli* MutS protein structure in complex with a G:T mismatch was solved by Lamers *et al*[2], but only a truncated form, consisting of the first 800aa, belonging to the N-terminal domain (Fig. 1. 3). The structure of the last 53aa (C-terminal domain) was determined fused to maltose binding protein[1] (Fig. 1. 6).

MutS is an asymmetric protein, resembling two praying hands in which the DNA is held between the fingers and the inwards folded thumbs [7] (Fig. 1. 4).

It is divided in several domains: mismatch binding, clamp, connector, core and lever, ATPase and helix-turn-helix domain (Fig.1.3).

DNA is held between the clamp and the DNA binding domain. The positively charged surface of the clamp domain interacts with the DNA backbone, forming several salt bridges. Only one monomer interacts specifically with the mismatch, with the highly conserved Phe-X-Glu motif[2]. The residue Phe36 wedges into the DNA, stacking with only one base of the mismatched pair and the Glu38 forms a hydrogen bond with a particular nitrogen on the thymine (N3) (Fig. 1. 5). In the G:T mismatch, Glu38 stacks with the thymine. The other monomer makes only unspecific interactions with the DNA backbone. In free DNA with a G:T mismatch, the bases were seen to form a wobble pair. In the MutS/G:T crystal structure, however, the mismatched bases are unstacked and distorted, adjusting to the kink induced by MutS[2].

The mismatch-binding domain possesses no overall positive charge, suggesting that it is the clamp domain that does the DNA scanning[2]. The DNA flexibility at the mismatch site conferred by the wobble G:T pair allows the protein to modulate the DNA conformation with its negative charges and to stack the Phe36 from the mismatch-binding domain.

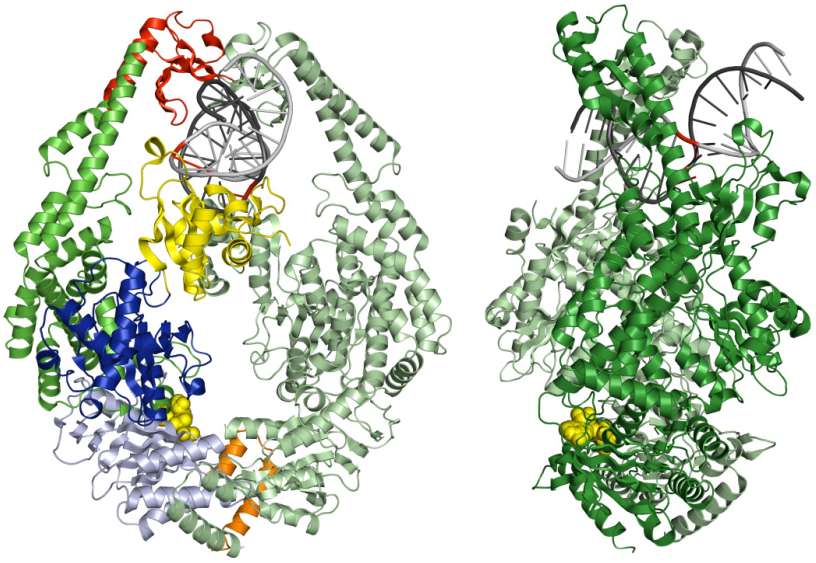

Fig. 1. 3: Crystal structure of E. coli MutS[2]. Each monomer consists of six domains: mismatch binding domain (yellow), clamp domain (red), lever and core domain (green), connector domain (dark blue), ATPase domain (light blue, with ADP showing in yellow spheres) and helix-turn-helix (orange). The DNA is shown in grey, with the mismatched bases in red.

The connector domain, formed by mostly parallel β-sheets, surrounded by 4 α-helices, connects the mismatch-binding domain to the core domain, from which two α-helices (lever domain) extend to surround the DNA, without contacting the helix. The clamp domain corresponds to the tip of the levers. The core domain also connects to the ATPase domain, which has a Walker A motif (GXXXXGKT/S, where XXXX is variable and serine can substitute threonine in some cases[14]).

The clamp, C-terminal ATPase and the HTH domains are involved in the MutS dimerization. The positive charge of the clamps prevents their interaction in the absence of

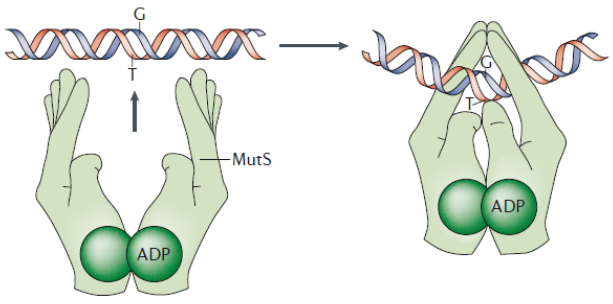

Fig. 1. 4: MutS resembles two praying hands, in which the finger tips correspond to the clamp domain, the thumbs to the mismatch-binding domain, the palms are the core and connector domains and the wrists the ATPase and HTH domains[7].

DNA, but the negative charge of the DNA backbone allows the clamp formation in the presence of DNA. The ATPase and HTH domains show a more extensive dimer interface. ADP is only seen bound to the mismatch-binding monomer, where the P-loop of the second monomer still needs to rearrange before it can bind the nucleotide[2].

The MutS C-terminal domain crystal structure, fused to maltose binding protein, was determined, as mentioned above (Fig. 1. 6). The C-terminal domain is comprised of 53aa; however, crystals were only obtained with a fragment of the residues 820-853, suggesting that the residues 801-819 constitute a flexible region. Each monomer interacts primarily with another monomer, forming a dimer, with an extensive interface. Each dimer then interacts with a second dimer, forming a tetramer with a relatively small interface. The monomers can be distinguished by either a loop-loop packed or a helix-helix packed interface, each dimer consisting of one loop-loop packed and one helix-helix packed monomer. Each loop from one monomer of one dimer interacts with the loop monomer on the other dimer; the same is true for the helix monomers. Electrostatic interactions play an important role in the tetramerization domain, where Arg840 of one loop monomer interacts with Asp833 and Asp835 of the other loop monomer (monomers in dark blue and in dark green from Fig. 1. 6); Arg840 of the one helix monomer interacts with Tyr847 and Glu844 on the other helix monomer[1].

The importance of the tetramer in the mismatch repair system is still under debate. No tetramer formation has been described for *Taq* or Human MutS and different reports give different importance to the tetramer role in *in vivo* MMR [1, 15].

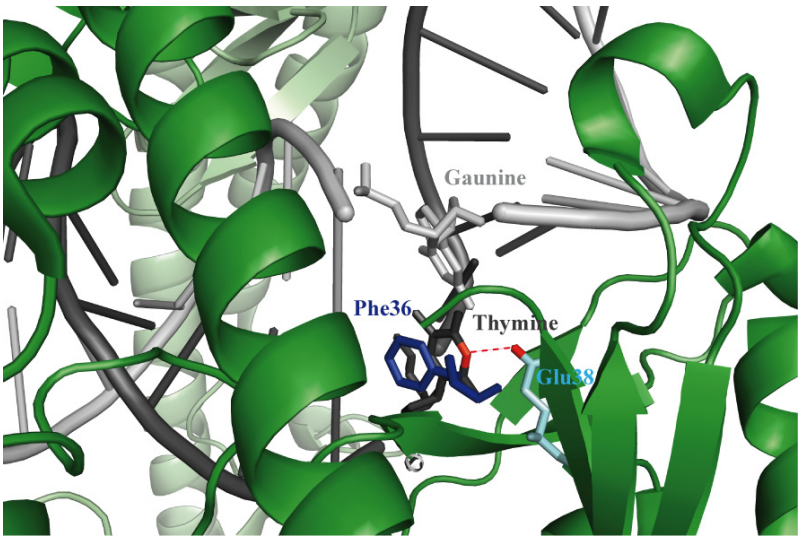

Fig. 1. 5: The mismatch recognition by occurs via the conserved Phe-X-Glu motif, in the mismatch binding domain. The Phe36 (dark blue) stacks onto the unpaired T of the G:T mismatch, while the Glu38 (light blue) makes a hydrogen bond (in red) with the N3 of the same T. The mismatch binding monomer is seen in dark green, while the second monomer is seen in light green.

A cysteine-free full-length dimer variant of MutS (MutS$^{CF/D835R}$) has been fully characterized by our gropu and was found to be impaired in *in vivo* MMR, while retaining the

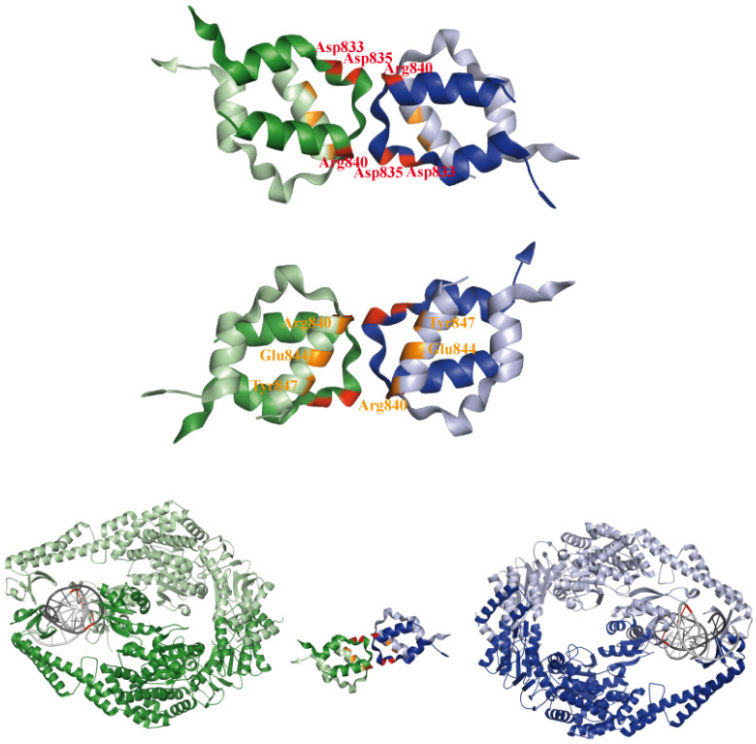

Fig. 1. 6: *E. coli* MutS tetramer[1]. a) Tetramerization domain of MutS (residues 820-853), solved by SAXS, shown from the loop-loop packed monomer view (top) or the helix-helix packed monomer view (bottom). Highlighted in red are the residues responsible for the loop monomer interactions and in orange the residues involved in the helix monomer interactions. b) Possible model for the MutS tetramer (full length), suggested by Mendillo *et al*. The residues 801-819, possibly forming the linker between the N-terminal and the C-terminal fragments are missing.

same DNA affinity as MutS^{CF}[15]. This suggests that the tetramer is important for MutH activation but not for mismatch recognition. The results from Mendillo *et al* showed that the introduction of the point mutations D835R and R840E had only a small effect on MMR[1].

1.3.1 Mismatch recognition

Mispaired or unpaired DNA bases with weakened base pairing are more susceptible to kink. MutS test the flexibility of the DNA and thus recognizes a broad range of mismatches. The energetic difference between a normal and mismatched base pair is thought to be around 2-3kcal/mol and this small difference translates to 100-1000fold higher affinity of MutS for mismatched vs. perfectly matched DNA[16]. The question arises of how MutS achieves such a high specificity and it was proposed that the ATPase activity of MutS might be the answer to this question. MutS hydrolyzes ATP quickly in the absence of a mismatch but when bound

to one, the burst of ATP hydrolysis is inhibited, allowing the MutS/DNA/ATP complex to form[16].

E. coli MutS was crystallized bound to five different mismatches: G:T, G:G, A:A, C:C and +T [2,17]. Common to all crystal structures is the 60º kink that the DNA undergoes at the mismatch site but the target base is different according to the mismatch. In the G:T and +T mismatch, the Glu38 interacts with the N3 of the pyrimidine T and in the C:A, A:A and G:G mismatches, MutS interacts with the N7 of the purines (A and G).

The importance of the DNA kinking at the mismatch site has been addressed in Atomic Force Microscopy studies (AFM) [18]. In this work, the bend angles induced by MutS at mismatch sites, as well as at homoduplex sites were analyzed by determining the DNA bend angle of MutS/DNA complexes seen in AFM images. This study found that MutS forms a bent and an unbent population, when in complex with a mismatch DNA (specific complex), but only a bent population when in complex with a homoduplex DNA substrate (unspecific complex) [19]. As a result, Wang *et al* propose that MutS unspecifically bends the DNA, while scanning it for mismatches; upon encountering one, it first specifically kinks the DNA at the mismatch (initial recognition complex, IRC), and then unbends it (ultimate recognition complex, URC), where this complex results from specific MutS/mismatch interactions.

$$\text{MutS+DNA} \leftrightarrow \text{MutS:DNA}_{\text{bent,NS}} \leftrightarrow \text{MutS:DNA}_{\text{kinked,SP}} \leftrightarrow \text{MutS:DNA}_{\text{unbent,SP}}$$

The DNA bent state refers to a smooth bend, spreading the bending over several bases (which would be seen in the unspecific complex), whereas the kinked DNA state implies a sharp DNA kink at the mismatch site, as seen in the specific complex captured by the crystal structures[18].

In a more detailed analysis, Tessmer *et al* studied the effect of *E. coli* residues Phe36 and Glu39 (Phe38 and Glu41 in *Taq* MutS) mutations on DNA bending[20]. The results showed that, despite the very low DNA affinity of the $MutS^{F36A}$ mutant, it still supports DNA bending at the mismatch site at high concentrations, similar to MutS wild type. Furthermore, Tessmer *et al* suggested that the Phe36 residue is responsible for the formation of the specific URC, seeing as the unbent complex is absent in $MutS^{F36A}$. The work published by Jacobs-Palmer *et al*[21], however, shows no interaction of *Taq* $MutS^{F39A}$ with DNA. The assay used by Jacobs-Palmer *et al* detects DNA kinking by aminopurine fluorescence. The adenine analogue aminopurine is placed adjacent to an extra T, which is recognized by *Taq* MutS, and will only emit fluorescence if MutS binds and kinks the mismatch. Thus, according to these results, *Taq* $MutS^{F39A}$ is no longer able to kink the mismatch, which contradicts the Tessmer *et al* data. In contrast, the E39A mutation still allowed MutS to form the kinked complex, but the unbent population (0º bend angle) was shifted to a slightly bent population (15º bend angle). This mutation was seen to cause severe MMR defects *in vivo* and shows enhanced ATP hydrolysis at mismatch binding (contrary to wild type, see below) [22]. The observation

that this mutant can no longer form the unbent population led Tessmer *et al* to suggest that the Glu38 residue is responsible for the formation of the unbent complex and for attaining the conformation necessary for the formation of the sliding clamp.

1.3.2 ATP binding, ATP hydrolysis and sliding clamp formation

The ATPase domain of MutS has been classified as belonging to the family of the ABC-transporters (ATP-Binding Cassette)[23]. The exact function of both MutS monomer's ATPase domain has been under intense study and is not yet fully understood. It was proposed that the exchange of ADP for ATP depends on mismatch binding. The ATP binding induces a conformational change in MutS, which forms a sliding clamp and in complex with MutL activates MutH. The ATPase domain activity facilitates the dissociation from DNA, more so of homoduplex DNA than of heteroduplex DNA, double-checking that it has in fact encountered a mismatch. Furthermore, the ATP hydrolysis burst is inhibited upon binding of mismatched DNA[24].

Lamers *et al* showed that the two chemically identical ATP binding sites are asymmetric in nucleotide binding and are coupled in ATP hydrolysis[25]. During steady-state ATP hydrolysis, one monomer at a time hydrolyzes ATP, in an alternating mechanism. The residue Arg697 seems to be responsible for this alternating mechanism, in which the residue in one monomer prevents the hydrolysis in the opposing monomer[25]. The asymmetry of the domains is observed before the DNA binding event and it is also present in human MutS, where only one of the monomers can bind the mismatch. Together, these facts suggest that dimer asymmetry is important for correct DNA binding (maybe conferring and extra orientation to MutL), but also later in the mismatch repair mechanism, hence the alternating hydrolysis mechanism.

The two ATPase sites in MutS have different affinities for di- and tri-nucleotides [26] and it seems that it is the mismatched DNA that modulates the affinity of a given nucleotide at a given site[27]. The monomer that binds the mismatch also possesses ATPase activity with higher affinity for ATP, whereas the other monomer retains low affinity for nucleotide while monomer 1 does not hydrolyze ATP. Upon hydrolysis of the trinucleotide in monomer 1, monomer 2 becomes the high affinity monomer, thus monomer 1 can release the product. The modulation of ADP and ATP binding to the ATPase sites modulates the movement of the clamp and mismatch binding domain, located at opposite ends of the protein (compare domains light blue with yellow and red in Fig. 1. 3).

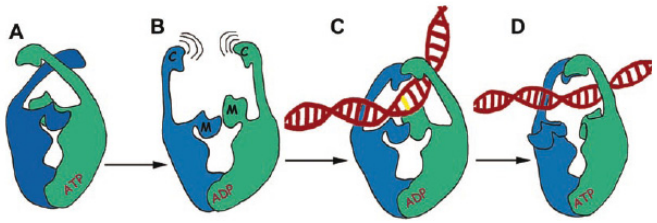

Fig. 1. 7: Proposed conformational changes of MutS modulated by nucleotide[27].

As Fig. 1. 7 suggests, in the DNA-free and ADP bound state, MutS is in an open state in which the clamps are open, flexible and ready to accommodate DNA. The inability to obtain a crystal structure of these domains in the absence of DNA corroborates this hypothesis[28]. DNA promotes the clamp closing, the DNA is kinked by insertion of Phe36, and Glu39 forms a hydrogen bond with the mismatched base. Meanwhile, ATP binds to the high affinity ATPase site, which promotes the tightening of the clamps around the DNA, but its hydrolysis is inhibited because of mismatch binding. The conformational changes attained thus far cause the mismatch binding domains to move away from another and MutS to form the sliding clamp[22, 27]. At this point it is still unclear which ATPase domain hydrolyzes first.

Jacobs-Palmer *et al* address the ATPase function of MutS with kinetic studies on a DNA substrate, in which 2-aminopurine was placed adjacent to an extra base, as a fluorescent reporter for MutS binding to mismatched DNA[21]. Based on the results, the following model for the ATPase activity of MutS has been proposed (Fig. 1. 8):

1. In the absence of a mismatch and nucleotide (a), MutS binds ATP, hydrolyzes it (b) and releases phosphate (Pi) rapidly (c)

2. When MutS is bound to DNA (d), it can also bind ATP rapidly (e), but hydrolysis is slow (f)

3. ADP-bound MutS (c) can also bind to a mismatch but the complex is short-lived (f) and it can either slide away (h) or dissociate directly from the mismatch (c)

4. If MutS is bound to the mismatch in the ADP form (f), it can readily replace ADP with ATP and become a long-lived complex (e)

5. When MutS is bound to the mismatch in the ATP form, it can slide away from the mismatch (g) in a closed form, until it hydrolyzed or released the nucleotide, or until downstream proteins have been activated for the subsequent MMR steps.

The conformational change the DNA undergoes upon the binding of MutS to a mismatch is a suitable FRET system, relying on the distance change between two fluorophores placed on either side of the mismatch (see below). Huang *et al* used this system to analyze the binding of MutS tetramer to all combinations of mismatches, perform kinetic studies on the binding and the role of nucleotide binding[29]. Their kinetic results show that the difference in the affinity of MutS for the different mismatches relies on the different dissociation rates, suggesting subtle changes in the recognition mode, from mismatch to mismatch. Furthermore, their results suggests that MutS tetramer exhibits a positive cooperativity in binding, modulated by nucleotides and with implications in the affinity of MutS for the mismatch, in agreement with Junop *et al*[24]. Huang *et al* propose that the functional unit for *E. coli* MutS is a tetramer, which binds to a mismatch with positive cooperativity. Subsequent ATP binding causes the loss of positive cooperativity between the two dimers, without changing the stoichiometry of the complex. Although the affinity for mismatched DNA decreases, the affinity for homoduplex DNA decreases even more, so that the MutS/homoduplex complex dissociates before it activates the downstream repair events, maintaining the high specificity that characterizes MMR.FRET studies on MutS and DNA

Several techniques allow us to have a more detailed look into the structure and conformational changes, like X-ray crystallography, NMR, cryo-electron microscopy or AFM. Although very insightful, these techniques give us mostly static information about the protein and protein complexes we want to study. The advances in the fluorescence field have made these techniques very strong and competitive when it comes to acquire dynamic and in

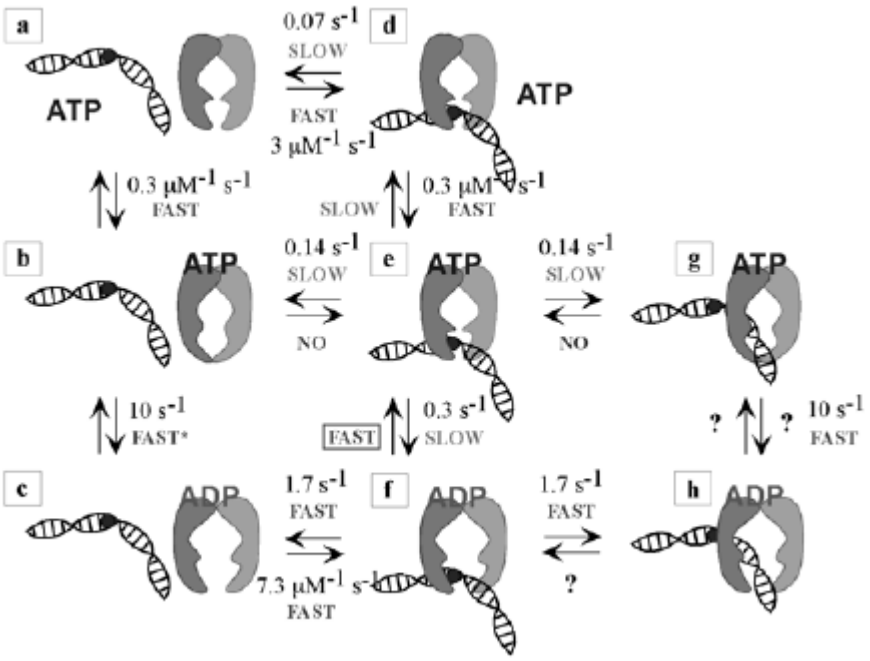

Fig. 1. 8: Model proposed by Jacobs-Palmer *et al* for ATPase activity of MutS.

solution information about a certain biomolecule[30].

Fluorescence is a very useful technique to detect changes in the surroundings of a fluorophore when attached to a protein or nucleic acid. In particular, Fluorescence Resonance Energy Transfer (FRET) is invaluable for studying small distance changes within those molecules, from 10 to 100Å. FRET requires the presence of two appropriate fluorophores, one donor and one acceptor fluorophore, within the mentioned range (FRET will be explained in detail in the Materials and methods section). FRET is useful for both DNA as well as protein studies and the only obstacle is the coupling of the fluorophore to the target molecule. DNA is easy to label as it can be synthesized with site-specific thiol groups or with modified nucleotides[31]. The labeling of proteins is more problematic, as explained below.

Although most proteins contain intrinsic fluorophores (the residues tryptophan and tyrosine have fluorescence properties), their quantum yield is low and their position on the protein might not be ideal. There is a wide range of extrinsic fluorophores with appropriate quantum yields and fluorescence properties to be used in FRET, which can be site-specifically coupled to the protein via a number of coupling methods (Table 1. 2). The most common conjugation chemistry for site-specific protein labeling are fluorophores with a succinimidyl ester linker, which target primary amines, or fluorophores with a thiol-reactive maleimide linker, which react with cysteines residues. Because proteins have many primary amines, the thiol reaction is more specific seing as cysteines residues can be introduced at specific sites via point mutations[31]. FRET can be used to study either conformational changes of one molecule, where both donor and acceptor fluorophore are coupled to the same molecule, or it can be used to study the interaction between two molecules, in which one is labeled with acceptor and one with donor fluorophore[32]. The extreme sensitivity of FRET to small distance changes between the fluorophores and the possibility to follow the FRET signal in real time and down to the single molecule level, makes this a very useful technique to

Table 1. 2: Conjugation methods for fluorophores[31, 33]

	Chemistry or method	Reactive group	Remark
DNA or RNA	Phosphoramidite or acetoxyethoxy methyl solid support synthesis		Direct incorporation into the backbone
	Amine reactive (—NH_2)	NHS ester	Amino C6-dT/dC (for internal labeling without backbone disruption)
	Thiol reactive (—SH)	Maleimide	Thiol modifier on a 3’ or 5’ end
Proteins	Amine reactive (—NH_2)	NHS ester	N-terminal or lysine amine group
	Thiol reactive (—SH)	Maleimide	Cysteine thiol group
	Ketone reactive (=O)	Hydrazine	Unnatural amino acid with ketone group

understand and “see” inter and intra-protein or DNA movements. As was mentioned before, the exact function of the hydrolysis of either ATP in both MutS monomers is still under study. Ideally, the monitoring of MutS conformational changes in the clamp domains while modulating the binding of nucleotide to one ATP binding site and then the other, would give us valuable information about the communication between the domains and the when and why ATP is hydrolyzed in the mismatch repair system.

1.3.3 Single molecule FRET studies

Although ensemble (or bulk) fluorescence measurements provide us with a large amount of information, it lacks the sensitivity of looking at each molecule individually and gives us only the average behavior of all different species in solution. The recent advances in single molecule techniques[34] allow us do just that, to look at each molecule individually and group them into subpopulations of a heterogeneous population.

Single molecule FRET has had a wide use in studying inter and intra molecular interactions, being largely accepted as the most promising single molecule technique. It can be divided in three subgroups, depending on the state of the observed molecule: surface tethered, freely diffusing or confined molecules[34]. Each subgroup has advantages and disadvantages; only the single molecule techniques in which the fluorescent molecule is diffusing freely in solution will be discussed here.

Freely diffusing fluorescent molecules are observed only when they diffuse through the confocal detection volume of about 2fl [4, 35]. The Multiparameter Fluorescence Detection (MFD) of the fluorophores allows the identification and quantification of single molecules (Fig. 1. 9). It uses pulsed excitation and time correlated single photon counting to simultaneously monitor the evolution of up to eight fluorescence dimensions of the protein/DNA-coupled fluorophore, as it travels through the observation volume. These eight fluorescence properties are: fundamental anisotropy, fluorescence lifetime, fluorescence intensity, time, excitation spectrum, fluorescence spectrum, fluorescence quantum yield and distance between fluorophores. Furthermore, as the fluorophores are freely diffusing through the observation volume, information about the diffusion time can also be obtained, which is a clear advantage over surface tethered techniques[35]. The subsequent offline Probability Distribution Analysis (PDA) separates the observed molecules into different groups according to their fluorescence properties, with statistically good results, as it can look at several thousand molecules in one sample. The PDA method calculates the theoretical probability of recording certain combination of red and green fluorescence, from which the FRET efficiency can be derived[36].

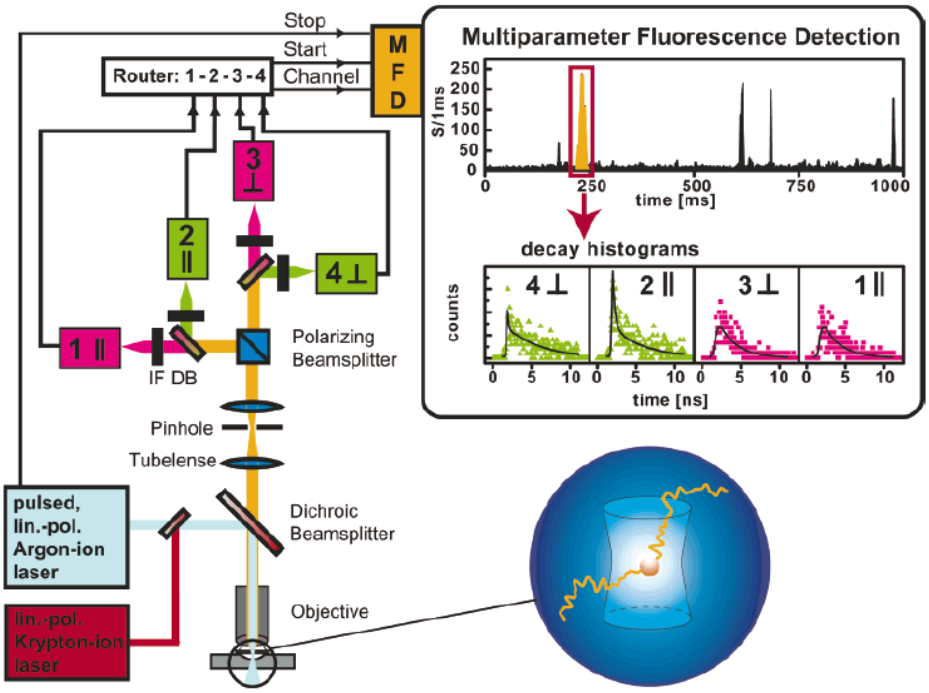

Fig. 1. 9: smMFD setup: the four channel confocal setup allows the simultaneous detection of spectral range, fluorescence intensity, lifetime, anisotropy (IF: interference filter, DB: dichroic beam splitter).

DNA damage is known to introduce structural changes into the DNA, either protein- or damage- induced. These conformational changes comprise distortion, bending or kinking of the DNA helix. smFRET has the potential to understand these damages and the repair systems that correct them, by giving us detailed information about the structural changes the DNA has suffered and allowing us to monitor its interaction with the repair proteins.

Advances in the use of single-molecule techniques to look at the DNA conformational changes was provided by Woźniak *et al*[37], in which MFD studies were performed on various DNA constructs, where the donor-acceptor fluorophore distance was systematically varied between 2 and 10nm. Their results showed that absolute distance between the D-A pair can be calculated with great accuracy, taking into account the orientation and positional variability conferred to the fluorophore by the linker. Their method has the potential to be applied to other double stranded DNA systems, including the study of the DNA bending/kinking by MutS in the mismatch repair system.

1.4 Aim

The specificity and efficiency of the mismatch repair system relies on the ability of MutS to recognize a lesion and to efficiently distinguish between matched and mismatched DNA, among the several thousand base pairs that comprise a genome. The fact that the energetic

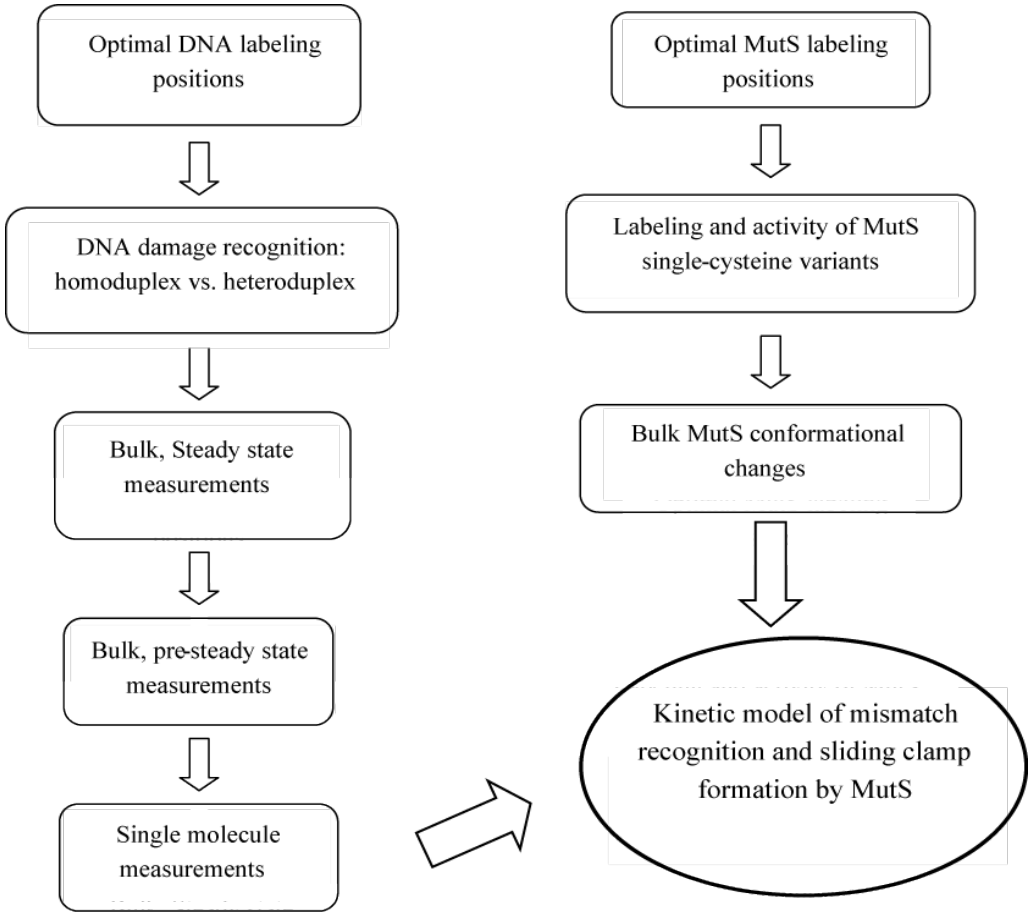

Fig. 1. 10: Layout of the this study.

difference between a correct and an incorrect base-pair of only 2-3kcal/mol makes for 100-1000 fold difference in binding to a homo- or a heteroduplex[16], increases the relevance of understanding the mismatch recognition event by MutS. Furthermore, the two asymmetric ATPase domains in MutS play an important role in the mismatch recognition and in the recruitment of MutL, although the specific function of the two ATPase domains is not fully understood. Moreover, in MutS the ATPase domain is located on the opposite side of the clamp domain which is responsible for the DNA binding and mismatch recognition, separated by more than 60Å. The importance of the ATPase activity of MutS in MMR is mirrored in the *in vivo* effects of eukaryotic proteins, where it was seen that mutants in which one of the ATPase domains was mutated were still mismatch repair proficient in complementation assays, but the double mutants are inactive[38].

The aim of this project is the study of the mismatch binding and recognition by MutS and the role the ATPase function plays in the recognition and in the formation of the sliding clamp. After information is gathered with bulk, steady-state and pre-steady state, and single molecule experiments, it will be used to derived a kinetic model of mismatch recognition and formation of the sliding clamp (Fig. 1. 10). The question was addressed by using fluorescently

labeled DNA substrates, to study the mismatch recognition, and double labeled MutS variants to understand the role of the nucleotide in promoting crucial conformational changes in MutS. Therefore, my role in this project included the development of FRET systems, suitable for the study of MutS DNA interaction and MutS conformational changes. What concerns the double labeled DNA substrates, it implied choosing the right set of fluorophores to use as a FRET pair, which had to be compatible for both bulk and single molecule measurements. In addition, the labeling position on the DNA needed to be optimized, as the fluorophores cannot affect or be affected by the activity of MutS. What concerns the double labeled MutS mutants, my project implied the choice of suitable single-cysteine MutS variants for fluorescent labeling, while retaining the activity in mismatch recognition and signaling. My role in the Mismatch Repair Group was thus to develop fluorescence techniques for the study of in solution MutS binding to DNA and ATP hydrolysis.

II. Materials and Methods

2.1 Materials

2.1.1 Reagents

Table 2. 1: Reagents used in this study.

Name	Company
Acetic acid	Roth
Acrylamide-bisacrylamide (1:29) 40%	AppliChem
ADP	Sigma
ADPnP	
Agar	AppliChem
Ampicillin	AppliChem
ATP	Sigma
Benzamidine	Sigma
BSA	
Coomassie brilliant blue R250 and G250	AppliChem
κ-casein from bovine milk	Sigma
dNTPs	Roth
DTT	MBI Fermentas
EDTA	AppliChem
EtBr	Roth
Glycerol	AppliChem
Glycine	Serva
HEPES	AppliChem
KCl	Merck
Imidazole	AppliChem
IPTG	ApliChem
$MgCl_2$	Merck
Ni-NTA agarose	Biorad
PMSF	AppliChem
Rifampicin	Sigma
SDS	Sigma
TCEP	Sigma
TEMED	AppliChem
Tween 20	Merck
Tris	AppliChem

2.1.2 Fluorophores

All DNA labeled oligos were purchased at Purimex (3x HPLC purified). They were received already dissolved and were stored at -20 ºC.

i. DNA labels

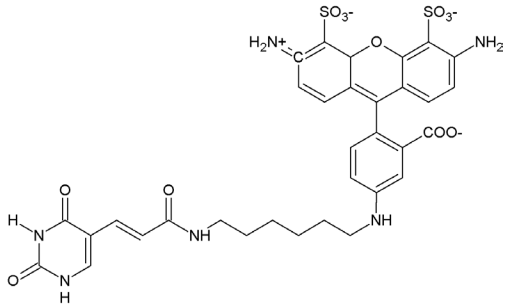

Fig. 2. 1:Chemical structure of Alexa Fluor 488 (Alexa 488 or A488) with a C6 amino linker coupled to position 2' of the thymine (C6-2'-dT).

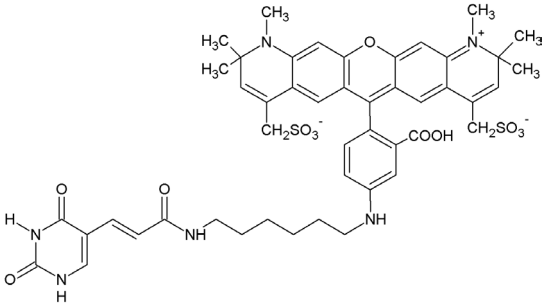

Fig. 2. 2: Chemical structure of Alexa Fluor 594 (Alexa 594 or A594) with an amino linker C6 coupled to position 2' of the thymine (C6-2'-dT).

Table 2. 2: Physical properties of DNA-conjugated Alexa 488 and Alexa 594.

	Alexa 488	Alexa 594
λ absorbance maximum (nm)	494	590
λ emission maximum (nm)	517	617
ε (max abs) (M^{-1} cm^{-1})	71 000	73 000
ε * (M^{-1} cm^{-1})	38 000	52 000
MW (g/mol)	643.5	819.9
CF	0.30	0.43

***corresponds to the ε at the used excitation wavelength for Alexa 488 (470nm) and Alexa 594 (575nm); CF is the correction factor used for the determination of the degree of labeling.**

Table 2. 3: Fluorescent labeled single strand oligonucleotide used in fluorescence measurements.

ssOligonucleotide	Extinction coefficient, ($M^{-1}cm^{-1}$)
G_XhoI_A594_A	390800
G_XhoI_A594_C	386400
G_XhoI_A594_G	391000
G_XhoI_A594_T	388500
G_XhoI_A594_G_I	390150
G_XhoI_A594_T_I	387630
T_HindIII_A488_A	419130
T_HindIII_A488_C	411930
T_HindIII_A488_G	415620
T_HindIII_A488_T	413100
T_HindIII_A488_G_I	405900
T_HindIII_A488_T_I	403380

ii. Protein labels

For protein labeling, the fluorophores, coupled with a maleimide linker, were purchased at Molecular Probes, Invitrogen. The necessary amount for each labeling reaction was dissolved in DMSO, immediately before use and the concentration was determined by absorbance at 280nm. The remaining stock was stored at -20 ºC.

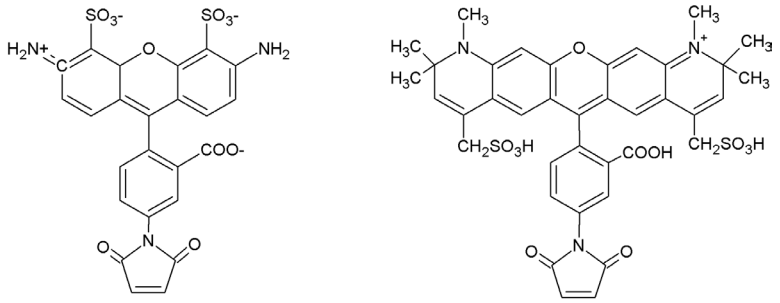

Fig. 2. 3: Chemical structure of Alexa Fluor 488 C5-maleimide (Alexa 488-mal or A488-mal; left) and Alexa Fluor 594 C5-maleimide (Alexa 594-mal or A594-mal; right).

Table 2. 4: Physical properties of the Alexa-maleimide fluorophores used for protein modification.

	Alexa 488	Alexa 594
λ absorbance maximum (nm)	495	590
λ emission maximum (nm)	519	617
ε (M^{-1} cm^{-1})	71 000	73 000
ε * (M^{-1} cm^{-1})	38 000	52 000
MW (g/mol)	720.6	908.9
CF	0.12	0.57

*corresponds to the ε at the used excitation wavelength for Alexa 488 (470nm) and Alexa 594 (575nm); CF is the correction factor used for the determination of the degree of labeling.

Prior to the labeling reaction, the protein was incubated with a reducing agent, TCEP, to reduce possible disulfide bridges, so that the thiol groups were available for reaction with the maleimide group coupled to the fluorophores (Fig. 2. 4 and Fig. 2. 5). Contrary to DTT, which contains thiols and would decrease the labeling efficiency by reacting with the maleimide group coupled to the fluorophore, TCEP does not contains thiols (Fig. 2. 6).

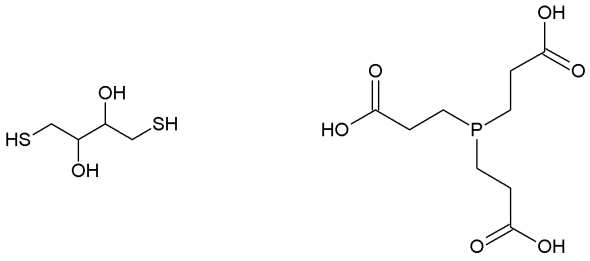

Fig. 2. 4: Chemical structure of DTT (left) and TCEP (right).

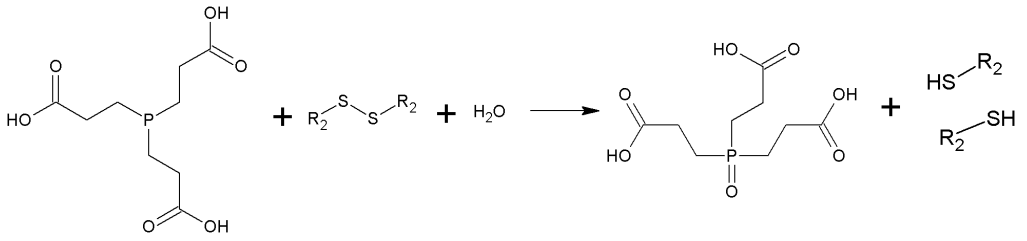

Fig. 2. 5: Schematic representation of the reduction of disulfide bridges by TCEP.

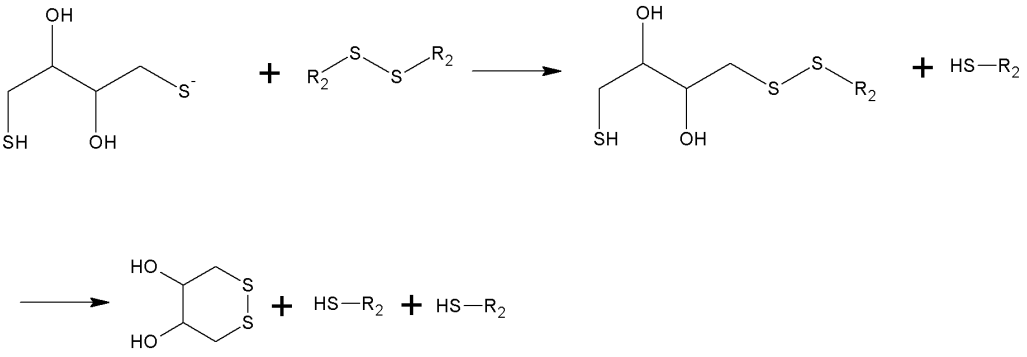

Fig. 2. 6: Schematic representation of the reduction of disulfide bridges by DTT.

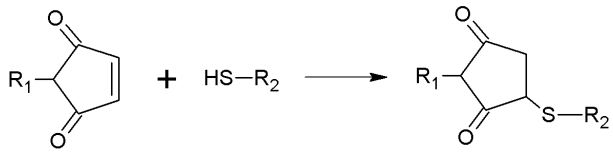

Fig. 2. 7: Reaction of a maleimide group with a thiol group (SH) located on the surface of the protein. R_1: fluorophore; R_2: protein.

The labeling reaction (Fig. 2. 7) was stopped with 10mM DTT.

iii. Degree of labeling

The degree of labeling (DOL) for both DNA and protein was calculated with the following equation:

$$DOL = \frac{A_{F,max} \times \varepsilon_{protein\ /DNA}}{\left(A_{280nm\,/260nm} - A_{F,max} \times CF\right) \times \varepsilon_{max}} \qquad \textbf{Equation 2.1}$$

where,

$$CF = \frac{A_{280nm\,/260nm}}{A_{F,max}} \qquad \textbf{Equation 2.2}$$

A_{max} corresponds to the maximum absorbance of the fluorophore, A_{280nm} corresponds to the absorbance at 280nm (for proteins) and A_{260nm} corresponds to the maximum of absorbance at 260nm (for DNA). $\varepsilon_{protein}$ is the extinction coefficient of the protein, ε_{DNA} the extinction coefficient of the DNA (Table 2. 5: Name and components of the buffers used.). ε_{max} is the extinction coefficient of the fluorophore at the maximum absorbance wavelength. CF introduces a correction factor for the absorbance of the fluorophore at 280nm or 260nm (for proteins and DNA respectively) and corresponds to the absorbance at 280nm or 260nm, in relation to the absorbance at the maximum.

2.1.3 Buffers

Table 2. 5: Name and components of the buffers used.

	Buffer	Components
MutHLS purification	**Binding buffer**	20 mM Tris-HCl, pH 7.9, 1 M NaCl, 5 mM imidazole, 10% glycerol, 1 mM PMSF, 1 mM benzamidine
	Washing buffer	20 mM Tris-HCl, pH 7.9, 1 M NaCl, 20 mM imidazole, 10% glycerol, 1 mM PMSF, 1 mM benzamidine
	Elution buffer	20 mM Tris-HCl, pH 7.9, 1 M NaCl, 500 mM imidazole, 10% glycerol
	MutS/MutL dialysis buffer	10 mM HEPES-KOH, pH 7.9, 200 mM KCl, 1 mM EDTA, 1 mM DTT, 10% glycerol
	MutH dialysis buffer	10 mM HEPES-KOH, pH 7.9, 500 mM KCl, 1 mM EDTA, 1 mM DTT, 50% glycerol
	STE	10 mM Tris-HCl, pH 8.0, 100 mM NaCl, 0.1 mM EDTA
EMSA	**Binding buffer**	25mM Tris/HCl, pH 7.5, 125mM KCl, 5mM $MgCl_2$
	Stop buffer	50% glycerol
• Protein modification	**FB125**	25mM Tris/HCl, pH 7.5, 125mM KCl, 5mM $MgCl_2$
	FB150	25mM Tris/HCl, pH 7.5, 150mM KCl, 5mM $MgCl_2$
• Acitvity assay	**Activity buffer**	10mM Tris/HCl, pH 7.9, 125mM KCl, 5mM $MgCl_2$
Gel running buffers	**TPE**	Tris (109g), Phosphoric acid (15ml), EDTA 2mM; pH 8.2 adjusted with Phosphoric acid
	TBE	TBE 1x: Tris 100mM, Boric acid 100mM, EDTA 2.5mM; pH 8.3 adjusted with Boric acid
	TAE	TAE 1x: Tris 40nM, Sodium acetate 20nM, EDTA 1mM; pH 8 adjusted with Glacial acetic acid

2.1.4 DNA primers

Table 2. 6: Sequence (5'-3') of the 42bp oligonucleotides used to generate 42bp double strand and double labeled DNA substrates

Name	Short name	Sequence
G_XhoI_A594_A	G_A594_A	TATTAATTT*CGCGGGCTCGAAAGCTTCATCCTCTACGCCGGA
G_XhoI_A594_C	G_A594_C	TATTAATTT*CGCGGGCTCGACAGCTTCATCCTCTACGCCGGA
G_XhoI_A594_G	G_A594_G	TATTAATTT*CGCGGGCTCGAGAGCTTCATCCTCTACGCCGGA
G_XhoI_A594_G_14	G_A594(14)_G	TATTAAT*TTCGCGGGCTCGAGAGCTTCATCCTCTACGCCGGA
G_XhoI_A594_T	G_A594_T	TATTAATTT*CGCGGGCTCGATAGCTTCATCCTCTACGCCGGA
G_XhoI_A594_G_I	G_A594_G_I	TATTAATTT*CGGATGAAGCTGTCGAGCCCGCTCTACGCCGGA
G_XhoI_A594_T_I	G_A594_T_I	TATTAATTT*CGGATGAAGCTTTCGAGCCCGCTCTACGCCGGA
T_HindIII_A488_A	T_A488_A	TCCGGCGT*AGAGGATGAAGCTATCGAGCCCGCGAAATTAATA
T_HindIII_A488_C	T_A488_C	TCCGGCGT*AGAGGATGAAGCTCTCGAGCCCGCGAAATTAATA
T_HindIII_A488_G	T_A488_G	TCCGGCGT*AGAGGATGAAGCTGTCGAGCCCGCGAAATTAATA
T_HindIII_A488_T	T_A488_T	TCCGGCGT*AGAGGATGAAGCTTTCGAGCCCGCGAAATTAATA
T_HindIII_A488_G_I	T_A488_G_I	TCCGGCGT*AGAGCGGGCTCGAGAGCTTCATCCGAAATTAATA
T_HindIII_A488_T_I	T_A488_T_I	TCCGGCGT*AGAGCGGGCTCGATAGCTTCATCCGAAATTAATA

T* indicates which thymine is coupled to the fluorophore. Bases underlined indicate the position of the mismatch.

Primer for the generation of a single point mutation:

Table 2. 7: Sequence (5'-3') of the primers used in mutagenesis

Name	Sequence
MutS_D835R_Cfr13I	GGTGAGTGATCTCGGGTCCAGATTTTCCA
MutS_CTD	GTTATTAAGCGCGCACGGCAAAAGCTG

Table 2. 8: Sequence (5'-3') of the primers used in screening for the point mutation.

Name	Sequence
BBseqB	CTTCCTTTCGGGCTTTGTTAG
BBseqA	CCCGCGAAATTAATACGACTC

Primers for the generation of 406bp and 484bp substrate

1) Unlabeled 406bp substrate

Table 2. 9: Sequence (5'-3') of the primers used for the generation of a 406bp unlabeled substrate

Name	Sequence
Back_21_P	P-TCCGGCGTAGAGGATGAAGCT
T_HindIII_T	TCCGGCGTAGAGGATGAAGCTTTCGAGCCCGCGAAATTAATA
T_HindIII _C	TCCGGCGTAGAGGATGAAGCTCTCGAGCCCGCGAAATTAATA
T_HindIII_ A_P	P-TCCGGCGTAGAGGATGAAGCTGTCGAGCCCGCGAAATTAATA
T_HindIII_ G	TCCGGCGTAGAGGATGAAGCTATCGAGCCCGCGAAATTAATA
BBSeqB111	TCATCCTCGGCACCGTCAC
BBSeq111B_P	P-TCATCCTCGGCACCGTCAC

P- indicates a phosphorilated base. T* indicates which thymine is coupled to the fluorophore. Bases underlined indicate the position of the mismatch.

2) Single labeled 406bp substrate

Table 2. 10: Sequence (5'-3') of the primers used for the generation of a 406bp single labeled substrate

Name	Sequence
Back_21_P	P-TCCGGCGTAGAGGATGAAGCT
T_HindIII_A488_T	TCCGGCGT*AGAGGATGAAGCTTTCGAGCCCGCGAAATTAATA
T_HindIII_A488 _C	TCCGGCGT*AGAGGATGAAGCTCTCGAGCCCGCGAAATTAATA
T_HindIII_A	P-TCCGGCGTAGAGGATGAAGCTATCGAGCCCGCGAAATTAATA
T_HindIII_A488_G	5TCCGGCGT*AGAGGATGAAGCTATCGAGCCCGCGAAATTAATA
BBSeqB111	TCATCCTCGGCACCGTCAC
BBSeq111B_P	P-TCATCCTCGGCACCGTCAC

P- indicates a phosphorilated base. T* indicates which thymine is coupled to the fluorophore. Bases underlined indicate the position of the mismatch.

3) Double labeled 406bp substrate

Table 2. 11: Sequence (5'-3') of the primers used for the generation of a 406bp double labeled substrate

Name	Sequence
MM_A364_P_28	P-CGACTCACTATAGGGGAATTGTGAGCGG
T_HindIII_A488_T	TCCGGCGT*AGAGGATGAAGCTTTCGAGCCCGCGAAATTAATA
T_HindIII_A488 _C	TCCGGCGT*AGAGGATGAAGCTCTCGAGCCCGCGAAATTAATA
T_HindIII_A	P-TCCGGCGTAGAGGATGAAGCTATCGAGCCCGCGAAATTAATA
T_HindIII_A488_G_P	P-TCCGGCGT*AGAGGATGAAGCTATCGAGCCCGCGAAATTAATA
G_XhoI_A594_G_P	P-TATTAATTT*CGCGGGCTCGAGAGCTTCATCCTCTACGCCGGA
G_XhoI_A594_T	TATTAATTT*CGCGGGCTCGATAGCTTCATCCTCTACGCCGGA
BBSeqB111	TCATCCTCGGCACCGTCAC
BBSeq111B_P	P-TCATCCTCGGCACCGTCAC

P- indicates a phosphorilated base. T* indicates which thymine is coupled to the fluorophore. Bases

4) 484bp substrate

Table 2. 12: Sequence (5'-3') of the primers used for the generation of a 484bp unlabeled substrate

Name	Sequence
BBSeqB111	TCATCCTCGGCACCGTCAC
BBSeq111B_P	P-TCATCCTCGGCACCGTCAC
BBSeqA302	ATCTTCCCCATCGGTGATGTC
BBSeqA302_P	P-ATCTTCCCCATCGGTGATGTC

P- indicates a phosphorilated base

2.1.5 Enzymes

Table 2. 13: Restriction endonucleases and DNA modifying enzymes

Type	Name	Company	Recognition sequence
Restriction endonucleases	Cfr13I	MBI Fermentas	5' G^GNCC 3'
	DpnI	MBI Fermentas	5' GA^TC 3'
	HindIII	MBI Fermentas	5' A^AGCTT 3'
	XhoI	MBI Fermentas	5' C^TCGAG 3'
DNA modifying enzymes	Pfu polymerase	In house synthesis (I. Dern)	
	Taq polymerase	In house synthesis (I. Dern)	
	λ exonuclease	MBI Fermentas	5'→3' exodeoxynuclease; selectively digests the phosphorilated strand of DNA double strand

2.1.6 Kits

Table 2. 14: Commercial kits used.

Name	Company
O'RangeRuler^{TM} DNA Marker	MBI Fermentas
PageRuler^{TM} Protein Ladder	MBI Fermentas
Zeba Protein-desalting spin columns	Pierce
pUC Mix Marker, 8	MI Fermentas
QIAprep Spin Miniprep	Qiagen
Promega PCR purification kit	Promega

2.1.7 Strains

TX2929: A *mutS* $^{-}$ cell line used for *in vivo* complementation assays. TX2929 is a descendent of the CC106 K12 strain in which the *mutS* gene was deactivated by the insertion of transposon.

Genotype: E. coli K12, CC106: (P90C [*ara*Δ[*lac-pro*XIII] [F'*laciZ proB*$^{+}$]).

TX2929: CC106 *mutS201*::Tn*5*;Km^{r}.

HMS174 (λDE3) (Novagen): Expression strain used to generate MutS and MutL proteins. Cells were transformed with vectors derived from pET-15b containing *mutS* or *mutL* genes.

HMS174 (λDE3) carries the T7 RNA polymerase gene, which enhances the expression of gene products under control of the T7 promotor.
Genotype: F^-, *recA1hsdR* ($r_{K12}^- m_{K12}^+$)(Rif^r)(DE3).

XL1 blue MRF' (Stratagene): Cell line used to overexpress MutH protein and for cloning mutagenized plasmids.
Genotype: recA1 endA1 gyrA96 thi-1 hsdR17 supE44 relA1 lac [F' proAB $lacI^qZ\Delta M15$ Tn10 (Tet^r)].

2.1.8 Plasmids

pTX412: pET-15b (Novagen) derived plasmid containing the *mutS* gene (kindly provided Dr M. Winkler)
pTX418: pET-15b (Novagen) derived plasmid containing the *mutL* gene (kindly provided Dr. M. Winkler).
pMQ402: pBAD18 derived plasmid containing the *mutH* gene (kindly provided Dr. M. Marinus).

2.2. Methods

2.2.1. Annealing

The DNA sample containing both complementary oligonucleotides is heated at 95 ºC for 5mins and allowed to slowly cool down to room temperature. Alternatively, the oligonucleotides were annealed in a thermocycling machine, by heating the sample at 95ºC for 2mins and cooling down the sample to 4ºC in 0.5ºC/30s steps. Oligonucleotides were annealed to a final concentration of at least 20µM and stored at -20 ºC.

2.2.2. Electrophoretic Mobility Shift Assay (EMSA)

Double labeled DNA binding by MutS was analysed through electrophoretic mobility shift assays. Different concentrations of MutS (0-400nM) were incubated with 50nM of double labeled 42bp oligonucleotides, for 10mins at 37 ºC, with 125mM KCl, 25mM Tris/HCl and 5mM $MgCl_2$. The 20µl reaction was stopped with 4µl of 50% glycerol and the tubes placed on ice. The complexes were loaded, under current, onto a 4% polyacrylamide gel, which was run at 60V for 90mins, at 4 ºC, in 40 mM Tris-HCl (pH 7.5), 20 mM sodium acetate, 1 mM EDTA. The bands were visualized without staining under U.V. light (Geldoku).

Competitive titrations were performed under the same conditions. MutS and DNA concentrations were kept constant (400nM and 50nM, respectively) and the complex was titrated with increasing concentrations of unlabeled G:T and A:T 42bp oligonucleotides (0.1 to 1µM).

2.2.3. Generation of MutS substrates

The various mismatch substrates with a single GATC site were generated based on the procedure published by Thomas *et al*[39]. Briefly, two PCR reactions were setup, using as a template 2 different pET-15b plasmids, one with a XhoI (pET-15b_XhoI) and one with a HindIII (pET-15b_HindIII) cleavage site, in the same position (Fig. 2. 8). One of the primers in each PCR reaction is 5' phosphorilated, a preferred substrate for λ exonuclease. After the purification of the PCR products with a Promega PCR-cleanup kit, the phosphorilated strand was digested, and the single strands annealed. After annealing, the G:T mismatch substrate was again purified with a Promega PCR-cleanup kit.

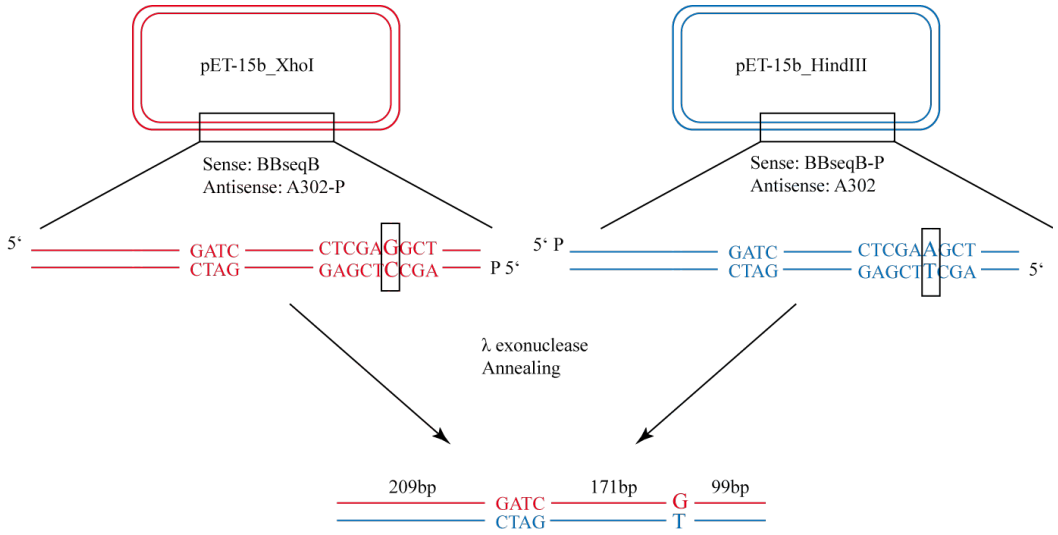

Fig. 2. 8: Schematic representation of the generation of 484bp mismatch substrate.

To generate the 406bp substrates, small changes were introduced into the protocol. The antisense primers introduce the mismatch and they can be either unlabeled (generating unlabeled 406bp substrate) or labeled with A488 (originating either single or double labeled 406bp substrate).

The generation of unlabeled or single labeled substrate is depicted in Fig. 2. 10. The sense primers are the same as for the 484bp substrate. The antisense primer vary, depending on which substrate is to be generated (G:T or T:G, unlabeled or single labeled). The template used while generating the 406bp substrate can be either pET-15b_XhoI or pET-15b_HindIII,

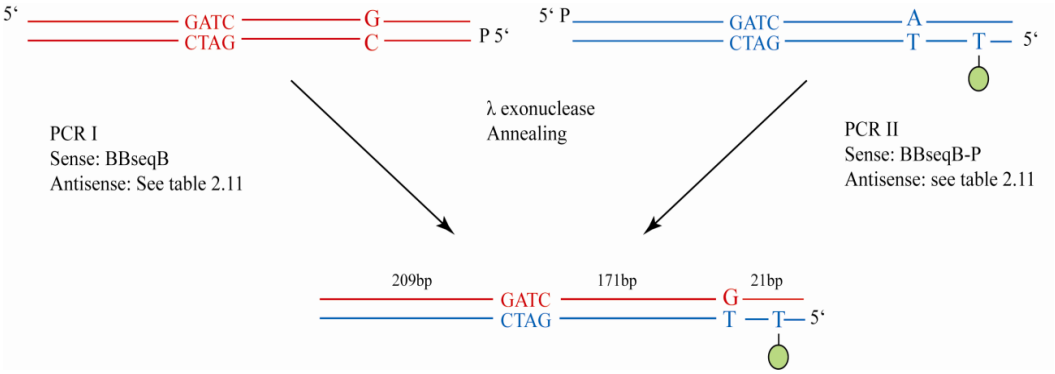

Fig. 2. 10: Schematic representation of the generation of the 406bp unlabeled/single labeled substrate. The PCR II antisense primer introduces the fluorophore in the case of the single labeled substrate. The antisense primers will decide which mismatch is introduced.

since the mismatch will be introduced via the antisense primer. The primers are shown in Table 2. 10.

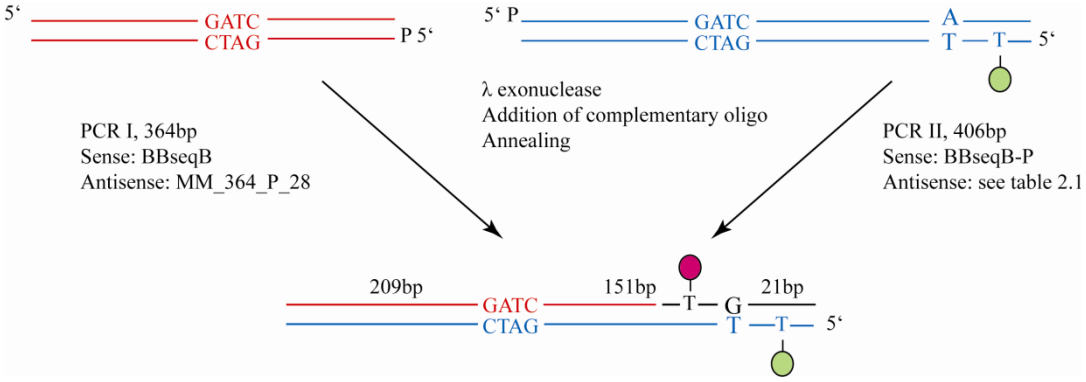

Fig. 2. 9: Schematic representation of the generation of the 406bp double labeled substrate. The product of PCR I (red) is shorter than the product of PCR II (blue), leaving a gap that will be filled by the acceptor labeled oligo (black). The green circle represents the coupled Alexa 488 and the pink circle represents the coupled Alexa 594.

The generation of the double labeled substrate requires two single strands of different length (Fig. 2. 9) and an acceptor-labeled 42bp oligo that is annealed on the 5’ end of the longer PCR product, which carries the donor label. The mismatch is also introduced via the oligo (see Table 2. 11Table 2. 15 for the required oligos). This substrate contains a nick between the 42bp oligonucleotide and the top 364bp strand.

2.2.4. Mismatch-provoked MutH endonuclease activity

The activity of MutS, MutL and MutH was determined in a mismatch-provoked MutH endonuclease activity assay. 10nM DNA substrate was incubated with 500nM MutH, 400nM MutS (unless otherwise mentioned) and 1µM MutL for 0 to 30mins at 37 ºC, in Activity buffer. After each time point, 10µl reaction solution were removed and stopped with 4µl AAP and loaded onto a 6% polyacrylamide gel. The products were separated for 30 to 60mins at

Table 2. 15: Description of the primers necessary for each substrate.

Antisense primer for PCRI	Antisense primer for PCRII		Complementary oligo for double labeled susbtrate	Mismatch
	Unlabeled substrate	Single/double labeled substrate		
Back-21-P	T_HIndIII_T	T_HindIII_A488_T	G_XhoI_A594_G	G:T
T_HindIII_A-P	T_HindIII_G	T_HindIII_A488_G	G_XhoI_A594_T	T:G

35W in Tris, Phosphate, EDTA buffer and visualized with Ethidium Bromide staining. The results were analyzed with TotalLab (Nonlinear Dynamics).

The cleavage of the 484bp substrate produces two fragments of 209bp and 275bp length and the cleavage of the 406bp substrates originate two fragments of 209bp and 197bp.

The first order rate was calculated with the following equation:

$$\%S = A \times e^{-kt} + BL,$$

where %S is percentage of substrate cleaved, A is amplitude, *k* is the pseudo-first order rate constant, t is time in minutes and BL is baseline.

2.2.5. Protein expression and purification

Protein expression: MutS and MutL were expressed from the *E. coli* cell strain HMS174 (λDE3) (Novagen) and MutH was expressed from the *E. coli* cell strain XL1 blue MRF' (Stratagene).

500ml of LB-medium, containing 100µg/ml of ampiciline, were inoculated with 1/100 dilution of an o/n culture and grown at 37 ºC, with constant shaking, until reaching an $O.D._{600}$ of 0.7-0.9. Protein expression was induced with IPTG, to a final concentration of 1mM (MutS and MutL) or 25g/l arabinose (MutH) for 4h or 3h, respectively, at 28 ºC. After this period, the cultures were harvested by centrifugation for 15 min (Beckman J6-HC), at 4 ºC, 3640x*g* and washed once with 15mls 10mM Tris/HCL, 100mM NaCl and 0.1mM EDTA buffer. Following a second centrifugation step, the pellets were stored at -20 ºC.

Protein purification: All purification steps were done at 4 ºC. After carefully thawing the pellet, the cells are ressuspended in ice-cold binding buffer, supplemented with 1mM benzamidine and 100mM PMSF (protease inhibitors), and sonicated for 6-8 min. The cells were centrifuged for 30 min. at 4 ºC, 25 000×*g* (Beckman J2-HS). The clear lysate was incubated with 0.5ml Profinity IMAC Ni-charged resin (Biorad) (1ml per liter of culture), pre-equilibrated with binding buffer, for 30 min. with gentle shaking. The Ni-resin/protein suspension is then centrifuged for 5 minutes 206 *g* (Beckman J6-HC), the supernatant is discarded and the suspension is washed 3x with 15mls washing buffer. Following the last

wash step, the Ni-resin/protein pellet is ressuspended in 7.5ml of washing buffer and loaded into a clean Biorad column. After letting the Ni-resin settle at the bottom of the column, the wash buffer was allowed to run through the column and the protein was eluted with 4x 500µl of elution buffer. The protein was incubated with 10mM DTT for 20min., on ice, and dialysed o/n against ~700ml dialysis buffer (the buffer was changed at least 2x). Following dialysis, the protein was transferred into 1.5ml tubes, centrifuged at 4º for 30min, >16,000 *g* (Eppendorf 5417C). The supernatant was collected and the concentration determined through the absorbance value at 280nm in Nanodrop. The protein was aliquoted, snapped freezed with liquid nitrogen and stored at -80 ºC. MutH was dialysed against MutH dialysis buffer and stored at -20 ºC.

2.2.6. Plasmid isolation

LB-medium containing 100µg/ml ampiciline was inoculated and cells were grown o/n, at 37 ºC, with shaking. The following morning, the cells were harvested and the plasmid was isolated with the QIAprep Spin Miniprep kit, according to the manufacturer's instructions.

2.2.7. PCR purification

PCR product was purified using the Promega PCR cleanup kit, according to the manufactures instructions.

2.2.8. Site-specific labeling

Single-cysteine variants of MutS were incubated with a molar excess of fluorophore (Alexa 488 or Alexa 594) over protein, in 25mM Tris/HCl pH7.5, 125mM KCl and 5mM $MgCl_2$, for 30 to 60mins at 4 ºC. After labeling, the reaction was stopped with DTT and the free fluorophore was removed with the 0.5ml Pierce desalting columns, according to the manufacturer's instructions.

The degree of labeling was determined as described in Degree of labeling.

Alternatively, the protein was modified immediately after purification. In this case, the protein was purified and eluted as described above. Instead of reducing the disulfide bridges with DTT, TCEP was added in 2x excess over protein and incubated for 30 minutes on ice. The labeling reaction was carried out in the elution buffer, with 2x excess of fluorophore over protein (in case of single labeled protein) or with a premixture of 0.5x Alexa 488 and 4x Alexa 594 (in case of double labeled protein). The proteins were allowed to label for 30 minutes on ice, after which the free fluorophore was removed with 5ml Pierce desalting columns, according to the manufacturer's instructions. Next, the protein was transferred into 1.5ml tubes, centrifuged for 30min, at 4 ºC, >16,000 *g* (Eppendorf 5417C). The supernatant

was collected and the concentration determined through the absorbance value at 280nm in Nanodrop and the DOL as described previously. The protein was aliquoted, snapped freezed with liquid nitrogen and stored at -80 ºC.

2.2.9. Site-directed mutagenesis

Site-directed mutagenesis was performed as describe by Kirsch and Joly[40]. Briefly, the protocol consists of two phases: in the first phase, a DNA fragment is amplified by PCR, using the gene of interested as a template and introducing the mutation with one of the primers along with a silent restriction marker; in the second phase, the amplified fragment of the first phase is used as a "megaprimer" to complete the sequence of the gene. This protocol relies on the fact that the in vitro synthesized DNA is not methylated, contrary to the parental DNA, rendering it resistant to digestion by DpnI.

The cysteine-free *muts* plasmid pTX412-CF was used as template to generate the *muts* pTX412-CF-D835R, using the primers MutS_D835R_Cfr13I, that introduces the mutation, and MutS_CTD. The thermal cycler was programmed as follows: 95ºC for 2'; 95ºC for 30''; 20x (50ºC for 1'; 69ºC for 1'; 50ºC for 1'); 68ºC for 5' and then cooled down to 4ºC. Approximately 100ng of the 162bp product was then used as a megaprimer in the second amplification cycle: 95ºC for 2', 16x (95ºC for 50'', 55ºC for 55'', 68ºC for 25') and 68ºC for 7'. Following this amplification step, the product was digested with 10U of DpnI, the undigested DNA was recovered by ethanol purification and ressuspended in 10µl of water. 6µl of the ressuspended DNA were then used to electrotransform XL blue E. coli cells; the nicked plasmid is repaired in vivo. The target region was amplified by PCR and screened for the mutation with the restriction enzyme that corresponds to the marker. Positive colonies were grown overnight in LB medium, containing 100µg/ml of ampiciline. The mutated gene was sequenced (SeqLab).

2.2.10. Transformation

Electrotransformation of E. coli XL Blue electrocompetent cells: Plasmid DNA was added to the electrocompetent XL Blue cells, previously thawed on ice, and incubated on ice for 1min. After the ice incubation, the suspension was introduced in an electroporation cuvette (previously cooled on ice) and submitted to an electric pulse of 1250V. LB-medium (500µl) was added into the cuvette, the suspension was carefully mixed and transferred into a 1.5ml eppendorf tube and incubated for 60mins at 37 ºC. Following the incubation, the cells were centrifuged for 4mins, at 4 200rpm, most of the supernatant was discarded, the cells were ressuspended in approximately 50µl supernatant and spread on plates with tetracycline and ampiciline (100µg/ml) resistance. The plates were incubated o/n at 37 ºC.

Transformation of E. coli HMS 174 (λDE3) competent cells: After recovering the plasmid from an o/n culture of the positive clones, 100-150ng was added to HMS cells, previously defrosted on ice. The suspension was incubated on ice for 30 to 60mins, followed by a heat shock for 1 to 2mins at 42 ºC and 1 to 5mins incubation on ice. LB-medium (800µl) was added to the cell suspension, which was then incubated at 37 ºC for 1h followed by 4mins centrifugation at 4 200 rpm. Most of the supernatant was discarded, the cells were ressuspended in 50µl supernatant and spread on ampiciline (100µg/ml) plates.

2.2.11. Modeling of a kinked DNA structure

In order to better understand how the fluorophores interact with DNA and with the protein bound to a mismatch, the 42bp oligonucleotide was modeled into a kinked structure using the parameters of the kinked DNA from the crystal structure, and fluorophore clouds were attached to the appropriate base.

The crystal structure DNA is 17bp long and is characterized by base-pair and base-pair step parameters (available with the crystal structure, PDB ID 1e3m [2]) that define the distortion of the helix. As the DNA used in the FRET studies is 42bp long, the crystal structure parameters was used to define the mismatch region, assigning the mismatch position of the crystal structure (template) to the mismatch position of the desired sequence (target). The unkinked 42bp oligonucleotide parameters were used to describe the missing bases (12bp 5' to the mismatched G and 13bp 3' to the G) (Table A. 1). The 42bp unkinked parameters with the target sequence were obtained by a three-dimensional nucleic acid visualization software, 3D DART [41]. The 42bp sequence and the derived parameters were introduced into the software and the 42bp G:T kinked 3D structure was obtained. The Pymol Molecular Graphics System (Delano Scientific, Palo Alto, CA, USA) was used to align the target DNA, obtained from 3D DART, to the template DNA, from the crystal structure. The fluorophore clouds, together with four bases (the T to which it is attached, plus two bases before and one base after, to increase the certainty of the cloud's position) were then modeled onto the labeled thymine (T) and aligned with the bases of the kinked DNA. The T:G was obtained by switching the two strands: the top strand in G:T is the bottom strand in T:G and vice-versa, while maintaining the G:T unaltered (Table A. 2). This way, the same parameters can be used to describe both mismatches.

2.2.12. Fluorescence

All fluorescence measurements were performed with a Steady State Benchtop Spectrofluorometer from HORIBA Jobin Yvon. For details, see below.

i. Theory

Fluorescence is the phenomenon of emission of light from excited states. By light absorption of a certain wavelength, an electron is excited from the ground state to higher energy level. If the electron in the excited state keeps its spin in the opposite orientation from the one that was left in the ground state, the electron is said to be in an excited singlet state, and the transition of this electron back to the ground state results in fluorescence emission. If, on the other hand, the electron in the excited state has the same spin orientation as the electron in the ground state, the electron is said to be in an excited triplet state, and the return to the ground state causes the emission of phosphorescence[42](Fig. 2. 11). The emission rates of fluorescence are in the range of $10^8 s^{-1}$, so that typical fluorescence lifetimes are around 10ns[43] (see below). After excitation, energy is lost in collisions between the excited molecules and the solvent, which causes vibrational or even electronic (internal conversions) changes in the excited molecules, with no emission of light. In unconjugated molecules there is great vibrational freedom, which can cause the return to the ground state by the excited molecule. In contrast, in highly conjugated molecules, like aromatic molecules, where the vibrational freedom is restricted, the mentioned processes can carry the excited molecule only to the lowest vibrational level of the lowest excited singlet state. Return to the ground state from this state occurs by the emission of fluorescent light, so molecules with one or more aromatic rings usually have fluorescence properties. If, instead of returning to the ground state, the molecule suffers a photochemical reaction or a change of spin of one of the electrons it is said to undergo a intersystem crossing, resulting in the creation of the lowest triplet state[42].

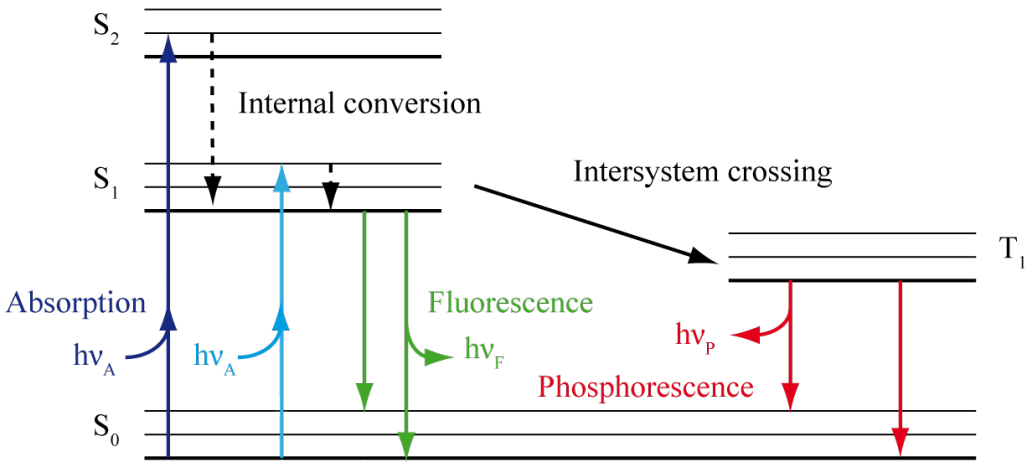

Fig. 2. 11: One form of the Jablonski diagram[43]. hν stands for energy, where the subscript refers to the type of energy: absorbed (A), emited by fluorescence (F) or emited by phosphorescence (P). Energy levels: S_0 (ground state), S_1 (lowest energy level of the first excited state), S_2 (highest energy level of the first excited state) and T_1 (first triplet state).

ii. Fluorescence quantum yield and lifetime

Quantum yield (Q) corresponds to the number of photons emitted relative to number of photons absorbed. The excited state can be depopulated by the radiative decay or by non-radiative decay, so the quantum yield can be calculated by:

$$Q = \frac{\Gamma}{\Gamma + k_{nr}} \qquad \textbf{Equation 2.3}$$

where, Γ is the radiative decay rate and k_{nr} is the non-radiative decay rate. When Q of a substance is close to unity, the non-radiative decay is much smaller than the radiative decay and the substance has very bright emission[43].

The excited state lifetime (τ) of a fluorophore is defined as the average time a fluorophore stays in the excited state, before returning to the ground state:

$$\tau = \frac{1}{\Gamma + k_{nr}} \qquad \textbf{Equation 2.4}$$

In the absence of non-radiative processes (k_{nr}=0), the lifetime of a fluorophore is called the intrinsic or natural lifetime[43].

Quantum yield determination*:* The quantum yield of a fluorophore is determined by comparison with standards of known quantum yield. The quantum yields of the compounds are mostly independent of excitation wavelength, so the standards can be used wherever they display useful absorption.

Determination of the quantum yield is generally accomplished by comparison of the wavelength-integrated intensity of the unknown to that of the standard. The optical density is kept below 0.05 (abs max below 0.05 and at ex. wavelength around 0.03) to avoid inner filter effects. The quantum yield of the unknown sample is calculated using:

$$\phi_{F,sample} = \frac{Abs_{ref} \times F_{sample} \times n^2_{sample} \times \phi_{F,ref}}{Abs_{sample} \times F_{ref} \times n^2_{ref}} \qquad \textbf{Equation 2.5}$$

$\phi_{F,sample}$ is the quantum yield of the measured sample; $\phi_{F,ref}$ is the quantum yield of the standards; n is the refractive index of the solution in which you measure both standards and sample. If the solution is the same, this term cancels itself. F is the fluorescence of both standards and sample excited at the same wavelength. The fluorescence signal should not exceed 10^5 counts.

The chosen standards were Rhodamine 110 (for A488) and Rhodamine 101 (for A594). All measurements were done using the same cuvette (different for each sample), the

measurements were carefully corrected for the buffer background (both for fluorescence and absorbance measurements).

iii. Fluorescence anisotropy

When a sample is excited with polarized light, the emission of light can also be polarized. The extent of the emission polarization is defined as anisotropy (r). Anisotropy depends on the transition moments for absorption and emission, that lie along specific directions within the fluorophore structure.

In an homogeneous solution, the fluorophores are randomly oriented. When they are exposed to polarized light, the fluorophores with their dipoles oriented along the vector of the light source are preferentially excited, conferring an average anisotropy to the solution.

The anisotropy is given by:

$$r = \frac{I \parallel - I \perp}{I \parallel + 2I \perp} \qquad \textbf{Equation 2.6}$$

where I ‖ is the emission polarizer oriented parallel to the excitation polarizer and I ⊥ is the emission polarizer oriented perpendicular to the excitation polarizer. The lower term of the equation 2.6 corresponds to the total intensity of the sample, in which twice the intensity of the perpendicular emission polarization is added because there are two perpendicular emission axis. Anisotropy is a dimensionless property, it does not depend on the total intensity of the sample and is independent of the fluorophore concentration[43].

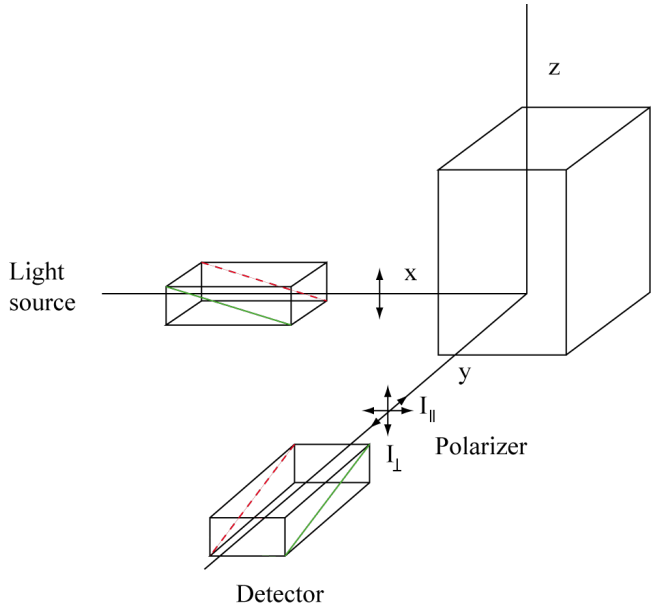

Fig. 2. 12: Scheme for anisotropy measurements.

Fluorescent anisotropy is a useful technique to determine protein-protein or DNA-protein interaction in solution due to the molecular rotations that the fluorophore undergoes during its excited state which depolarizes its fluorescence. If the emission is completely depolarized, I ∥ = I ⊥, and r = 0. If the emission is completely polarized along the transmission direction of the polarizer, I ∥ = 0, and r = 1, which is hardly ever observed. As the molecular rotations are size dependent, the values of anisotropy obtained are useful to determine the interactions of two molecules. It is important, however, to bear in mind the relation between the fluorescence lifetime of the fluorophore and the rotational correlation time of the labeled molecule, in the presence and absence of an interaction partner.

The anisotropy of a conjugated fluorophore depends on three factors: the mean correlation time (φ), due to the rotational motion, which depends on the size and shape of the macromolecule and on the type of linker used; the lifetime of the fluorophore (τ), dependent on the photophysics of the probe and the molecular environment; the limiting anisotropy (r_0), which can be determined by measuring the steady-state anisotropy in a highly viscous environment, to slow the rotation down. The relation between these three factors can be appreciated with the Perrin equation[43]:

$$r = \frac{r_0}{1 + {}^{\tau}/_{\rho}} \qquad \textbf{Equation 2.7}$$

- If the molecule is rotating slow, φ>>>τ, ${}^{\tau}/_{\rho} = 0$ and $r = r_0$
- If the molecule is rotating fast, τ>>>φ, ${}^{\tau}/_{\rho}$ very large and r approaches 0

In non-viscous solutions, the anisotropy is primarily determined by the rotational motion of the fluorophore. It is important to note, though, that DNA oligonucleotides longer that 40bp, due to its high molecular weight, will exhibit only a very small change in anisotropy, independently of the size of the formed complex[44].

All fluorescence anisotropy measurements were performed with the polarization module of the Steady State Benchtop Spectrofluorometer Fluoromax 4 from HORIBA Jobin Yvon. Slits were kept constant at 4nm and the samples were excited at 470nm (Alexa 488) or 575nm (Alexa 594). For each anisotropy measurement, the fluorescence spectrum was also recorded, excited at the same wavelength.

The titration measurements were performed by starting at a high protein concentration (1μM) and doing 1:2 dilution steps with a solution containing the same DNA concentration (10nM) and the same nucleotide concentration (1mM). The fluorescence spectrum was always recorded first, followed by the anisotropy measurement, which consists of 10 repeats,

with the final anisotropy value being an average of the repetitions. The titration curve was fitted to Sigmoidal Logistic [45] equation:

$$y = \frac{y_{max} - y_{min}}{1 + \left({}^{x}/_{K_D}\right)^{n}} + y_{min} \qquad \textbf{Equation 2.8}$$

where n is the Hill coefficient and K_D is the dissociation constant.

iv. Fluorescence Resonance Energy Transfer (FRET)

As was mentioned in the introduction, FRET is a very useful biochemical tool for looking at conformational changes in DNA and protein and at protein-protein interactions.

FRET occurs between two fluorophores, one donor (D) and one acceptor (A) fluorophore. The donor fluorophore is directly excited by a specific wavelength and the acceptor fluorophore is excited by the emission of the donor. As a result, the emission of the donor fluorophore decreases (the donor fluorescence is quenched) and the acceptor emission increases (FRET). It is a process that does not involve the emission or re-absorption of a photon and it is the result of long-range dipole-dipole interactions. For FRET to take place, three conditions have to fulfilled:

1. Overlap of the emission spectrum of the donor with the excitation spectrum of the acceptor

2. The two fluorophores need to have the correct spatial orientation, in relation to one another

3. The distance between the two fluorophores should be between 10 and 100Å.

FRET is strongly dependent on the distance, being proportional to r^6 (r is the distance between Donor and Acceptor):

$$E = \frac{R_0^6}{R_0^6 + r^6} \qquad \textbf{Equation 2.9}$$

The distance at which FRET efficiency is 50% is called the Förster distance (Fig. 2. 13).

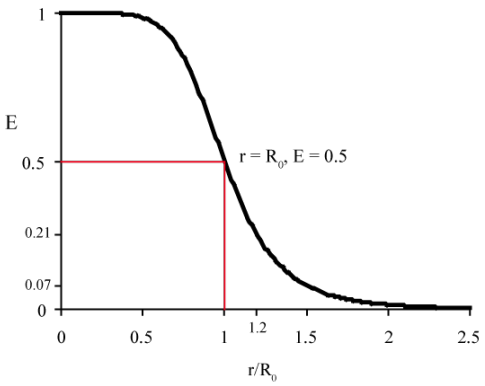

Fig. 2. 13: Dependence of FRET efficiency (E_{FRET}) on the donor-acceptor distance. When donor-acceptor distance is equal to the R_0 (r/R_0=1), E is 50%.

R_0 (in Å) is specific for each FRET pair and can be calculated from experimentally known values:

$$R_0 = 0.211\ (\kappa^2 n^{-4} Q_D J(\lambda))^{1/6} \qquad \textbf{Equation 2.10}$$

n is the refractive index of the medium and it is a value of 1.4 for biomolecules in aqueous solutions. $\mathbf{Q_D}$ is the quantum yield of the donor in the absence of acceptor (0.65 in the case of Alexa 488 attached to 42bp oligonucleotides) and **J(λ)** ($M^{-1}cm^{-1}nm^4$) is the overlap integral of the donor emission and acceptor excitation. Both Q_D and J(λ) are specific for each DA pair.

$\boldsymbol{\kappa^2}$ describes the DA dipole-dipole orientation factor, which is very difficult to determine experimentally. It can take values between 0 (perpendicular) to 4 (parallel) and it is generally assumed to be approximately 2/3 in biological systems, which has an upper error of 35%. The basis for this assumption is that the fluorophore is most commonly attached to the protein/DNA by a long linker, that allows the fluorophores to move freely within a cone and the energy transfer is averaged over all DA orientations. Alternatively, however, one can derive from anisotropy measurements that a range of static donor-acceptor orientations are present, which do not change during the lifetime of the excited state, and assume a κ^2 of 0.476 [43].

According to Clegg[46], the FRET efficiency can be calculated by four methods: 1) enhanced fluorescence of the acceptor; 2) decreased quantum yield of the donor; 3) decrease in the donor lifetime; 4) change in the fluorescence anisotropy of the donor and acceptor. Only the first case will be dealt with here.

v. Determining FRET efficiency by enhanced fluorescence of the acceptor for bulk measurements

When working with labeled biomolecules (DNA or proteins) in FRET experiments, it is important to bear in mind that the labeling reactions are usually not 100% efficient and that

the unlabeled molecules should be corrected for when determining FRET efficiencies. When working with double labeled DNA, the labels are placed at opposite strands, so that there can be the following species in solution:

d^+ = donor labeled DNA strand

d^- = unlabeled donor DNA strand

a^+ = acceptor labeled DNA strand

a^- = unlabeled acceptor DNA strand

$$(d^+ + d^-) = (a^+ + a^-) = 1$$
$$(d^+ + d^-) \times (a^+ + a^-) = d^+a^+ + d^+a^- + d^-a^+ + d^-a^- = 1$$

Knowing this, an expression translating the total fluorescence intensity can be derived, taking into account the degree of labeling of each DNA species. The actual measured emission fluorescence intensity from a solution containing both donor and acceptor results from the contribution of three emission processes: enhanced emission from A due to FRET, A emission from direct excitation and D emission from direct excitation of the D. The total emission $F_{em}(\lambda_{ex}, \lambda_{em})$, excited at λ_{ex} and emitted at λ_{em} is thus proportional to:

Acceptor fluorescence resulting from FRET

Acceptor fluorescence resulting from direct excitation

$$F_{em}(\lambda_{ex}, \lambda_{em}) \propto [Sd^+a^+]E\varepsilon_D(\lambda_{ex})\phi_A(\lambda_{em}) + \{[Sd^-a^+] + [Sd^+a^+]\}\varepsilon_A(\lambda_{ex})\phi_A(\lambda_{em}) +$$

$$\underbrace{\{(1-E)[Sd^+a^+] + [Sd^+a^-]\}\varepsilon_D(\lambda_{ex})\phi_D(\lambda_{em})}_{\text{Donor fluorescence}} \qquad \textbf{Equation 2.11}$$

$\varepsilon_D(\lambda_{ex})$ = Molar extinction coefficient of the donor, excited at λ_{ex}

$\varepsilon_A(\lambda_{ex})$ = Molar extinction coefficient of the acceptor, excited at λ_{ex}

$\phi_D(\lambda_{em})$ = Donor quantum yield

$\phi_A(\lambda_{em})$ = Acceptor quantum yield

$[Sd^+a^+]$ = concentration of double labeled dsDNA

$[Sd^+a^-]$ = concentration of dsDNA labeled only with donor

E = FRET efficiency

The superscripts D and A refer to Donor and Acceptor, respectively. The equation is valid even if donor and acceptor strands are not 100% labeled and therefore it follows that:

$$[Sd^+a^+] = [S]d^+a^+$$
$$[Sd^+a^-] = [S]d^+a^-$$
$$[Sd^-a^+] = [S]d^-a^+$$
$$[Sd^-a^-] = [S]d^-a^-$$

where [S] is total DNA concentration.

Equation 2.11 can be rewritten as:

$$F_{em}(\lambda_{ex},\lambda_{em}) \propto [S]\{\varepsilon_D(\lambda_{ex})\phi_A(\lambda_{em})Ed^+a^+ + \varepsilon_A(\lambda_{ex})\phi_A(\lambda_{em})a^+ + \varepsilon_D(\lambda_{ex})\phi_D(\lambda_{em})[(1-E)]d^+[(1-E)a^+ + a^-]\} = F_A(\lambda_{ex},\lambda_{em}) + F_D(\lambda_{ex},\lambda_{em}) \quad \textbf{Equation 2.12}$$

A derived emission spectrum containing only the emission from the acceptor, after subtracting the donor contribution is:

$$F^A_{em}(\lambda_{ex},\lambda_{em}) \propto [S]\{\varepsilon_D(\lambda_{ex})\phi_A(\lambda_{em})Ed^+a^+ + \varepsilon_A(\lambda_{ex})\phi_A(\lambda_{em})a^+\} \quad \textbf{Equation 2.13}$$

This is done experimentally by taking an emission spectrum of the double labeled sample and an emission spectrum of the sample labeled only with donor. This last spectrum is then normalized to the emission maximum and subtracted from the double labeled emission spectrum. The resulting spectrum is the FRET-induced acceptor emission spectrum of the double labeled sample, without the contribution of the donor.

The fluorescence intensity, which is not an absolute number, must be normalized by a standard, proportional to the concentration of the DNA. This standard can be the fluorescence of the direct excitation of the acceptor.

So, two fluorescence measurements with double labeled species need to be performed: one in which the solution is excited at the donor wavelength ($F^A_{em,FRET}(\lambda_{exD},\lambda_{em\,A_1})$) and one in which the solution is excited at the acceptor wavelength $F^A_{em,dir}(\lambda_{exA},\lambda_{em\,A_2})$. The following ratio can then be formed:

$$(ratio)_A = \frac{F^A_{em,FRET}(\lambda_{exD},\lambda_{em\,A_1})}{F^A_{em,dir}(\lambda_{exA},\lambda_{em\,A_2})} \quad \textbf{Equation 2.14}$$

$F^A_{em,FRET}(\lambda_{exD},\lambda_{emA})$ = Fluorescence of the acceptor due to FRET

$F^A_{em,dir}(\lambda_{exA},\lambda_{emA})$ = Fluorescence of the acceptor directly excited

$$(ratio)_A = \frac{[S]\left[\varepsilon_D(\lambda_{exD})\phi_A(\lambda_{em\,A_1})Ed^+a^+ + \varepsilon_A(\lambda_{exD})\phi_A(\lambda_{em\,A_1})a^+\right]}{[S]\left[\varepsilon_A(\lambda_{exA})\phi_A(\lambda_{em\,A_2})a^+\right]}$$

$$= \frac{\varepsilon_D(\lambda_{exD})\phi_A(\lambda_{em\,A_1})Ed^+ + \varepsilon_A(\lambda_{exD})\phi_A(\lambda_{em\,A_1})}{\varepsilon_A(\lambda_{exA})\phi_A(\lambda_{em\,A_2})}$$

$$= \left[Ed^+\frac{\varepsilon_D(\lambda_{exD})}{\varepsilon_A(\lambda_{exA})} + \frac{\varepsilon_A(\lambda_{exD})}{\varepsilon_A(\lambda_{exA})}\right] \times \frac{\phi_A(\lambda_{em\,A_1})}{\phi_A(\lambda_{em\,A_2})} \qquad \textbf{Equation 2.15}$$

The extinction coefficient values are know, d^+ is the labeling degree of the donor labeled strands and it can be calculated. Because $\lambda_{em\,A_1} = \lambda_{em\,A_2}$, the last term is 1 and so:

$$(ratio)_A = \left[Ed^+\frac{\varepsilon_D(\lambda_{exD})}{\varepsilon_A(\lambda_{exA})} + \frac{\varepsilon_A(\lambda_{exD})}{\varepsilon_A(\lambda_{exA})}\right] \qquad \textbf{Equation 2.16}$$

Considering equations 2.14 and 2.15:

$$\frac{F^A_{em,FRET}(\lambda_{exD},\lambda_{em\,A_1})}{F^A_{em,dir}(\lambda_{exA},\lambda_{em\,A_2})} = \left[Ed^+\frac{\varepsilon_D(\lambda_{exD})}{\varepsilon_A(\lambda_{exA})} + \frac{\varepsilon_A(\lambda_{exD})}{\varepsilon_A(\lambda_{exA})}\right]$$

$$\Leftrightarrow \frac{F^A_{em,FRET}(\lambda_{exD},\lambda_{em\,A_1})}{F^A_{em,dir}(\lambda_{exA},\lambda_{em\,A_2})} - \frac{\varepsilon_A(\lambda_{exD})}{\varepsilon_A(\lambda_{exA})} = Ed^+\frac{\varepsilon_D(\lambda_{exD})}{\varepsilon_A(\lambda_{exA})}$$

$$\Leftrightarrow \boldsymbol{E}$$

$$= \left[\frac{\boldsymbol{F^A_{em,FRET}(\lambda_{exD},\lambda_{emA_1})}}{\boldsymbol{F^A_{em,dir}(\lambda_{exA},\lambda_{emA_2})}} - \frac{\boldsymbol{\varepsilon_A(\lambda_{exD})}}{\boldsymbol{\varepsilon_A(\lambda_{exA})}}\right] \times \frac{\mathbf{1}}{\boldsymbol{d^+}} \times \frac{\boldsymbol{\varepsilon_A(\lambda_{exA})}}{\boldsymbol{\varepsilon_D(\lambda_{exD})}} \qquad \textbf{Equation 2.17}$$

The emission of the acceptor, Alexa 594, can be considered negligible when excited at the donor, Alexa 488, excitation wavelength (470nM). Thus, it follows that the term $\frac{\boldsymbol{\varepsilon_A(\lambda_{exD})}}{\boldsymbol{\varepsilon_A(\lambda_{exA})}}$ is 0. E is then defined by:

$$E = \left[\frac{F^A_{em,FRET}(\lambda_{exD},\lambda_{em\,A_1})}{F^A_{em,dir}(\lambda_{exA},\lambda_{em\,A_2})}\right] \times \frac{1}{d^+} \times \frac{\varepsilon_A(\lambda_{exA})}{\varepsilon_D(\lambda_{exD})} \qquad \textbf{Equation 2.18}$$

The donor excitation wavelength was set at 470nM and for the acceptor wavelength at 575nm. The corrected extinction coefficients are then:

$\varepsilon_A(\lambda_{ex\,575nm})$ = 52 000 $M^{-1}cm^{-1}$, $\varepsilon_D(\lambda_{ex\,470nm})$ = 38 000 $M^{-1}cm^{-1}$

The degree of labeling for the donor (d^+) was calculated for the donor single strand as described in section 2.1.2. E is now defined by:

$$E = \left[\frac{F^A_{em,FRET}(\lambda_{ex470nm}, \lambda_{em617nm})}{F^A_{em,dir}(\lambda_{ex575nm}, \lambda_{em617m})}\right] \times \frac{1}{d^+} \times \frac{\varepsilon_A(\lambda_{ex57nm})}{\varepsilon_D(\lambda_{ex470nm})} \qquad \textbf{Equation 2.19}$$

From equation 2.9and equation 2.19 it follows:

$$r = \left[R_0^6 \times \left(\frac{1}{E} - 1\right)\right]^{1/6} \qquad \textbf{Equation 2.20}$$

$F^A_{em,FRET}(\lambda_{ex470nm}, \lambda_{em617nm})$ is the spectrum of a double labeled sample (in this case **DNA DA**, red line in Fig. 2. 14), excited at the donor wavelength and corrected for the donor emission. It is obtained by taking two spectra (see Fig. 2. 14), one for **DNA DA** (red line) and one for **DNA donor only** (green line). The **DNA donor only** spectrum is then normalized by its maximum (donor only normalized, not shown) and used to generate the donor emission component of the DNA DA spectrum, the **DNA DA Donor emission (normalized)** spectrum (orange line), by multiplying the donor only normalized spectrum by the Donor DA spectrum. This contribution is then subtracted from the DNA DA spectrum to give the **pure acceptor from DNA DA** spectrum (light blue). The maximum of this spectrum was then used in equation 2.18. $F^A_{em,dir}(\lambda_{ex575nm}, \lambda_{em617m})$ corresponds to the maximum of the spectrum of direct excitation of the acceptor in the DNA DA sample (pink line).

The same procedure was repeated for the determination of FRET efficiency in the presence of MutS, using the DNA+MutS spectra, respectively.

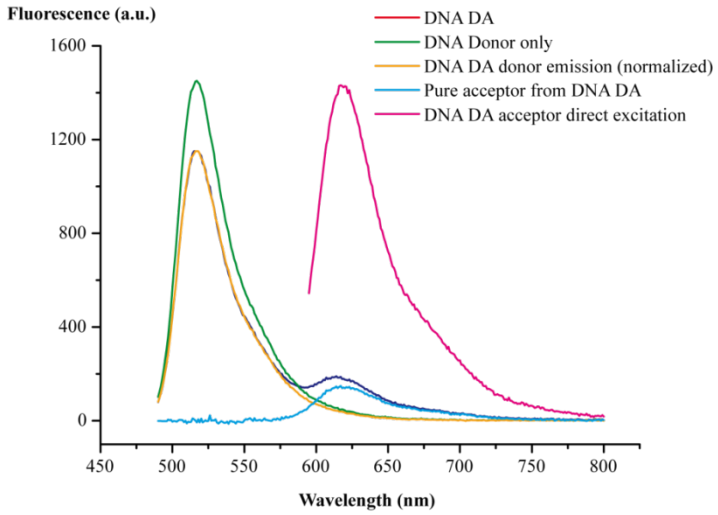

Fig. 2. 14: Spectral analysis for FRET efficiency determination.

The advantages of this method for the FRET efficiency calculation are:

1. All fluorescence measurements are done with the same sample, reducing the occurrence of errors;
2. The fluorescence quantum yield does not enter into the E calculations;
3. The normalization with the acceptor fluorescence circumvents the necessity of knowing the concentration of the labeled molecule
4. The labeling efficiency of the acceptor does not have to be necessarily 100%.

Equation 2.19 is also used to calculate the FRET efficiency for measurement in which: 1) the protein is double labeled or 2) both DNA and protein are labeled with a FRET pair. In 1) d^+ is the degree of labeling (see section 2.2 of the Materials and Methods) of the protein with donor and in 2) d^+ is the degree of labeling of either the protein or the DNA, depending on the experiment.

The fluorescence measurements were performed in quartz cuvette at room temperature. The slits opening was varied between 2.5 and 4nm, according to the measurement. All experiments were performed in 20m Tris/HCl pH7.5, 125mM KCl and 5mM $MgCl_2$. In some measurements, 0.05% Tween 20 was added as a stabilizing agent. Alexa 488 was excited at 470nm and the emission spectrum was measured from 490 to 800nm. Alexa 594 was excited at 575nm and the spectrum registered from 590 to 800nm.

vi. Determining FRET efficiency by the fluorescence intensity ratio F_D/F_A in smMFD

The detected signal intensities (S_G, green signal, and S_R, red signal) are calculated by dividing the number of photons by the burst duration. F_D and F_A are obtained from S_G and S_R after correcting for background counts (B_G and B_R), spectral crosstalk, α, and the ratio of the detection efficiencies, g, between the green and the red chanels (g_G/g_R)[4]:

$$F_D = \frac{S_G - S_R}{g_G} = \frac{F_G}{g_G} \qquad \textbf{Equation 2.21}$$

$$F_A = \frac{(S_R - B_R) - \alpha(S_G - B_G)}{g_R} = \frac{F_R}{g_R} \qquad \textbf{Equation 2.22}$$

If the quantum yield of the acceptor, ϕ_{FA}, is taken into account, FRET efficiency can be calculated as:

$$E_{FRET} = \frac{\frac{F_A}{\phi_{FA}}}{\frac{F_A}{\phi_{FA}} - \frac{F_A}{\phi_{FD(0)}}} = \frac{1}{1 + \frac{\phi_{FA}}{\phi_{FD(0)}} \frac{S_G - B_G}{(S_R - B_R) - \alpha(S_G - B_G)} \frac{g_R}{g_G}}$$ **Equation 2.23**

$\phi_{FD(0)}$ corresponds to the fluorescent quantum yield of the donor in the absence of acceptor. The determined acceptor quantum ϕ_{FA} yield was 0.95. From equation 2.21 and 2.22, it follows that:

$$R_{DA} = R_0 \left(\frac{\phi_{FA}}{\phi_{FD(0)}} \frac{F_D}{F_A} \right)^{1/6}$$ **Equation 2.23**

The Förster radius (R_0) was determined to be 53.2Å, for double labeled DNA.

The fluorescence lifetime is determined for each burst in two steps: (i) by generating a histogram of photon arrival times, and (ii) by fitting the histograms to a single exponential using a maximum likelihood estimator and iterative convolutions to account for the scatter contribution [47]. The FRET efficiency can be calculated through the ratio of the donor fluorescence lifetime, in the absence ($\tau_{D(0)}$) and presence of acceptor ($\tau_{D(A)}$), as follows:

$$E_{FRET} = 1 - \frac{\tau_{D(A)}}{\tau_{D(0)}}$$ **Equation 2.25**

vii. Double labeled DNA bending

As mentioned in the Introduction, MutS kinks the DNA by 60º upon finding a mismatch while scanning the DNA, being an important part in activation of downstream events. As can be seen from Fig. 2. 15, if one fluorophore is located on each side of the mismatch, the induced kink will reduce the distance between the two fluorophores. The binding of MutS to the mismatch will thus be signaled by an increase in FRET and a decrease of the donor signal. A FRET setup was designed so that, by switching only the mismatch bases, X:Y, all the possible mismatches could be tested for bending in 42bp oligonucleotides.

Altogether, 16 oligonucleotides can be derived by combination of the bases and they can be divided in three groups: asymmetric heteroduplexes, symmetric heteroduplexes and homoduplexes.

The position at which the fluorophores are placed is chosen according to three main points:

1. For a distance change to be observed, the fluorophores cannot be placed too far away from each other. Ideally, they should be placed around the R_0 for the FRET pair. For the pair Alexa 488 and Alexa 594, the R_0 is approximately 53Å.

2. The fluorophores cannot be placed too close to the protein as protein-fluorophore interactions must be taken into account and can influence the measure FRET efficiency.

3. The experiments that will be carried out. In the particular case of the current study, the fluorophores also have to be appropriate for the MFD experiments.

In these experiments, the bending effect of MutS was analyzed. MutS was allowed to bind to 42bp oligonucleotides (heteroduplex and homoduplex) double-labeled with donor and acceptor fluorophore. The stock DNA solution (20 or 30µM) was first diluted to 1µM and then to 20nM. MutS was added to the DNA in 50µl buffer solution to a final concentration of 400nM of MutS dimer. The FRET efficiency was determined as described () and used to compare the different DNA substrates.

For the determination of the dissociation constant (K_D), MutS was added to the 10nM DNA solution containing 1mM ADP to a final concentration of 500nM and diluted down in 1:2 dilution steps with a solution containing 10nM double labeled DNA and 1mM ADP, in order to keep the DNA and ADP concentration constant, until reaching a final concentration of 0.5nM. The data points were fitted to a Sigmoidal Logistic function [45]: $y = \frac{y_{min} - y_{max}}{1+(x/K_D)^n} +$

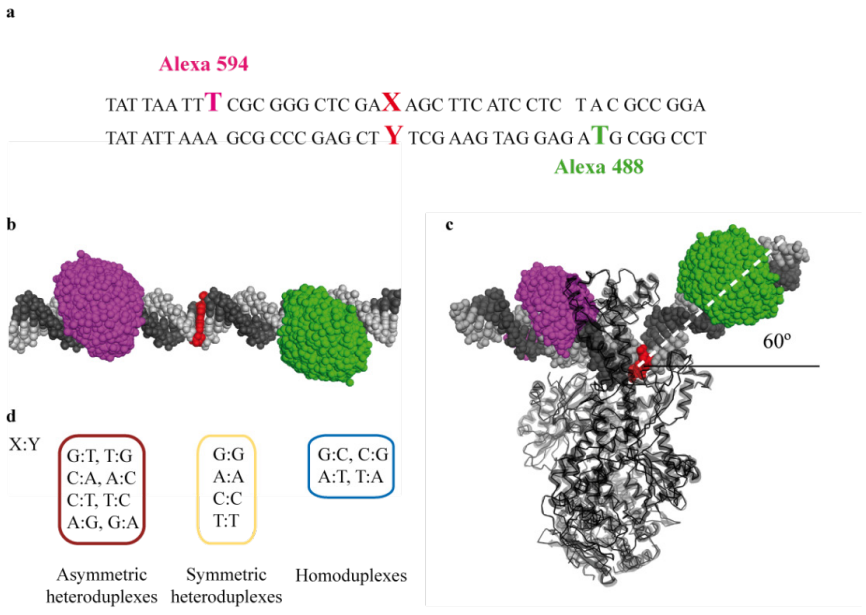

Fig. 2. 15: Experimental FRET Setup. a) Sequence and position of the mismatched bases (red), of Alexa 594 at position -12 (pink, on the top strand) and Alexa 488 at position -14 (green, on the bottom strand). X and Y indicate the position of the mismatch, with X representing the base on the Alexa 594 labeled strand and Y representing the base on the Alexa 488 labeled strand. b) model of the 42bp double-labeled DNA (DNA DA), unbent (left) and kinked by 60° (c), with the fluorophore clouds depicted in pink (Alexa 594) and green (Alexa 488). d) combination of X:Y bases tested.

y_{max} (equation 2.26). K_D is the dissociation constant and n corresponds to the Hill coefficient.

viii. Protein-DNA interaction studies (DNA/MutS FRET)

The interaction between labeled MutS and labeled 42bp oligonucleotides, either a G:T or a T:G heteroduplex, or a G:C homoduplex was analyzed. In one experiment, the DNA was labeled with donor and MutS with acceptor fluorophore; in the second experiment, the DNA was labeled with acceptor and MutS with donor fluorophore. The DNA concentration was kept at 20nM (both labeled with Alexa 488 and Alexa 594) and MutS was added to the DNA to a final concentration of 100nM (both labeled with Alexa 488 and Alexa 594) in 50µl buffer. The donor-labeled molecule was always added first and the spectrum was recorded, followed by the acceptor-labeled molecule. The FRET efficiency was determined as described previously and used to compare the measurements.

ix. Double labeled MutS

To determine the stability of the MutS dimer, double labeled protein was diluted down in 1:2 dilution steps, from 1µM to 4nM, in the absence and presence of 1mM ADP, ADPnP and ATP. To determine the effect of ADP, ADPnP and ATP in the stability of the dimer, 200nM double labeled MutS was incubated in the presence of 1µM unlabeled cysteine-free MutS and in the absence or presence of 1mM ADP, ADPnP and ATP. The fluorescence spectrum was registered 2 in 2 minutes to monitor the FRET signal change. To analyze the conformational changes of the clamps in the presence of the different nucleotides and in the presence of plasmid DNA and 42bp oligonucleotides, 200nM MutS were measured, varying the DNA and the nucleotide present and the order of addition. The fluorescence spectrum was again registered every 2 minutes and the F_A/F_D ratio plotted vs. time. Furthermore, to determine the approximate K_D for the ADP and ADPnP, the nucleotides were titrated into a 500nM double labeled MutS solution and fluorescence spectra were registered at different time points.

From the fluorescence spectra obtained from each measurement, the maximum of the donor and acceptor (FRET) peak was used to determine the ratio Donor fluorescence/Acceptor fluorescence (F_A/A_D). The higher the ratio (high acceptor signal, low donor signal), the higher the FRET efficiency. The F_A/A_D ratio was then plotted vs. MutS concentration or vs. time, accordingly. When mentioned, the data points were fitted to a Sigmoidal Logistic function [45]: $y = \frac{y_0 - y_{max}}{1+(x/K_D)^n} + y_{max}$ (equation 2.26).

2.2.13. Stopped flow

All experiments were performed in 25mM Tris (pH7.5), 125mM KCl and 5mM $MgCl_2$ by using a Applied Photophysics SX20 with dual detection stopped flow apparatus (deadtime 1.1ms, according to the manufacturer), with Alexa 488 excitation at 493nm and Alexa 594

excitation at 593nm. Donor and acceptor fluorescence was separated by two bandpass filters with the following ranges: HQ 520/35nm (green) and HQ 645/75nm (red).

The curves were fitted to a single, double or triple exponential:

$$\text{Single: } y = y_0 + Ae^{-x/t} \qquad \textbf{Equation 2.27}$$

$$\text{Double: } y = y_0 + A_1e^{-x/t_1} + A_2e^{-x/t_2} \qquad \textbf{Equation 2.28}$$

$$\text{Triple: } y = y_0 + A_1e^{-x/t_1} + A_2e^{-x/t_2} + A_3e^{-x/t_3} \qquad \textbf{Equation 2.29}$$

y_0 corresponds to the offset, A_1, A_2, A_3 correspond to the amplitudes of decay constants t_1, t_2 and t_3 and $t=1/k_{obs}$.The error percentage was calculated for the amplitudes and for the observed rates by dividing the standard deviation by the value of the variable and multiplying by 100.

i. Double labeled DNA bending kinetics

The measurements were performed in 25mM Tris/HCl pH 7.5, 5mM $MgCl_2$ and 125mM KCl. 42bp DNA oligonucleotide, with a G:T mismatch and double labeled with Alexa 488 and Alexa 594, and MutS unlabeled was used. The concentration of the reactants was twice the desired final concentration: 100µl of syringe 1 containing a 2x the final concentration of MutS and 2mM ADP (1mM final concentration) or ATP were rapidly mixed with 100µl of syringe 2 containing 30nM DNA (15nM final concentration). The association of MutS in the presence of ADPnP was measured by mixing 100µl of 30nM double labeled G:T oligonucleotide and 1µM MutS (500nM final concentration) preincubated with 2mM of ADPnP (1mM final concentration) The association of MutS to homoduplex was measured by mixing 100µl of 30nM double labeled G:C oligonucleotide (15nM final concentration) and 100µl of MutS (500nM final concentration).

For dissociation kinetics, different experiments were performed:

- 100µl of a pre-incubated 1µM MutS and 30nM of double labeled DNA from syringe 2 were rapidly mixed with 100µl of 2mM ATP, ADP or ADPnP and 2.25µM of unlabeled 42bp oligonucleotide (competitor) from syringe 1
- 100µl of a pre-incubated 1µM MutS, 30nM of double labeled DNA and 2mM ATP or ADP from syringe 2 were rapidly mixed with 100µl of 2.25µM of unlabeled 42bp oligonucleotide (competitor) from syringe 1
- 100µl of a pre-incubated 1µM MutS and 30nM of double labeled from syringe 2 were rapidly mixed with 100µl of a 2mM ATP or ADPnP solution from syringe 1

ii. Double labeled MutS kinetics

The measurements were performed in 25mM Tris/HCl pH 7.5, 5mM $MgCl_2$ and 125mM KCl. The concentration of the reactants was twice the desired final concentration. For these experiments, double-labeled $MutS^{R449C/D835R}$ was used and mixed different reactants as described below:

- 100µl of a 600nM MutS-DA solution from syringe 2 were rapidly mixed with 100µl buffer from syringe 1
- 100µl of a 600nM MutS-DA solution from syringe 2 were rapidly mixed with 100µl of a 2µM G:T or G:C solution from syringe 1
- 100µl of a 600nM MutS-DA solution from syringe 2 was rapidly mixed with a 2mM ATP solution from syringe 1
- 100µl of a 600nM MutS-DA solution pre-incubated with 2mM ATP or ADP from syringe 2 were rapidly mixed with 100µl of a 2µM G:T solution from syringe 1

2.2.14. Analytical Ultracentrifugation

Analytical ultracentrifugation (AUC) analysis was performed on the MutS dimer-tetramer equilibrium and on the interaction between the three MMR initiation proteins. The interaction between two or more proteins can be characterized as either static or dynamic[48]. In static interactions, the interaction is very slowly reversible or even irreversible during the measuring time, allowing the analysis of the different states of association due to the strong interaction between the interaction partners. These interaction are usually analyzed by Sedimentation Velocity (SV), where the rate transport is measured and the complexes are fractionated at high velocity according to their mass, shape and density. SV allows for the estimation of the sedimentation coefficient and molar mass of the complexes. In SV, the sedimentation coefficient *s* describes the linear velocity *u* of a macromolecule resulting from a centrifugal field $\omega^2 r$[49]:

$$s = \frac{u}{\omega^2 r} \qquad \text{Equation 2.30}$$

s is a molecular constant expressed in Svedberg units (S), with $1S = 10^{-3}$sec. In order to interpret the sedimentation coefficient in terms of hydrodynamic model shapes or compare it with predictions from hydrodynamic theory for a given structure, it is usual to correct the obtained s-value (s_{exp}) to an s-value that would be observed under standard conditions of water at 20ºC, $s_{20,w}$:

$$s_{20,w} = s_{exp}\left(\frac{\eta_{exp}}{\eta_{20,w}}\right)\left(\frac{1-\bar{\nu}\rho_{20,w}}{1-\bar{\nu}\rho_{exp}}\right) \qquad \text{Equation 2.31}$$

,where η refers to the viscosity, ρ to the density and $\bar{\nu}$ is the partial specific volume of the volume. In contrast to static association, dynamic association are rapidly reversible during measuring time and, although it is not possible to physically separate the different complexes formed, information about the concentration dependence of an interaction partner can be obtained. Usually, moderately strong composition-dependent interaction forces are involved and are usually analyzed by Sedimentation Equilibrium (SE). During this type of analysis, there is no net transport and the equilibrium distributions can be analyzed using thermodynamic models for association, such that composition dependence of signal-average buoyant mass is obtained.

Analytical Ultracentrifugation studies were performed with an analytical ultracentrifuge with fluorescence detection was used in the following measurements (Beckman Proteomelab XL-A XL-I).

Sedimentation velocity runs were performed with MutS labeled with Alexa 488 or 42bp DNA oligonucleotide, containing an Alexa 488 on position -14 on the T-Strand , in 25m Tris/HCl pH 7.5, 125mM KCl and 5mM $MgCl_2$. Labeled MutS was incubated either with unlabeled 42bp G:T oligonucleotide or a 505bp circular plasmid, containing one GATC site and one mismatch (G:T).

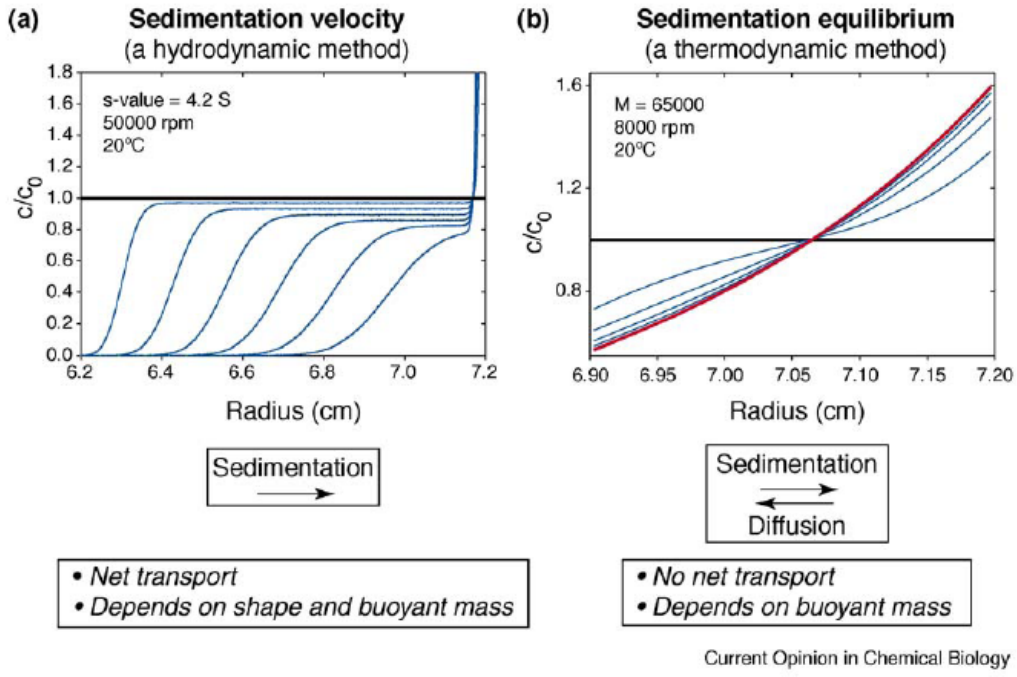

Fig. 2. 16: Simulation of ultracentrifugation sedimentation velocity and sedimentation equilibrium measurements of a 65kDa single species at 20° C with s-values of 4.2 S. c/c_0 is the protein concentration at a given radial position and time in relation to the loading concentration before centrifugation (black). a) High-speed sedimentation velocity (SV) experiments, where successive gradients correspond to elapsed time intervals of 5min. b) Low speed equilibrium experiment (SE), where successive gradients correspond to elapsed time intervals of 4h.the final gradient (red) is a close approximation to SE.

To test the dependence of MutS on the oligomerization state, the sedimentation profile of 1μM, 200nM, 40nM and $MutS^{R449C/D835R}$-Alexa 488 and $MutS^{R449C}$ in the presence of 1mM ADP or 1mM ADPnP. To determine the stoichiometry of MutS binding to a 42bp oligonucleotide, the 50nM 42bp G:TA488 was incubated with 100nM or 1μM of unlabeled MutS and the sedimentation profile was determined. Alternatively, 100nM of $MutS^{R449C/D835R}$-Alexa 488 was incubated with 25nM, 50nM and 500nM of unlabeled 42bp G:T and the sedimentation behavior of the complex was determined.

2.2.15. Single molecule Multiparameter Fluorescence Detection (smMFD)

i. Preparation of κ-casein coated slides

In order to avoid absorbance effects of the DNA onto the glass slides (Menzel-Glaeser, 24x60mm, #1.5), these were coated with κ-casein prior to each measurement. A drop of 80μl κ-casein (2mg/ml) was placed in the center of the glass plate and allowed to adhere to the surface for approximately 20mins. After the incubation period, the drop was washed 8x with 50μl of water and 2x with 50μl buffer used in the measurements. After the last buffer washing step, a drop of 50μl buffer was placed on the coated area.

ii. Single molecule measurements

For single molecule measurements, the DNA (20μM stock) was diluted in 3 steps in fluorescence buffer. The final concentrations of the dilutions was 20nM, 375pM and, finally, the last dilution was made into the 50μl sample drop, to a final concentration of 7.5-15pM. Measurements were typically performed for 1h30mins, at 20 ºC.

iii. Multiparameter Fluorescence Detection

The single molecule measurements of a very dilute (~15pM) solution of double labeled DNA molecules was performed with a confocal epi-illuminated microscope. The donor fluorophore (Alexa 488) is excited by a linearly polarized, active-mode-locked Argon-ion laser (476.5 nm, 73 MHz, 300 ps). The laser light is focused into the solution with a 60x/1.2 water immersion objective. Because the solution is very diluted, single bursts derived by single molecules are detected within the sample volume. This photon-train is divided initially into its parallel and perpendicular components via a polarizing beamsplitter and then into a wavelength ranges below and above 595 nm. Additionally, red (HQ 630/66 nm) and green (HQ 533/46 nm) filters in front of the detectors ensure that only fluorescence photons coming from the acceptor (Alexa 594) and donor (Alexa 488) molecules are registered. An estimate of the focal geometry is acquired by determining the diffusion correlation time of 200 ± 13 μs for Rhodamine 110 and knowing its diffusion coefficient of 0.34 ± 0.03 $\mu m^2/ms$. Moreover,

correction factors l_1 = 0.0308 and l_2 = 0.0368 are used to account for the mixing of polarization by the microscope objective and a factor G = 1.02 is applied to compensate for the slightly different detection efficiency of the two polarization components. Detection is performed using four avalanche photodiodes (SPCM-AQR-14, Laser Components, Germany). The signals from all detectors are passed through a passive delay unit and two routers to two synchronized time-correlated single photon counting boards (SPC 132, Becker and Hickl, Germany) which are connected to a PC. Fluorescence bursts are distinguished from the background of 1-2 kHz by applying certain threshold intensity criteria (~0.05 ms interphoton time, 50 photons minimum per burst). Bursts during which bleaching of the acceptor occurs are excluded from further analysis by applying a criterion regarding the difference in macroscopic times, T_G-T_R < 0.45 ms, where T_G and T_R are the average macroscopic times in which all photons have been detected in the green and red channels respectively during one burst.

iv. Probability Distribution Analysis (PDA)

The probability distribution analysis calculates the theoretical probability of recording a particular combination of red and green fluorescence from which the FRET efficiency, and thus distance, can be derived[36]. PDA quantitatively describes the shapes of FRET distributions measured by MFD, including the effect of background and shot-noise in the distribution. Both the mean and width of a distribution are the functions of the mean FRET efficiency[50]. With the PDA approach, a single parameter, which corresponds to the FRET efficiency mean, determines automatically the maximum width and asymmetry of the distribution that can be assigned to shot-noise. Any additional broadening is attributed to the real interdye distance distribution which can reveal biologically relevant heterogeneities in an ensemble of biomolecules [50].

Histograms of FRET efficiencies and distance for the donor-acceptor pair were calculated using equation 2.9, 2.20 and 2.21. Fits to experimental histograms were generated by applying the mentioned equations to theoretical distributions $P(S_G,S_R)$, calculated using the PDA theory[50] to the burst selection described above. The experimental histograms were fitted using in-house developed software, using a four-3state model. Each FRET state was fitted using an (apparent) Gaussian distribution of distances while a fixed R_{DA} at 110Å is used for donor-only species.

v. Fluorescence Correlation Spectroscopy

FCS is based on the analysis of the fluctuations of the fluorescence intensity. The origin of the fluctuations is not critical for the technique and thus FCS offers a unique tool for the direct study of phenomena like diffusion and photophysics. Through the before mentioned

phenomena, FCS can indirectly investigate biologically relevant processes like binding. From the Stokes-Einstein relation it follows than the bigger a molecule is, the slower it diffuses in a solution. In this study the binding of the labeled oligonucleotides to MutS was investigated by FCS since unbound oligonucleotides diffuse faster than the bound oligonucleotides. FCS curves were produced by correlating the signals coming from the green parallel and the green perpendicular detection channel. This was done to avoid antibunching. One should notice that the data registration scheme used for smMFD allows the use of the same data sets for correlation analysis. Moreover, it allows applying correlation analysis only to specific subpopulations of molecules. The diffusion times of the various FRET subpopulations were determined and compared in order to confirm that most of the molecules were in the bound state.

III Results

3.1 MutS can be site-specifically labeled with Alexa fluor dyes and is active after labeling

In the current report, the DNA/MutS interaction will be addressed from three points of view (Fig. 3. 1): a) DNA (3.2 and 3.3), b) DNA and MutS (3.2.3) and c) MutS alone (3.4).

FRET is a very powerful technique to study protein/DNA interactions and DNA or protein conformational changes, as it allows the monitoring of small distance in real time and in solution. To perform DNA conformational change studies, single labeled oligonucleotides were purchased and annealed, forming double labeled oligonucleotides, with various mismatches. To perform DNA/MutS interaction and MutS conformational change FRET studies, single-cysteine MutS (SC-MutS) variants need to be specifically modified with maleimide-coupled Alexa fluorophores, without significant loss of DNA binding and mismatch recognition ability, ATPase activity and, depending on the experiment, interaction with MutL. The labeling and activity of SC-MutS variants is addressed in this section.

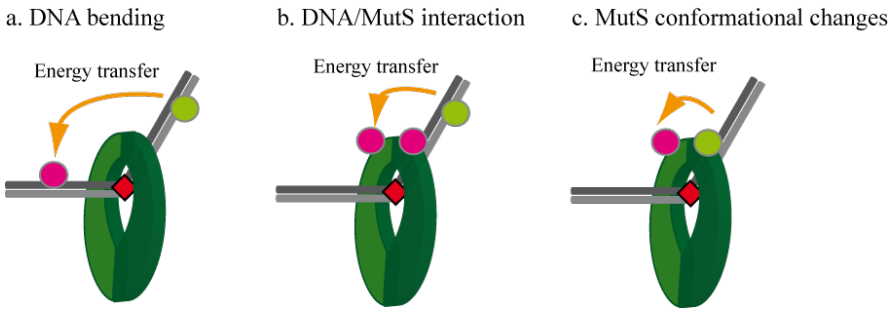

Fig. 3. 1: Schematic representation of the FRET systems used in the current report. a) DNA bending analyzed with short double labeled oligonucleotides; b) DNA/MutS FRET analyzed with single labeled single-cysteines MutS and single labeled DNA; c) Conformational changes in MutS, analyzed with double labeled single-cysteine MutS variants and unlabeled DNA.

MutS is site-specifically labeled with Alexa-maleimide fluorophores. For DNA/MutS interaction studies, SC-MutS^{R449C} (Fig. 3. 2a) was labeled with Alexa dyes (Alexa 488, Alexa 594 or both, according to the experiment), conjugated to a maleimide linker. As can be seen in Fig. 3. 2b, MutS^{R449C} is site-specifically labeled with Alexa 488; the cysteine-free (CF) variant of MutS is not labeled under the same reaction conditions.

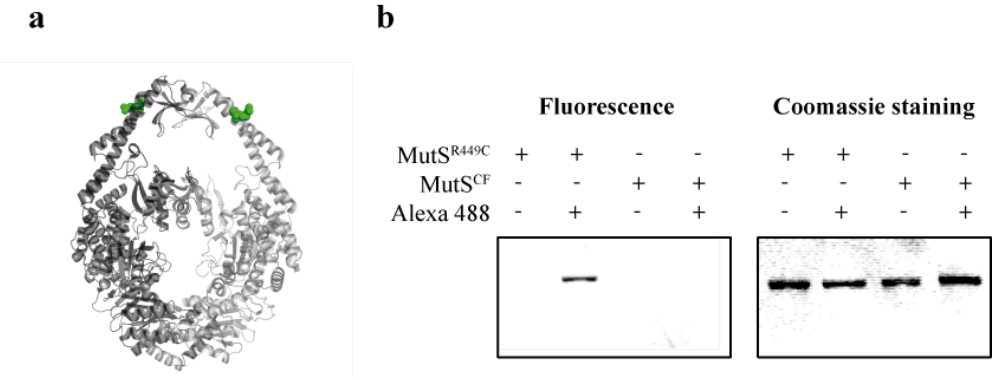

Fig. 3. 2: a) Crystal structure of MutS, with the residues 449 marked as green spheres. b) 10% SDS-Page gel of the labeling reaction of MutS and Alexa 488. Left: the labeled protein is observed without further staining, under U.V. light due to the fluorescent properties of Alexa 488. Right: the proteins were stained with colloidal coomassie.

As was mentioned in the Introduction, $MutS^{WT}$ can form tetramers, hence implying that in tetrameric SC variants of MutS four cysteine are available for modification with Alexa-maleimide fluorophores. As these four fluorophores complicate the analysis of fluorescence data, a dimer variant of MutS ($MutS^{CF/D835R}$) was used in the current experiments. This variant was previously shown to retain the same affinity for DNA as the tetramer ($MutS^{CF}$) and was considered suitable for the experiments[15]. The single-cysteine variant, $MutS^{R449C/D835R}$ was generated from the $MutS^{CF}$ variant by the mutation of an arginine to a cysteine. As can be seen from Fig. 3. 3, the ability of $MutS^{R449C/D835R}$ to induce mismatch provoked MutH activation is comparable to

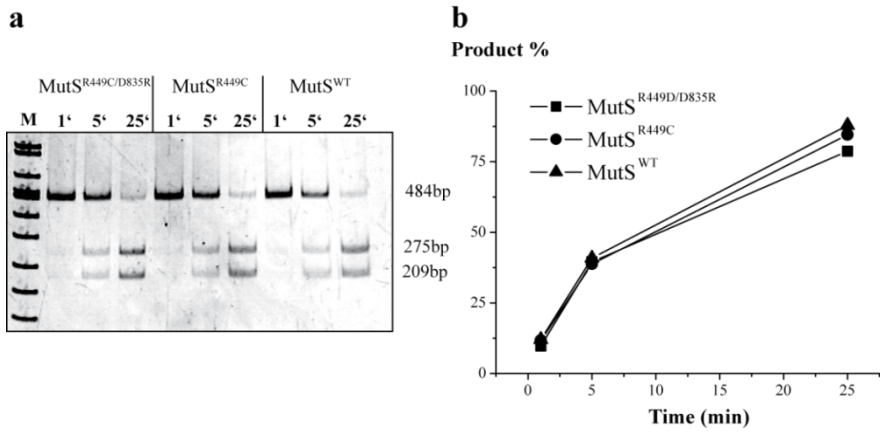

Fig. 3. 3: Activity of the dimeric SC-MutS variant $MutS^{R449C/D835R}$, $MutS^{R449C}$ and $MutS^{WT}$ in mismatch-provoked MutH activation. a) 10nM of 484bp DNA susbtrate containing one G:T mismatch and one GATC site were incubated in the presence of the different MutS variants, MutL, MutH and ATP, and samples were taken at 1', 5' and 25'. MutS binds the mismatch and activates MutL and MutH, which cleaves the DNA at the GATC site. The products (275 and 209bp) were separated on a 6% PAAG and analyzed with TotaLab. b) The % of product formed is plotted vs. time. Pseudo-first order cleavage rate *k* were determined for the cleavage reaction: $MutS^{R449C/D835R}$ A induces a *k* of 0.08min^{-1}, $MutS^{R449C}$ induces a *k* of 0.09min^{-1} and $MutS^{WT}$ a *k* of 0.1min^{-1}.

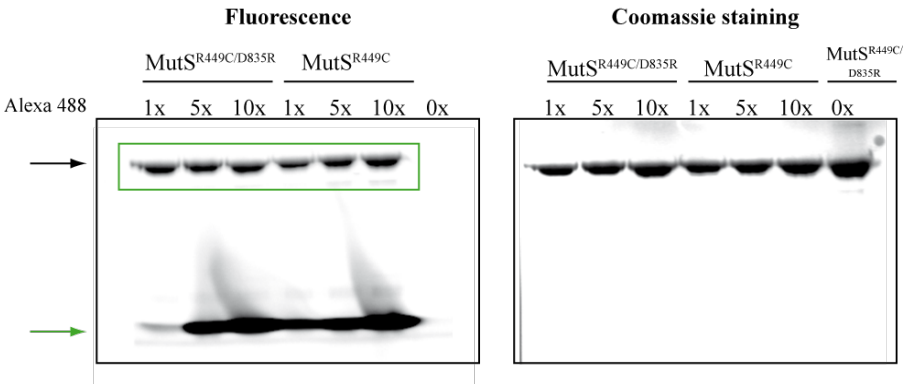

Fig. 3. 4: Labeling of MutS$^{R449C/D835R}$ and MutS^{R449C} with Alexa 488. Left: visualization of the fluorescence proteins under U.V. light. The black arrow indicates the band of the labeled protein and the green arrow indicates the free fluorophore, which was not removed after labeling. Right: colloidal coomassie staining of the labeled and unlabeled proteins (0x indicates unlabeled MutS$^{R449C/D835R}$, only visible after the colloidal coomassie staining).

MutS^{R449C} and MutS^{WT}.

Unless otherwise stated, the measurements were performed with MutS$^{CF/D835R}$ (unlabeled) or MutS$^{R449C/D835R}$ (labeled).

Next, the labeling reaction was optimized for MutS^{R449C} and MutS$^{R449C/D835R}$ (Fig. 3. 4). Dimer and tetramer variants were labeled with 1x, 5x, 10x excess of Alexa 488 over MutS. Both variants are labeled with a similar efficiency.

MutS is active after single- or double-labeling with Alexa 488 and/or Alexa 594. For the purpose of FRET studies, single-labeled MutS$^{R449C/D835R}$ with Alexa 488 (MutS$^{R449C/D835R}$-D) or Alexa 594 (MutS$^{R449C/D835R}$-A) and double-labeled with both (MutS$^{R449C/D835R}$-DA) were required. MutS$^{R449C/D835R}$ was therefore tested for labeling and activity with all three combinations of fluorophores. To avoid labeling before each measurement and in order to perform the measurements with the same batch of protein, MutS was labeled immediately after purification, followed by storage of the labeled protein at -80ºC. MutS was successfully labeled with Alexa 594 (Fig. 3. 5a) and there was not a significant loss of protein after the purification procedure, and the free fluorophore was removed to a good extent (pink box). After purification and labeling, the proteins were tested for heteroduplex discrimination in a mismatch-provoked MutH activation assay, where the MutS activity on a heteroduplex (G:T) was compared to the activity on a homoduplex (G:C) (Fig. 3. 5b). The unlabeled and labeled protein showed comparable levels of G:T vs. G:C discrimination (4.8x and 3.4x, respectively).

Single labeled MutS (with Alexa 488 or Alexa 594) was used in DNA/MutS FRET studies in section 3.2.3.

Next, the labeling reaction of MutS$^{R449C/D835R}$ with both Alexa 488 and Alexa 594 was optimized. Ideally, the protein should be labeled equally with both fluorophores. As this is difficult to obtain and as only the FRET signal is of interest and the donor is directly excited, a lower DOL for Alexa 488 and a higher DOL for Alexa 594 are sufficient. To optimize the ratios for double labeling, the MutS/A488 ratio was kept constant at 1:0.5 and the amount of A594 was varied, as shown in Table 3. 1.

Table 3. 1: MutS$^{R449C/D835R}$ was labeled with a mixture of Alexa 488 and Alexa 594, where the excess of Alexa 594 was varied and Alexa 488 and MutS concentrations remained constant. DOL A488 refers to the degree of labeling of the donor fluorophore in the double labeled protein and the same applies to DOL A594 and the acceptor fluorophore (Section 2.1.2.iii). The Total DOL is the sum of DOL A488 and DOL A594. The shaded ratio is the one chosen for subsequent labeling reactions.

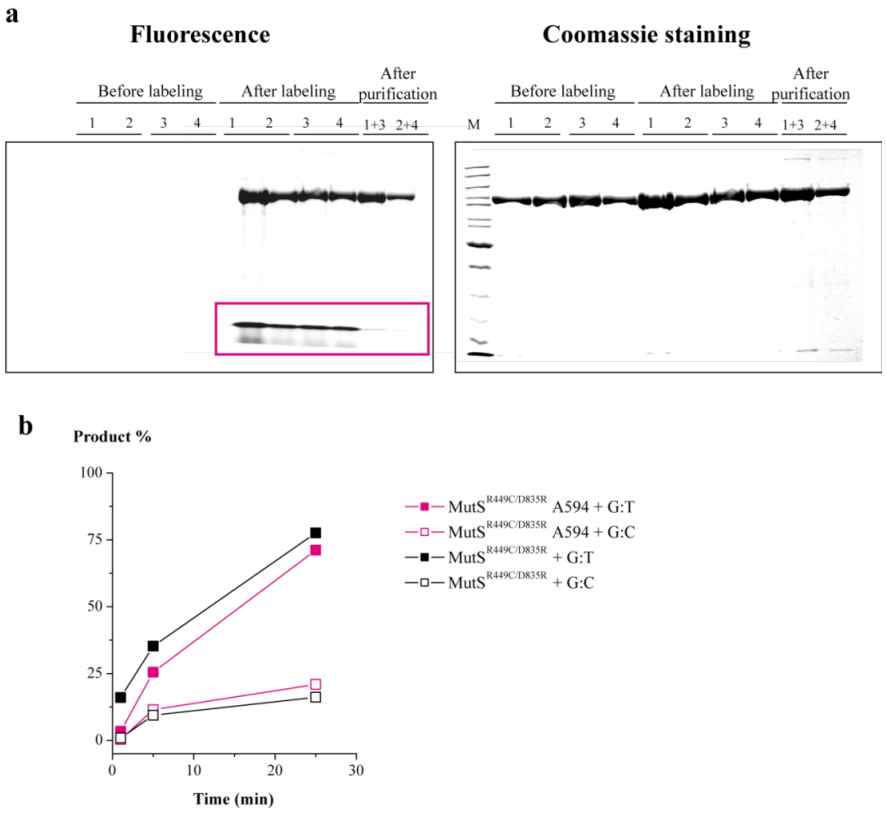

Fig. 3. 5: Labeling and *in vitro* activity of MutS$^{R449C/D835R}$. a) MutS$^{R449C/D835R}$ was labeled with Alexa 594 in a 1:1 ratio and the excess fluorophore was removed, as described previously. The product of the labeling reaction and of the purification step were visualized on a 10% SDS gel. Left) The labeled proteins can be seen, without further staining, under U.V. light. The pink box marks the excess fluorophore and the difference between after labeling and after purification shows the extent to which the free fluorophore was removed. Right) Coomassie staining of the labeled and unlabeled proteins. b) The activity of MutS after labeling was tested in a mismatch-provoked MutH endonuclease activity on a 484bp DNA substrate and the products were separated on a 6% PAAG. The % of product formed is plotted vs. time. Pseudo-first order cleavage rates *k* were determined for the cleavage reaction: MutS$^{R449C/D835R}$ A induces a *k* of 0.052min^{-1} (G:T) vs 0.01min^{-1} (G:C) whereas MutS$^{R449C/D835R}$ induces a *k* of 0.073min^{-1} (G:T) and 0.008min^{-1} for G:C.

MutS:A488:A594 ratio	DOL A488	DOL A594	Total DOL
1:0.5:0:5	0.25	0.14	0.40
1:0.5:1	0.24	0.18	0.42
1:0.5:2	0.2	0.53	0.73
1:0.5:3	0.2	0.56	0.75
1:0.5:4	0.13	0.6	0.73
1:0.5:5	0.13	0.75	0.88

The best ratio is the one that provides the highest Alexa 488 DOL (but lower that Alexa 594 DOL) and at the same time yields a high Alexa 594 DOL. The chosen working MutS/A488/A594 labeling ratio was thus 1:0.5:3.

Next, MutS^{R449C} and MutS$^{R449C/D835R}$ were labeled both with Alexa 488 (in a 1:0.5 ratio) and with Alexa 488/Alexa 594 (in a 1:0.5:3 ratio), and tested for induction of MutH activation. Both dimer and tetramer MutS^{R449C} variants are labeled and active after labeling (Fig. 3. 6 a and b). The study of conformational change with double labeled MutS will be addressed in section 3.4.2. Nucleotide modulates the clamp state of MutS.

In addition to MutS$^{R449C/D835R}$, also another single-cysteine variant, MutS$^{D246C/D835R}$, was labeled with either both Alexa 488 and Alexa 594 or with Alexa 594 only. After labeling, the

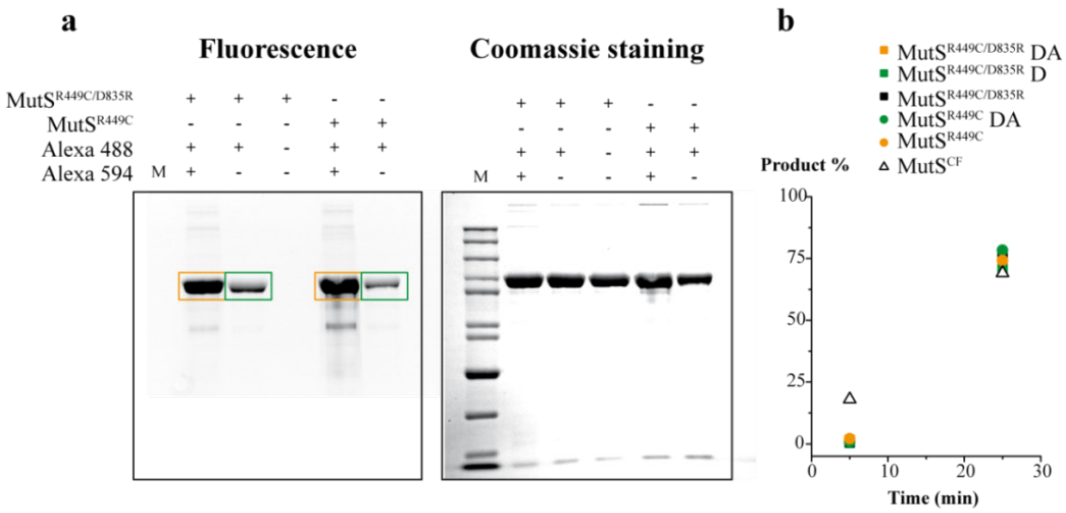

Fig. 3. 6: MutS$^{R449C/D835R}$ and MutS^{R449C} were purified and single-labeled with Alexa 488 (D, green) or double-labeled with Alexa 488 and Alexa 594 (DA, orange) and tested for activity in mismatch-provoked MutH activation, as described. a) The products of the labeling reaction were run on a 10% SDS gel; the proteins can be visualized by either fluorescence alone, resulting from the fluorescent tag, or by coomassie staining. b) Activity of labeled and unlabeled MutS$^{D246C/D835R}$ in the mismatch-provoked MutH endonuclease activity, on a 484bp DNA substrate, containing a single G:T mismatch and a single GATC site. Samples were taken as indicated and run on a 6% PAAG. The graph shows the comparison between the percentage of product formed after activation by the labeled and unlabeled MutS$^{D246C/D835R}$ and unlabeled MutS$^{R449C/D835R}$.

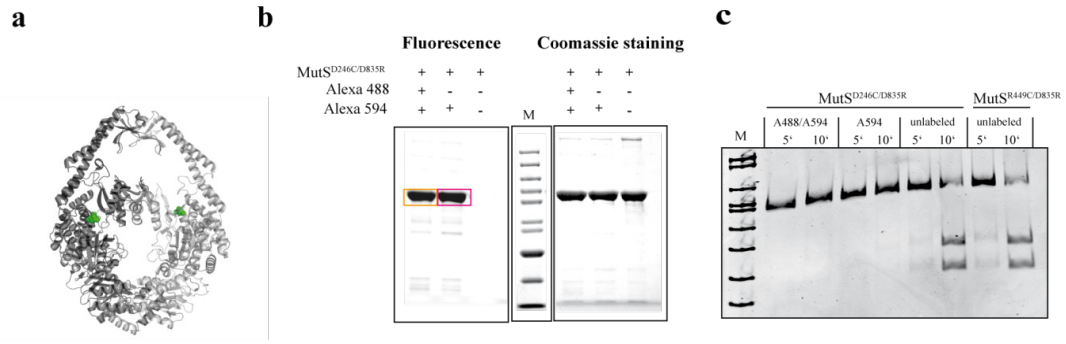

Fig. 3. 7: MutS$^{D246C/D835R}$ was purified, single-labeled with Alexa 594 (A, pink), double-labeled with Alexa 488 and Alexa 594 (DA, orange) and tested for activity in mismatch-provoked MutH activation, as described. a) Crystal structure of MutS, with the residues 246 marked as green spheres. b) The product of the labeling reaction were run on a 10% SDS gel; the proteins can be visualized by either fluorescence alone, resulting from the fluorescent tag, or by coomassie staining. c) Activity of labeled and unlabeled MutS$^{D246C/D835R}$ in the mismatch-provoked MutH endonuclease activity, using a 484bp DNA substrate, containing one single G:T mismatch and one single GATC site. Samples were taken as indicated and run on a 6% PAAG.

variants were tested for MutH activation and compared with unlabeled MutS$^{R449C/D835R}$. Fig. 3. 7 shows that both variants are labeled but that MutS$^{D246C/D835R}$ is no longer able to activate the MutH endonuclease activity after labeling.

The loss of activity of this variant could be attributed to impaired DNA binding or to impaired interaction with MutL. The DNA binding ability of both variants is addressed below (Section 3.2.3.). The interaction between MutS and MutL is currently being characterized in detail by our group using a variety of different methods, e.g. crosslinking (Ines Winkler, personal communication).

3.2 MutS binds mismatches with preferred orientations

To investigate the binding and bending/kinking of DNA by MutS in solution, double labeled 42bp oligonucleotides bearing all 16 combinations of base-base pairs at one position were used (Fig. 2. 15 and Fig. 3. 1). The variable base-base pair is located centrally on the DNA and a donor and a acceptor fluorophore are placed on either side of the mismatch. Binding of MutS to the mismatch induces a change in the Donor-Acceptor (DA) distance and is measurable with FRET. The DNA/MutS association was addressed in bulk (steady state and pre-steady state) and in the single molecule level.

3.2.1 DNA kinking at mismatches by MutS monitored by FRET

The kinking/bending of the designed oligonucleotides was tested with MutS^{D835R}. Unlabeled MutS (500nM monomer MutS) was added in excess to double labeled DNA (DNA-DA), with

mismatch (G:T-DA) and without (G:C-DA). There is a clear difference in the fluorescence emission spectra between both substrates in the presence of MutS (Fig. 3. 8):.the emission spectra of G:T/MutS displayed an increase in FRET, i.e. a decrease of the donor fluorescence with concomitant increase of the acceptor fluorescence – but addition of MutS to a G:C substrate led to a donor quench with unsignificant change of the acceptor signal.

A constant concentration of DNA was titrated with increasing MutS concentrations (Fig. 3. 9). Plotting the ratio of F_A/F_D against the concentration of MutS revealed a striking difference between the G:T and the G:C-DA substrates. (Fig. 3. 9c). A Sigmoidal Binding Model (Equation 2.26) was fitted to the G:T-DA data with a K_D of 11nM±0.89 (n=1.2±0.11). In contrast, since no obvious saturation of the F_A/F_D ratio was reached with G:C-DA, fitting of the binding model to the data was not possible.

Next, the FRET efficiencies (E, see Equation 2.19) were measured in the presence and absence of MutS. An excess of MutS over DNA was again used to assure that all mismatches are bound. The ratio of FRET efficiencies of bound and unbound DNA ($E_{bound}/E_{unbound}$) is shown in Fig. 3. 10 for all 16 base-base combinations as described (see also Section 2.2.12.vii).

The theoretical FRET efficiency for the unbound DNA substrates was around 0.09 (see Section 3.2.3) whereas the experimentally derived FRET efficiencies varied between 0.13 and 0.18 with an average of 0.15±0.01 (Table 3. 2). The fluctuation may be explained by different flexibilities of the mismatched DNA). A $E_{bound}/E_{unbound}$ ratio of approximately 1 was obtained for the four homoduplex substrates, indicating no change in the FRET efficiency before and after adding MutS. In contrast, the ratios for the 12 heteroduplex substrates was higher, albeit the variation was large (Table 3. 2 and Fig. 3. 10).

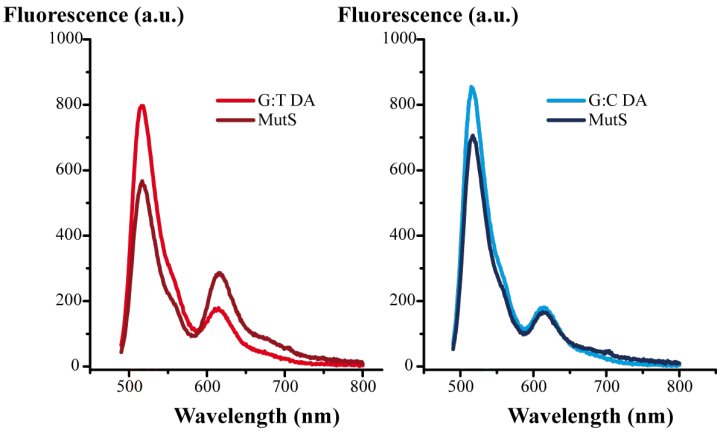

Fig. 3. 8: Emission spectra showing the effect induced by MutS effect upon binding to G:T DA and G:C DA. 500nM MutS were added to 10nM double-labeled DNA in the presence of 1mM ADP. The addition of MutS to G:T oligo (left) induces a strong increase in the FRET due to the DNA kinking. In contrast, the addition of MutS to G:C oligo (right) has no effect on the FRET signal, albeit a small quench of the donor signal.

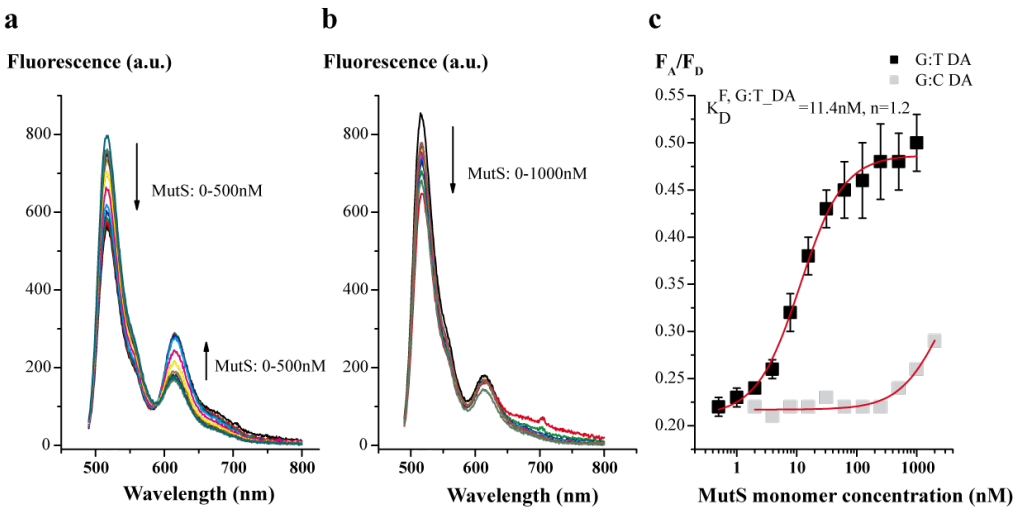

Fig. 3. 9: Emission spectra of G:T and G:C titration with MutS in the presence of ADP: increasing amounts of MutS were added to 10nM of G:T (a) and G:C (b) oligonucleotides, leading to an increase in the FRET signal of the G:T but not of the G:C oligonucleotide. The acceptor fluorescence/donor fluorescence ratio (F_A/F_D) was plotted for both cases vs. MutS concentration (c) and fitted to equation 2.7 (red curve), revealing a K_D of ~11nM±0.89 for the MutS/G:T complex, with n=1.2. The K_D for G:C cannot be determined due to the weak DNA binding.

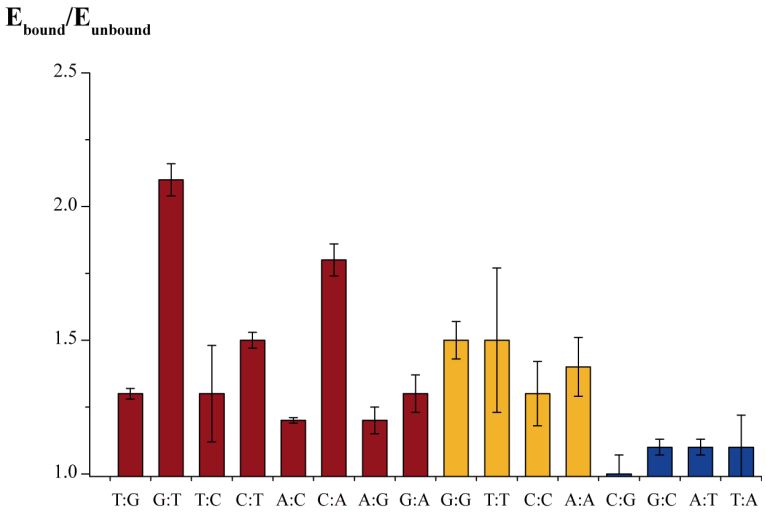

Fig. 3. 10: Binding of MutS to 16 different double labeled substrates. 42bp oligonucleotides, with all possible X:Y combinations were tested in the FRET assay for MutS-induced kinking. 20nM of DNA were incubated with 400nM of MutS. The asymmetric heteroduplexes are shown in red, the symmetric heteroduplexes in yellow and the homoduplexes are shown in blue..

To compare the effect of MutS binding to each mismatch, the ratio of the FRET efficiencies, $E_{bound}/E_{unbound}$, was calculated, which gives information about the relative change induced by the binding of MutS. A high $E_{bound}/E_{unbound}$ ratio means significant increase in FRET efficiency after the addition of MutS. G:T, C:A and C:T show the highest $E_{bound}/E_{unbound}$ ratio, whereas the

complementary mismatches T:G, A:C and T:C show a much lower $E_{bound}/E_{unbound}$ ratio. In contrast, there is no major difference between G:A and A:G. Comparing the symmetric mismatches, T:T and G:G show the highest $E_{bound}/E_{unbound}$ ratio, whereas C:C and A:A show the lowest $E_{bound}/E_{unbound}$ for the symmetric mismatches.

Table 3. 2: FRET efficiency between the fluorophores for bound and unbound DNA-DA measured in bulk in the absence of 1mM ADP, as indicated. G:T/T:G and C:A/A:C are marked in bold. The FRET efficiency was calculated according to section 2.2.12 and equation 2.19 and the distance was according to equation 2.19. σ corresponds to the standard deviation of at least 2 experiments.

DNA DA	$DNA_{unbound}$ $E_{mean} \pm\sigma$	DNA_{bound} $E_{mean} \pm\sigma$	$E_{bound}/E_{unbound}$ ($\pm\sigma$)
T:G	**0.13±0.00**	**0.16±0.00**	**1.3±0.02**
G:T	**0.17±0.00**	**0.37±0.03**	**2.1±0.06**
T:C	0.15±0.02	0.19±0.00	1.3±0.2
C:T	0.16±0.00	0.25±0.00	1.5±0.03
A:C	**0.15±0.01**	**0.18±0.01**	**1.2±0.01**
C:A	**0.15±0.00**	**0.27±0.01**	**1.8±0.06**
A:G	0.14±0.01	0.17±0.01	1.2±.05
G:A	0.14±0.00	0.18±0.01	1.3±0.07
G:G	0.14±0.01	0.21±0.00	1.5±0.07
T:T	0.14±0.03	0.22±0.01	1.5±0.3
C:C	0.18±0.00	0.22±0.03	1.3±0.1
A:A	0.13±0.01	0.18±0.00	1.4±0.1
C:G	0.13±0.00	0.13±0.01	1.0±0.07
G:C	0.15±0.01	0.16±0.00	1.1±0.03
A:T	0.15±0.00	0.16±0.00	1.1±0.03
T:A	0.14±0.02	0.15±0.00	1.1±0.1
T:G ADP	**0.16±0.01**	**0.2±0.006**	**1.2±0.08**
G:T ADP	**0.13±0.001**	**0.32±0.008**	**2.5±0.04**

Although in principle, a G:T mismatch is similar to a T:G mismatch, the observed ratios of $E_{bound}/E_{unbound}$ are significantly different. The difference in FRET efficiency change observed for the various bound mismatched substrates and in particular, the difference between G:T and T:G, can be explained by the following points:

1. MutS does not bind to certain mismatches due to lower affinity for different sequence contexts [51-53]
2. MutS interacts differently with the various mismatches (different binding orientations). This leads to different fluorophore/protein geometries, thereby influencing the photophysical properties of the dyes and thus the FRET efficiency.

3. MutS binds but does not bend/kink the mismatches to the same extent, maybe due to the sequence context

Point 1 and 2 are addressed by the following experiment (Fig. 3. 11).

To understand the difference between G:T and T:G, two DNA substrates were generated (T:G-I and G:T-I) in which the outside flanking sequences were switched (Fig. 3. 11a). As a consequence, the inside flanking sequences around the mismatch were kept unchanged (10bp 3' and 5' from the mismatch) but the fluorophores were switched. Hence MutS should bind and bend/kink the corresponding substrate in a similar way (i.e. G:T should correspond to G:T-I). The results are shown in Table 3. 3 and Fig. 3. 11b.

Table 3. 3: FRET efficiency between the fluorophores for bound and unbound T:G-I and G:T-I.

DNA DA	$DNA_{unbound}$ E_{mean} ±σ	DNA_{bound} E_{mean} ±σ	$E_{bound}/E_{unbound}$ ±σ
G:T-I	0.12±0.02	0.15±0.03	1.3±0.03
T:G-I	0.15±0.03	0.22±0.04	1.5±0.02
T:G	**0.13±0.01**	**0.16±0.01**	1.3±0.02
G:T	**0.17±0.01**	**0.37±0.03**	2.1±0.06

The FRET efficiency was calculated according to section 2.2.12 and equation 2.18 and the distance was according to equation 2.19. σ corresponds to the standard deviation of at least 2 experiments.

The FRET efficiencies of free DNA were in the same range as measured before (Table 3. 2). Binding of MutS to G:T-I resulted in a similar efficiency as the binding of MutS to T:G (0.15 vs. 0.16, respectively). On the other hand binding of MutS to T:G-I resulted in a FRET efficiency of 0.22, in comparison to 0.37 obtained with G:T. In summary, these results indicate that the mismatch flanking sequences is not responsible for the low FRET efficiency of the T:G/MutS complex. The results suggest that the primary reason for the observed differences in FRET efficiencies are due to the orientation of the fluorophores with respect to the mismatch, rather than the direct sequence context around the mismatch (see Section 3.2.2). Nevertheless, the lower $E_{bound}/E_{unbound}$ ratio of T:G-I/MutS complex suggests that the sequence context around the mismatch can have an effect on the affinity of MutS for DNA mismatch, as described in the literature for *E. coli* MutS and human MutSα[51, 53]. This aspect will further addressed below.

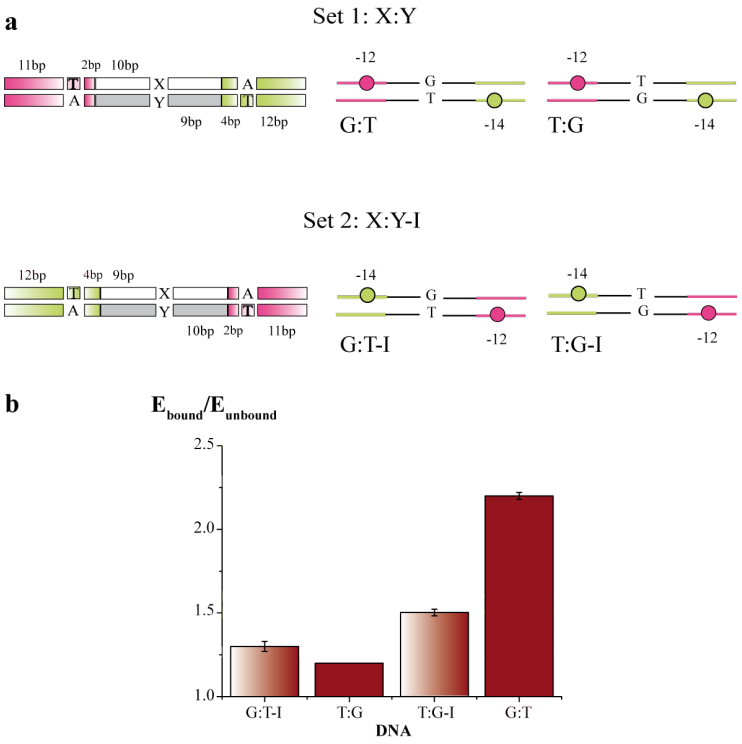

Fig. 3. 11: New set of 42bp oligonucleotides tested for MutS bending. The sequence surrounding both fluorophores was inverted for G:T and T:G, giving rise to two new oligonucleotides, T:G-I and G:T-I, while the sequence surrounding the mismatch was kept identical (see text for details). a) Left: Scheme for X:Y and X:Y-I oligonucleotides. The bases that were switched along with the fluorophore are shown in pink (for Alexa 594, represented by the pink boxed T) and green (for Alexa 488, represented by the green boxed T). The distance in bp between the end of the exchanged sequence and the fluorophores, and between the mismatch and the unchanged sequence is given. The white boxes refer to the sequence surrounding the X base from the mismatch and the grey boxes represent the sequence surrounding the Y mismatch base. Right: schematic representation of G:T/T:G in comparison to T:G-I/G:T-I. b) Effect on the FRET efficiency induced by MutS binding. 20nM DNA were incubated with 400nM MutS (n=3). The $E_{bound}/E_{unbound}$ ratio is plotted for each DNA substrate tested in comparison to G:T and T:G, with error bars corresponding to the standard deviation of a least 3 repetitions.

3.2.2 MutS has similar affinity for G:T and for T:G

MutS has similar binding affinity for double-labeled G:T and T:G. As stated above, the binding affinity of MutS for mismatches is known to be sequence context dependent and a lower affinity of MutS for T:G would further decrease the observed FRET efficiency. As such, Electrophoretic mobility shift assays were performed with both G:T and T:G double labeled 42bp oligonucleotides, to independently compare both substrates. As a control, the binding for G:C double-labeled homoduplex was also tested. The resulting binding curves (Fig. 3. 12) show

indeed a slightly higher K_D for T:G than for G:T, as predicted by the fluorescence experiments, demonstrating that in fact there is a difference in affinity due to the surrounding bases. However, the difference in affinity (K_D of 122nM vs. 145nM) is small. In addition, competition experiments carried out with the unlabeled G:T and T:G resulted in similar K_D-values indicating that the observed difference with the double-labeled oligonucleotides are not due to fluorophore-dependent (data not shown).

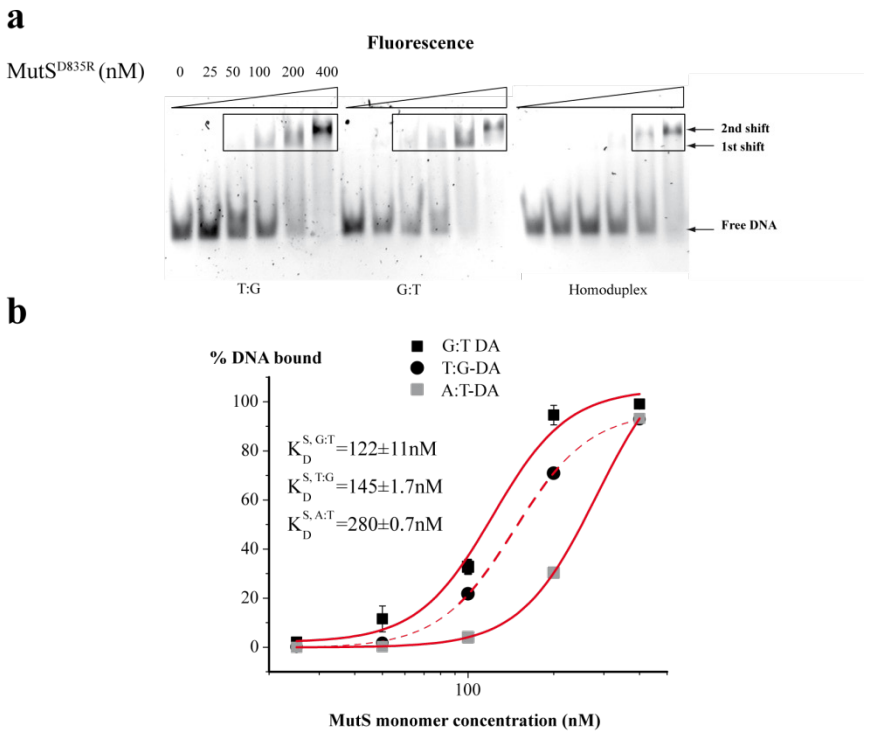

Fig. 3. 12: Binding of MutS to double-labeled G:T, T:G and G:C was determined with EMSA. a) MutS concentration was varied from 25-400nM (monomer) and the DNA-DA concentration was held constant at 50nM. The bands were visualized by fluorescence. b) The shifts were analyzed with the gel analysis software TotalLab and the % of DNA bound was plotted against the MutS concentration. A sigmoidal binding model (equation 2.7) could be fit to the data points, with n=3.3. The obtained K_D values for G:T was approximately 122±11nM and for T:G was approximately 145±2nM.

The EMSA experiments also showed that at high concentrations a second complex with lower mobility was formed, indicating that more than one MutS bind to the DNA at high concentrations. The oligonucleotide used in EMSA studies is 42bp long, with the mismatch at the center of the DNA. When MutS is bound to the mismatch, it occupies approximately 15bp, around 7 bases on either side of the mismatch, leaving sufficient space next to it for a second MutS. The second MutS could have bound next to the first MutS, which was bound to the mismatch, or to the free DNA ends as was observed for *E. coli* MutS in AFM studies [54].

Mismatch provoked activation of MutH on double-labeled 406bp G:T and T:G substrate. The *in vitro* activity of MutS was tested with 406bp long heteroduplex DNA containing the 42bp double labeled oligonucleotide, to determine to what extent the fluorophore is recognized as a mismatch. Alexa 488 and Alexa 594 labeled 406bp mismatch substrates were synthesized with either a G:T or a T:G mismatch or a G:C homoduplex. The unlabeled control substrates were generated with exactly the same process (described in Section 2.2.3) except that the primers used were unlabeled. Fig. 3. 13 shows the results of the cleavage reaction with MutS/L/H. In general, DNA generated by the mentioned procedure is cleaved faster than a "bona fide" homoduplex-control (G:C-PCR). However, both G:T and T:G containing DNAs are cleaved better than the corresponding G:C homoduplex controls, regardless whether fluorophores are present or absent.

The fact that both unlabeled and double labeled homoduplex strands are 5 to 10x more cleaved than the PCR substrate, is an indication that mismatches might arise in the substrates during its generation. Furthermore, the substrate contains a nick next to the G, which could contribute to enhanced activity on the homoduplex strands, by providing the homoduplex with a low energy site, prone to be recognized by MutS.

The 406bp double labeled DNA substrates were also tested for DNA binding by determining the fluorescence emission spectra. Since the donor–acceptor distance is the same as in the oligonucleotides, the $E_{bound}/E_{unbound}$ ratio is expected to be similar. This is in fact the case, as shown in Fig. 3. 14. 406bp G:T DA shows high FRET efficiency as MutS binds to the mismatch,

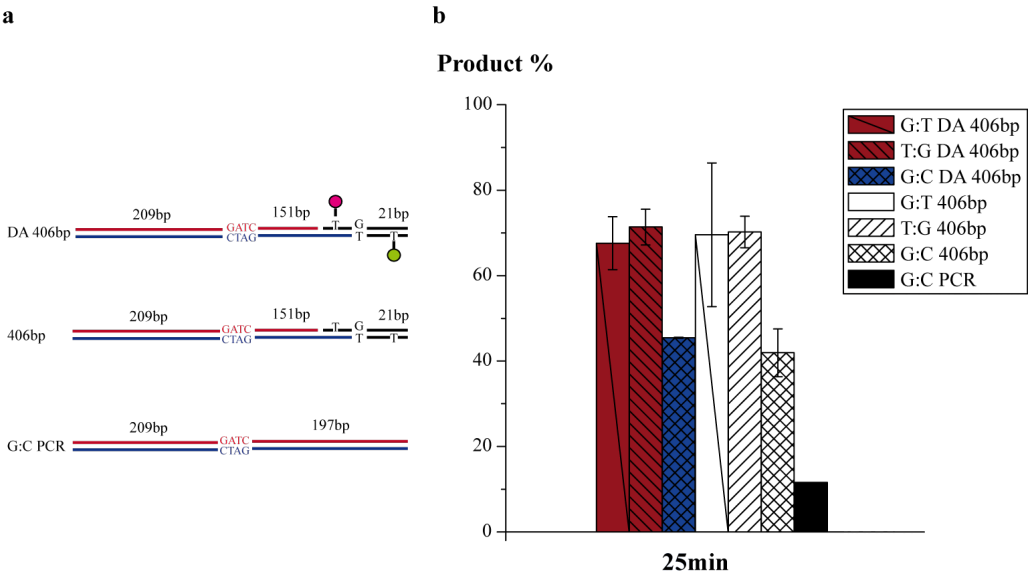

Fig. 3. 13: Mismatch-provoked MutH endonuclease activity of 406bp substrates, labeled and unlabeled. a) Schematic representation of the substrates. Unlabeled and double labeled 406bp G:T, T:G and G:C substrates were tested for MutH activation. b) 10nM DNA was incubated with MutS, MutL, MutH and ATP, samples were taken at 5' and 25' and the cleavage products (209bp and 197bp) were separated on a 6% PAAG and analyzed with TotalLab. The product percentage formed after 25min is plotted.

whereas T:G exhibits a very low FRET efficiency. Noteworthy, however, is that, comparing the G:C spectrum from Fig. 3. 10 and from Fig. 3. 14, the donor fluorescence is quenched in the short oligonucleotide but not in the long substrate. As the fluorophores are sensitive to their surroundings, this observation suggests that MutS, although without specifically bending, is binding oligonucleotide homoduplex DNA. This difference was no longer observed in the long homoduplex DNA because MutS has more binding sites.

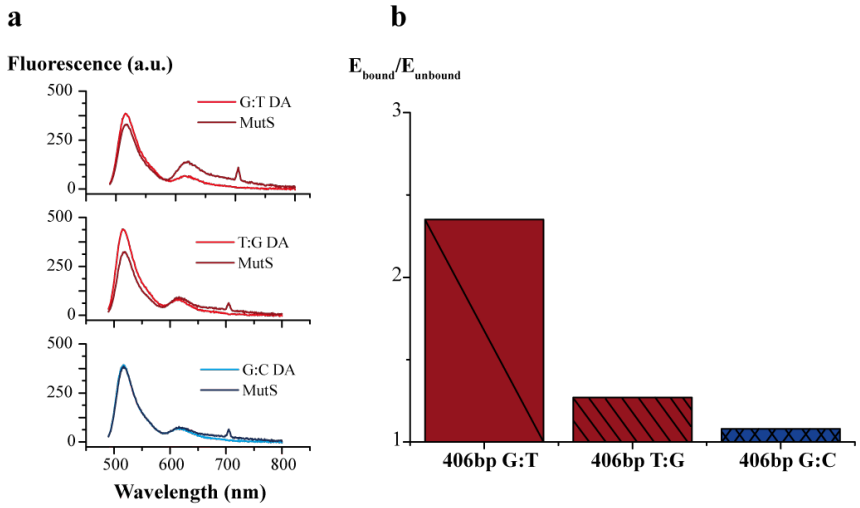

Fig. 3. 14: FRET efficiency change upon binding of MutS to 406bp G:T-DA, T:G-DA and G:C-DA in the absence of ADP. a) Emission spectra of 20nM double labeled 406bp DNA in the presence and absence of 400nM MutS. b) FRET efficiency change after addition of MutS. The $E_{bound}/E_{unbound}$ ratio is plotted for each substrates.

3.2.3 MutS has preferential binding modes for DNA mismatches

Molecular modeling of fluorophore and DNA. The fluorophores are sensitive to their surrounding: interacting with a nearby protein can quenched the emitted fluorescence or the constrict the rotational freedom of the dye. In both cases, the energy transfer efficiency could be affected. It was shown that the difference in the FRET efficiency of the G:T/MutS and T:G/MutS complexes is not related to the sequence context. However, it could be related to different

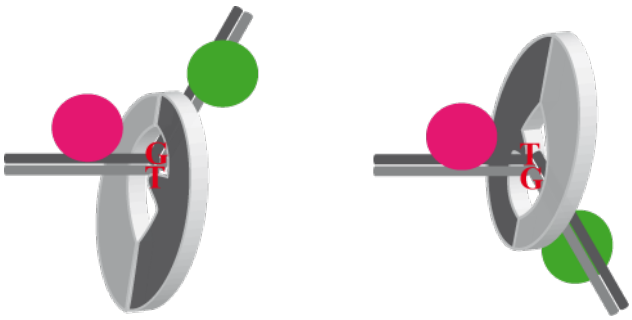

Fig. 3. 15: Proposed binding orientations of MutS on the G:T-DA and T:G-DA substrate. Note that the fluorophores introduce the asymmetry into the substrates. Without them, G:T would be equal to T:G.

contacts between protein and fluorophores. This would imply different orientations of the protein in relation to the mismatch and thus to the fluorophores in both complexes (Fig. 3. 15).

In order to get more information about the protein/fluorophore interactions, the fluorophores were modeled onto the appropriate position on the DNA, as described in Section 2.2.11. The

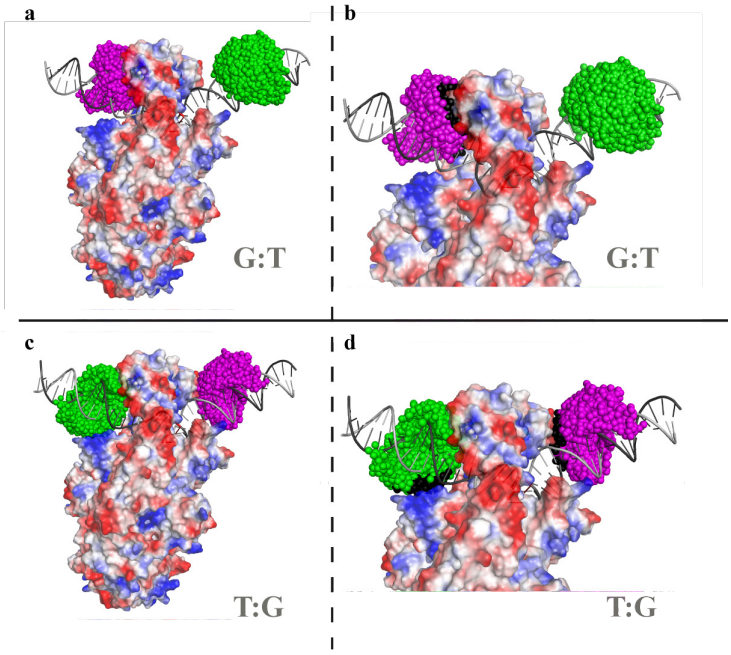

Fig. 3. 16: Modeled G:T and T:G 42bp kinked DNA structures with fluorophores, bound to MutS. MutS was depicted showing the surface electrostatic potential, according to the charge of the residues. Red represents the negatively charge residues and blue represents the positively charged residues. The clouds are constituted by 5193 possible positions. a) MutS bound to a 42bp kinked DNA with G:T mismatch. Alexa 488 was modeled onto position -14 on the T-strand (dark grey) and Alexa 594 was modeled onto position -12 on the G-strand (light grey). b) Detail of the interaction of MutS and Alexa 594. The black patch indicates the positions of the fluorophore cloud which are within 5Å of MutS, and represent a possible preferential orientation of the fluorophore. The center of mass for total Alexa 488 and Alexa 594 cloud was mapped to position 461. The center of mass for the black patch on was position 4505. c) MutS bound to a 42bp kinked DNA with T:G mismatch. Alexa 488 was modeled onto position -14 on the G-strand (dark grey) and Alexa 594 was modeled onto position -12 on the T-strand (light grey). d) The black patch indicates the positions of the fluorophore clouds (both Alexa 488 and Alexa 594) which are within 5Å of MutS, and represent a possible preferential orientation of the fluorophore. The center of mass for the total Alexa 488 and Alexa 594 cloud was mapped to position 461. The center of mass for the black patch on Alexa 488 was position 2085 and for Alexa 594 was position 3782.

clouds were designed taking into account the size of the linker with which they are attached to DNA and represent the rotational freedom of the fluorophore[37]. Both Alexa 488 and Alexa 594 were assumed to have the same linker length and, thus, comparable rotational freedom (Fig. 3. 16a, c and e). In order to assess the possible interactions with the bound MutS, the clouds were

analyzed for MutS-contacts. Linker-allowed fluorophore positions that fall in an area within 5Å of MutS were considered to make MutS/fluorophore interactions and marked with a black patch on the fluorophore cloud (Fig. 3. 16b, d and f). To determine the effect of a preferential population of these positions by the fluorophore, the theoretical distance between the center of mass of each fluorophore of either the total cloud or the patches was determined. To understand the effect of the charge of the residues n the surface of MutS, its electrostatic potential was determined (Pymol Molecular Graphics System (Delano Scientific, Palo Alto, CA, USA)). The calculated distances can be seen in Table 3. 4, Table 3. 5).

After the molecular modeling analysis, the influence of MutS on the fluorophores can be interpreted as follows: when MutS is bound to G:T-DA, Alexa 594 interacts with the protein whereas Alexa 488 does not (Fig. 3. 16b). From the 5193 possible fluorophore positions in the cloud, 1172 (22%) are within 5Å distance of MutS.

Since Alexa 594 is negatively charged it might be influenced by the positive residues from the internal part of the clamp. This could lead to a higher FRET efficiency and result in a calculated distance of 54Å (E_{FRET} of 0.48) instead of 59Å (E_{FRET} of 0.35), expected for a freely rotating fluorophore. The position at which Alexa 488 is attached to is at a large nough distance not to interact with MutS and its rotational freedom is unaffected. As mentioned previously, the expected efficiency for free DNA is lower than the experimental E_{FRET} and this was attributed to a high flexibility of the free DNA. When MutS binds to DNA, the theoretical and experimental FRET efficiency should be similar as the MutS binding and kinking decreases the flexibility of the DNA. In fact, the experimental E_{FRET} is in agreement with the theoretical E_{FRET} (0.37 vs. 0.35, respectively), for the case of unrestricted fluorophores. This observation suggests that the restriction of the rotational freedom of the acceptor does not largely influence the FRET

Table 3. 4: Theoretical distances between Alexa 488 and Alexa 594 in the unbent and kinked state of the G:T DNA, derived from the modeled structures.

		Alexa 488 (461)	Theoretical E_{FRET}	Exp. E_{FRET}
Kinked G:T	Alexa 594 (4505)	54	0.48	0.37
	Alexa 594 (461)	59	0.35	
Unkinked G:T	Alexa 594 (461)	78	0.09	0.17

The calculated distance corresponds to the distance between the center of mass with constricted (black patches) and unconstricted rotation (total cloud). Alexa 594 (4505) represents the center of the mass of the black patch and Alexa 594 (461) of the total cloud on this fluorophore. Alexa 488 (461) represents the center of the mass of the total cloud on this fluorophore. The theoretical FRET efficiency (E_{FRET}) was calculated from the theoretical distance (eq. 2.9), using a R_0 of 53.2Å. For the experimental E_{FRET} see E_{bound} in Table 3. 2.

efficiency.

When MutS is bound to T:G, both fluorophores seem likely to be affected byMutS and only the FRET efficiencies will be compared (as the calculation of distances requires freely rotating fluorophores). Both Alexa 488 and Alexa 594 are close enough to MutS to permit contacts, as the black patches imply. Alexa 488 has 5% of its cloud within the 5Å range and also in this case a patch of positively charged residues could influence the position of the fluorophore (in Fig. 3. 16d it can be seen that the black is closely in contact with a blue patch on the protein). Alexa 594 has less than 4% of its cloud in contact with MutS; in this case, however, the fluorophore/MutS interaction occurs with negatively charged residues and instead of attracting the fluorophore, the charge repulsion might push it away (Fig. 3. 16d). The theoretical distance was calculated considering that the fluorophore is unlikely to occupy the black patch and the center of mass used was that of the magenta cloud excluding the black patch. In the case of T:G, there are four possible scenarios: 1) the interaction of MutS with both fluorophores is negligible and the FRET efficiency between fluorophores in kinked DNA is 0.31; 2) Alexa 488 is affected by the negative residues in the vicinity but Alexa 594 is not; the expected FRET efficiency in this case would be 0.25; 3) Alexa 594 is affected by the neighboring positive residues and is pushed away by the positive residues but Alexa 488 is not; in this case the FRET efficiency would be 0.29; 4) both fluorophores are affected; the FRET efficiency between them is 0.23. Experimentally, the FRET efficiency between the fluorophores after binding of MutS to T:G is approximately 0.16 (Table 3. 2). This FRET efficiency is lower than the predicted efficiencies for all possible scenarios. However, the MutS-Alexa488 clashes could lead to a fluorophore quench by the protein, explaining the lower experimental FRET efficiency.

Table 3. 5: Theoretical distances between Alexa 488 and Alexa 594 in the unbent and kinked state of the T:G DNA, derived from the modeled structures.

		Alexa 488 (2085)	**Alexa 488 (461)**	**Theoretical E_{FRET}**	**Exp. E_{FRET}**
Kinked T:G	Alexa 594 (4337)	65	62	0.23/0.29	0.16
	Alexa 594 (461)	64	61	0.25/0.31	
Unkinked T:G	Alexa 594 (461)	–	79	0.09	0.13

The calculated distance corresponds to the distance between the determined center of mass with constricted (black patches) and unconstructed rotation (total cloud). Alexa 594 (4337) represents the center of the mass of the pink cloud, excluding the black patch and Alexa 594 (461) of the total cloud on this fluorophore. Alexa 488 (2085) represents the center of the mass of the black patch and Alexa 488 (461) of the total cloud on this fluorophore. The theoretical FRET efficiency (E_{FRET}) was calculated from the theoretical distance (eq. 2.9), using a R_0 of 53.2Å. For the experimental E_{FRET} see E_{bound} in Table 3. 2.

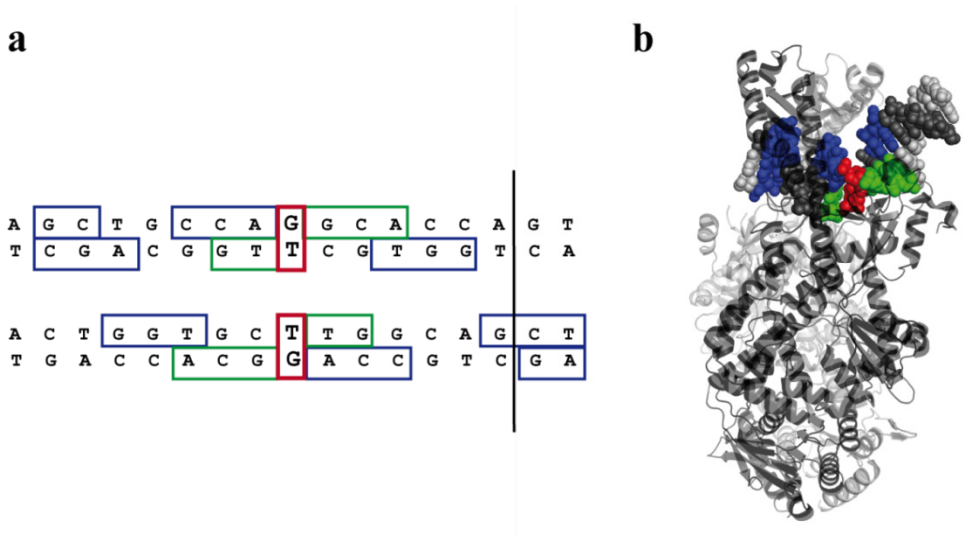

Fig. 3. 17: Crystal structure of MutS interacting with G:T DNA. a) DNA contact map derived from the co-crystal structures[2] for G:T and T:G (assuming the proposed binding orientation). The black line indicates where the 6bp-end substrate ends. The green boxes indicate specific contacts and blue boxes indicate unspecific protein-DNA contacts and the red box indicates the mismatch. b) Crystal structures of MutS and DNA, highlighting the specific and unspecific contacts as in a) MutS makes more interactions with the DNA on the right side than on the left. The mismatch can be seen in red, in blue are shown the unspecific and in green the specific interactions.

M*ismatch provoked MutH endonuclease activity*. The crystal structure of MutS and DNA shows that MutS interacts with up to 4bp on one side and up to 8bp on the other side of the mismatch (Fig. 3. 17).

Two substrates with different distances between the mismatch and the end of the substrate were designed. The substrates were used to test the ability of MutS in provoking MutH endonuclease activity (see Fig. 3.17a). The 390bp long substrates are designed so that, if MutS binds G:T only in one orientation, T:G mismatches 6bp to the end do not allow all contacts to DNA, whereas G:T mismatches 6bp to end do. This leads to an impaired or inhibited *in vitro* T:G-dependent MutH activation, while activation on short G:T substrate is unaffected. In contrast, both 406bp long substrates are bound by MutS.

The results show that both substrates, G:T 406 and G:T 390 can be cleaved with similar apparent rate constants k ($0.032\text{min}^{-1}\pm0.0014$ and $0.03\text{min}^{-1}\pm9\times10^{-4}$, respectively) (Fig. 3. 18b and c). Similarly, T:G 406 is cleaved with an apparent rate constant k of $0.027\text{min}^{-1}\pm0.008$. However, T:G 390 can only activate MutH with the efficiency of a homoduplex. This indicates that MutS has indeed a preferential binding orientation on a G:T mismatch and its prevention as consequences in the ability of *in vitro* mismatch-dependent MutH activation.

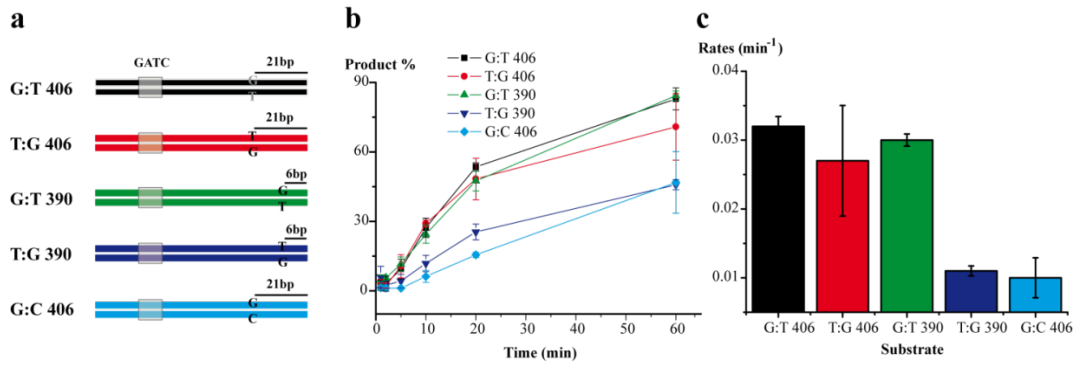

Fig. 3. 18: Mismatch provoked MutH endonuclease activity on different unlabeled substrates. a) scheme of the different substrates used in the assay. G:T/T:G/G:C 406 represents a 406bp long linear substrate where the distance from the mismatch to the end is 21bp. G:T/T:G 390 represents a 390bp long linear substrate, where the distance from the mismatch to the end of the DNA is 6bp. b) mismatched provoked MutH activation is less efficient with T:G 390 and G:C 406, with a similar pseudo first order cleavage rate *k* of approximately 0.01min^{-1}, 3x lower than for the G:T/T:G 406 and G:T 390 (c). The shaded box in a) represents the GATC site, recognized by MutH.

Distinct binding orientations measured by anisotropy. As was mentioned above, determining the association of a protein to a DNA oligonucleotide longer than 40bp by anisotropy change is too insensitive. However, if a long linker is used between the fluorophore and the DNA base, the motional constraint of the fluorophore is reduced and the anisotropy of the conjugated fluorophore is low. Despite this, the possible interaction between the fluorophore and a protein binding to DNA can reduce the rotational freedom of the fluorophore. This interaction in turn can lead to a reduced κ^2, which is an important factor in the transfer efficiency in FRET (see Section 2.2.12.iii. To test the influence of MutS binding to DNA on the free rotation of the fluorophores, anisotropy measurements were performed for both Alexa 488 and Alexa 594 with single labeled oligonucleotides.

Fig. 3. 19 compares the effect on the fluorophore anisotropy of MutS binding to G:T, G(14):T, T:G and G:C oligonucleotides. Fig. 3. 19a shows the titration of MutS with GA594:T and GA594:C. The anisotropy of the Alexa 594 in the G:T oligonucleotide is strongly dependent on the MutS concentration and fitting the data to Equation 2.26 yielded a K_D of 14nM for G:T-DA, comparable to data from the literature [54] and FRET-experiments (Fig. 3. 9). Contrary to Alexa 594, the anisotropy of Alexa 488 on G: oligonucleotides is hardly influenced by increased MutS concentrations (Fig. 3. 20b). From the model in Fig. 3. 16a and b, it was seen that when MutS binds to G:T, Alexa 594 will interact with the protein but not Alexa 488. This explains the increase in the acceptor anisotropy at low concentrations. An increase in the donor fluorophore anisotropy is seen at high MutS concentrations, possibly but the EMSA experiments showed that at high concentrations a second MutS can bind to the same substrate, possibly binding close to the donor. The affinity of MutS for homoduplex is too weak to determine a K_D value with anisotropy.

Nevertheless, the MutS concentration at which the anisotropy of the donor in G:T started to increase corresponds to the increase in anisotropy of both donor and acceptor in G:C, supporting the idea of homoduplex binding. Similar results were obtained with the double labeled DNA (GA594:TA488) (data not shown).

The effect on the anisotropy of MutS binding to GA594(14):T was also analyzed. In this substrate Alexa 594 is coupled to position -14 and not to position -12 (2bp further away from the mismatch than in the G:T substrate) (Fig. 3. 20c) and the anisotropy change is expected to be less pronounced. However, the anisotropy change is similar in both GA594:T and GA594(14):T substrates.

As the anisotropy change in the Alexa 594 of G:T is a good indication of MutS binding to the oligonucleotide, MutS affinity for DNA was also assessed in the presence of 1mM ADPnP and

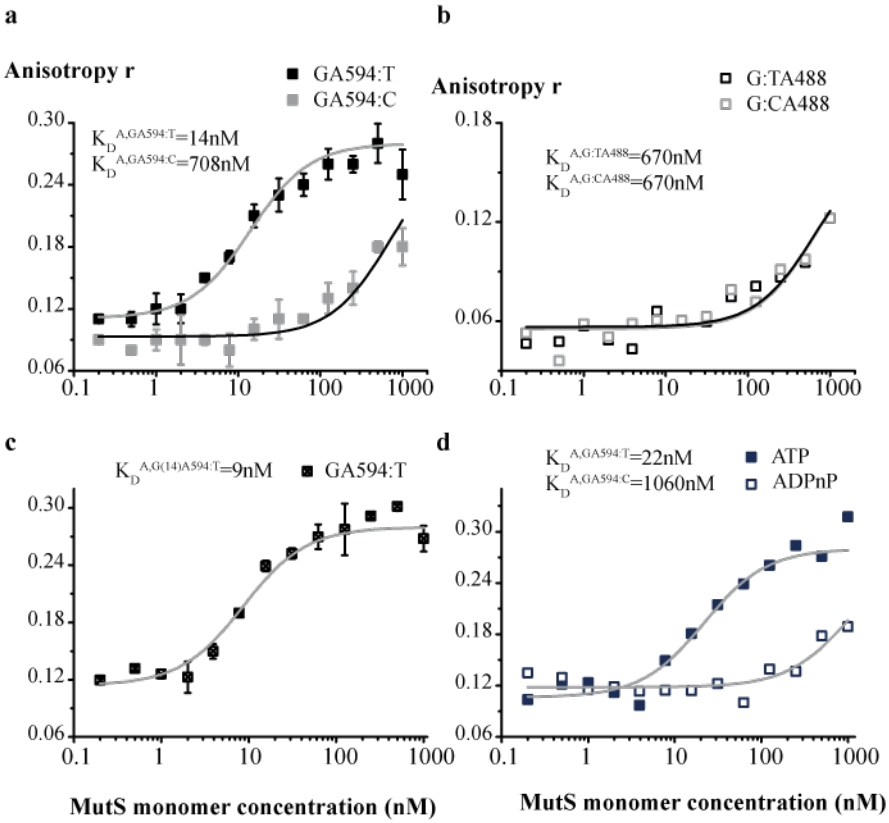

Fig. 3. 19: Anisotropy of MutS binding to single labeled 42bp oligonucleotide. a) Comparison of the anisotropy effect of MutS binding to a G:T (black squares) or G:C oligonucleotide (grey squares), where Alexa 594 is located 12bp away from the mismatch on the G-strand, in the presence of 1mM ADP. b) Comparison of the anisotropy effect of MutS binding to a G:T (black open squares) or G:C oligonucleotide (grey open squares), where Alexa 488 is located 14bp away from the mismatch on the G-strand, in the presence of 1mM ADP. c) Anisotropy effect of MutS binding to G:T oligonucleotide, where Alexa 594 is located 14bp away from the mismatch on the G-strand, in the presence of 1mM ADP. d) Comparison between MutS binding to a G:T oligonucleotide, with Alexa 594 12bp away from the mismatch on the G-strand, in the presence of 1mM ATP (closed squares) or 1mM ADPnP (open squares).

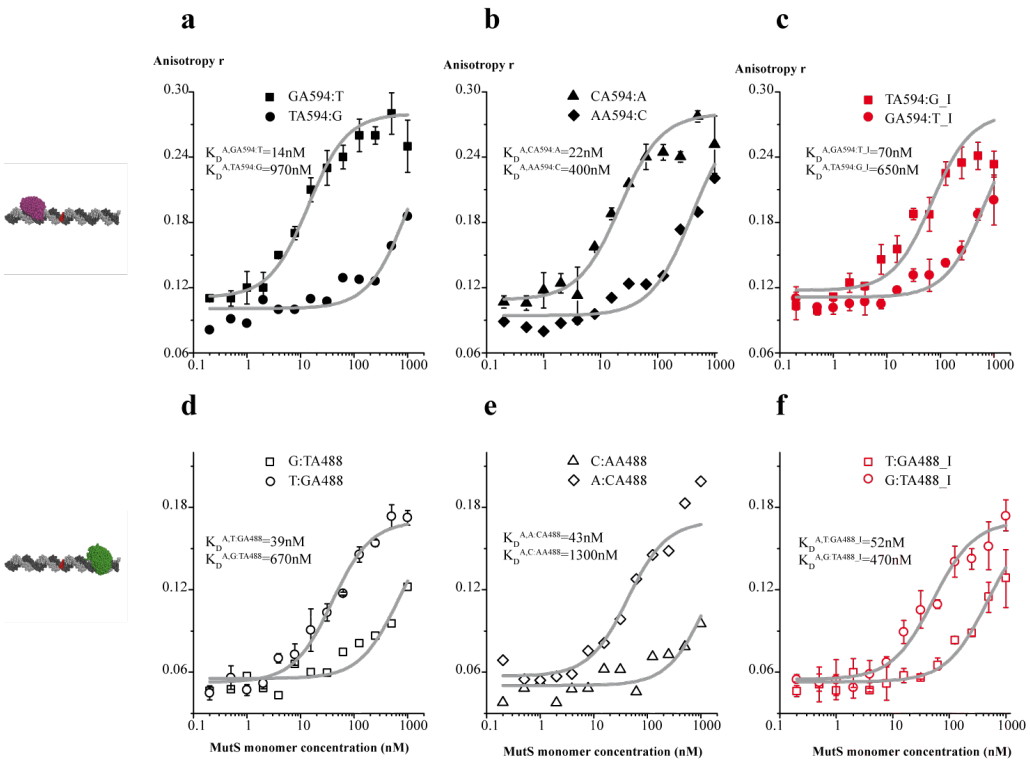

Fig. 3. 20: Anisotropy effects caused by MutS binding to Alexa 594 single labeled a) G:T and T:G; b) C:A and A:C; c) T:G-I and G:T-I; and Alexa 488 single-labeled oligonucleotides d) G:T and T:G; e) C:A and A:C; f) T:G-I and G:T-I. MutS was diluted from 1µM to 0.2nM in the presence of 10nM of 42bp oligonucleotides single-labeled either on the top strand (Alexa 594) or on the bottom strand (Alexa 488); the resulting anisotropy is plotted vs. MutS monomer concentration (nM). The curves were fitted sigmoidal logistic curve, with n=1.2 and the maximum of 0.28 for the Alexa 594 labeled oligonucleotides and 0.17 for the Alexa 488 labeled oligonucleotides (derived from the G:T binding curves).

ATP. The obtained K_D in the presence of ATP is of similar magnitude as the K_D determined in the presence of ADP (22nM instead of 14nM). In contrast, no saturation was reached in the presence of ADPnP and an anisotropy change is only observed at very high concentrations of MutS.

Next, the influence of MutS binding to GA594:T and TA594:G (Fig. 3. 20a) and to CA594:A and AA594:C (Fig. 3. 20b) was compared. From the analysis in Fig. 3. 15c and d, it was expected that if MutS binds to T:G with an inverted orientation in comparison to G:T, the rotational freedom of Alexa 488 is affected in the T:G/MutS complex but not in the G:T/MutS complex. The anisotropy results agree with the expected results. In addition, it is interesting to compare the influence of MutS on the Alexa 594 of G:T and C:A, as both substrates showed a high FRET increase in the DNA bending experiments. The Alexa 594 anisotropy of both oligonucleotides shows a strong dependence on the concentration of MutS and the obtained K_D are similar (14nM and 22nM, respectively). In contrast, the anisotropy of Alexa 488 is hardly influenced in either case (G:TA488 and C:AA488).. In addition, the results with T:G and A:C are the opposite: the influence of MutS on the Alexa 594 labeled T:G and A:C is negligible. In contrast, the anisotropy

change of Alexa 488 on T:GA488 and A:CA488 is significant and K_D-values of 39nM and 43nM, respectively, were obtained.

The same experiment was performed with T:G-I and G:T-I, both single labeled with Alexa 488 or Alexa 594 (Fig. 3. 20c and f). TA594:G-I shows a stronger effect on Alexa 594 than GA594:T-I (c). In contrast, G:TA488-I shows a stronger effect of increasing MutS concentration than T:GA488-I. Comparing the overall anisotropy results for these substrates with those of G:T and T:G indicates that G:T-I is similar to T:G and T:G-I to G:T, which confirms the results obtained in Fig. 3. 11. This experiments confirms the proposed preferential binding orientation of MutS. In addition, it extended the conclusions for C:A (equivalent to G:T) and A:C mismatches (equivalent to T:G).

Finally, it is interesting to note the difference in the initial values of anisotropy, depending on the fluorophore: Alexa 594 labeled oligonucleotides have an initial anisotropy of approximately 0.1 whereas Alexa 488 labeled oligonucleotides have an initial anisotropy value of approximately 0.05. This effect can be related to different Alexa488/DNA and Alexa594/DNA interactions, due to slightly different photophysical properties of the fluorophores.

Table 3. 6: Dissociation constants determined by anisotropy change of the Alexa 594 or Alexa 488.

	$K_D^{Alexa\ 594}$	$K_D^{Alexa\ 488}$
G:T	**14±2.3**	670±110
G(14):T	**8.6±1.5**	-
G:T DA	**6.4±2.3**	57±27
G:T ATP	**22±4.0**	-
G:T ADPnP	1060±240	-
G:C	708±111	670±120
T:G	971±162	**39±6**
C:A	**22±4**	1300±330
A:C	400±63	**43±9.0**
T:G-I	**70±14**	471±61
G:T-I	652±140	**52±7**

MutS-DNA FRET. In the previous section it was shown that MutS has a preferred binding orientation for a specific mismatch that could explain the low FRET efficiency of the T:G DA/MutS complex. Nevertheless, the low FRET efficiency can also be explained by the inability of MutS to bend T:G substrates. In order to determine the validity of this argument, protein-DNA FRET experiments were carried out with two different MutS variants, $MutS^{R449C/D835R}$ and $MutS^{D246C/R835R}$, labeled with Alexa 488 or Alexa 594, and three different DNA substrates, G:T, T:G and G:C, labeled with the either Alexa 594 or Alexa 488.

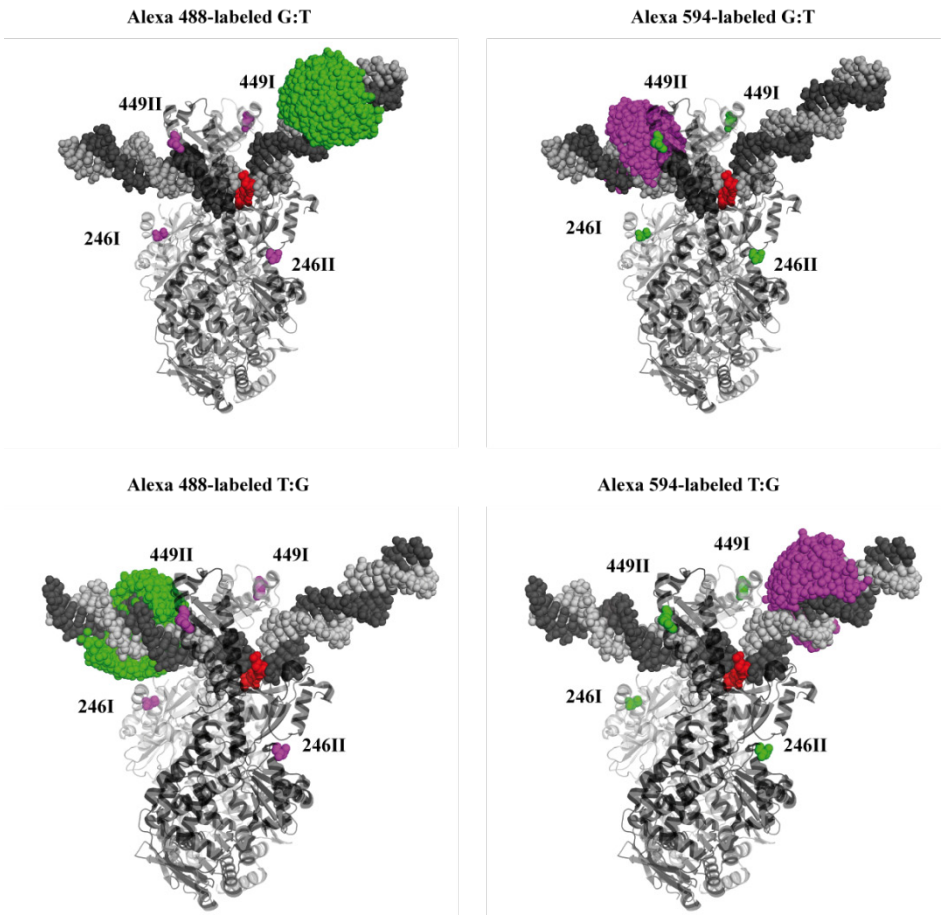

Fig. 3. 21: Scheme of the MutS-DNA FRET experiment. MutS monomer I is the non-mismatch binding monomer (light grey) and monomer II is the mismatch binding monomer (dark grey). 449 I or 246 I refer to the appropriate fluorophore position on monomer I and 449 II or 246 II refer to the fluorophore position on monomer II. The notation D refers to Alexa 488 (donor, green) labeled MutS or DNA, accordingly, and A refers to Alexa 594 (acceptor, magenta) labeled molecules.

In the first experiment, the binding of Alexa 594 labeled $MutS^{R449C/D835R}$ to Alexa 488 labeled G:T, T:G and G:C 42bp oligonucleotides was compared to the binding of $MutS^{D246C/D835R}$ to the same DNA substrates. The two MutS variants differ in the relative position of the cysteines to the DNA, so that different orientations can be distinguished. The expected FRET efficiencies for each MutS/substrate combination were calculated assuming 100% of labeling and binding (Fig. 3. 20 Table 3. 8). In the second experiment, the labels were switched: MutS is now labeled with Alexa 488 and the DNA are labeled with Alexa 594.

The fluorophore positions on the DNA are the same as described previously (Fig. 2. 15. As MutS is a dimer, two cysteines are available for modification and thus the expected FRET efficiency will be calculated from the shortest theoretical distance only.

Table 3. 7: Degree of labeling for the labeled MutS variants used in this assay.

	DOL Alexa 488	DOL Alexa 594
$MutS^{R449C/D835R}$	0.5	1
$MutS^{D246C/D835R}$	0.5	0.9

Table 3. 7 shows the labeling degrees obtained for each MutS variant. The DOL for Alexa 488-labeled MutS is only 50% whereas the DOL for Alexa 594 close to 100%.; The FRET efficiency calculations will take into account the different DOL but as the MutS variants contain two cysteines, the measured FRET efficiency will depend on which of the cysteines is labeled in case of DOL<100% (see below).

Due to the expected rotational restrictions (Fig. 3. 16), only the FRET efficiency between MutS and G:TA488 and TA594:G will be analyzed (as well as G:CA488 and GA594:C). The theoretical predictions for FRET efficiencies in every case are listed in Table 3. 8 and are again compared with the experimental results in Fig. 3. 22.

1. **MutS-A and G:T-D** (Fig. 3. 22a). Theoretically, it is expected that $MutS^{R449C/D835R}$-A will originate higher FRET efficiency with G:T-D than $MutS^{D246C/D835R}$-A. The experimental results show that this is the case, although the absolute values are lower than predicted.

2. **MutS-D and T:G-A** (Fig. 3. 22b). The expected FRET efficiency for the $MutS^{R449C/D835R}$-D in complex with T:G-A is higher than the expected FRET between $MutS^{D246C/D835R}$-D and T;G-A. The experimental results again agree qualitatively with the predictions. In addition, as was said before, the low FRET efficiency seen for the T:G-DA/MutS complex could be explained if MutS does not bend the T:G substrate. To account for this possibility, the expected FRET efficiency was determined for an unbent T:G/MutS complex. This was only done for the T:G-A/MutS-D complex because only one of the DNA ends is kinked by MutS (the acceptor arm in the case of T:G). The donor side does not suffer major conformational changes. If the T:G is not kinked upon MutS binding, the FRET efficiency between Alexa 594 on the DNA and Alexa 488 at position 246 in MutS is 2x higher than the FRET efficiency between Alexa 594 on the DNA and Alexa 488 at position 449 in MutS. The experimental results indicate that this is not the case as the contrary is verified. The FRET efficiency between T:G-A and $MutS^{R449C/D835R}$ is twice as high as the FRET efficiency between T:G-A and $MutS^{D246C/D835R}$. It is thus unlikely that MutS binds to T:G without kinking.

3. **MutS binding to homoduplex.** Another interesting point is that the FRET efficiency between labeled MutS and labeled G:C > 0, indicating MutS binding of homoduplex DNA. Furthermore, the FRET efficiency between $MutS^{D246C/D835R}$-D and G:C-A is higher than $MutS^{D246C/D835R}$-D in complex with TG-A. When MutS is binding to T:G-A, the acceptor arm is bent and the FRET with the donor-labeled 246 residues on MutS will decrease. In the case of a G:C bound MutS, the DNA would be unbent and the acceptor arm closer to the 246 residues,

Table 3. 8: Theoretical FRET efficiency between each position on the DNA and on the protein.

Alexa 594	Kinked E Alexa 488	Kinked E Alexa 488	Alexa 488	Kinked E Alexa 594	Kinked E Alexa 594	Unkinked E Alexa 594
	G:T D	T:G D		G:T A	T:G A	
$MutS^{R449C/D835R\ I}A$	0.9	–	$MutS^{R449C/D835R\ I}D$	–	1.0	0.6
$MutS^{R449C/D835R\ II}A$	0.6	–	$MutS^{R449C/D835R\ II}D$	–	0.6	0.4
$MutS^{D246C/D835R\ I}A$	0.09	–	$MutS^{D246C/D835R\ I}D$	–	0.2	0.1
$MutS^{D246C/D835R\ II}A$	0.5	–	$MutS^{D246C/D835R\ II}D$	–	0.5	0.95

The FRET efficiencies were derived from the theoretical distance (equation 2.9) between the center of mass of the fluorophore and the Cα of the residue, measured with Pymol.

leading to higher FRET efficiencies. The theoretical values for the G:C DNA cannot be predicted theoretically because there are several possible binding positions for MutS and not a specific one, as in the case of a mismatch. The measured efficiency with G:C is thus an average value of all the FRET efficiencies originated by unspecific MutS binding.

In general, the predicted FRET efficiency is higher than the experimental FRET efficiency. The expected values are based on the assumption of 100% DOL of the proteins and 100% binding. If MutS is not 100% labeled, it implies that there are single labeled molecules in solution and either cysteine can be coupled to the fluorophore. As the two cysteines are at different distances from the fluorophore on the DNA, the FRET efficiency will depend on which monomer

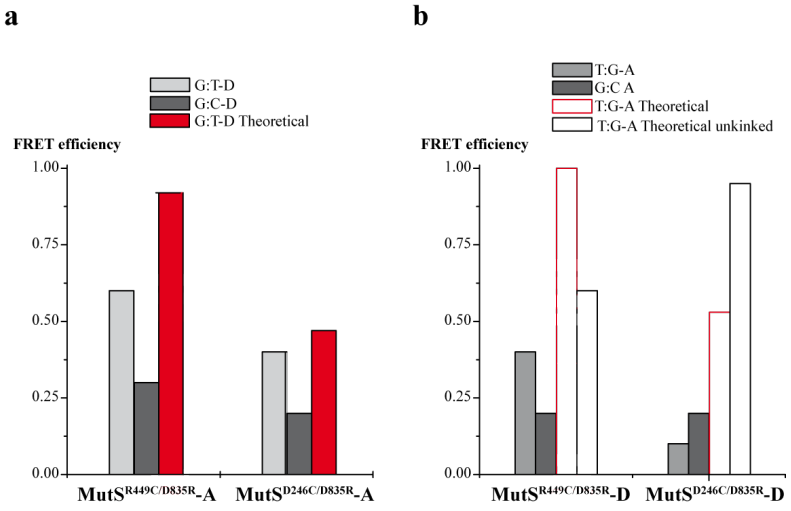

Fig. 3. 22: MutS-DNA FRET. a) measured FRET efficiency between Alexa 488-labeled MutS and Alexa 594-labeled DNA. b) measured FRET efficiency between Alexa 594-labeled MutS and Alexa 488-labeled DNA. The FRET efficiency was determined according to Section 2.2.12 and equation 2.19. The theoretical distance was measured between position 449 or 246 on MutS and position -12 on the bottom strand of G:T, T:G and G:C or position -14 on the top strand of G:T, T:G and G:C (see Table 3. 8).

is labeled (see Table 3. 7 and Table 3. 8). In addition, the discrepancy between theoretical and experimental values can also be related to different affinities of MutS for G:T and T:G. The anisotropy measurements showed that the K_D for G:T is 14nM and for T:G is 39nM.

3.2.4 G:T and T:G have different populations in single-molecule Multiparameter Fluorescence Detection (smMFD)

In order to get more insight into the binding mode of MutS to various DNA mismatches, the binding of MutS to G:T-DA, T:G-DA, G:G-DA and G:C-DA oligonucleotides was analyzed with smMFD (Section 2.2.15). The bursts of freely diffusing complexes were arranged in a histogram according to FRET efficiency (E_{FRET}) and the donor lifetime in the presence of acceptor ($\tau_{D(A)}$). Fig. 3. 23 shows the 2D frequency histogram of E_{FRET} vs. $\tau_{D(A)}$ obtained for all measurements, after a burst selection was performed (see Appendix, Fig. A. 1). Panels A, B and C show the measurements of G:T, G:G and T:G alone: all three substrates show similar FRET populations, with an average donor lifetime of 3.5ns and a donor anisotropy close to 0, indicating the rotational freedom of the donor. Although the lifetime of free Alexa 488 is approximately 4ns, the lifetime of a fluorophore bound to DNA and in the presence of an acceptor fluorophore will decrease the lifetime. Specially in the case of G:G and T:G (panels A and C), a population of donor-only can be observed, with a low FRET efficiency and a lifetime of approximately 4ns, possibly corresponding to free donor or to donor-only oligonucleotide. As this population does not change after the addition of protein, it was considered background and not further analyzed.

The binding of MutS to the different substrates (panels D, E and F) originate different FRET populations (as was seen in the bulk measurements). The G:G/MutS complex (D) shows a very broad population, at higher FRET efficiencies, the G:T/MutS complex (E) shows a smaller population at high FRET efficiencies and the T:G/MutS complex (F) shows only a broad populations at low FRET efficiencies. In addition, the donor lifetime decreases for all three substrates and the anisotropy increases. Here it is important to note that the anisotropy change is not identical for all three substrates. G:T shows only a small anisotropy increase and it is accompanied by a decrease in the donor lifetime, characteristic for FRET. To make this more clear, the anisotropy was fitted to a Perrin equation with a rotational correlation time (ρ) of 1ns and the center of G:T/MutS population moves along the line corresponding to the fit. In contrast, G:G and T:G show a population in which the anisotropy is increased without a change in the donor lifetime, suggesting that this change is FRET-independent and thus could represent a protein-fluorophore interaction.

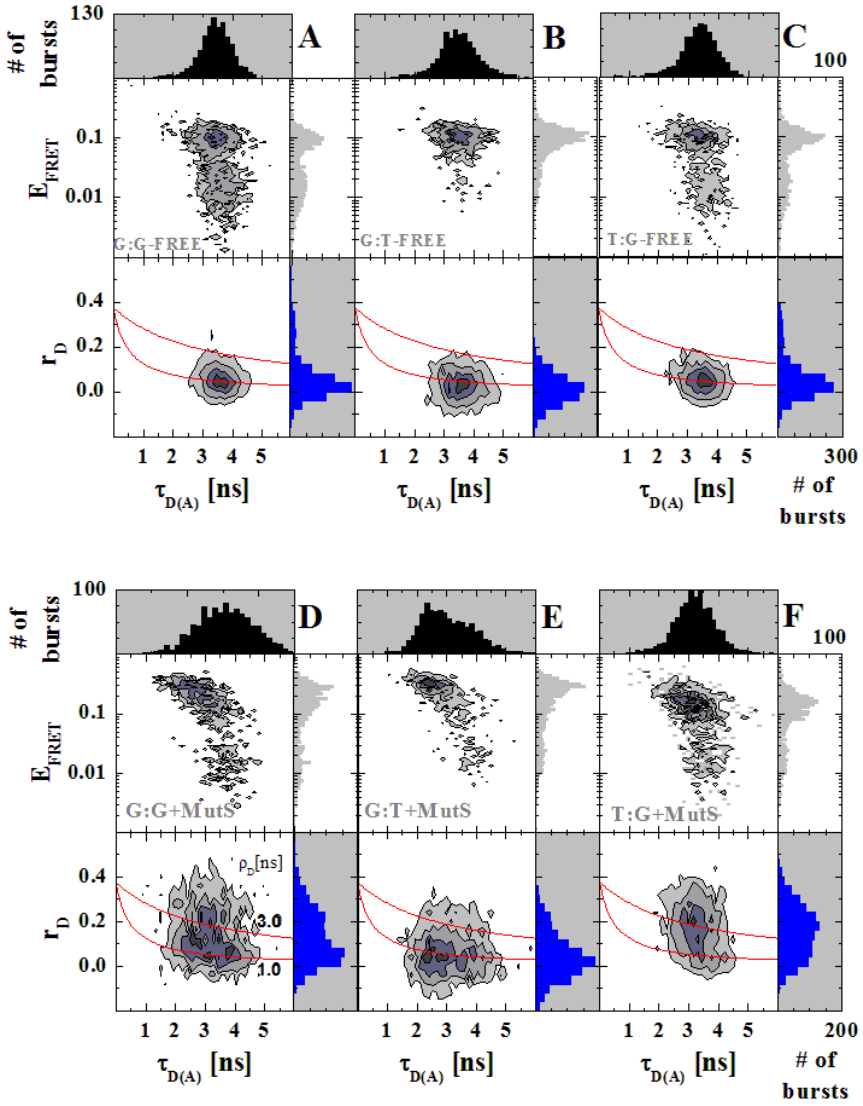

Fig. 3. 23: Two-dimensional frequency histogram of the smMFD measurements of MutS bound to double labeled G:T, G:G or T:G, where frequency increases from white to black (normalized to a total of 1000 bursts). FRET efficiency (E_{FRET}) and donor anisotropy (r_D) is plotted vs. $\tau_{D(A)}$ (donor lifetime in the presence of acceptor). Direct excitation of the acceptor is negligible. FRET efficiency is determined from green and red signals after background correction, detections efficiencies and crosstalk[4] (see section 2.2.12.v.). The donor quantum yield was determined to be 0.65 and 0.85 in the absence of MutS. The red curve computed Perrin equation $r = r_0/(1 + \tau/\rho)$, using fundamental anisotropy r_0 of 0.37 and a rotational correlation time ρ of 3ns (top) and of 1ns (bottom). The data treatment was done by Evangelos Sisamakis. Data analysis was done in close collaboration with Evangelos Sisamakis, Dr. Paul Rothwell and Prof. Claus Seidel (University of Düsseldorf).

A population is present in G:G/MutS and T:G/MutS that cannot be fitted to the Perrin equation with a ρ of 1ns but only with a ρ of 3ns, indication of the rotational constraint of the donor. These results are thus in agreement with the bulk anisotropy measurements for G:T , T:G (Fig. 3. 19) and G:G (data not shown).

To quantitatively analyze the FRET populations a Probability Distribution Analysis (PDA) was performed on the information obtained from each burst. Prior to PDA additional burst selection criteria were applied in order to reduce the donor-only population and to exclude bursts for which photobleaching has occurred (see Appendix). Fig. 3. 24 shows the results from the PDA on the data from Fig. 3. 23, and the populations obtained for each measurement are plotted, in terms of number of events vs. distance in Å. Comparing all the DNA alone measurements (right side) can be seen that all mismatches show similar distance between the fluorophores when in the unbound state. A highly populated low FRET species is distinguished in all DNA free samples at approximately 76Å, corresponding to the unbent DNA (in agreement with the predicted value, Table 3. 4). In addition, a minor populated FRET species can be distinguished at shorter distances, possibly corresponding to a preferential conformation of the mismatched DNA. When MutS is added to each substrate, the heterogeneity between the different mismatches already seen in the bulk measurements is also observed in the single molecule measurements.

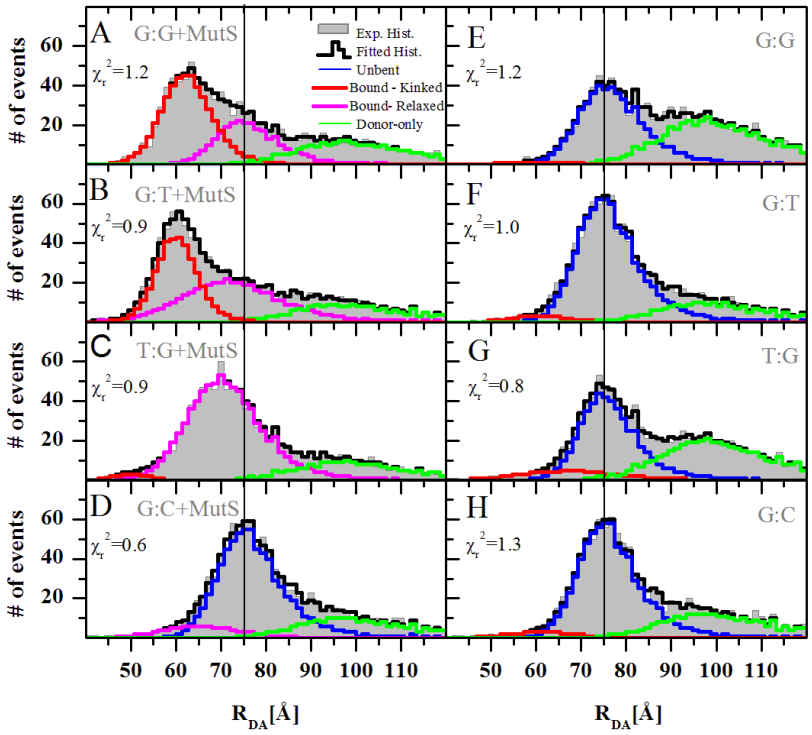

Fig. 3. 24: Probability distribution analysis of the data obtained from the single molecule measurements. The R_{DA} is plotted vs. number of events and for each fit the corresponding chi-square value is presented. The R_0 used in the distance calculation was 53.2Å and a κ^2 of 2/3 was assumed. Each panel shows the experimental histogram, the fitted histogram, the unbent population, the bound-kinked population, the bound-relaxed population and the donor-only population for bound and unbound G:G, G:T, T:G and G:C. The black line indicates the position of the unbent DNA. The theoretical DA distance in the unbent DNA is 78Å and in the kinked DNA is 59Å. The data treatment was done by Evangelos Sisamakis. Data analysis was done in close collaboration with Evangelos Sisamakis, Dr. Paul Rothwell and Prof. Claus Seidel (University of Düsseldorf).

The addition of MutS to G:T (panel B) induces a shift of the low FRET population seen in the free G:T measurement to higher FRET efficiencies and can now be seen at 59.7Å, with a narrow half-width, indicative of a specific complex (the expected distance was 59Å, Table 3. 4). This population is attributed to the sharply kinked DNA in complex with MutS and is thus termed "bound-kinked". A second population is observed at lower FRET efficiencies, at a distance of 70Å and has a very broad width. This suggests that the high FRET population is a specific G:T/MutS complex, whereas the low FRET population is a more unspecific complex (hence the term "bound-relaxed"). Both FRET species are similarly populated (see Table 3. 9). The G:G+MutS measurement (A) shows that the very broad population seen in the 2D histograms are in fact 2 populations, one centered at approximately 63Å (with a relative amplitude of 63%), like the "bound-kinked" population in G:T+MutS and one centered at 77Å ("bound-relaxed"), with a narrow width and a relative amplitude of 37%. Both populations seem to correspond to specific G:G/MutS complexes. The T:G+MutS measurement (C), shows that the "kinked-bound" population is not present but that the bound relaxed population is present at 71Å, with a relative amplitude of 97%. Although a second population can be observed in T:G+MutS, it has an amplitude of only 2.7Å and is thus not considered any further. The "bound-relaxed" population present in G:T, G:G and T:G is slightly shifted from substrate to substrate. However, the error estimation for each measurement reveals that all three are within the error and thus correspond to the same population (see Fig. 3. 24).

Table 3. 9: Statistical analysis of the populations from Fig. 3. 23.

	Gaussian 1				**Gaussian 2**				**Fixed Ratio at 110 [Å]**	
	R_{mean} [Å]	**HW [Å]**	**A [%]**	**Rel. A [%]**	**R_{mean} [Å]**	**HW [Å]**	**A [%]**	**Rel. A [%]**	**A [%]**	**X_r^2**
FREE G:G	77.7	5.0	39.8	97.0	61.3	7.3	1.2	3.0	59.0	1.2
G:G + MutS	76.8	4.7	23.8	37.2	63.1	4.6	40.2	62.8	36.0	1.2
FREE G:T	76.6	4.4	66.6	95.2	61.6	5.5	3.3	4.8	30.1	1.0
G:T + MutS	73.7	10.5	38.1	53.8	60.8	3.3	32.8	46.2	29.1	0.9
FREE T:G	76.8	3.9	38.4	83.6	68.8	10.6	7.5	16.4	54.0	0.8
T:G + MutS	71.7	7.1	68.9	97.3	50.8	2.7	1.9	2.7	29.2	0.9
FREE G:C	76.9	4.4	60.1	94.3	62.6	8.0	3.7	5.7	36.2	1.3
G:C + MutS	77.4	4.6	60.6	87.7	66.4	8.0	8.7	12.3	30.9	0.6

R_{mean} corresponds to the average distance between the fluorophores and HW to the half width of the distribution. A refers to the amplitude of the given population, in relation to all the populations, rel. A. refers to the relative amplitude of the population in relation only to the FRET populations. Fixed ratio at 110Å refers to the donor-only population, considered fixed at 110Å.

Addition of MutS to homoduplex (G:C) showed no significant change of the FRET species: the unbent species is highly populated as before but the diffusion coefficients indicate that the DNA is bound (data not shown). A small "bound-relaxed" population (12.3%) forms nevertheless after the addition of MutS. These results confirm the bulk measurements, in which homoduplex DNA exhibited no significant bending, but did exhibit binding by MutS.

In all measurements, a population corresponding to a donor-only species can be seen at very low FRET efficiencies, despite the burst selection. The origin of the donor-only population is unclear, as the oligonucleotide was annealed with the acceptor strand in excess, specifically to minimize the donor-only population. The low DNA concentration used in the single molecule measurements (10 to 15pM) in addition with the sample heating by the laser might contribute to some instability of the duplex, which is only 42bp long, leading to the melting of the duplex. Another source of donor-only DNA is the incomplete labeling of the acceptor strand, leading to duplex with only the donor fluorophore. However, as the donor-population does not significantly change with the addition of protein, it is considered a fixed ratio and a large distance of 110Å is attributed to this population.

Single molecule MFD measurements showed that different FRET species are present when MutS binds to mismatched oligonucleotides. With G:T, a high FRET population (specific complex) and a low FRET population (unspecific complex) are present, with no observed constrains of the donor anisotropy. When bound to T:G, MutS induces only a low FRET population and the donor anisotropy is constrained. This observation confirms the existence of a preferred binding mode. The addition of MutS to G:G induces the formation of two FRET

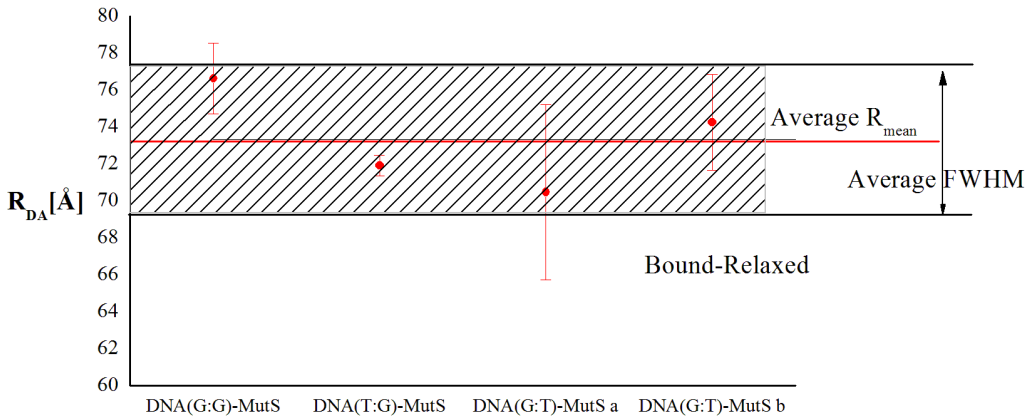

Fig. 3. 25: Statistical analysis of the "bound-relaxed" population seen with G:T+MutS, G:G+MutS and T:G+MutS. The points correspond to distance (R_{mean}) resulting from each individual fit and its associated error estimation. The red line denotes the average of R_{mean} and the grey area the average FWHM (Full Width at Half-Maximum) calculated from all the fits. Since all points lie within the shaded area it is justified to claim that these population represent the same state. The data treatment was done by Evangelos Sisamakis. Data analysis was done in close collaboration with Evangelos Sisamakis, Dr. Paul Rothwell and Prof. Claus Seidel (University of Düsseldorf).

populations, one with high FRET, as G:T and one with low FRET, as T:G, suggesting that there is not a preferred binding mode with G:G, but that both are allowed. The donor anisotropy of G:G is also affected by the addition of MutS.

In summary, it was shown in this section that MutS specifically binds and kinks heteroduplex DNA at the mismatch site. MutS has lower affinity for homoduplex DNA and bending or kinking of the homoduplex DNA was not observed (neither in single molecule nor in bulk measurements). In addition, the data suggests that MutS has two binding orientations for the same mismatch ("G:T-binding mode" and "T:G-binding mode"), identified by lower FRET efficiency of the T:G/MutS complex and confirmed by the FRET populations observed in smMFD. The low FRET efficiency of T:G/MutS is due to different photophysical properties of the fluorophores and not to unbent DNA. The binding orientations are independent of the sequence context surrounding the mismatch. In addition, the different binding orientations can be distinguished by strategically placing the fluorophores so that their anisotropy is affected when MutS is bound in one orientation but not in the other. Since it was shown that the donor fluorophore in the G:T substrate is freely rotating even in the presence of MutS, the subsequent experiments were carried out only with G:T.

3.3 Nucleotide influence on DNA binding and bending by MutS

The ATPase cycle of MutS is known to be extremely important in the fine tuning of mismatch recognition and discrimination, and in the formation of the sliding clamp that activates MutL and initiates the repair mechanism[25]. Although thoroughly investigated, the ATPase cycle is yet not fully understood, specially what concerns the function of both ATPase domains. In order to shed more light into the kinetics of DNA/MutS association and dissociation, in the presence and absence of nucleotides, stopped flow measurements were preformed with the double labeled G:T

Table 3. 10: Kinetic parameters determined from the MutS/DNA association in the presence of 1mM ADP.

[S] (nM)	A_1±%E	k_{obs1} (s^{-1})±%E	A_2±%E	k_{obs2} (s^{-1})±%E
600	2.7±5.2	15.0±10.7	0.1±25.9	1.2±19.0
500	2.4±4.7	12.5±11.7	0.1±8.5	1.2±19.3
400	2.3±9.7	10.2±18.2	0.1±13.3	0.9±32.0
300	2.1±6.3	7.8±16.6	0.1±27.1	0.8±42.9
200	1.9±0.2	5.5±22.7	0.1±28.5	0.6±35.4
100	1.4±0.1	3.0±18.7	0.3±22.2	0.7±24.4
50	0.9±0.11	2.1±3.5	0.2±18.8	0.4±13.3

A_1 corresponds to the amplitudes of the fast association rate k_{obs1} and A_2 corresponds to the amplitudes of the slow association rate k_{obs2}. [S] is the concentration of MutS. E corresponds to the error percentage.

oligonucleotide used in the previous section. In addition, smMFD measurements were also performed to better understand the dynamics of the kinked G:T/MutS complex in the presence of ADP, ATP and ADPnP.

3.3.1 DNA/MutS association is fast and biphasic

The developed FRET-binding assay can be used to follow the MutS/DNA association by stopped-flow with fluorescence detection to extract kinetic information about the binding step. The substrate used was a double labeled 42bp G:T oligonucleotide and the FRET signal was

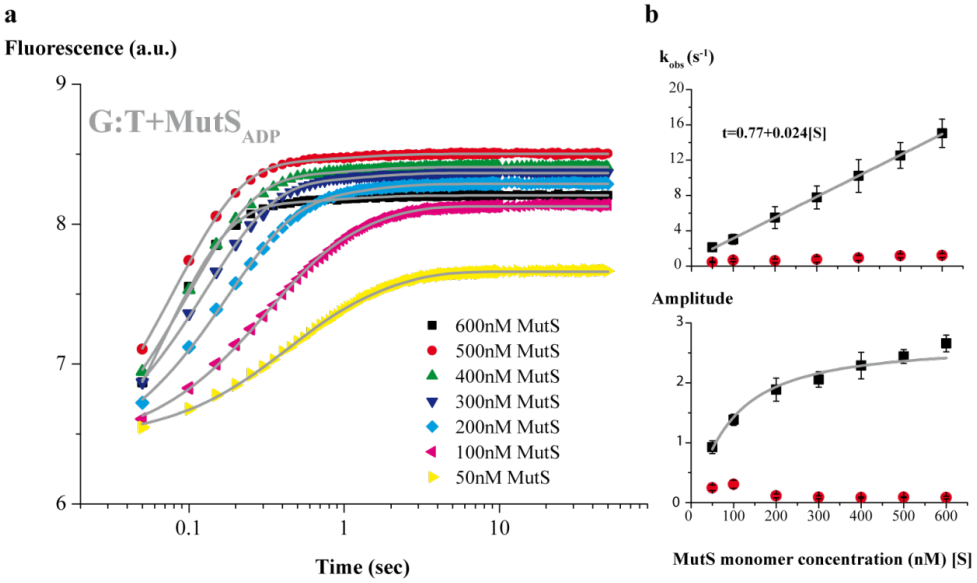

Fig. 3. 26: Stopped-flow measurement of MutS binding to double-labeled G:T oligonucleotide in the presence of 1mM ADP. The MutS monomer concentration was increased from 50 to 600nM, as indicated, while the DNA concentration was kept constant at 15nM. MutS was pre-incubated with ADP. a) The acceptor fluorescence is plotted vs. time in seconds. The data was fitted to a double exponential (grey line). b) The observed rates (top) and amplitudes (bottom) resulting from the fitting to a double exponential are plotted vs. MutS monomer concentration. The fitting revealed one concentration dependent (black squares) and one concentration independent (red circles) rate. The amplitudes are fitted with a sigmoidal logistic curve (Equation 2.26) and the rates with a linear regression.

monitored over time.

Fig. 3. 26 shows the association kinetics of G:T-DA and different concentrations of MutS in the presence of 1mM ADP. Two rates can be derived from the data (Table 3. 10). The fastest rate increases with increasing concentrations suggesting a second-order reaction, i.e. MutS binding to DNA. An association rate K_{on} of 24$\mu M^{-1}s^{-1}$ is obtained for the G:T/MutS$_{ADP}$ complex. The slowest rate is concentration independent, suggesting a first-order reaction, like a conformational change in the complex (MutS+DNA⇌MutS/DNA⇌MutS/DNA*). The average rate k_{obs2} for this process is 0.8s^{-1} and the average amplitude A_2 is 0.1 (Table 3. 10 and Fig. 3. 32, steps 1 to 3).

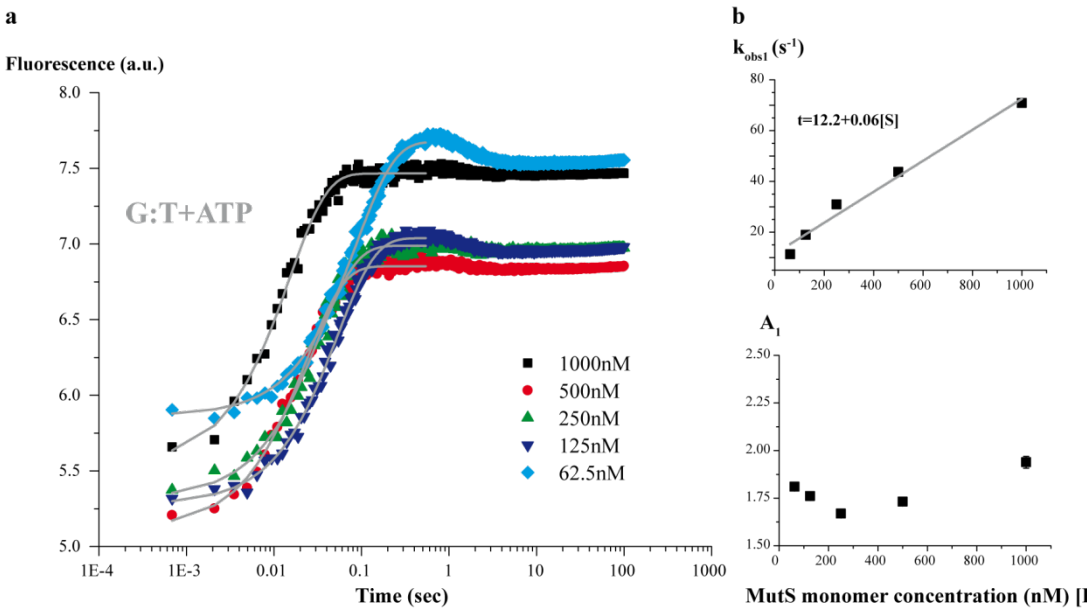

Fig. 3. 28: Stopped-flow measurement of MutS binding to double-labeled G:T oligonucleotide in the presence of 1mM ATP. The MutS monomer concentration was increased from 62.5 to 1000nM, as indicated, while the DNA concentration was kept constant at 15nM. MutS was pre-incubated with ATP. a) The acceptor fluorescence is plotted vs. time in seconds. The data was fitted to a single exponential (grey line), between the time range of 0.7msec and 0.54s. b) The observed rates (top) and amplitudes (bottom) resulting from the fitting to a double exponential are plotted vs. MutS monomer concentration. kobs1 resulting from the association curves were fitted to a linear regression with a slope of 0.06.

Since the MutS/DNA association seems to be accompanied by a large amplitude, it is possible that the binding and the bending events are not discernable. If the binding event is slow in comparison to the bending step, the later will appear to be a second order reaction due to the concentration dependence of the first step. The kinetic data is summarized in Fig. 3. 32.

Fig. 3. 28 shows the association of MutS and G:T DA in the presence of 1mM ATP. Since MutS hydrolyzes ATP to ADP, MutS will be present as a mixture of $MutS_{ATP}$ and $MutS_{ADP}$ (see Fig. 3. 27). Two phases are clearly distinguished in the association curves and the second phase is

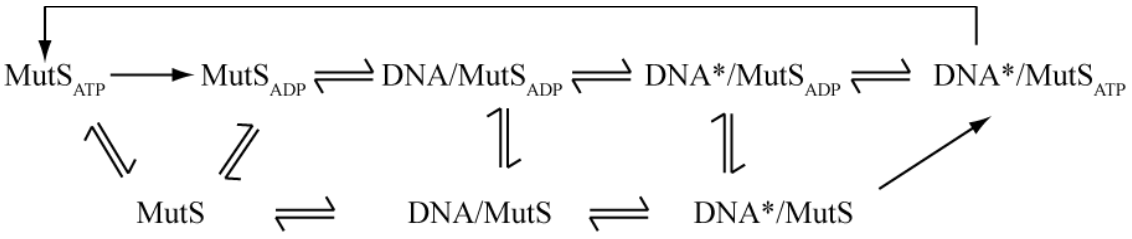

Fig. 3. 27: Nucleotide states for MutS in the presence of ATP and DNA. $MutS_{Free}$ (MutS) can bind ADP or ATP and form $MutS_{ADP}$ or $MutS_{ATP}$. $MutS_{ATP}$ can hydrolyze to $MutS_{ADP}$ and bind DNA at the mismatch site ($DNA/MutS_{ADP}$). $DNA/MutS_{ADP}$ suffers a conformational change, still bound to the mismatch and ADP/ATP exchange occurs. $DNA^*/MutS_{ATP}$ can then dissociate into $MutS_{ATP}$+DNA, with hydrolysis occurring during or after dissociation. DNA/MutS binds ADP and forms $DNA/MutS_{ADP}$ and possibly the same is true for DNA*/MutS.

most prominent at lower MutS concentrations. Also in the presence of ATP, k_{obs1} increases linearly with increasing MutS concentration, indicating that the binding occurs via a second-order rate process. An association rate K_{on} of 60µM^{-1}s^{-1} was determined for the G:T/MutS$_{ATP/ADP}$ complex. k_{obs2} is 10 to 20x slower that k_{obs1}, suggesting that MutS adopts a different conformation after the first DNA binding event (Fig. 3. 29 and Table 3. 11).

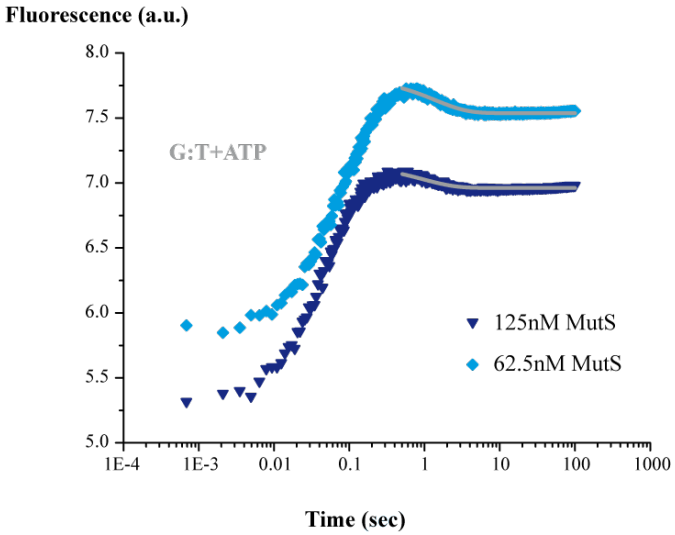

Fig. 3. 29: Fitting of the second phase, distinguished at 125 (dark blue) and 62.5nM (light blue) MutS. The data was fitted with a single exponential (grey line), between the time range of 0.5 and 100 seconds.

Table 3. 11: Kinetic parameters determined from the MutS/DNA association in the presence of 1mM ATP.

[S] nM	A_1±%E	k_{obs1} (s^{-1})±%E	A_2±%E	k_{obs2} (s^{-1})±%E
1000	1.9±1.22	67.4±0.0004	n.d.	n.d.
500	1.7±0.92	43.6±0.0008	n.d.	n.d.
250	1.7±1.21	30.9±0.0023	n.d.	n.d.
125	1.8±0.61	18.9±0.0035	-0.2±4.8	1.1±4.2
62.5	1.8±0.52	11.3±0.0100	-0.3±1.9	0.8±4.4

A_1 corresponds to the amplitudes of the fast association rate k_{obs1} and A_2 corresponds to the amplitudes of the slow association rate k_{obs2}. [S] is the concentration of MutS. E corresponds to the error percentage.

The MutS$_{ADP}$ and MutS$_{ATP}$ association curves were performed with different protein batches and comparing the same measurement performed with the different batches (500nM MutS$_{ADP}$+15nM G:T) indicated that the second batch is approximately 2x more active than the first (data not shown). Although this aspect rather difficults the analysis, it appears nevertheless that the association of MutS in the presence of ATP (meaning ATP/ADP equilibrium) is faster than the association in the presence of ADP (see Fig. 3. 32, step 6).

Fig. 3. 30 shows the association of MutS to homoduplex G:C in the absence of nucleotide and to G:T in the presence of ADPnP. Although the addition of MutS to G:C did not show a change in the FRET signal in steady state measurements, the pre-steady state results show a slow association (k_{obs} of 0.26s^{-1}) with a very small amplitude of 0.04 (Table 3. 12). This rate does not

seem to be present in the G:T/MutS association: at 500nM MutS, the k_{obs1} is 12.5s^{-1} and k_{obs2} is 1.2s^{-1}. Most likely, this rate and amplitude are too small to be detected in the G:T/MutS association and corresponds to MutS binding to unspecific DNA. In the presence of ADPnP, the G:T/MutS association is inhibited, with no significant change in the FRET signal. Possibly, MutS adopts a rigid closed conformation in the $MutS_{ADPnP}$ state, which is no longer able to bind DNA (as seen with the anisotropy data in Fig. 3. 19 and in the smMFD experiments in Fig. 3. 23). This aspect will be further addressed below.

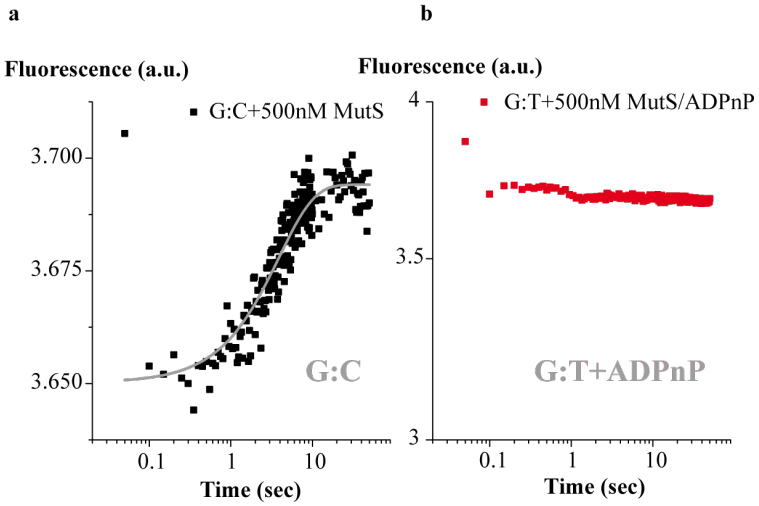

Fig. 3. 30: Stopped-flow measurement of 500nM MutS binding to double-labeled G:C oligonucleotide (a) and to double-labeled G:T in the presence of 1mM ADPnP. The DNA concentration was 15nM. The MutS/G:C DA association curve was fitted to a single exponential.

Table 3. 12: Kinetic parameters determined for the association of MutS to G:C DA and of MutS incubated with 1mM ADPnP to G:T DA.

s1	s2	A_1±%E	k_{obs1} (s^{-1})±%E
15nM G:C	500nM MutS	0.04±3.1	0.26±6.81
15nM G:T	500nM MutS+1mM ADPnP	n.d.	n.d.

Syringe 1 and 2 are indicated by s1 and s2, respectively. E corresponds to the error percentage.

The influence of nucleotide (ADP, ATP or ADPnP) on the dissociation kinetics of G:T/MutS was analyzed next (Table 3. 13). To prevent re-association of MutS and DNA, the different complexes were chased with competitor DNA, which shared the same sequence as the labeled DNA but without fluorophores. The results are shown in Fig. 3. 31 and summarized in Fig. 3. 32. The dissociation of MutS from G:T is faster when MutS is pre-incubated with 1mM ATP (a). Also in this case, an ATP/ADP equilibrium needs to be considered. The dissociation rate of the G:T/MutS complex is 1.9s^{-1} when chased with ATP and competitor DNA (steps 4 to 6 in Fig. 3. 32). MutS was pre-incubated with G:T DNA prior to mixing step, thus existing in the DNA*/MutS or in the DNA*/$MutS_{ADP}$ form (at the mismatch). The addition of ATP allows the

exchange of ADP for ATP and the dissociation in the sliding clamp form (step 4 to 5 in Fig. 3. 32).

When the G:T/MutS complex pre-incubated with ATP was chased with competitor alone, the dissociation rate is only $0.3s^{-1}$. Since MutS was pre-incubated with ATP and DNA prior to the addition of competitor, the complex present in solution is G:T/$MutS_{ATP/ADP}$. Comparing this

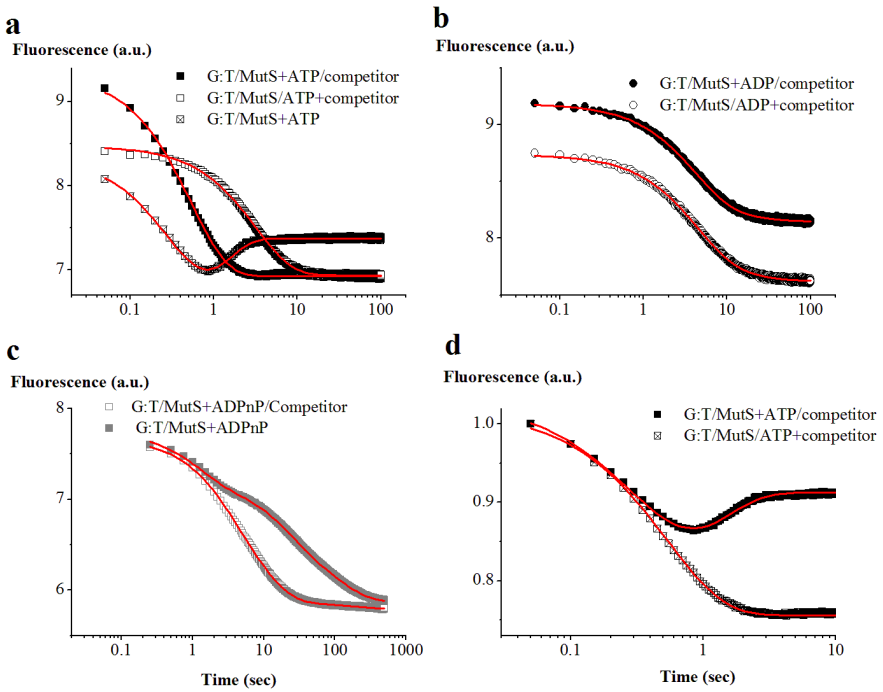

Fig. 3. 31: Stopped flow measurement of the dissociation of MutS from the double labeled G:T DNA. a) The effect of ATP on the dissociation of MutS from G:T was tested by 1) competing for MutS binding with a mixture of 1mM ATP and 100x excess of competitor (closed squares); fitted with a single-exponential; 2) pre-forming the complex in the presence of 1mM ATP and competing for MutS binding by adding 100x excess of competitor (open squares); fitted with a single-exponential; 3) and adding 1mM ATP to the pre-formed complex (open circles); fitted with 2 exponentials. c) The effect of ADPnP on the dissociation of MutS from the DNA was analyzed by pre-incubating the complex in the absence of ADPnP and competing for MutS binding with 1mM ADPnP (close squares) or with a mixture of 1mM ADPnP and 100x excess of competitor. the curves were fitted to a triple-exponential. d) The effect of ADP on the dissociation was analyzed by pre-incubating the complex in the absence of ADP and by adding 100x excess of competitor with 1mM ADP (closed circles) or by pre-incubating the complex in the presence of 1mM ADP and adding 100x excess of competitor. The curves were fitted to a double-exponential. d) Detail of the initial decay for G:T/MutS+ATP/competitor and G:T/MutS+ATP. The curves were normalized to the maximum of each curve

experiment with the chase of the G:T/$MutS_{ADP}$ complex with competitor (b), the rates are comparable, suggesting that the MutS state dissociating in G:T/$MutS_{ATP/ADP}$ is mostly ADP-bound (6 to 5 in Fig. 3. 32). Furthermore, comparing the amplitudes in both ATP experiments, addition of ATP and competitor to the G:T/MutS complex causes a larger change in amplitude than the addition of competitor to the G:T/$MutS_{ATP/ADP}$ complex, although the end value is the same. This

suggests that the fast dissociation of $MutS_{ATP}$ from DNA slightly shifts the G:T+MutS ⇌ G:T/MutS equilibrium in the direction of unbound MutS or unbent DNA. Pre-incubation of G:T/MutS with ATP thus causes a partial dissociation of MutS from the DNA and the addition of competitor captures the unbound MutS proteins. When MutS is in the ATP-free form, the mentioned equilibrium is shifted in the direction of bound MutS and the amplitude change is larger.

The addition of ATP to MutS bound to G:T is more complex, as can be seen by the resulting curve. Two phases can be clearly distinguished, first a dissociation phase, with a k_{obs1} of $2.4s^{-1}$, followed by an association phase, fitted with 1 exponential and a k_{obs2} of $1.4s^{-1}$. The initial dissociation corresponds to the dissociation step seen when G:T/MutS is chased with ATP and competitor (compared Fig. 3. 31a and d). The immediate re-association of MutS after the first dissociation partly masks the first dissociation event, which has a smaller amplitude. The association phase indicates that there is a second binding event after the dissociation of the $G:T/MutS_{ATP/ADP}$ complex (4 to 6 in Fig. 3. 32). The association constant determined for this event is approximately 10x slower than the association constants determined above for the $G:T/MutS_{ATP}$ complex, suggesting that this is yet another MutS conformation. This step might correspond to the second binding event mentioned in the $G:T/MutS_{ATP}$ experiments.

The dissociation of the G:T/MutS complex was determined in the presence of ADPnP with or without competitor (c). ADPnP is a non-hydrolysable analog of ATP and MutS is thought to adopt the $MutS_{ATP}$ conformation when bound to ADPnP; these experiments were performed to better understand the kinetics of the ATP experiments. However, the dissociation of MutS from the G:T substrate when chased with ADPnP or ADPnP and competitor is more complex than the ATP experiments. Both dissociation curves were fitted with three exponentials but the dissociation of MutS in the presence of ADPnP and competitor was faster than the dissociation of

Table 3. 13: Dissociation rates of MutS from G:T in the presence of different nucleotides, with or without competitor (C).

s1	s2	A_1±%E	k_{obs1} (s^{-1})± %E	A_2±%E	k_{obs2} (s^{-1})± %E	A_3±%E	k_{obs3} (s^{-1})± %E
G:T/MutS	ATP/C	2.4±0.4	**1.9**±0.5	–	–	–	–
G:T/MutS/ ATP	C	1.5±0.2	**0.3**±0.2	–	–	–	–
G:T/MutS	ATP	3.5±9.2	**2.4**±3.4	-2.5±12.9	1.4±3.4	–	–
G:T/MutS	ADPnP	0.6±0.8	**0.9**±1.3	0.7±0.3	0.05±0.6	0.7±0.3	0.01±0.3
G:T/MutS	ADPnP/C	0.7±1.5	**0.4**±1.6	1.1±1.1	0.10±0.7	0.08±0.8	0.01±1.8
G:T/MutS	ADP/C	0.9±0.6	**0.2**±0.8	0.1±4.5	0.05±4	–	–
G:T/MutS/ ADP	C	1±0.7	**0.2**±0.8	0.2±3.7	0.06±2.8	–	–

Syringe 1 and 2 are indicated by s1 and s2, respectively. %E corresponds to the error percentage.

MutS in the presence of ADPnP alone. This suggests that after an initial dissociation event, $MutS_{ADPnP}$ can still rebind DNA. However, the G:T/$MutS_{ADPnP}$ association experiment showed that $MutS_{ADPnP}$ does not bind DNA (Fig. 3. 30). It is possible though, that the high affinity ATPase site of MutS is still occupied by ADP not lost during purification[25]. For ADPnP to bind both ATPase sites, an ADP-ADPnP exchange step needs to occur suggesting that when MutS has only one of the ATPase domains occupied with ADPnP it can still bind DNA until the second ATPase site is also occupied with ADPnP. This event would not be detected when competitor is present in solution because unbound MutS will bind to the unlabeled DNA, as is indeed the case. The k_{off} determined in the presence of ADPnP and competitor is nevertheless 10x slower than in the presence of ATP and competitor, suggesting that there is a difference between $MutS_{ATP}$ and $MutS_{ADPnP}$ complexes. In addition, one of the k_{off} rates obtained in the presence of ADPnP and competitor is similar to the fastest k_{off} rate determined in the presence of ADP. The fact that MutS cannot hydrolyze ADPnP seems to confer a conformation to $MutS_{ADPnP}$ that is similar to $MutS_{ADP}$ when bound to DNA.

The stopped flow data can be summarized in the following scheme:

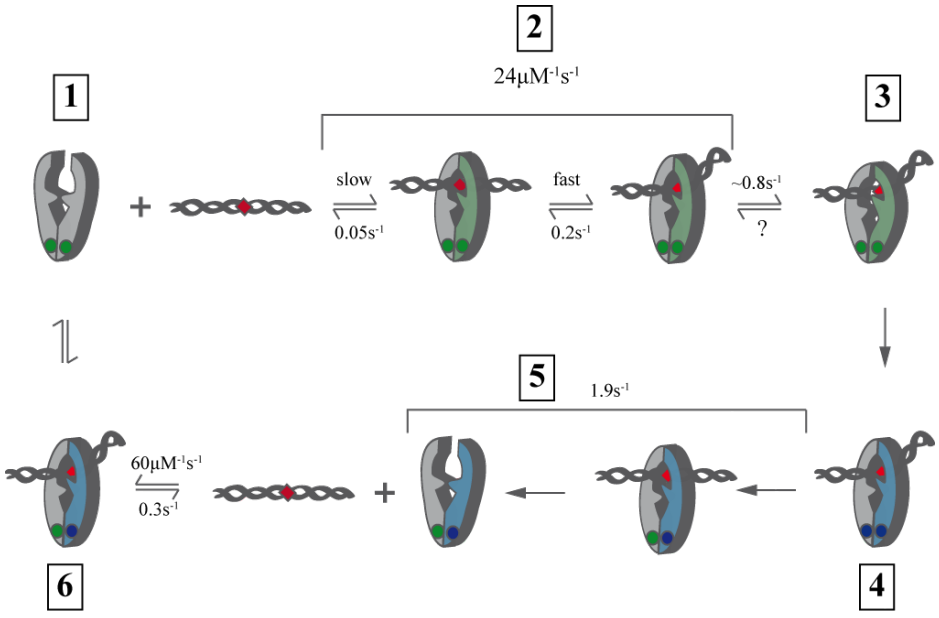

Fig. 3. 32: Scheme for the data obtained from the stopped flow measurements of DNA/MutS association and dissociation in the presence of different nucleotides. The circles indicate the ATPase sites, one in each monomer and the red square represents the mismatch. Green indicates the binding of ADP and the mismatch-binding monomer is colored in green. Blue indicates the binding of ATP and the mismatch binding monomer is colored in blue. The rates given for different phases were obtained from the stopped flow measurements.

The association of DNA and MutS in the presence of ADP correspond to steps 1 to 3. MutS binds to DNA, finds the mismatch, bends the DNA at the mismatch site (1 and 2) and finally induces the specific kink (3). The k_{off} in the presence of ADP is biphasic, indicating a two step dissociation. In the presence of ATP, ADP/ATP exchange occurs, stimulated by the presence of DNA, and MutS turns into a sliding clamp. The dissociation is fast and occurs in one phase. As

the DNA used in the stopped flow experiments was short and had open ends, MutS slides off the DNA with concomitant ATP hydrolysis (5) and rebinds DNA (6). The k_{off} in the presence of ATP is 10x faster than in the presence of ADP, suggesting a different MutS conformation. In the presence of ADPnP, hydrolysis is inhibited and the second binding step was not observed, indicating that $MutS_{ATP/ATP}$ cannot bind DNA.

3.3.2 The DNA-kinked population is modulated by nucleotide

The binding of MutS to the double labeled 42bp oligonucleotides and the influence of nucleotide on the bound and bent/kinked populations was analyzed with smMFD.

Fig. 3. 33 shows the PDA corresponding to nucleotide measurements, after a burst selection

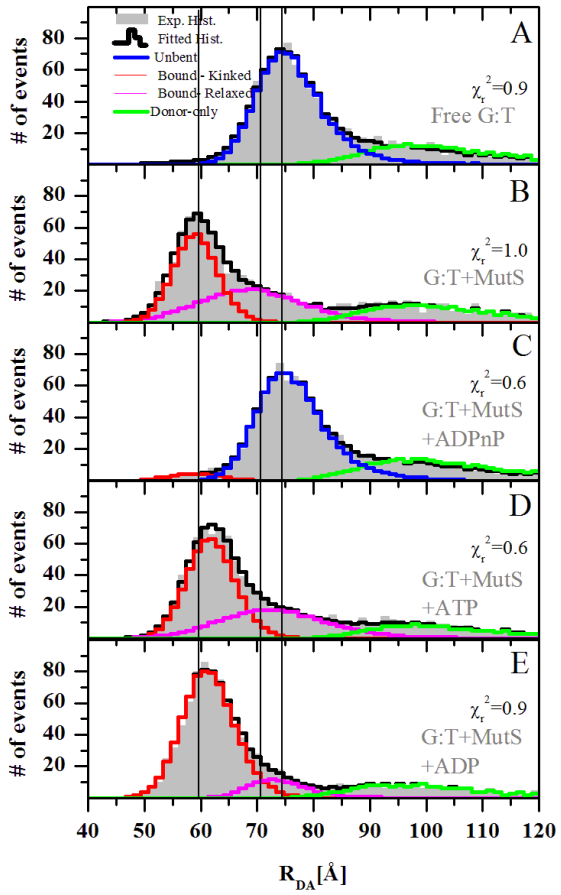

Fig. 3. 33: Probability distribution analysis of the data obtained from the single molecule measurements. The R_{DA} is plotted vs. number of events and for each fit the corresponding chi-square value is presented. The R_0 used in the distance calculation was 53.2Å. Each panel shows the experimental histogram, the fitted histogram, the unbent population, the bound-kinked population, the bound-relaxed population and the donor-only (fixed ratio) population for unbound G:T and bound G:T in the absence of nucleotide or in the presence of ADP, ATP or ADPnP. Data analysis was done in close collaboration with Evangelos Sisamakis, Dr. Paul Rothwell and Prof. Claus Seidel (University of Düsseldorf).

was performed (see Appendix, Fig. A. 1). The number of events vs. the distance (Å) is now plotted. The G:T and G:T+MutS measurements were analyzed previously. The addition of ADPnP causes a shift in the G:T populations: the high (red) and low (pink) FRET populations are shifted to the position of unbent DNA. The diffusion time of the low FRET population indicates that the DNA is free (Fig. 3. 34), meaning that the binding of ADPnP to MutS inhibits the re-association of MutS. The addition of ADP and ATP to G:T/MutS led to a decrease in the pink population ("bound-relaxed" DNA) and a slight increase of the kinked population. This indicates that MutS exists in a more structured form when bound to nucleotide, avoiding unspecific complexes. As the measuring time is approximately 1h30minutes, ATP has been hydrolyzed by

Table 3. 14: Statistical analysis of the populations from Fig. 3. 30.

	Gaussian 1				Gaussian 2				Fixed Ratio at 110 [Å]	
	R_{mean} [Å]	HW [Å]	A [%]	Rel. A [%]	R_{mean} [Å]	HW [Å]	A [%]	Rel. A [%]	A [%]	X_r^2
FREE DNA (G:T)	76.4	3.9	67.8	94.7	65.1	7.9	3.8	5.3	28.3	0.9
G:T+MutS	69.9	9.0	32.3	47.2	59.7	3.0	36.1	52.8	31.6	1.0
G:T+MutS+ ADPnP	76.6	3.9	66.8	95.3	59.6	4.2	3.3	4.7	29.9	0.6
G:T+MutS+ ATP	73.8	9.2	30.3	39.7	62.5	3.6	46.1	60.3	23.6	0.6
G:T+MutS+ ADP	74.3	4.8	10.5	14.2	62.0	3.5	63.3	85.8	26.2	0.9

R_{mean} corresponds to the average distance between the fluorophores and HW to the half width of the distribution. A refers to the amplitude of the given population, in relation to all the populations, rel. A. refers to the relative amplitude of the population in relation only to the FRET populations. Fixed ratio at 110Å refers to the donor-only population, considered fixed at 110Å. Data analysis was done in close collaboration with Evangelos Sisamakis, Dr. Paul Rothwell and Prof. Claus Seidel (University of Düsseldorf).

MutS and the form present is $MutS_{ADP/ATP}$ (or $MutS_{ADP}$). The diffusion times indicate that in the presence of ADP and ADPnP all populations correspond to bound DNA (Fig. 3. 34).

The statistical analysis of the PDA is summarized in Table 3. 14. The free DNA (G:T) was fitted with two Gaussians: one at 76.4Å, with a narrow width of 3.9Å, and one at 65.1Å, with a very broad width of 7.9Å. The low FRET population is highly populated (94.7% relative amplitude) and corresponds to the unbent DNA, whereas the higher FRET is poorly populated (only 5.3% of relative amplitude) and might correspond to a preferential conformation of the mismatched DNA. The high FRET population in the G:T/MutS complex ("bound-kinked") has a maximum at 59.7Å, with a half-width of 3Å. The low FRET population ("bound-relaxed") is located at 70Å and has a broad half-width of 9Å. This suggests that the high FRET population is a

specific G:T/MutS complex, whereas the low FRET population is a more unspecific complex (hence the term "bound-relaxed"). Confirming this idea, the measurements in which ATP and ADP were added showed a lower relative amplitude of the unspecific complex (39.7% and 14.2%, for ATP and ADP respectively, vs. 47.2% for no nucleotide). In addition, the presence of ADP seems to favor even more the specific G:T/MutS complex, where both the low and high FRET populations showed a narrow width. The "bound-relaxed" population present with ATP was centered at 74.3Å and could possibly belong to the unbent yet bound DNA (Fig. 3. 33). The width of the population was very broad, suggesting that it is an unspecific complex. The analysis of different time windows (1 to 3ms) indicate that the bent population is static in the mentioned time range (not shown). Furthermore, the analysis of the macroscopic time (total measuring time, 1h to 1h30min) also does not indicate a dynamic bent population. Nevertheless, a conformational change of DNA from kinked to unbent cannot be excluded, as the stopped-flow measurements showed that it was at least biphasic. However, the time windows available in the smMFD measurements are not suitable to observe the dynamics that are occurring in the upper msec/sec range. The addition of ADPnP to G:T/MutS results in the low FRET population seen with free DNA (at 76.6Å with a half-width of 3.9Å), and also in this case no dynamics could be detected. This result is in agreement with the stopped flow measurements, which showed that the G:T/$MutS_{ADPnP}$ complex dissociates within 500 seconds and MutS+ADPnP did not result in the formation of any significant amount of complexes with high FRET.

The average donor-only population corresponds to approximately 28% of the total populations present. Again, it is considered as a fixed ratio, as it does not change significantly in amplitude and in distance within the different measurements.

The comparison of the diffusion time of each population clearly indicates that both the unbound and the donor-only population are indeed unbound in the absence of protein and in the presence of ADPnP (Fig. 3. 34). In general, the diffusion time of free DNA is approximately 1.5ms, while the DNA/MutS complex exhibits an average diffusion time of 2.3ms.

In this section, the effect of nucleotide on the DNA binding and bending by MutS was analyzed. The stopped flow results showed that the association of $MutS_{ADP}$ and DNA occur in a two step process, in which one step is bimolecular (MutS and DNA association) and one is unimolecular (DNA conformational change). The equilibrium is shifted in the direction of kinked DNA, indicated by the high FRET population observed for the G:T/$MutS_{ADP}$ complex in smMFD. The association of $MutS_{ATP}$ and DNA is also biphasic, although in this case the second step possibly corresponds to a slow binding phase. The G:T/$MutS_{ATP}$ complex seems to be more dynamic, indicated by the faster K_{on} and k_{off} determined with the stopped flow measurements and also by the presence of a "bound-relaxed" population in smMFD. When MutS is bound to a mismatch, ADP is rapidly exchanged by ATP and $MutS_{ATP}$ dissociates rapidly (sliding clamp). In

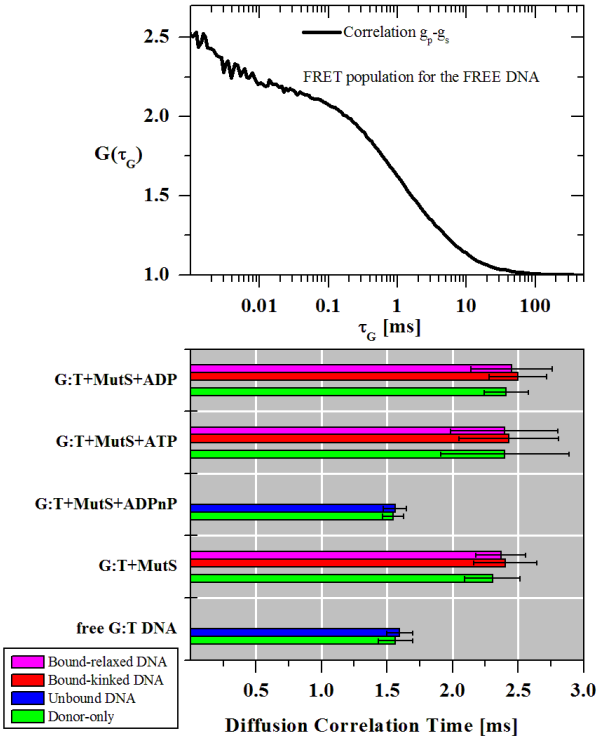

Fig. 3. 34: Fluorescence correlation spectroscopy results derived from the single molecule measurements. a) Fluorescence autocorrelation function for the free DNA population. b) Comparison of the correlation diffusion times diffusion obtained from the FCS analysis for bound-relaxed DNA, bound-kinked DNA, free DNA and no FRET population.

the absence of competitor, $MutS_{ATP}$ is hydrolyzed to $MutS_{ADP}$ and a second binding event is observed. Both stopped flow and single molecule data indicates that $MutS_{ADPnP}$ cannot bind DNA.

3.4 Communication between ATPase and clamp domain of MutS monitored by FRET

As introduced in the previous section, the ATPase activity of MutS is very important in the correct identification of mismatches. The binding and hydrolysis of the nucleotide comes with large conformational changes that spread across the protein and control the state of the clamp that encircles DNA. These conformational changes have been predicted but little experimental data is available. In the next section, FRET will be used to monitor these conformational changes in solution and to analyze the effect of nucleotide and DNA on the conformation of MutS.

3.4.1 MutS$^{R449C/D835R}$ is a stable dimer in solution in the presence of nucleotide

The dimer-tetramer equilibrium of MutS was analyzed by analytical ultracentrifugation with fluorescence detection. Tetramer and dimer-forming MutS MutS^{R449C} and MutS$^{R449C/D835R}$ labeled with Alexa 488 were subjected to sedimentation velocity runs.

The sedimentation coefficient distribution of MutS$^{R449C/D835R}$ is shown in Fig. 3. 35a. The sedimentation distribution shows a clean preparation, with minor impurities at low Svedberg values. The sedimentation distribution does not show a concentration dependent sedimentation coefficient. At the concentrations tested, the sedimentation coefficient is around 8.1 or 8.2S,

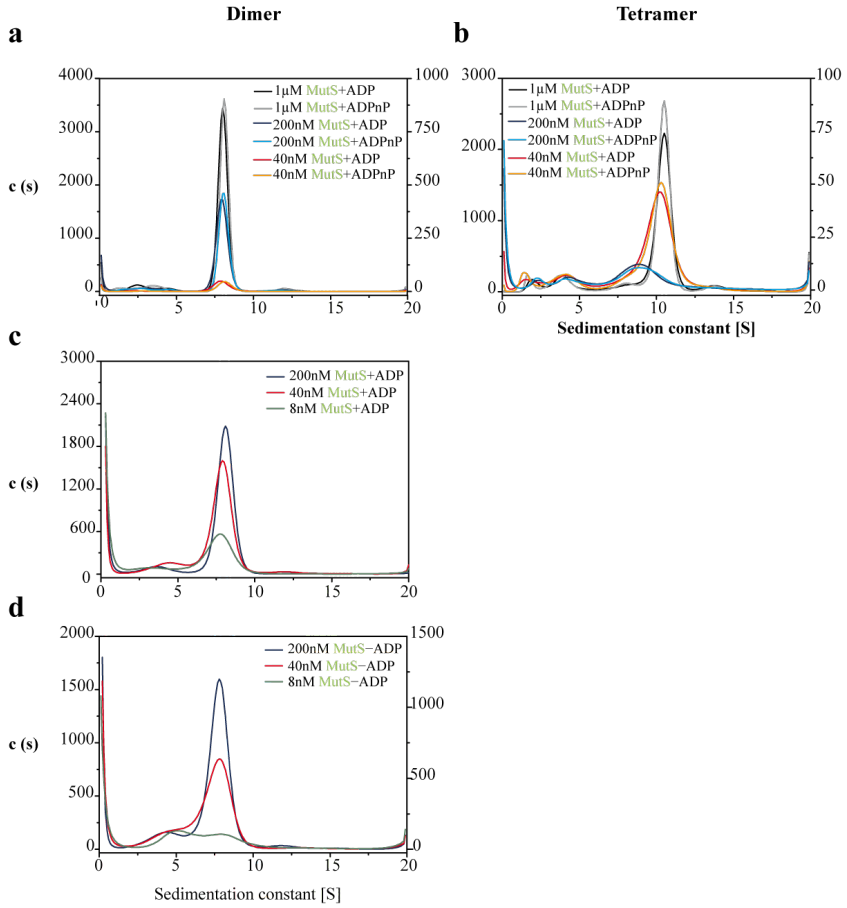

Fig. 3. 35: Sedimentation coefficient distribution obtained from sedimentation velocity runs of Alexa 488 labeled MutS in the presence and absence of nucleotides. The Lamm equation solution is plotted vs. the sedimentation constant. a) 1µM, 200nM and 40nM of MutS^{R449C}-Alexa 488 were analyzed in the presence of 1mM ADP or 1mM ADPnP. Due to the difference in the signals amplitude, the 200nM and 40nM are plotted on the secondary axis. The 200nM run was corrected by a factor of 5 and the 40nM run by a factor of 20. b) 200nM and 40nM of MutS$^{R449C/D835R}$-Alexa 488 were analyzed in the presence of 1mM ADP or 1mM ADPnP. The 40nM distribution profile was plotted on the secondary axis. The 200nM run was corrected by a factor of 5 and the 40nM run by a factor of 20. c) Sedimentation profile of MutS$^{R449C/D835R}$ was obtained at 200nM (blue), 40nM (red) and 8nM (green), in the presence of 1mM ADP. d) Sedimentation profile of MutS$^{R449C/D835R}$ was obtained at 200nM (blue), 40nM (red) and 8nM (green), in the absence of ADP. Analysis performed by Dr. Ute Curth, Medizinische Hochschule Hannover.

suggesting that MutS$^{R449C/D835R}$ is a stable dimer at these concentrations. Furthermore, the type of nucleotide binding to MutS (ADP or ADPnP) has no influence in the dimerization state. However, the ADP runs are slightly shifted to lower s-values when compared to the ADPnP runs. It is known that MutS adopts different conformations when bound to ADP and ADPnP and this difference could be detected by the small difference in sedimentation coefficients.

In contrast, the sedimentation profile of MutS^{R449C}-Alexa 488 shows a concentration dependence sedimentation coefficient (Fig. 3. 35b). At 1µM, the sedimentation coefficient is approximately 10.6S but it is difficult to determine if this value corresponds to the tetramer or to another MutS-state without further analysis. When moving to lower MutS concentrations, the distributions also shift to lower s-values and become broader, suggesting an equilibrium between two states (maybe dimer-tetramer equilibrium). The preparation of MutS^{R449C}-Alexa 488 is not very clean and degradation products can be seen at low s-values, which difficults the analysis. In

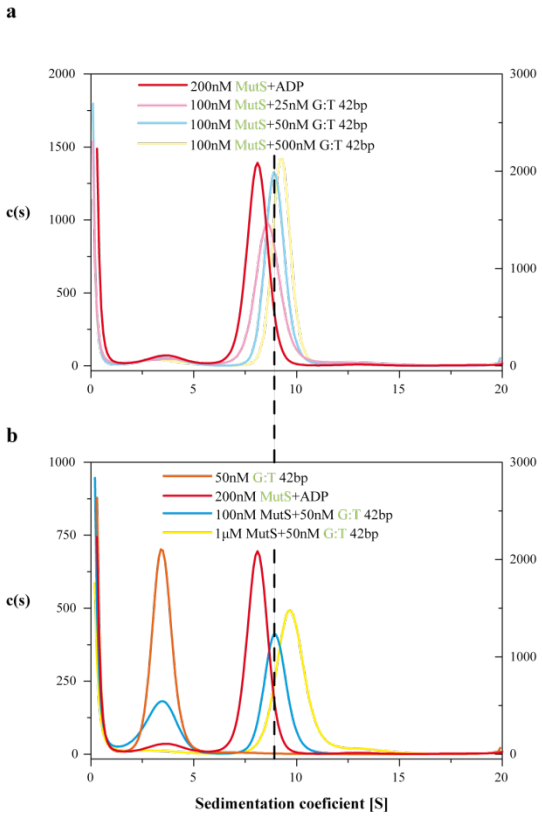

Fig. 3. 36: Sedimentation coefficient distribution obtained from sedimentation velocity runs of Alexa 488 labeled 42bp oligonucleotide. The Lamm equation solution is plotted vs. the sedimentation constant. Sedimentation velocity run of 50nM 42bp oligonucleotide labeled with Alexa 488 alone (orange), in the presence of 100nM (blue) and 1µM (yellow) unlabeled MutS MutS$^{CF/D835R}$. The sedimentation profile from 200nM MutS$^{R449C/D835R}$-Alexa 488 in 1mM ADP from figure 3.34c was also plotted (red). b) Sedimentation coefficient distribution obtained from sedimentation velocity runs of 100nM Alexa 488 labeled MutS$^{R449C/D835R}$ in the absence and presence of different concentrations of unlabeled 42bp oligonucleotide. The Lamm equation solution is plotted vs. the sedimentation constant. The concentration of DNA oligonucleotide added was as follows: 25nM (red), 50nM (green) and 500nM (blue).

addition, similar to what was seen for MutS$^{R449C/D835R}$, the oligomerization state of MutS^{R449C} shows no dependence on the nucleotide. The tetramer, however, does not show a shift in the ADP runs, when compared to ADPnP. Possibly, if the ADPnP induces a different conformation on MutS, it cannot be distinguished in the tetramer.

Next, the influence of the presence or absence of ADP in the dimer-tetramer equilibrium of the MutS$^{R449C/D835R}$ was analyzed (Fig. 3. 35c and d). Three different Alexa 488-labeled MutS (200nM, 40nM and 8nM) were sedimented in presence and absence of 1mM ADP, in the absence of DNA. At 200 and 40nM MutS and in the presence of ADP, the maximum of the distribution is centered at around 8.1-8.2, as was seen before. At 8nM, however, the s-value decreases and the maximum is now around 7.8S (Fig. 3. 35c).

In the absence of nucleotide, the sedimentation distributions appear to be broader than in the presence of ADP and the maximum is slightly shifted: the 200 and 40nM runs show a maximum at around 7.9S and the 8nM run at around 8S, although the sensitivity at this concentration is very low (Fig. 3. 35d). These results suggest that MutS is stable both in the presence and absence of nucleotide. In the absence of ADP, however, a monomer-dimer equilibrium is starting to be noticeable, specially at low concentrations (8nM).

Alexa 488 labeled MutS was sedimented in the presence of different concentrations of 42bp oligonucleotides. The sedimentation profile of 100nM of MutS$^{R449C/D835R}$-A488 was analyzed in the presence of 25, 50 and 500nM unlabeled oligonucleotide. The results can be seen in Fig. 3. 36a. The distributions obtained for these experiments were compared with the sedimentation profile obtained for 200nM MutS$^{R449C/D835R}$-A488 alone in the presence of ADP (Fig. 3. 35c). A clear dependence on the DNA concentration can be seen in each sedimentation run: increasing the DNA concentration from 0 to 500nM shifts the sedimentation distribution to higher s-values. The working MutS concentration was 100nM monomer (50nM dimer). Free labeled dimer MutS has a s-value of 8.3 (red), in complex with DNA in a 1:2 stoichiometry the s-value increases to 8.7 (pink), in a 1:1 stoichiometry the sedimentation coefficient increases to 9.0S (blue) and in a 10:1 stoichiometry the distribution shows a s-value of 9.4 (yellow). In the 50nM DNA run the DNA/MutS ratio is 1:1 and under these conditions there should not be free MutS in solution. However, the addition of 500nM DNA further shifts the sedimentation coefficient to higher s-values, suggesting that there is still free MutS and DNA when the DNA/MutS stoichiometry is 1:1.

Next, 50nM of Alexa 488 labeled 42bp oligonucleotide was sedimented alone and in the presence of 100nM or 1μM MutS$^{R449C/D835R}$ (see Fig. 3. 37b). Again in this experiment, the results were compared to the sedimentation profile of 200nM of free MutS$^{R449C/D835R}$ (with ADP), with a sedimentation coefficient of 8.2S (red distribution). The labeled oligonucleotide alone has a sedimentation constant of 3.5 (orange distribution). When the DNA/MutS stoichiometry is 1:1, approximately 30% of the oligonucleotide is free, while 70% appears to be in the MutS-bound

form, with a s-value of 9 (blue distribution). This s-value corresponds to the s-value obtained for the same conditions, but with labeled MutS and unlabeled DNA (blue in Fig. 3. 37a). With this experiment the free-DNA can be detected and the previous assumption that free DNA is still present when the DNA/MutS ratio is 1:1 is confirmed. The addition of 1µM MutS (yellow distribution) to 50nM G:T-A488 then shifts the equilibrium to higher s-values (9.8S) and no free DNA is detected. At these concentrations it is possible that two MutS proteins bind to the 42bp oligonucleotide (DNA/($MutS^{R449C/D835R}$)x2 complex). This complex could correspond to a tetramer MutS bound to DNA. However it was seen previously that the tetramer alone is thought to have a sedimentation coefficient of 10.6S (Fig. 3. 36b) and the tetramer bound to DNA would show an even higher s-value. The s-value obtained for the 1µM MutS and 50nM G:T-A488 run is approximately 9.8S, lower than expected for a tetramer alone. If the 10.6S sedimentation coefficient corresponds to the tetramer, it could be possible that a mix of oligonucleotide with 2 MutS and with 1 MutS is present in solution. This would also explain the slightly broader distribution. Furthermore, it is not known how the tetramer binds to DNA. Possibly the shapes of a DNA/$MutS^{R449C}$ and of DNA/($MutS^{R449C/D835R}$)x2 are different and could also account for different sedimentation coefficients.

In summary, the dimer variant of MutS is a stable dimer in the presence of ADP and ADPnP. In the absence of nucleotides, the dimer dissociates at low MutS concentrations. In the presence of DNA, the majority of MutS is in the bound state.

3.4.2 Nucleotide modulates the clamp state of MutS

To understand the dynamics of the dimer exchange, and specially the movement of the clamp domain, double labeled $MutS^{R449C/D835R}$ was incubated in the absence or presence of different nucleotides, as well as several types of DNA, i.e. G:T/G:C 42bp oligonucleotide or plasmid DNA.

$MutS^{R449C/D835R}$ is fully active in a functional assay after labeling (Fig. 3. 6) and well suited for this analysis. The position of the cysteines are on the clamp domain in the right distance for FRET experiments, to monitor the clamp opening and closing.

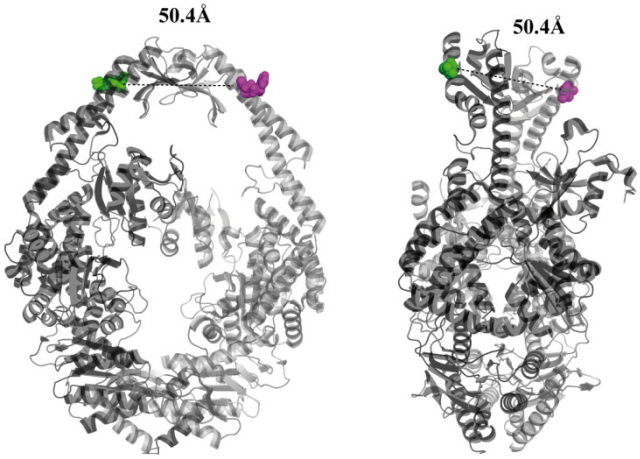

Fig. 3. 37: MutS was double labeled with Alexa 488 (green) and Alexa 594 (pink) on position R449C. The measured Cα-Cα distance is 50.4Å.

Monomer exchange is possible in the absence of nucleotide. AUC analysis of Alexa 488-labeled MutS$^{R449C/D835R}$ revealed that the stability of the dimer is dependent on the presence of ADP or ADPnP (Fig. 3. 35). To obtain information about the dynamics of the monomer/dimer equilibrium, MutS$^{R449C/D835R}$-DA was incubated with MutS$^{CF/D835R}$ in the presence or absence of nucleotide and the F_A/F_D ratio was monitored over time. If the dimer dissociates into monomers, monomers of labeled and unlabeled MutS can form mixed dimers; as a consequence, the F_A/F_D will decrease over time (Fig. 3. 38a).

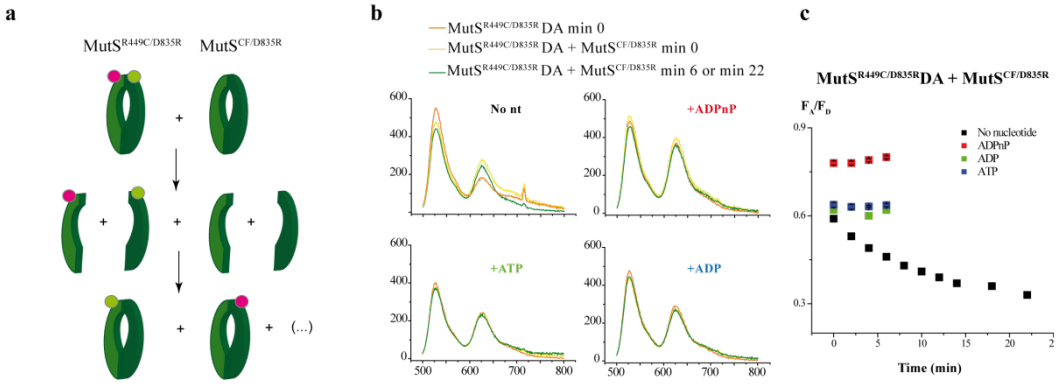

Fig. 3. 38: 200nM of MutS$^{R449C/D835R}$-DA was incubated in the absence of nucleotide or in the presence of 1mM ADPnP, ADP or ATP and in the presence of 2µM MutS$^{CF/D835R}$. The fluorescence spectra was taken every 2 minutes for 22 minutes (no nucleotide) or for 6 minutes (ADP, ATP and ADPnP). a) Scheme for the dimer exchange of double labeled MutS. If the dimer dissociates into monomers, MutS monomers can re-associate with unlabeled dimers and the FRET will decrease (i.e. the F_A/F_D ratio) over time. If the dimers are stable in solution, the F_A/F_D ratio will stay constant over time. b) Fluorescence spectra for each nucleotide of MutS$^{R449C/D835R}$ DA alone (orange line), for MutS$^{R449C/D835R}$-DA and MutS$^{CF/D835R}$ after 0 minutes incubation (yellow line) and after 22 minutes (no nucleotide) and 6 minutes incubation (ADP, ATP and ADPnP). c) The F_A/F_D ratio is plotted vs. time in minutes.

The experimental data indicates that this is the case but only in the absence of nucleotide (Fig. 3. 38b and c). Fig. 3. 38a shows the fluorescence spectra of the double labeled MutS in the absence of unlabeled MutS and after 0 and 22 minutes incubation. In the absence of nucleotide, the decrease in FRET was significant whereas in the presence of nucleotide no significant change in the FRET signal was observed. Noteworthy, the MutS FRET signal was higher in the presence of ADPnP. This suggests that the protein in the ADPnP-bound form adopts a conformation in which the distance between the two fluorophores, and thus the clamps, is shorter.

The sliding clamp conformation can be detected in the presence of plasmid DNA and ATP. Next, the influence of the DNA on the MutS clamp conformation was analyzed (Fig. 3. 39 and Fig. 3. 40). In Fig. 3. 39, plasmid DNA was added to MutS$^{R449C/D835R}$-DA, followed by addition of ADPnP, ADP or ATP. MutS was initially incubated in the absence of nucleotide for 14 minutes. As expected, in the absence of nucleotide, MutS dissociates into monomers, resulting in a decrease of the observed F_A/F_D. Upon addition of plasmid DNA (at 14min) an increase of F_A/F_D was observed. This suggests that MutS binds to DNA in the absence of nucleotide and the dimer is stabilized. The addition of either ADPnP or ATP resulted in a strong increase in the F_A/F_D ratio of MutS bound to plasmid DNA. This observation indicates that the binding of either nucleotide to the ATPase domain induces a slow but significant conformational change in the clamp domain of MutS. In addition, the dimerization of MutS monomers also leads to a FRET increase, but to a lower extent, as seen for the addition of ADP to the MutS/plasmid complex. In contrast to the

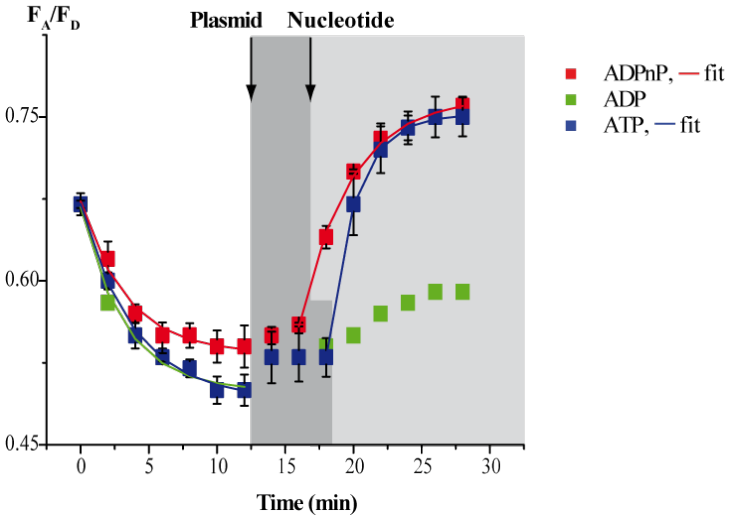

Fig. 3. 39: 200nM MutS$^{R449C/D835R}$ DA was incubated in the absence of nucleotide. At minute 14, 1µM plasmid DNA (2794bp) was added to the MutS and alternatively, ADPnP, ADP or ATP was added to MutS/plasmid complex as indicated. The F_A/F_D ratio is plotted vs. time in minutes. The curves were fitted to a single exponential. The initial decrease in FRET signal shows an average k_{obs1} of 0.29min^{-1}; the ADPnP k_{obs2} is approximately 0.27min^{-1} and ATP k_{obs2} is approximately 0.5min^{-1}. The ADP k_{obs2} was not determined.

experiments performed without DNA, F_D/F_A with ATP was similar to F_A/F_D with ADPnP.

Next, the type of DNA was varied: 42bp G:T oligonucleotide, 42bp G:C oligonucleotide or a homoduplex plasmid (Fig. 3. 40a, b and c). In all experiments, the fluorescence emission spectra was first measured in the absence of nucleotide and DNA. After the first measurement, either ADPnP, ADP or ATP was added to MutS (at 2min), followed by the addition of DNA at min. 12. Also here can be seen that the addition of ADPnP causes a rapid increase in the F_A/F_D ratio; in contrast, the addition of ADP and ATP causes a small decrease in the F_A/F_D ratio. In all experiments with ADPnP, the FRET signal stays constant and the addition of DNA has no significant effect. In the case of ADP and ATP, the signal still increases slightly during the first 10 minutes. The addition of G:T and G:C oligonucleotide to MutS in the presence of ADP leads to a strong decrease in the FRET signal, whereas the addition of plasmid has no effect on the FRET signal. The conformation adopted by MutS in the presence of an oligonucleotide is independent of a mismatch. However, MutS is known to recognize DNA ends and thus this conformation could correspond to the mismatch binding conformation. It could also represent the conformation of MutS binding to the ends of the DNA and thus this conformations is not present

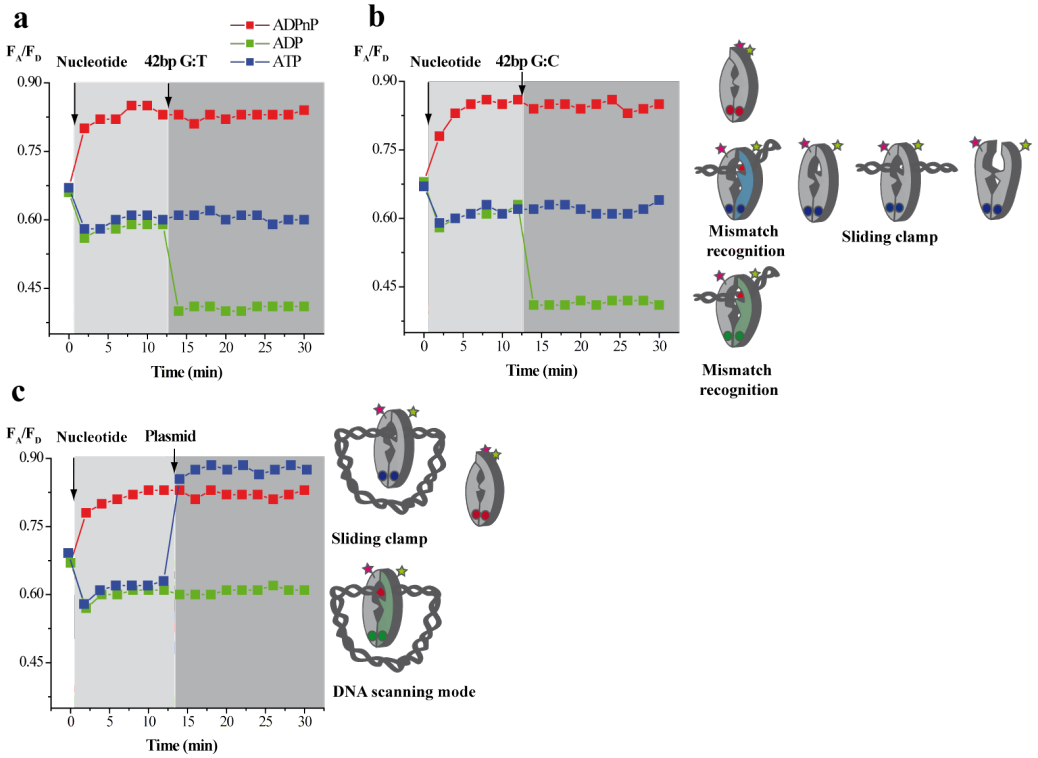

Fig. 3. 40: 200nM MutS$^{R449C/D835R}$ DA was incubated in the presence of ADPnP, ADP or ATP for 10 minutes. At minute 12: a) 2µM of 42bp G:T, b) G:C oligonucleotide or c) 1µM of plasmid DNA (2794bp) was added. The F_A/F_D ratio is plotted vs. time in minutes. The light grey shaded areas indicate the measuring period in the presence of ADPnP (red), ATP (blue) or ADP (green); the dark shaded areas indicate the measuring period in the presence of DNA. Next to representative measurements, a cartoon depicts possible conformations of MutS, with either bound ATP, ADP or ADPnP, with special focus on the mismatch binding and sliding clamp conformations. For simplicity, the same nucleotide was considered to

with plasmid DNA. In the case of ATP, the addition of neither oligonucleotide, G:T or G:C, has a significant effect on the FRET signal. It is likely that all bound and free MutS conformations are present with ATP (ADP/ATP equilibrium) but as this measurement was performed in bulk, these cannot be distinguished. The addition of plasmid, however, causes a strong increase in the FRET signal. As the plasmid DNA has no open ends, MutS cannot slide off the DNA and either remains bound or dissociates by opening of the clamps.

To summarize the results of this section: without nucleotide, MutS exists in a monomer/dimer equilibrium. Addition of ATP, ADP or ADPnP stabilizes the dimer. Conformations of the clamp are similar in the presence of ADP or ATP and closed in the presence of ADPnP (corresponding to the plasmid/$MutS_{ATP}$ conformation). Since MutS is known to be mainly in its ADP-bound form (Fig. 3. 33) in the presence of ATP, only the $MutS_{ADP}$ and $MutS_{ADPnP}$ states can be analyzed by FRET (each state by itself can be a mixture of states, i.e. open/closed, not resolved in bulk measurements). In the presence of excess oligonucleotide, the majority of MutS will be in a DNA-bound state (the exception is $MutS_{ADPnP}$ which cannot bind DNA). Surprisingly, although $MutS_{ADP/ATP}$ and $MutS_{ADP/ADP}$ are similar, in the presence of plasmid DNA significant differences were observed. This indicates that binding of ADP and ATP induce different conformational states. With ADP (see smMFD), the majority of the species present was DNA/$MutS_{ADP}$. This state has a lower F_A/F_D than the $MutS_{ADP}$ state, suggesting a larger distance of the clamps (this is the only state for which a structure is available). Interestingly, the absence of a mismatch on the oligonucleotide does not influence the conformation of MutS significantly. In contrast, on plasmid DNA MutS adopts a state similar to the $MutS_{ADP}$ state. The major difference between the two DNAs is the presence/absence of ends. Since MutS binds to DNA ends with high affinity, the $MutS_{ADP}$ state on G:C oligonucleotides may be bound to DNA ends in a similar conformation as when bound at mismatches. With ATP and DNA, a highly dynamic system is most likely formed,

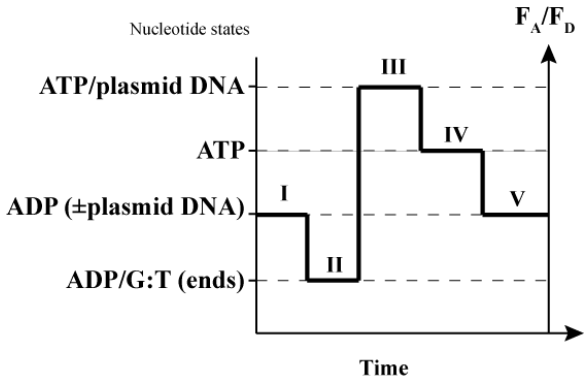

Fig. 3. 41: Representation of the clamp conformation in the various nucleotide and DNA states of MutS along a arbitrary time line. The change in the F_A/F_D ratio represents the state of the clamp (high F_A/F_D, closed clamp; low F_A/F_D, open clamp). Each clamp state corresponds to a different phase and a different state (I-V) in the functional cycle of MutS.

hence MutS exists in an equilibrium of states (DNA stimulates the ADP/ATP exchange). In the absence of DNA ends, this equilibrium is shifted towards a high FRET state, which prevents the dissociation of the sliding clamps.

The relation between the conformational states (Fig. 3. 41) and the kinetic phases is summarized in Table 3. 15: State I corresponds to DNA and MutS association in the presence of ADP, with a fast K_{on} rate, and medium F_A/F_D ratio. The clamp is in a flexible and open state. When MutS binds a mismatch (or DNA ends), it adopts a closed and tight state (State II), characterized by a decrease in the F_A/F_D ratio. The mismatch-induced ADP/ATP exchange increases the F_A/F_D ratio, the clamps are wide and closed (State III), and the sliding clamp forms. The fast dissociation of the sliding clamp corresponds to phase III and the hydrolysis of ATP in phase IV leads to the decrease of F_A/F_D to $MutS_{ADP}$ levels in state V. The DNA/$MutS_{ADP}$ re-

Table 3. 15: Relation between MutS nucleotide and DNA states and the associated event.

F_A/F_D			Rate
Medium	State I	$MutS_{ADP}$ + G:T	
	Phase I	Binding	$24\mu M^{-1}s^{-1}$
Low	State II	G:T/$MutS_{ADP}$	
	Phase II	Nucleotide exchange	
High	State III	G:T/$MutS_{ATP}$	
	Phase III	Sliding/dissociation	$1.9s^{-1}$
High	State IV	$MutS_{ATP}$ + G:T	
	Phase IV	Hydrolysis	
Medium	State V	$MutS_{ADP}$ + G:T	
	Phase V	Binding	$60\mu M^{-1}s^{-1}$

The measured F_A/F_D ratio are shown in the first column and the measured rate in the last column.

association in phase V possibly corresponds to a different MutS conformation ($MutS_{ADP/ATP}$?) and a different K_{on} is attributed.

Fast conformational changes of the clamp in the presence of nucleotide. To get insights into the fast dynamics of clamp movement, pre-steady state experiments were performed. The steady state experiments showed that the dimer variant of MutS is unstable in the absence of nucleotide. This effect was observed also in the rapid mixing of $MutS^{R449C/D835R}$DA with buffer, where the FRET signal is seen to decrease steadily with time (Fig. 3. 39a). The rapid mixing of $MutS^{R449C/D835R}$-DA with 1µM G:T or G:C oligonucleotide shows a rapid decrease of the FRET signal within the first second (Fig. 3. 42a). Although part of the decrease can be due to the instability of the dimer, the kinetics was clearly different in the case where DNA was added and could be due to binding of MutS to DNA, resulting in a more open conformation.

In the absence of DNA, the addition of ATP to MutS$^{R449C/D835R}$-DA caused decrease of the F_A/F_D ratio in the steady-state experiments (blue squares and light grey area in Fig. 3. 40). Fig. 3. 43b shows that adding ATP induces a rapid decrease (in 1s) followed by a slow increase (in 2-3s) of the FRET signal, suggesting an opening and subsequent closing of the clamp domain. The different phases might correspond to the binding and hydrolysis of ATP. Although there is a rapid change in the FRET signal, the overall change in amplitude is small, as was seen in the steady state.

The addition of G:T to MutS$^{R449C/D835R}$-DA$_{ADP}$ induces a small decrease in the FRET signal, possibly due to the opening of the clamp in the presence of DNA. In contrast, when G:T oligonucleotide was added to MutS$^{R449C/D835R}$-DA preincubated with ATP (blue squares and dark grey area in Fig. 3. 40a), there was again a fast decrease in the FRET signal (DNA binding), followed by an increase in the FRET signal (ADP/ATP exchange). Since MutS exists primarily in an ADP-bound state in the presence of ATP, the initial decrease could correspond to the binding of DNA, similar to the fast association in the presence of ADP (green curve). As ATP is in excess, the second phase could then correspond to the ADP/ATP exchange, catalyzed by the presence of a mismatch. In the steady state measurements it was observed that the addition of G:T oligonucleotide to MutS$^{R449C/D835R}$-DA$_{ATP}$ caused no significant change of the FRET signal; in the stopped flow measurements, however, the initial and final FRET signal is different. The initial

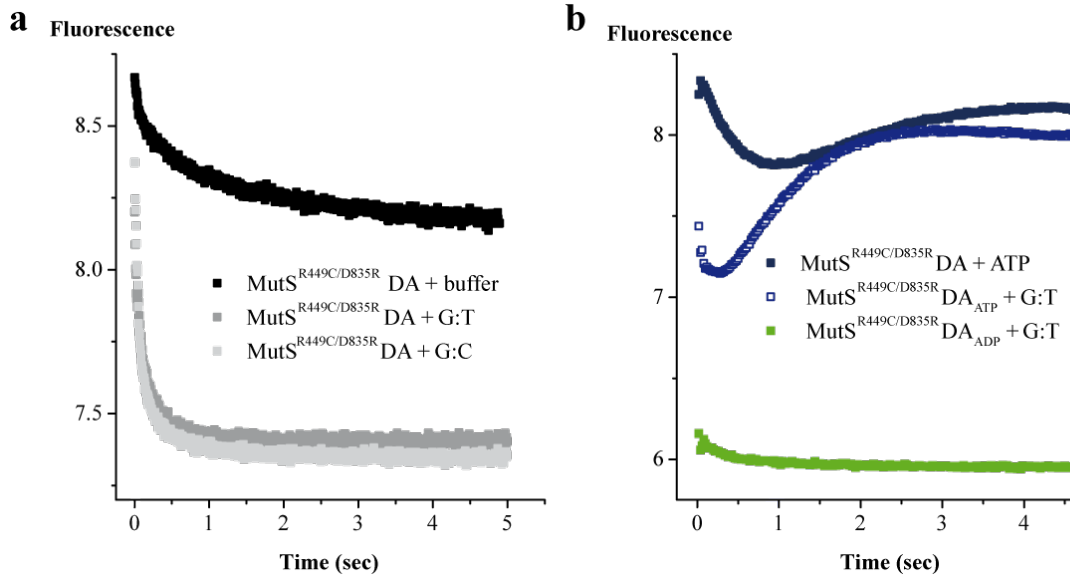

Fig. 3. 42: Stopped-flow analysis of the fast movement of the clamp induced by nucleotide and DNA. The FRET signal is plotted vs. time in seconds. Data from 3 injections were averaged for each experiment. MutS concentration was 300nM, the DNA concentration 1µM and the nucleotide concentration 1mM. a) MutS$^{R449C/D835R}$DA was rapidly mixed with buffer (black squares), 1µM G:T (dark grey squares) or 1µM G:C (light grey squares). b) MutS$^{R449C/D835R}$DA was rapidly mixed with 1mM ATP (filled blue squares), pre-incubated with 1mM ATP and rapidly mixed with 1µM G:T (open blue squares) or pre-incubated with 1mM ADP and rapidly mixed with 1µM G:T (green squares).

FRET decrease is fast and it is possible that a decrease happens in the dead time of the stopped flow apparatus. It follows that the actual initial FRET signal is higher, closer to the end FRET signal and so the overall amplitude change also insignificant.

Effect of nucleotide on the stabilization of the dimer. The previous sections showed that the conformational changes undergone by MutS depend on the type of nucleotide binding to the ATPase domains and that the different conformations can easily be monitored with FRET. In addition, the stability of the dimer is directly related to the presence of nucleotide (Fig. 3. 38). The binding of ADPnP causes a high F_A/F_D ratio and ADP a medium F_A/F_D ratio. If the dimer is unstable, the F_A/F_D ratio decreases slowly over time, but a decrease in the F_A/F_D ratio due to a conformational change is fast. However, MutS has two ATPase sites and thus far this aspect has not been addressed. To better understand the relation between the two ATPase sites and the difference between having one or two sites occupied, double labeled $MutS^{R449C/D835R}$ was titrated with different nucleotides and the effect on the F_A/F_D ratio was analyzed.

Four different concentrations of ADPnP (100µM, 10µM, 1µM and 100nM) were added to MutS and the effect on the F_A/F_D ratio registered over time. The results are shown in Fig. 3. 43a. Adding 100µM or 10µM ADPnP has no effect on the F_A/F_D ratio over time. After the addition of 1µM, the F_A/F_D ratio decreases fast before stabilizing at level that is located between the F_A/F_D value of $MutS_{ADPnP}$ and $MutS_{ADP}$ (compare the values of ADPnP and ADP in the absence of DNA in Fig. 3. 40 and the red filled triangle in Fig. 3. 43a). In contrast, the addition of 100nM of ADPnP causes a slow decrease of the F_A/F_D ratio, without reaching the saturation, suggesting that the monomers dissociate at 100nM ADPnP. Together, these results suggest that there are two

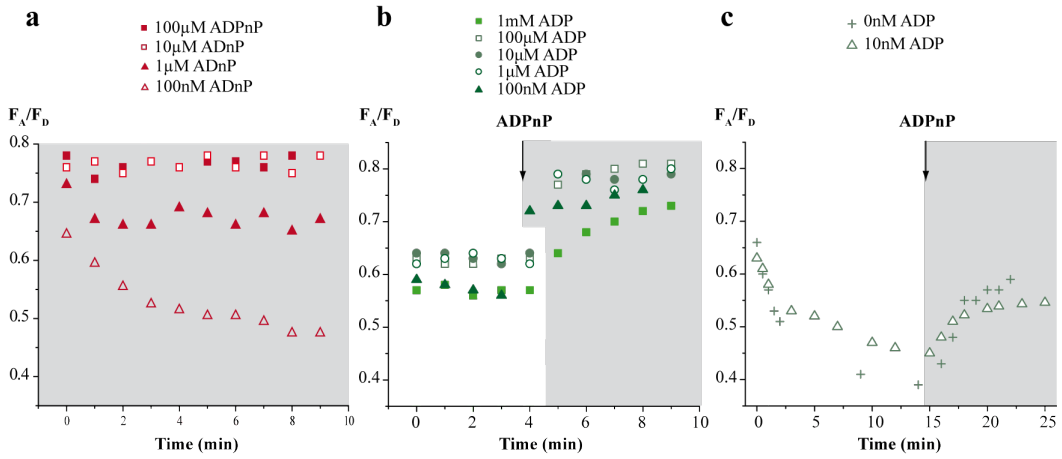

Fig. 3. 43: 500nM MutS DA was incubated in the presence of different concentrations of ADP and ADPnP, with 0.05% Tween 20. a) MutS was incubated with ADPnP at the indicated concentrations and fluorescence spectra were recorded at the indicated time. F_A/F_D ratio was plotted vs. time (min). b+c) MutS was incubated with ADP at the indicated concentrations and fluorescence spectra were recorded at the indicated time. F_A/F_D ratio was plotted vs. time (min). 1mM ADPnP was added as indicated.

nucleotide levels in MutS: one that is responsible for a conformational change (between 10 and 1µM) and one that is related to the stabilization of the dimer (below 1µM).

To better understand where the second level is located, MutS was incubated with six different concentrations of ADP and 1mM ADPnP was added after a certain incubation time. The incubation of MutS with the different ADP concentrations showed that the dimer dissociates when less than 100nM ADP is present (Fig. 3. 43c). In addition, adding 1mM ADPnP to 1mM ADP induced a slow increase in F_A/F_D, suggesting an ADPnP/ADP exchange followed by the conformational change characteristic for $MutS_{ADPnP}$ (Fig. 3. 44 III). In contrast, the incubation of MutS in 100nM ADP (closed triangles) causes a small decrease in the F_A/F_D ratio in the first 4 minutes (already seen with 100nM ADPnP). Addition of 1mM ADPnP caused an abrupt increase in the F_A/F_D ratio, followed by a slow change to the MutSADPnP level. Possibly, the $MutS_{ADPnP/ADPnP}$ conformation is different from the $MutS_{ADP/ADP}$ (II) and probably from the $MutS_{ADP/ADPnP}$ (III) but this effect is difficult to distinguish. According to the estimated K_D, at 1 and 10µM, at least one ATPase site is occupied and the added ADPnP fills the second, with concomitant increase in F_A/F_D. This suggests that a mixed state (ADP/ADPnP) has a similar conformation as $MutS_{ADPnP/ADPnP}$, but the difference is difficult to distinguish. The measurement

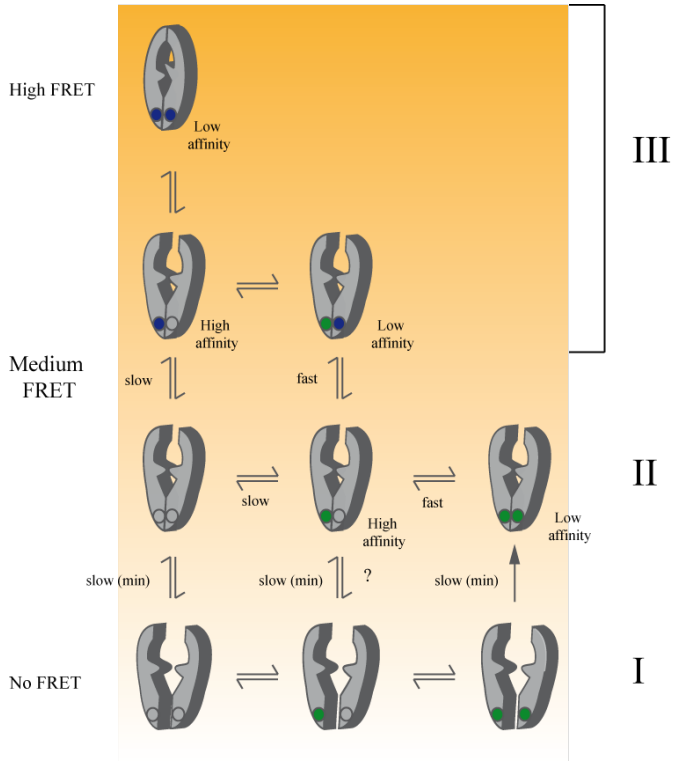

Fig. 3. 44: Schematic representation of the clamp state when one or two nucleotides are bound to the ATPase site (circles) of MutS. State I corresponds to monomers, seen in the absence of nucleotide, state II corresponds to loose dimers, observed in the presence of ADP, and state III refers to rigid dimers, formed in the presence of ATP/ADPnP. Although the experiments were performed with ADPnP, ATP is represented in the scheme. The conformations of $MutS_{ADPnP}$ and $MutS_{ATP}$ prior to hydrolysis are in theory the same.

was repeated in the presence of 10nM ADP (Fig. 3. 43c) and compared with 0nM ADP. The F_A/F_D ratio decreased slowly but steadily in both cases (II to I). The addition of 1mM ADPnP caused a slow increase in the F_A/F_D ratio. When 1mM ADPnP was added to the MutS/0nM ADP solution, the increase in F_A/F_D is faster. This suggests that in the first case, ADP has to be exchanged by ADPnP before ADPnP can bind and induce the conformational change signaled by the FRET increase. In neither case, however, does the FRET efficiency reach the high FRET seen previously. Furthermore the initial drop is more significant than in the experiment from Fig. 3. 39, suggesting that the longer the protein is incubated without nucleotide, the longer it takes to recover the dimeric state.

In summary, the results from this section showed that in the absence of nucleotides, the MutS dimer slowly dissociates into monomers and the FRET is low. When nucleotide is bound to MutS, the dimers are stable and the FRET increases, but the re-association of monomers is slow. The K_D of the low affinity site is located between 1 and 10μM and the K_D for the high affinity site is below 100nM. When ATP (or ADPnP, blue) is binding to at least one ATPase site, the FRET increases.

The results from this section highlight the importance of the conformational changes induced by nucleotide binding and the strong effect of the presence of ATP instead of ADP in the ATPase domain of MutS. The presence of nucleotide stabilizes the dimer and induces different conformations on the clamp domain of MutS. Two conformations of free MutS are distinguished, $MutS_{ADP}$ and $MutS_{ADPnP}$ (corresponding to $MutS_{ATP}$ before hydrolysis), and three conformations of DNA-bound MutS: plasmid DNA/$MutS_{ADP}$, mismatch/$MutS_{ADP}$, plasmid DNA/$MutS_{ATP}$. $MutS_{ADPnP}$ corresponds to a rigid closed conformation, unable to bind DNA, while $MutS_{ADP}$ is flexible and ready to bind DNA. The plasmid DNA/$MutS_{ADP}$ conformation is similar $MutS_{ADP}$, and smMFD and AUC measurements showed that the majority of MutS is bound under these conditions. Plasmid DNA/$MutS_{ATP}$ is a closed conformation.

The fast kinetics of MutS binding to ATP shows a rapid conformational change, not observed in steady state. The fast kinetics of $MutS_{ATP}$ and G:T association shows that the binding comes with is a fast conformational change in the clamp domain, absent in the $MutS_{ADP}$ and G:T association, attributed to the DNA binding, followed by ADP/ATP exchange.

The nucleotide titration to double labeled MutS allowed the determination of the K_D for the high (100nM) and low affinity (between 1 and 10μM) ATPase site by analyzing the dimeric state of double labeled MutS. In addition, three clamp states were proposed related to the F_A/F_D ratio and to the nucleotide state of MutS: monomers (I), loose dimers (II) and closed dimers (III).

IV. Discussion

Fluorescence Resonance Energy Transfer (or FRET) is an very useful technique for studying conformational changes between 10 to 100Å, a range in which conformational changes usually occur within DNA and proteins. However, attaching one or more fluorophores to DNA or proteins is not a trivial task. Fluorophores are bulky and rigid molecules and there is always the risk that they interfere with the biological function of the target which needs to be controlled. At the same time, the spectral and fluorescence properties of the fluorophore ideally should be unaltered by the DNA or the protein, in order to prevent an influence on the FRET efficiency. This later topic will be dealt with in detail in the next chapter.

4.1 Choice of labeling positions and fluorophores

Fluorescence labeling of protein and DNA usually requires several steps: the first important decision is the chemistry of fluorescence labeling. As discussed in the Introduction, maleimide-based linkers to attack the thiol group of cysteines is more specific that the succinimidyl ester linkers to target amine groups. In case of MutS an active cysteine-free variant of MutS had been generated before[15], hence introduction of thiol group to generate single-cysteine variants was possible. Care should be taken that neither the mutation nor the chemical modification is interfering with the function of the protein which has to be controlled experimentally. Depending on the positions chosen and the available detection methods appropriate pairs of fluorophore dyes suitable for FRET have to be selected. In the case presented here, the fluorophore dyes were selected based on compatibility with the smMFD setup available at Prof. Seidel's group at the University of Düsseldorf.

A cysteine-free variant of MutS is available and single cysteines can be introduced in specific positions for FRET studies. Since MutS exists in dimer-tetramer equilibrium, for the sake of clarity in data analysis and interpretation, studies were carried out with a MutS variant that is unable to from tetramers. It had been shown previously, that a single point mutation (D835R) in the C-terminal domain of MutS is sufficient to prevent tetramerization of the protein without seriously affecting the *in vitro* and *in vivo* activities of MutS [15].

The movement of the clamp domain has been implicated to play an important role in the ATPase/DNA binding cycle of MutS. For the work presented here the single-cysteines MutS variants were modified with Alexa-maleimide fluorophores, on position 449 in the clamp domain and as a control on position 246 in the connector domain of MutS. The latter domain was suspected to undergo only limited change in position, since for *Taq*-MutS the structure of the

unbound and bound protein were very similar in this domain[28]. Position 449 is located on the clamp domain of MutS, above the DNA, making it suitable for MutS-DNA FRET. Position 246 is located on the connector domain, below the DNA, and also suitable for MutS-DNA FRET. As the two residues are located on opposite sides with respect to the bound DNA, measured FRET efficiencies will yield complementary information about the binding orientation of MutS to DNA. Furthermore, using MutS labeled with two different fluorophores was used to study the movement of the clamp domains in relation to one another (see below) (Fig. 3. 21).

Both positions are surface-exposed and could be labeled with Alexa 488 or Alexa 594 or both dyes simultaneously to high yield. The labeled $MutS^{R449C/D835R}$ retained its *in vitro* activity in mismatch-provoked MutH endonuclease activity and the ability to discriminate between homo and heteroduplex (Fig. 3. 5); in contrast, the labeled $MutS^{D246C/D835R}$ was inactive in the mismatch-provoked MutH activation assays (Fig. 3.7). Since DNA binding of the labeled variant was not affected (Fig. 3.21), the fluorophore might interfere with one of the subsequent steps of the mismatch repair pathway, most likely the recruitment of MutL. Possibly this position overlaps with the MutS/MutL interaction interface (Ines Winkler, personal communication).

4.2 MutS binds mismatches with preferred orientations

Gorman *et al* proposed that MutS scans the DNA as a clamp searching for local helix distortions[55]. When MutS finds a flexible and bent region with lower energy in the DNA, it can recognize it as a mismatch. Regions without a lesion but that are intrinsically bent might serve as deep energy traps for MutS[55]. The encounter of MutS with such a trap, which mimics a mismatch, causes a conformational change in the protein, such as the Phe residue insertion, and turns it into an immobile clamp. In the absence of nucleotide, MutS resumes the mobile clamp state and continues scanning the DNA, eventually falling of the ends or dissociating by opening of the clamps. In the presence of nucleotide, however, MutS binds to 1 or 2 ATP molecules and assumes the sliding clamp mode, which is now able to activate MutL and MutH[55].

The initial step of this process is the discrimination between a flexible sequence in the DNA from a true mismatch. To analyze the mismatch recognition process in detail, a FRET system was designed in which a donor and an acceptor fluorophore were attached to a 42bp oligonucleotide, such that the mismatch was located between the two dyes, separated by 26bp. From a model of MutS bound to a G:T heteroduplex DNA containing the two fluorophores, it was inferred that upon DNA kinking the distance between the two fluorophores changes from 76Å (B-DNA) to 59Å (60º kinked DNA) (Fig. 3. 16) resulting in a measurable change in FRET-efficiency. The oligonucleotide design had the advantage that all possible 16 base-pairs could be tested and

compared. Noteworthy, although a G:T mismatch, for which the setup was designed, is identical to a T:G mismatch, this is only true for palindromic sequences embracing the mispair. In the present case neither the sequence nor orientation of the two fluorophore is palindromic. Since sequence context has an influence on mismatch recognition and repair efficiency this point was addressed and is discussed below in detail.

The measurement of the change in FRET efficiency of unbound and bound DNA led to two main observations:

1) An increase in FRET efficiency is only observed upon binding of MutS to heteroduplex DNA but not to any of the four homoduplex DNAs (Fig. 3. 10).

Homoduplex DNA is bound under the experimental conditions used (Fig. 3. 12 and Fig. 3. 24) nevertheless the addition of MutS does not change the FRET efficiency. This observation does not exclude kinking/bending of homoduplex DNA, rather it shows that MutS binds homoduplex DNA unspecifically at various positions (including DNA ends). Indeed, addition of MutS to dual-labeled 42bp homoduplex DNA resulted in a quench of the donor and acceptor fluorescence, without any increase of FRET, indicating that MutS binds to DNA at sites in close proximity to either donor and/or the acceptor fluorophore. This DNA binding is not dominated by the dye, as little if any fluorescence quenching by MutS is observed with a double-labeled 406bp long homoduplex DNA substrate (Fig. 3. 14). In contrast, the 406 bp long DNA containing a single G:T mismatch between the two fluorophores displayed a similar increase in FRET efficiency as observed with the 42-bp G:T oligonucleotides. However, smMFD showed that the presence of only a low FRET species for the G:C/MutS complex (Fig. 3. 24), suggesting that if a bent/kinked complex exists, it is short lived and undetectable. These results suggest that MutS binds heteroduplex DNA site-specifically, thereby changing the local conformation of the DNA (probably resulting in a DNA kink at the mismatch).

2) Depending on the orientation of the mismatch with respect to the surrounding sequence and the two fluorophores, a significant difference in the increase of FRET-efficiencies was observed.

All experimental data (discussed in detail below) suggest that MutS binds certain mismatches (i.e. G:T and C:A) with a preferred orientation, e.g. in a G:T mismatch the T is always in contact with Phe-36. The observed differences in FRET-efficiencies, e.g. between G:T and T:G, can be explained by a combination of three factors: different MutS affinities for the G:T and T:G sequence context, different MutS-induced DNA-kinking at the mismatch and different interaction between the protein and the two fluorophores depending on the binding orientation of the protein. The data showed that the different FRET efficiency is explained by a preferred binding orientation of MutS.

Sequence context is not a major determinant for the observed differences in FRET-efficiency observed in the G:T/MutS vs. T:G/MutS complex

The affinity of MutS for mismatches is known to be dependent on the sequence context surrounding the mismatch[51, 52, 56]. To rule out the possibility that the different FRET efficiencies are due to sequence context effects, G:T was placed in the sequence context of T:G (T:G-I) and T:G in the sequence context of G:T (G:T-I) (Fig. 3. 11). The results showed that the difference in the FRET efficiency after MutS binding to the two substrates remains, although the effect is less pronounced, i.e. the difference between both substrates is smaller. This indicates that MutS binds G:T and T:G with different orientations but that the sequence surrounding the mismatch affects the binding affinity. This was confirmed by the anisotropy measurements, where it was shown that the K_D for G:T is 2x higher than the K_D for T:G (Fig. 3. 20). A closer look into the FRET populations of DNA/MutS with smMFD confirmed the existence of different FRET populations with G:T and T:G. Moreover, binding of MutS to G:G allows the formation of both binding modes, although favoring the higher FRET population (corresponding to the "G:T-binding mode"), possibly due to higher affinity of MutS for the surrounding sequence context. In addition, a bound but unbent T:G substrate cannot be responsible for the low FRET efficiency as DNA/MutS FRET measurements showed that T:G is bent when bound to MutS (Fig. 3. 22).

The accumulated evidence indicates that MutS has a preferred orientation when binding a G:T mismatch. The co-crystal structure of G:T/MutS showed that MutS interacts specifically with the T whereas in the structure of A:C/MutS, MutS interacts with C. If MutS has a preference to bind one base over the other, this could have an effect in the mismatch recognizing ability of MutS. The importance of having a preferred binding mode was tested in the mismatch-provoked MutH activation. MutS does not recognize T:G if the distance from the mismatch to the end is only 6bp, whereas the recognition of G:T mismatch in the same context is unaffected (Fig. 3. 18). This indicates that the inhibition of the preferred binding orientation may have consequences for efficient mismatch recognition.

In addition, the data showed thus far does not account for the existence of an unbent G:T/MutS complex as suggested by Wang *et al*[18]. However, if the complex is low populated, none of the techniques employed would show an unbent but bound DNA state. The labeled $MutS^{D246C/D835R}$ could be employed in the DNA/MutS FRET pre-steady state measurements to allow the distinction of the unbent state. The 246 residue is located below the DNA and the unbending of the DNA will increase the FRET efficiency between the protein and a fluorophore located on the bent arm of the DNA.

Protein-dye interactions influences FRET-efficiencies

The question of why the two pairs of mismatches (i.e. G:T/T:G and C:A and A:C) show different FRET efficiencies still remains to be answered. Based on the models, even if MutS binds

G:T and T:G with different orientations, the FRET efficiency should be similar as the DNA is always kinked by 60º. However, since the fluorophores are influenced by their environment, e.g. contacts to the protein, protein-dependent anisotropy effects were tested for, in the two proposed different binding orientations.

As predicted by the "DNA-fluorophore clouds" (Fig. 3. 16), Alexa 488 and Alexa 594 show different effects when MutS binds to G:T and T:G (Fig. 3. 20). The binding of MutS to T:G decreases the rotational freedom of Alexa 488, indicated by an increase in the anisotropy of this fluorophore, also seen in the smMFD measurements (Fig. 3. 23). In contrast, the binding of MutS to G:T does not affect Alexa 488 (confirmed with the single molecule measurements) but instead decreases the rotational freedom of Alexa 594, signaled by an increase of its anisotropy. These results are consistent with preferred binding orientations and in addition explain why the binding of MutS to T:G induces only a small FRET increase. The rotational freedom of the fluorophores is an important aspect in FRET as the assumption of a κ^2 of 2/3 is only applicable in the case of freely rotating fluorophores. Although in the G:T/MutS complex, the acceptor fluorophore Alexa 594 is also affected by the protein, the theoretical and the experimental values measured for this complex agree (Table 3. 4) whereas for the T:G complex they do not. This indicates that if the acceptor is rotationally restricted, the effect on the FRET efficiency is small but if the donor is affected, as in the T:G case, the measured efficiencies cannot be used to accurately determine distances.

These results highlight the well known problem of the rotational freedom of the fluorophores in a FRET system. This aspect is commonly ignored and fluorophores are placed on DNA and protein in positions that most likely affect the rotational freedom. Care must be taken when choosing labeling positions and the anisotropy should always be controlled in order to avoid artifacts.

Biological consequences of a preferred binding orientation

Preferential binding orientations for mismatches have been suggested for human MutSα [57, 58] and should be addressed using the above mentioned approach in future experiments. The

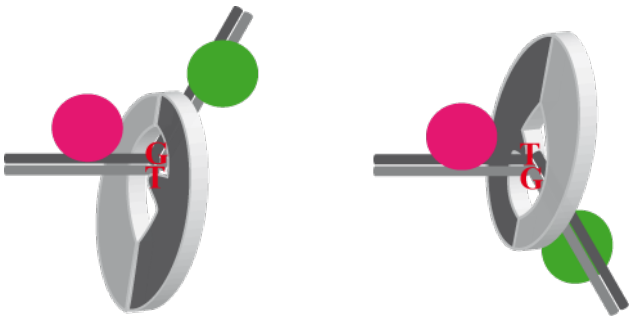

Fig. 4. 1: Different binding orientations proposed for MutS. Left: "G:T-binding mode"; Right: "T:G-binding mode".

intrinsic asymmetry of the heterodimeric MutSα (MSH2-MSH6) leads to an interesting hypothesis: If MutSα is loaded onto the replicated strand, possibly via interaction with PCNA[59], the orientation of the heterodimer will determine whether certain mismatches can be recognized or not. Although there is only limited data available on the mutation rates of specific mismatches with respect to the orientation of the replication fork (i.e. leading vs. lagging strand), a recent study by the Kunkel group revealed that T:G mismatches (T on the parental strand) are repaired more efficiently by the yeast MMR system than the corresponding G:T mismatch[60]. This might be a consequence of a preferential loading and recognition of yMutSα, however, without more detailed information this remains a highly speculative hypothesis.

Given a preferred binding orientation of MutS to a mismatch and the bi-directionality of the MMR-process raises the question whether either the active complex of MutS and MutL is asymmetric and mobile (which would offer the possibility to act on signals both upstream and downstream of the mismatch), or loses its asymmetry after mismatch recognition in order to act in both directions. The fact that eukaryotic MutSα and MutLα are both heterodimers strongly favors the former hypothesis, i.e. a mobile MutSL-complex.

4.3 Nucleotide influence on DNA binding and bending by MutS

The step of mismatch recognition by MutS has been intensively investigated by various methods, e.g. fluorescence[21, 61], AFM[62], SPR[63]. In particular, the kinetics of MutS binding to DNA have been analyzed with fluorescence methods by Huang and Crothers for *E. coli* MutS tetramer and Jacobs-Palmer *et al* for *Taq* MutS[21, 61]. In both studies, the DNA/MutS association was fitted to a one-step mechanism. Despite great effort, the mechanism of mismatch recognition is yet not fully understood.

The double labeled G:T substrate was shown in the previous section to be suitable for monitoring the binding and bending of MutS by FRET change. To unravel the initial steps of DNA/MutS, the same substrate was used in pre-steady state kinetics and the effect of nucleotides in the association and dissociation of the complex was studied. The rates obtained independently from different measurements were introduced into a kinetic model (Fig. 3. 32 and Fig. 4. 2) but it is far from being complete due to the complexity of the functional cycle of MutS.

The DNA/MutS$_{ADP}$ association is biphasic

The results presented here show that the G:T/MutS association in the presence of ADP is a two-step reaction, composed by a binding/bending step and a conformational change. A binding/bending step was attributed to the initial binding and recognition of a mismatch, with a K_{on} of 24 $\mu M^{-1}s^{-1}$, followed by a slow conformational change, attributed to the sharp kink induced

by MutS specifically at mismatched sites. Wang *et al* suggested that the interaction of MutS and DNA occurs by a kinking and an unkinking step but an unkinking step could not be distinguished in the current experiments[18].

The dissociation of $MutS_{ADP}$ from DNA is slow suggesting that the G:T/$MutS_{ADP}$ complex is stable, evidenced by the smMFD, where the majority of the MutS is in complex with a bound and kinked DNA (Fig. 3. 32).

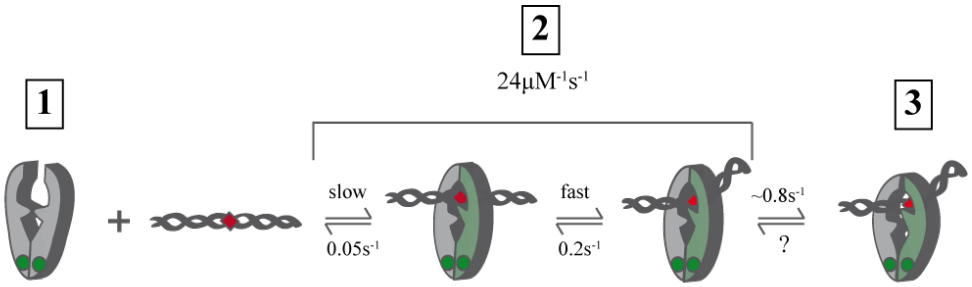

Fig. 4. 2: Schematic representation of the association of MutS and DNA, where the kinetic rates obtained with the stopped flow measurements were introduced. The green circle indicates binding of ATP to the ATPase site and in green the DNA binding monomer is highlighted.

In the present report a two step mechanism is suggested for the DNA/MutS association, in contradiction to previously published data[21, 29]. However, a one-step mechanism is insufficient to explain the data presented here. The previously reported kinetic data was performed with either $MutS^{WT}$ (tetramer) or with *Taq* MutS and the results might be accordingly different.

The G:T/$MutS_{ATP}$ is dynamic and unstable

The association of MutS and DNA in the presence of ATP is faster, with a K_{on} of $60\mu M^{-1}s^{-1}$ and the complex is more unstable (or dynamic). This observation was supported by the dissociation/association cycle observed after the addition of ATP to the G:T/MutS complex, and by the increase of the "bound-relaxed" population in smMFD (Fig. 3. 33). These observations contrast with previous work done by Jacobs-Palmer *et al*, where it was reported that the presence of ATP stabilizes MutS on the mismatch[21]. However, Jacobs-Palmer *et al* used *Taq* MutS instead of *E. coli* MutS, which could lead to slightly different results. In addition, it was reported elsewhere that MutS adopts a sliding clamp conformation when bound to ATP [64], implying that it rapidly slides away from the mismatch upon binding the nucleotide. It was reported that MutS only hydrolyzes ATP during or after the dissociation event and not while bound to DNA[64]. It is likely thus that ATP hydrolysis occurs in between the dissociation and association step, at least in one of the monomers, as MutS cannot bind DNA in the ATP/ATP conformation (corresponding to the $MutS_{ADPnP}$ conformation). Interestingly, the conformation of $MutS_{ADPnP}$ is not the same as $MutS_{ATP}$, indicated by the far more complex dissociation kinetics of the $MutS_{ADPnP}$ complex. It is likely that the dissociation of MutS from DNA requires ATP hydrolysis, which would explain the

more complex and slower dissociation kinetic of $MutS_{ADPnP}$. Such a mechanism was also suggested by Lamers *et al*, who showed that the hydrolysis driven MutS dissociation was prevented in a hydrolysis-deficient MutS mutant[25]. Furthermore, the kinetic analysis showed that the $MutS_{ADPnP}$ complex is unable to bind DNA, as long as both ATPase sites are occupied with ADPnP. This was seen in the smMFD measurements as well, where the addition of ADPnP to the G:T/MutS complex causes the unbending and release of the DNA (Fig. 3. 33C).

The asymmetric ATPase site of MutS increases the complexity of the functional cycle of MutS

It is difficult to assess in which nucleotide state both the ATPase sites are in each step. When MutS is pre-incubated with ATP, an ATP/ADP equilibrium is most likely present as MutS hydrolyzes ATP quickly in the presence of DNA and slowly in the absence of DNA (Fig. 3. 27). Therefore, the dissociation of the G:T/MutS complex pre-incubated with ATP and chased with competitor is similar to the dissociation of the G:T/$MutS_{ADP}$ complex. In addition, during the association of $MutS_{ATP}$ and DNA, MutS is likely to be in a $MutS_{ADP/ATP}$ state, as $MutS_{ATP/ATP}$ does not bind DNA and $MutS_{ADP/ADP}$ has a slower DNA association. Furthermore, the results with ADPnP suggest that when one ATPase site is bound to ADP, MutS can still bind to DNA. This observation is possibly related to the asymmetry in the nucleotide-binding sites and in the dimer during DNA binding. Reportedly, the high affinity ATPase site is also the one that binds the mismatch[25]. Thus, $MutS_{ADPnP/ADP}$ might still be able to bind mismatched DNA until ADP is replaced by ADPnP. When both ATPase sites are occupied by ADPnP, MutS adopts a closed rigid conformation unable to bind DNA, shown by anisotropy (Fig. 3. 19), stopped flow association kinetics (Fig. 3. 30) and smMFD (Fig. 3. 33).

In summary, the DNA/MutS association in the presence of both ADP and ATP is biphasic. The DNA/MutS complex dissociates fast after being challenged with ATP and competitor, in a conformation corresponding to the sliding clamp. The binding of ATP to MutS in complex with G:T induces the fast dissociation of MutS in the sliding clamp conformation and allows the re-association of the complex. The dissociation of $MutS_{ADPnP}$ is more complex than the dissociation of $MutS_{ATP}$, but $MutS_{ADPnP}$ is not allowed to rebind DNA.

The double labeled DNA is quite suitable for the analysis of the DNA/MutS association kinetics. The information obtained from the decay and association curves is nevertheless quite dense and insufficient to fully understand the complexity of the functional cycle of MutS. Surely, the two ATPase sites and the alternating hydrolysis mechanism play an important role in the modulation of the activity of MutS, as had already been seen for other proteins belonging to the ABC transporter family, such as Rad50[65, 66]. This aspect will be further address in the next chapter.

4.4 Communication between ATPase and clamp domain of MutS

The single-cysteine $MutS^{R449C}$ variant, both in its dimeric and its tetrameric form is well suited for fluorescent labeling and in solution analysis. MutS is known to undergo large conformational changes, modulated by the binding and hydrolysis of ATP[27], however, little experimental data is available that show the proposed conformational changes. Using the double fluorescently labeled MutS variant allowed for the first time monitoring of the conformational changes modulated by nucleotides and DNA in solution and in real time.

$MutS^{R449C/D835R}$ is stable dimer in solution in the presence of nucleotide

$MutS^{R449C/D835R}$, a dimeric single-cysteine variant of MutS was site specifically labeled with the FRET pair Alexa 488 and Alexa 594, without significant effects on the *in vitro* activity of the protein (Fig. 3. 5and Fig. 3. 6). Sedimentation velocity analysis and FRET studies showed that the stability of the $MutS^{R449C/D835R}$ dimer is dependent on the presence of nucleotide (Fig. 3. 35 and Fig. 3. 37). In the absence of nucleotide, the dimer slowly dissociated into monomers. This phenomenon was exploited for the formation of mixed dimers, consisting of labeled and unlabeled monomer or dimers composed of two different variants (e.g. $MutS^{R449C/D835R}$ /$MutS^{CF/D835R}$). This indicates that nucleotide binding is important for dimerization, probably because the two ATPase sites are in close proximity to the dimerization domain. Interestingly, it had been suggested by Lamers *et al* that the binding of ATP promotes the dimerization but binding of ADP promotes the monomerization of MutS[27]. However, Lamers *et al* performed the experiments with the dimer variant $MutS^{800}$, where the last 53aa are missing (dimerization/tetramerization domain). Although $MutS^{800}$ is still able to dimerize, the dimer was unstable even in the presence of ADP.

Double labeled MutS allows the distinction of different MutS conformations in solution

Kato *et al* suggested that MutS exists in three different conformations modulated by the nucleotide state of the protein: nucleotide free, ADP bound and ATP bound[67]. The results presented here confirm the existence of several MutS conformations and in addition further conformations for mismatch-bound and DNA-scanning MutS are proposed.

$MutS_{ADPnP(ATP)}$ conformation. Analysis of the FRET, which is sensitive to the distance between the clamps of the two subunit, presented in this report showed that the ADPnP-bound form of MutS adopts a closed, compact conformation, unable to bind DNA, which is consistent with previous reports [27, 67]. These findings were corroborated by the faster sedimentation velocity of the ADPnP-bound MutS in comparison to the ADP-bound form (Fig. 3. 35). It is well documented for the members of the ABC ATPase-family, to which MutS belongs, that the

ATPase activity depends on the dimerization of the ATPase domains[68]. The $MutS_{ADPnP}$ conformation probably corresponds to the $MutS_{ATP}$ conformation, prior to hydrolysis. To confirm this, measurements need to be performed in the presence of ATP but absence of magnesium (to prevent hydrolysis). The addition of oligonucleotide did not significantly affect the observed FRET signal in steady-state experiment. However, it can be expected that a mixture of species will be present (Fig. 3. 40a and b). This is supported by the pre-steady analysis of the FRET signals, indicating a fast transition from a high FRET to a low FRET state within the first few seconds, possibly corresponding to a DNA-binding induced conformational change in MutS followed by phases of nucleotide exchange and ATP hydrolysis (Fig. 3. 42). Upon addition of either ADPnP or ATP to a complex of $MutS_{free}$ with circular homoduplex DNA, the FRET signal increased indicating the formation of a more compact form, possibly with the clamp tightening around the DNA (Fig. 3. 39). Acharya *et al* showed that in the presence of a mismatch on DNA with blocked ends ATP hydrolysis but not the ADP/ATP exchange is inhibited and MutS stays bound to DNA. For homoduplex DNA with blocked ends the ADP/ATP exchange is slowed down to the level of the free protein [64]. Thus, in the presence of ATP and circular DNA MutS may exist in a mixed state of $MutS_{ATP}$ and $MutS_{ADP}$. However, since the FRET signals in the presence of circular DNA followed by addition of either ATP or ADPnP were quite similar and well distinct from those adding ADP, in the presence of ATP the majority of MutS may still be in a $MutS_{ATP}$-state and this seems to be more similar to the $MutS_{ADPnP}$ form in the absence of DNA and clearly distinct to any of the state MutS adopts in the presence of ADP.

Mismatch-bound and DNA scanning conformations. As mentioned above, in the absence of DNA $MutS_{ADP}$ exists in more flexible and open conformation, and is well defined in contrast to mixture of states that can form in the presence of ATP. In the presence of oligonucleotide (with or without a mismatch), the clamp domain of MutS seems to be get even more open, in a conformation attributed to the mismatch-binding conformation (Fig. 3. 40a and b). The existence of a major, well defined conformation is supported by the smMFD data: In the presence of ADP and a G:T mismatch a single major population of DNA/$MutS_{ADP}$ was observed (Fig. 3. 33). Surprisingly, the presence or absence of a mismatch in the oligonucleotides did not affect the FRET signal. Given the well known DNA-end binding of MutS, the conformation observed with the homoduplex oligonucleotides might reflect a MutS conformation bound to the ends of the DNA rather than to a piece of homoduplex DNA. This idea is supported by the data obtained with MutS and circular homoduplex DNA in the presence of ADP which are clearly distinct from the data with the oligonucleotides (Fig. 3. 39c). As MutS is completely bound to DNA under the experimental conditions used, MutS is likely to be in its DNA scanning mode.

Rapid mixing of $MutS_{ADP}$ and G:T oligonucleotide resulted in a single exponential decrease of the FRET signal in contrast to the multiphasic signals obtained in the presence of ATP. This is

consistent with the idea that the second and third phase in the experiments with MutS/ATP and G:T oligonucleotide showing an increase in the FRET signal corresponds to either conformational changes induced by nucleotide release, ATP binding and/or ATP-hydrolysis (Fig. 3. 42). However, in order to dissect this pathway, additional experiments are required, e.g. under conditions that inhibit hydrolysis.

Progressive binding of nucleotide to one and then to the other ATPase site increases the stability of MutS dimer

Modrich and co-workers have demonstrated that MutS can simultaneously bind ADP and ATP, having one high affinity site for ADP in one subunit and a high affinity site for ATP in the other subunit[26]. Lamers *et al* showed that the two ATPase domains of *E. coli* MutS are asymmetric in nucleotide binding and hydrolysis[25]. One of the nucleotide binding sites has a higher affinity for ATP (corresponding to the ATPase site on the mismatch binding monomer) and hydrolysis of ATP alternates even in the absence of DNA binding. K_D-values for the high affinities sites were reported to be in the 100 nM range for ADP and ATPγS whereas K_D of 10 μM were estimated for the low affinity sites for ADP and ATP[25, 26]. To analyze the effect of nucleotides on the dimer stability and the conformation of the clamp domain, nucleotides were titrated to double labeled MutS using FRET to monitor signal changes. The results showed that in the absence of (added) nucleotide, the dimer was unstable and slowly dissociated into monomers. Under low ADP concentration (< 10 μM) only the high affinity site of MutS is occupied. In contrast, low concentrations sufficient to bind to the high affinity ATP-site of MutS were not unable to prevent dissociation of the dimer. However, conditions where both high affinity sites were filled with ADP and ADPnP resulted not only in a stabilization of the dimer but also in the formation of a compact closed clamp state, which remains closed in the absence of hydrolysis.

The above mentioned experiments together with the data on nucleotide binding in the literature allowed the distinction of three clamp states of MutS (Fig. 3. 44), related to the two K_D-values of the ATPase sites and to the type of nucleotide bound. State I corresponds to the presence of mostly monomers of MutS, in the absence of nucleotides, characterized by a very low F_A/F_D ratio (Fig. 3. 43c). State II corresponds to one ADP bound to the high affinity ADP-site of MutS characterized by intermediate F_A/F_D. Additional binding of ADP or ADPnP to the second, low affinity ADP-site (1 to 10μM), does not significantly change the F_A/F_D ratio and is difficult to distinguish. Finally, when both nucleotide binding sites are occupied by ADPnP, state III is formed characterized by a high F_A/F_D ratio (Fig. 3. 43a). The observed concentration dependency of the F_A/F_D ratio is in agreement with the published values for K_D for the high and low affinity site [25].

The steady state and pre-steady state analysis of double labeled $MutS^{R449C/D835R}$ yielded useful information regarding the coupling of the nucleotide binding domain to the clamp domain. Since the fluorophores of the FRET pair are located on the clamp domain, the effect of nucleotide binding can be (indirectly) observed. The obtained information gave insights into conformational changes in MutS that have thus far only been predicted and can now be used to understand the ATPase cycle of MutS. Similar conformational changes occur in ATPase, such as the ABC transporter family and the GHKL family (to which MutL belongs). However, further pre-steady state analysis of double labeled MutS in different positions will be required to dissect the ATPase cycle both in structural and dynamic terms. Such measurements will include the use of circular mismatched DNA (thereby avoiding the effect of DNA ends), different combinations of nucleotides (ADP, ADPnP, ATP+Mg^{2+}, ATP-Mg^{2+}) and DNA (G:C, G:T, circular and linear) as well selected protein variants affected in various functional domains. Finally, the addition of downstream repair proteins, in particular MutL, will be needed to understand the critical, mismatch-specific conformation of MutS required to initiate the repair reaction. Given the complexity of the system, already in the absence of DNA and co-repair proteins, single-molecule measurements in solution (e.g. smMFD) and on the surface (TIRFM: Total Internal Reflection Fluorescence Microscopy) are highly warranted to understand the order and kinetics of the conformational transitions.

4.5 Model for DNA and MutS conformational changes

The present thesis demonstrates that Fluorescence Resonance Energy Transfer turned out to be a very useful and insightful method to monitor specific conformational changes in solution in DNA and MutS, during the initial key events in the mismatch repair pathway: the recognition of a mismatch and the MutS conformational changes occurring during the DNA recognition and the ATPase cycle. The combination of the DNA bending FRET experiments and the double-labeled MutS FRET experiments led to the proposal of the following working model on this process:

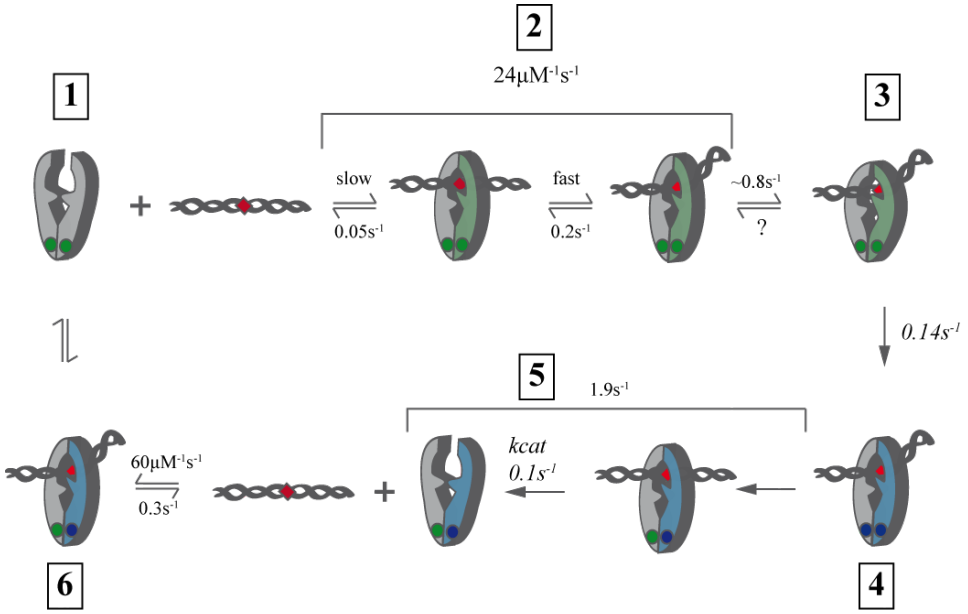

Fig. 4. 3: Model for DNA and MutS conformational changes monitored by FRET. The rates determined by stopped flow are shown. Rates in *italic* are obtained from the work published by Acharya *et al* and refer to the exchange of ADP by ATP ($0.14s^{-1}$) [64] and by Lamers *et al* referring to the burst of ATP hydrolysis measured in the presence of a mismatched oligonucleotide[26]. The green monomer indicates the mismatch binding monomer in G:T/$MutS_{ADP}$ and the blue monomer indicates the mismatch binding monomer in G:T/$MutS_{ATP}$.

When bound to ADP, MutS exists in conformation, where the clamp domain most likely is flexible (maybe fluctuating between open and closed states) and ready to bind DNA (1). Upon DNA binding, MutS (in an ADP-state) adopts a loose closed conformation able to rapidly scan the DNA[1]. After encounter with a mismatch, the DNA is specifically bent and kinked at the mismatch site by interaction of the Phe-X-Glu motif of the mismatch binding monomer (green) with only one bases of the mismatch (2) The DNA is recognized in a two step process and a sharp kink is induced (3). In this conformation the clamp domains are in a wide closed conformation. According to the association and dissociation rate constants and the smMFD FRET populations, the equilibrium is shifted in the direction of the kinked DNA/MutS complex in the presence of ADP. When MutS is bound at the kinked mismatch, ADP is readily exchanged for ATP in both subunits (4) [69], thereby converting the protein into a sliding clamp which detaches from the mismatch. In this state, the clamp domain most likely adopts a tight close conformation similar to the state in solution in the presence of ADPnP. This conformational change is predicted to involve also a movement of the mismatch binding domain away from the DNA [27] which might be the trigger to recruit MutL to the sliding $MutS_{ATP}$ [21, 64, 70, 71]. This movement of the mismatch-binding domain is highly speculative and needs experimental verification. However, a recent computational analysis using normal-mode analysis supported this model [71]. Moreover, a

[1] The fact that MutS in the presence of ADP can dissociate from DNA with blocked ends suggest, that the clamp domain is not fixed to a closed conformation.

crosslinking analysis performed in our group also provides first experimental evidence for a movement of the mismatch-binding domain (Ines Winkler, personal communication). As the DNA used in the stopped flow measurements has open ends, the sliding MutS dissociate rapidly from the DNA via the ends resulting in a $MutS_{ATP/ADP}$ (5). After dissociation, ATP is hydrolyzed to reset MutS to its initial $MutS_{ADP}$ state. Alternatively, the mixed $MutS_{ATP/ADP}$ can bind directly to DNA (6). It is likely that the fast dissociation of MutS from DNA requires ATP hydrolysis, as $MutS_{ADPnP}$ shows a more complex and slower dissociation kinetic than $MutS_{ATP}$. Furthermore, Lamers *et al*, showed that the hydrolysis driven MutS dissociation was prevented in a hydrolysis-deficient MutS mutant[25]. In addition, it was reported elsewhere that MutL induces the ATP-hydrolysis dependent reversibility of DNA binding by MutS but only in the presence of competitor DNA [64]. Possibly, mismatch-bound $MutS_{ATP}$ requires a molecular switch (provided by MutL?) to hydrolyze ATP and be recycled to $MutS_{ADP}$ to be able to rebind DNA. Since MutS possesses ATPase activity even in the absence of other proteins, MutL is likely to function as a catalyst, enhancing the ATPase activity of MutS in order to accelerate the recycling of the DNA binding form. A question that remains unanswered is the function of the two ATPase sites of MutS and the role of the alternating mechanism of hydrolysis. The two ATPase sites have different affinity for ATP, with the high affinity site located on the mismatch binding monomer[25, 72]. Furthermore, the mismatch binding monomer hydrolyzes ATP rapidly, while the non-mismatch binding monomer hydrolyzes it at a slower rate and the same holds true for human MutS heterodimer MSH2-MSH6, in which only MSH6 makes specific contacts with the DNA[72]. The conservation of the mechanism from bacteria to humans and the observation that ATP hydrolysis impaired MutS mutants are severely affected in *in vivo* MMR highlights the importance of the ATPase cycle in the fine-tuning of mismatch repair system.

The proposed mechanism of coupling mismatch recognition to strand discrimination suggests a 1D diffusion mode for the activation of MutH in *E. coli* MMR. A 1D diffusion intersite communication mechanism has recently also been proposed for Type III restriction endonucleases [73]. The similarities between the MMR and Type III restriction enzymes concerning the involvement of ATPase, the effect of roadblocks[70] and DNA-end blocking led the authors to suggest that a similar mechanism could be responsible for the mismatch site-GATC site communication in *E. coli* MMR. Many indirect observations accumulated over the years suggest that the formation of an active mobile complex of MutS is critical in MMR. The fluorescence resonance energy transfer studies present in this work support this hypothesis and led to the identification and monitoring of critical conformational transition both in the DNA and the MutS but also demonstrated that we are far from understanding the structural and dynamic complexity of this intriguing system. Future work further extending the single-molecule/kinetic approach using the fluorescently labeled DNA and MMR-proteins will help to unravel the details of the MMR-system.

V. References

1. Mendillo, M.L., C.D. Putnam, and R.D. Kolodner, *Escherichia coli MutS tetramerization domain structure reveals that stable dimers but not tetramers are essential for DNA mismatch repair in vivo.* J Biol Chem, 2007. **282**(22): p. 16345-54.
2. Lamers, M.H., A. Perrakis, J.H. Enzlin, H.H. Winterwerp, N. de Wind, and T.K. Sixma, *The crystal structure of DNA mismatch repair protein MutS binding to a G x T mismatch.* Nature, 2000. **407**(6805): p. 711-7.
3. Hoeijmakers, J.H., *Genome maintenance mechanisms for preventing cancer.* Nature, 2001. **411**(6835): p. 366-74.
4. Rothwell, P.J., S. Berger, O. Kensch, S. Felekyan, M. Antonik, B.M. Wohrl, T. Restle, R.S. Goody, and C.A. Seidel, *Multiparameter single-molecule fluorescence spectroscopy reveals heterogeneity of HIV-1 reverse transcriptase:primer/template complexes.* Proc Natl Acad Sci U S A, 2003. **100**(4): p. 1655-60.
5. Gidron, Y., K. Russ, H. Tissarchondou, and J. Warner, *The relation between psychological factors and DNA-damage: a critical review.* Biol Psychol, 2006. **72**(3): p. 291-304.
6. Schofield, M.J. and P. Hsieh, *DNA mismatch repair: molecular mechanisms and biological function.* Annu Rev Microbiol, 2003. **57**: p. 579-608.
7. Jiricny, J., *The multifaceted mismatch-repair system.* Nat Rev Mol Cell Biol, 2006. **7**(5): p. 335-46.
8. Li, G.M., *Mechanisms and functions of DNA mismatch repair.* Cell Res, 2008. **18**(1): p. 85-98.
9. Iyer, R.R., A. Pluciennik, V. Burdett, and P.L. Modrich, *DNA mismatch repair: functions and mechanisms.* Chem Rev, 2006. **106**(2): p. 302-23.
10. Lin, Z., M. Nei, and H. Ma, *The origins and early evolution of DNA mismatch repair genes--multiple horizontal gene transfers and co-evolution.* Nucleic Acids Res, 2007. **35**(22): p. 7591-603.
11. Dao, V. and P. Modrich, *Mismatch-, MutS-, MutL-, and helicase II-dependent unwinding from the single-strand break of an incised heteroduplex.* J Biol Chem, 1998. **273**(15): p. 9202-7.
12. Yamaguchi, M., V. Dao, and P. Modrich, *MutS and MutL activate DNA helicase II in a mismatch-dependent manner.* J Biol Chem, 1998. **273**(15): p. 9197-201.
13. Matson, S.W. and A.B. Robertson, *The UvrD helicase and its modulation by the mismatch repair protein MutL.* Nucleic Acids Res, 2006. **34**(15): p. 4089-97.
14. Ramakrishnan, C., V.S. Dani, and T. Ramasarma, *A conformational analysis of Walker motif A [GXXXXGKT (S)] in nucleotide-binding and other proteins.* Protein Eng, 2002. **15**(10): p. 783-98.
15. Manelyte, L., C. Urbanke, L. Giron-Monzon, and P. Friedhoff, *Structural and functional analysis of the MutS C-terminal tetramerization domain.* Nucleic Acids Res, 2006. **34**(18): p. 5270-9.
16. Yang, W., *Structure and mechanism for DNA lesion recognition.* Cell Res, 2008. **18**(1): p. 184-97.
17. Natrajan, G., M.H. Lamers, J.H. Enzlin, H.H. Winterwerp, A. Perrakis, and T.K. Sixma, *Structures of Escherichia coli DNA mismatch repair enzyme MutS in complex with different mismatches: a common recognition mode for diverse substrates.* Nucleic Acids Res, 2003. **31**(16): p. 4814-21.
18. Wang, H., Y. Yang, M.J. Schofield, C. Du, Y. Fridman, S.D. Lee, E.D. Larson, J.T. Drummond, E. Alani, P. Hsieh, and D.A. Erie, *DNA bending and unbending by MutS govern mismatch recognition and specificity.* Proc Natl Acad Sci U S A, 2003. **100**(25): p. 14822-7.
19. Kunkel, T.A. and D.A. Erie, *DNA mismatch repair.* Annu Rev Biochem, 2005. **74**: p. 681-710.
20. Tessmer, I., Y. Yang, J. Zhai, C. Du, P. Hsieh, M.M. Hingorani, and D.A. Erie, *Mechanism of MutS Searching for DNA Mismatches and Signaling Repair.* J Biol Chem, 2008. **283**(52): p. 36646-54.
21. Jacobs-Palmer, E. and M.M. Hingorani, *The effects of nucleotides on MutS-DNA binding kinetics clarify the role of MutS ATPase activity in mismatch repair.* J Mol Biol, 2007. **366**(4): p. 1087-98.
22. Lebbink, J.H., D. Georgijevic, G. Natrajan, A. Fish, H.H. Winterwerp, T.K. Sixma, and N. de Wind, *Dual role of MutS glutamate 38 in DNA mismatch discrimination and in the authorization of repair.* EMBO J, 2006. **25**(2): p. 409-19.

23. Gorbalenya, A.E. and E.V. Koonin, *Superfamily of UvrA-related NTP-binding proteins. Implications for rational classification of recombination/repair systems.* J Mol Biol, 1990. **213**(4): p. 583-91.
24. Junop, M.S., G. Obmolova, K. Rausch, P. Hsieh, and W. Yang, *Composite active site of an ABC ATPase: MutS uses ATP to verify mismatch recognition and authorize DNA repair.* Mol Cell, 2001. **7**(1): p. 1-12.
25. Lamers, M.H., H.H. Winterwerp, and T.K. Sixma, *The alternating ATPase domains of MutS control DNA mismatch repair.* EMBO J, 2003. **22**(3): p. 746-56.
26. Bjornson, K.P. and P. Modrich, *Differential and simultaneous adenosine di- and triphosphate binding by MutS.* J Biol Chem, 2003. **278**(20): p. 18557-62.
27. Lamers, M.H., D. Georgijevic, J.H. Lebbink, H.H. Winterwerp, B. Agianian, N. de Wind, and T.K. Sixma, *ATP increases the affinity between MutS ATPase domains. Implications for ATP hydrolysis and conformational changes.* J Biol Chem, 2004. **279**(42): p. 43879-85.
28. Obmolova, G., C. Ban, P. Hsieh, and W. Yang, *Crystal structures of mismatch repair protein MutS and its complex with a substrate DNA.* Nature, 2000. **407**(6805): p. 703-10.
29. Huang, S.Y. and D.M. Crothers, *The role of nucleotide cofactor binding in cooperativity and specificity of MutS recognition.* J Mol Biol, 2008. **384**(1): p. 31-47.
30. Hillisch, A., M. Lorenz, and S. Diekmann, *Recent advances in FRET: distance determination in protein-DNA complexes.* Curr Opin Struct Biol, 2001. **11**(2): p. 201-7.
31. Sapsford, K.E., L. Berti, and I.L. Medintz, *Materials for fluorescence resonance energy transfer analysis: beyond traditional donor-acceptor combinations.* Angew Chem Int Ed Engl, 2006. **45**(28): p. 4562-89.
32. Weiss, S., *Measuring conformational dynamics of biomolecules by single molecule fluorescence spectroscopy.* Nat Struct Biol, 2000. **7**(9): p. 724-9.
33. Roy, R., S. Hohng, and T. Ha, *A practical guide to single-molecule FRET.* Nat Methods, 2008. **5**(6): p. 507-16.
34. Joo, C., H. Balci, Y. Ishitsuka, C. Buranachai, and T. Ha, *Advances in single-molecule fluorescence methods for molecular biology.* Annu Rev Biochem, 2008. **77**: p. 51-76.
35. Widengren, J., V. Kudryavtsev, M. Antonik, S. Berger, M. Gerken, and C.A. Seidel, *Single-molecule detection and identification of multiple species by multiparameter fluorescence detection.* Anal Chem, 2006. **78**(6): p. 2039-50.
36. Antonik, M., S. Felekyan, A. Gaiduk, and C.A. Seidel, *Separating structural heterogeneities from stochastic variations in fluorescence resonance energy transfer distributions via photon distribution analysis.* J Phys Chem B, 2006. **110**(13): p. 6970-8.
37. Wozniak, A.K., G.F. Schroder, H. Grubmuller, C.A. Seidel, and F. Oesterhelt, *Single-molecule FRET measures bends and kinks in DNA.* Proc Natl Acad Sci U S A, 2008. **105**(47): p. 18337-42.
38. Iaccarino, I., G. Marra, F. Palombo, and J. Jiricny, *hMSH2 and hMSH6 play distinct roles in mismatch binding and contribute differently to the ATPase activity of hMutSalpha.* EMBO J, 1998. **17**(9): p. 2677-86.
39. Thomas, E., A. Pingoud, and P. Friedhoff, *An efficient method for the preparation of long heteroduplex DNA as substrate for mismatch repair by the Escherichia coli MutHLS system.* Biol Chem, 2002. **383**(9): p. 1459-62.
40. Kirsch, R.D. and E. Joly, *An improved PCR-mutagenesis strategy for two-site mutagenesis or sequence swapping between related genes.* Nucleic Acids Res, 1998. **26**(7): p. 1848-50.
41. Lu, X.J. and W.K. Olson, *3DNA: a software package for the analysis, rebuilding and visualization of three-dimensional nucleic acid structures.* Nucleic Acids Res, 2003. **31**(17): p. 5108-21.
42. Swarbrick, J. and J.C. Boylan, *Encyclopedia of pharmaceutical technology*. 2002, New York: Marcel Dekker.
43. Lakowicz, J.R., *Principles of fluorescence spectroscopy*. 2006, New York: Springer.
44. Rusinova, E., V. Tretyachenko-Ladokhina, O.E. Vele, D.F. Senear, and J.B. Alexander Ross, *Alexa and Oregon Green dyes as fluorescence anisotropy probes for measuring protein-protein and protein-nucleic acid interactions.* Anal Biochem, 2002. **308**(1): p. 18-25.
45. Yang, C.P., *Origin (Version 7)*. 2003, OriginLab Corporation: Northampton, MA.
46. Clegg, R.M., *Fluorescence resonance energy transfer and nucleic acids.* Methods Enzymol, 1992. **211**: p. 353-88.

47. Eggeling, C., S. Berger, L. Brand, J.R. Fries, J. Schaffer, A. Volkmer, and C.A.M. Seidel, *Data registration and selective single-molecule analysis using multi-parameter fluorescence detection.* J Biotechnol, 2001. **86**(3): p. 163-80.
48. Howlett, G.J., A.P. Minton, and G. Rivas, *Analytical ultracentrifugation for the study of protein association and assembly.* Curr Opin Chem Biol, 2006. **10**(5): p. 430-6.
49. Schuck, P.W., *Protein interactions : biophysical approaches for the study of complex reversible systems*. 2007, New York: Springer.
50. Kalinin, S., S. Felekyan, M. Antonik, and C.A. Seidel, *Probability distribution analysis of single-molecule fluorescence anisotropy and resonance energy transfer.* J Phys Chem B, 2007. **111**(34): p. 10253-62.
51. Joshi, A. and B.J. Rao, *MutS recognition: multiple mismatches and sequence context effects.* J Biosci, 2001. **26**(5): p. 595-606.
52. Jiricny, J., S.S. Su, S.G. Wood, and P. Modrich, *Mismatch-containing oligonucleotide duplexes bound by the E. coli mutS-encoded protein.* Nucleic Acids Res, 1988. **16**(16): p. 7843-53.
53. Mazurek, A., C.N. Johnson, M.W. Germann, and R. Fishel, *Sequence context effect for hMSH2-hMSH6 mismatch-dependent activation.* Proc Natl Acad Sci U S A, 2009.
54. Yang, Y., L.E. Sass, C. Du, P. Hsieh, and D.A. Erie, *Determination of protein-DNA binding constants and specificities from statistical analyses of single molecules: MutS-DNA interactions.* Nucleic Acids Res, 2005. **33**(13): p. 4322-34.
55. Gorman, J., A. Chowdhury, J.A. Surtees, J. Shimada, D.R. Reichman, E. Alani, and E.C. Greene, *Dynamic basis for one-dimensional DNA scanning by the mismatch repair complex Msh2-Msh6.* Mol Cell, 2007. **28**(3): p. 359-70.
56. Mazurek, A., C.N. Johnson, M.W. Germann, and R. Fishel, *Sequence context effect for hMSH2-hMSH6 mismatch-dependent activation.* Proc Natl Acad Sci U S A, 2009. **106**(11): p. 4177-82.
57. Warren, J.J., T.J. Pohlhaus, A. Changela, R.R. Iyer, P.L. Modrich, and L.S. Beese, *Structure of the human MutSalpha DNA lesion recognition complex.* Mol Cell, 2007. **26**(4): p. 579-92.
58. Jiang, J., L. Bai, J.A. Surtees, Z. Gemici, M.D. Wang, and E. Alani, *Detection of high-affinity and sliding clamp modes for MSH2-MSH6 by single-molecule unzipping force analysis.* Mol Cell, 2005. **20**(5): p. 771-81.
59. Iyer, R.R., T.J. Pohlhaus, S. Chen, G.L. Hura, L. Dzantiev, L.S. Beese, and P. Modrich, *The MutSalpha-proliferating cell nuclear antigen interaction in human DNA mismatch repair.* J Biol Chem, 2008. **283**(19): p. 13310-9.
60. Nick McElhinny, S.A., D.A. Gordenin, C.M. Stith, P.M. Burgers, and T.A. Kunkel, *Division of labor at the eukaryotic replication fork.* Mol Cell, 2008. **30**(2): p. 137-44.
61. Huang, F., G. Settanni, and A.R. Fersht, *Fluorescence resonance energy transfer analysis of the folding pathway of Engrailed Homeodomain.* Protein Eng Des Sel, 2008. **21**(3): p. 131-46.
62. Wang, H. and J.B. Hays, *Mismatch repair in human nuclear extracts: effects of internal DNA-hairpin structures between mismatches and excision-initiation nicks on mismatch correction and mismatch-provoked excision.* J Biol Chem, 2003. **278**(31): p. 28686-93.
63. Blackwell, L.J., K.P. Bjornson, D.J. Allen, and P. Modrich, *Distinct MutS DNA-binding modes that are differentially modulated by ATP binding and hydrolysis.* J Biol Chem, 2001. **276**(36): p. 34339-47.
64. Acharya, S., P.L. Foster, P. Brooks, and R. Fishel, *The coordinated functions of the E. coli MutS and MutL proteins in mismatch repair.* Mol Cell, 2003. **12**(1): p. 233-46.
65. Hopfner, K.P., A. Karcher, D.S. Shin, L. Craig, L.M. Arthur, J.P. Carney, and J.A. Tainer, *Structural biology of Rad50 ATPase: ATP-driven conformational control in DNA double-strand break repair and the ABC-ATPase superfamily.* Cell, 2000. **101**(7): p. 789-800.
66. Rees, D.C., E. Johnson, and O. Lewinson, *ABC transporters: the power to change.* Nat Rev Mol Cell Biol, 2009. **10**(3): p. 218-27.
67. Kato, R., M. Kataoka, H. Kamikubo, and S. Kuramitsu, *Direct observation of three conformations of MutS protein regulated by adenine nucleotides.* J Mol Biol, 2001. **309**(1): p. 227-38.
68. Holland, I.B. and M.A. Blight, *ABC-ATPases, adaptable energy generators fuelling transmembrane movement of a variety of molecules in organisms from bacteria to humans.* J Mol Biol, 1999. **293**(2): p. 381-99.

69. Bjornson, K.P., D.J. Allen, and P. Modrich, *Modulation of MutS ATP hydrolysis by DNA cofactors.* Biochemistry, 2000. **39**(11): p. 3176-83.
70. Pluciennik, A. and P. Modrich, *Protein roadblocks and helix discontinuities are barriers to the initiation of mismatch repair.* Proc Natl Acad Sci U S A, 2007. **104**(31): p. 12709-13.
71. Mukherjee, S., S.M. Law, and M. Feig, *Deciphering the mismatch recognition cycle in MutS and MSH2-MSH6 using normal-mode analysis.* Biophys J, 2009. **96**(5): p. 1707-20.
72. Antony, E., S. Khubchandani, S. Chen, and M.M. Hingorani, *Contribution of Msh2 and Msh6 subunits to the asymmetric ATPase and DNA mismatch binding activities of Saccharomyces cerevisiae Msh2-Msh6 mismatch repair protein.* DNA Repair (Amst), 2006. **5**(2): p. 153-62.
73. Ramanathan, S.P., K. van Aelst, A. Sears, L.J. Peakman, F.M. Diffin, M.D. Szczelkun, and R. Seidel, *Type III restriction enzymes communicate in 1D without looping between their target sites.* Proc Natl Acad Sci U S A, 2009. **106**(6): p. 1748-53.
74. Eggeling, C., J. Widengren, L. Brand, J. Schaffer, S. Felekyan, and C.A. Seidel, *Analysis of photobleaching in single-molecule multicolor excitation and Forster resonance energy transfer measurements.* J Phys Chem A, 2006. **110**(9): p. 2979-95.

Appendix

DNA modeling:

Table A. 1: Base-base and base-step parameters for the modeling of the 42bp G:T kinked structure. The pink shaded area corresponds to the sequence for which the crystal structure DNA parameters were used.

Seq.	shear	stretch	stagger	buckle	propeller	opening	shift	slide	rise	tilt	roll	twist
5' T-A	-0.03	-0.1	0.09	0.04	-15.13	-1.88	0	0	0	0	0	0
A-T	0.03	-0.1	0.09	-0.05	-15.14	-1.88	0	0.47	3.36	0	1.71	36.26
T-A	-0.03	-0.1	0.09	0.04	-15.13	-1.87	0	0.44	3.35	0	1.72	35.67
T-A	-0.03	-0.1	0.09	0.04	-15.15	-1.87	0	0.45	3.36	0	1.7	35.96
A-T	0.03	-0.1	0.09	-0.04	-15.13	-1.88	0	0.47	3.36	-0.01	1.71	36.25
A-T	0.03	-0.1	0.09	-0.04	-15.11	-1.89	-0.01	0.45	3.36	0.01	1.71	35.97
T-A	-0.03	-0.1	0.09	0.04	-15.13	-1.88	0	0.44	3.35	0.01	1.7	35.67
T-A	-0.03	-0.1	0.09	0.05	-15.14	-1.86	0	0.45	3.36	0	1.72	35.96
T-A	-0.03	-0.1	0.09	0.04	-15.14	-1.87	0	0.45	3.36	0	1.71	35.96
C-G	0.14	-0.18	0.1	-0.27	-15.14	-1.3	0.03	0.5	3.37	0.01	1.71	37.13
G-C	-0.14	-0.18	0.1	0.27	-15.15	-1.32	0	0.41	3.34	-0.01	1.71	33.92
C-G	0.14	-0.18	0.1	-0.27	-15.14	-1.3	0	0.54	3.38	0	1.71	38
G-C	0.28	-0.42	-0.62	-4.89	-6.49	0.84	0.01	0.47	3.36	-0.03	1.71	35.96
G-C	0.04	-0.16	0.08	-3.75	-2.39	-4.58	-1.20	-0.09	3.23	-9.99	2.37	37.80
G-C	-0.14	0.03	0.30	-5.23	-7.75	1.19	-0.58	-0.34	3.32	-1.69	2.97	31.84
C-G	-0.45	-0.12	0.33	-4.98	-14.48	-1.41	-0.67	-0.09	3.24	-1.07	5.23	30.36
T-A	-0.02	-0.29	-0.25	-4.40	4.28	-4.67	0.86	1.04	3.40	4.33	-1.78	40.80
C-G	0.02	-0.15	0.09	0.32	-14.13	-1.31	-1.10	0.33	3.24	-4.78	-0.75	35.34
G-C	0.23	-0.01	-0.04	2.00	-10.65	1.10	0.42	-0.16	3.23	2.57	6.41	31.98
A-T	0.32	-0.12	0.18	11.34	-5.40	0.35	0.54	0.72	3.09	2.27	4.03	36.03
G-T	**4.65**	**0.17**	**-0.71**	**-31.99**	**-2.58**	**-55.37**	**-1.85**	**1.48**	**6.72**	**9.71**	**54.87**	**33.32**
A-T	-0.26	0.01	-0.31	-22.42	-10.59	-4.85	2.65	0.58	3.24	-4.22	1.64	8.07
G-C	0.07	-0.14	-0.29	11.45	5.64	0.89	1.10	0.01	2.73	-0.46	20.21	23.34
C-G	-0.13	-0.04	0.07	14.41	-11.73	2.28	0.09	-0.53	3.41	-1.48	8.48	31.96
T-A	-0.02	-0.21	-0.26	15.10	-17.49	0.19	0.28	-1.00	3.30	0.05	0.16	33.58
T-A	-0.02	-0.13	-0.06	7.72	-8.17	3.05	0.62	0.04	3.64	6.31	5.03	34.54
C-G	0.27	-0.07	0.36	9.31	-5.86	0.35	-0.80	0.54	3.22	-4.40	7.91	32.74
A-T	-0.23	-0.32	0.56	1.94	-3.29	2.34	0.72	-0.94	3.37	-2.49	4.07	32.98
T-A	0.25	-0.20	0.55	1.44	-5.48	-1.62	-0.08	-0.71	3.31	1.59	3.48	38.79
C-G	0.14	-0.18	0.1	-0.26	-15.16	-1.3	0.03	0.5	3.37	0.01	1.71	37.13
C-G	0.14	-0.18	0.1	-0.25	-15.16	-1.32	-0.01	0.47	3.36	0.03	1.71	35.95
T-A	-0.03	-0.1	0.09	0.04	-15.12	-1.89	-0.03	0.42	3.35	0.01	1.7	34.8
C-G	0.14	-0.18	0.1	-0.26	-15.14	-1.29	0.03	0.5	3.37	0.02	1.72	37.14

T-A	-0.03	-0.1	0.09	0.05	-15.13	-1.87	-0.03	0.42	3.35	0	1.7	34.79
A-T	0.03	-0.1	0.09	-0.03	-15.13	-1.89	0	0.47	3.36	0	1.7	36.24
C-G	0.14	-0.18	0.1	-0.26	-15.17	-1.3	0.02	0.49	3.36	0.03	1.7	36.84
G-C	-0.14	-0.18	0.1	0.26	-15.14	-1.3	0	0.41	3.34	0	1.7	33.92
C-G	0.14	-0.18	0.1	-0.26	-15.14	-1.29	0	0.54	3.38	0	1.73	38
C-G	0.14	-0.18	0.1	-0.26	-15.14	-1.3	-0.01	0.47	3.36	0.03	1.7	35.96
G-C	-0.14	-0.18	0.1	0.26	-15.14	-1.3	0	0.41	3.34	0.01	1.7	33.93
G-C	-0.14	-0.18	0.1	0.25	-15.15	-1.31	0.01	0.47	3.36	-0.03	1.71	35.96
3' A-T	0.03	-0.1	0.09	-0.04	-15.12	-1.88	-0.03	0.5	3.37	-0.01	1.71	37.12

Table A. 2: Base-base and base-step parameters for the modeling of the 42bp T:G kinked structure. The pink shaded area corresponds to the sequence for which the crystal structure DNA parameters were used.

	shear	**stretch**	**stagger**	**buckle**	**propeller**	**opening**	**shift**	**slide**	**rise**	**tilt**	**roll**	**twist**
5' T-A	-0.03	-0.1	0.09	0.04	-15.13	-1.88	0	0	0	0	0	0
C-G	0.14	-0.18	0.1	-0.26	-15.15	-1.3	0.03	0.5	3.37	0.01	1.72	37.12
C-G	0.14	-0.18	0.1	-0.26	-15.14	-1.29	-0.01	0.47	3.36	0.03	1.71	35.97
G-C	-0.14	-0.18	0.1	0.26	-15.14	-1.29	0	0.41	3.34	0	1.7	33.92
G-C	-0.14	-0.18	0.1	0.26	-15.15	-1.3	0.01	0.47	3.36	-0.03	1.71	35.97
C-G	0.14	-0.18	0.1	-0.26	-15.15	-1.31	0	0.54	3.38	0	1.72	37.99
G-C	-0.14	-0.18	0.1	0.26	-15.15	-1.3	0	0.41	3.34	0	1.7	33.92
T-A	-0.03	-0.1	0.09	0.04	-15.13	-1.87	-0.02	0.49	3.36	-0.02	1.71	36.83
A-T	0.03	-0.1	0.09	-0.04	-15.13	-1.87	0	0.47	3.36	0	1.71	36.25
G-C	-0.14	-0.18	0.1	0.26	-15.15	-1.3	0.03	0.42	3.35	-0.01	1.7	34.8
A-T	0.03	-0.1	0.09	-0.04	-15.13	-1.88	-0.03	0.5	3.37	-0.01	1.72	37.12
G-C	-0.14	-0.18	0.1	0.26	-15.15	-1.3	0.03	0.42	3.35	-0.01	1.7	34.79
G-C	-0.14	-0.18	0.1	0.26	-15.15	-1.29	0.01	0.47	3.36	-0.03	1.71	35.96
A-T	0.28	-0.42	-0.62	-4.89	-6.49	0.84	0.01	0.47	3.36	-0.03	1.71	35.96
T-A	0.04	-0.16	0.08	-3.75	-2.39	-4.58	-1.20	-0.09	3.23	-9.99	2.37	37.80
G-C	-0.14	0.03	0.30	-5.23	-7.75	1.19	-0.58	-0.34	3.32	-1.69	2.97	31.84
A-T	-0.45	-0.12	0.33	-4.98	-14.48	-1.41	-0.67	-0.09	3.24	-1.07	5.23	30.36
A-T	-0.02	-0.29	-0.25	-4.40	4.28	-4.67	0.86	1.04	3.40	4.33	-1.78	40.80
G-C	0.02	-0.15	0.09	0.32	-14.13	-1.31	-1.10	0.33	3.24	-4.78	-0.75	35.34
C-G	0.23	-0.01	-0.04	2.00	-10.65	1.10	0.42	-0.16	3.23	2.57	6.41	31.98
T-A	0.32	-0.12	0.18	11.34	-5.40	0.35	0.54	0.72	3.09	2.27	4.03	36.03
G-T	**4.65**	**0.17**	**-0.71**	**-31.99**	**-2.58**	**-55.37**	**-1.85**	**1.48**	**6.72**	**9.71**	**54.87**	**33.32**
T-A	-0.26	0.01	-0.31	-22.42	-10.59	-4.85	2.65	0.58	3.24	-4.22	1.64	8.07
C-G	0.07	-0.14	-0.29	11.45	5.64	0.89	1.10	0.01	2.73	-0.46	20.21	23.34
G-C	-0.13	-0.04	0.07	14.41	-11.73	2.28	0.09	-0.53	3.41	-1.48	8.48	31.96
A-T	-0.02	-0.21	-0.26	15.10	-17.49	0.19	0.28	-1.00	3.30	0.05	0.16	33.58
G-C	-0.02	-0.13	-0.06	7.72	-8.17	3.05	0.62	0.04	3.64	6.31	5.03	34.54
C-G	0.27	-0.07	0.36	9.31	-5.86	0.35	-0.80	0.54	3.22	-4.40	7.91	32.74
C-G	-0.23	-0.32	0.56	1.94	-3.29	2.34	0.72	-0.94	3.37	-2.49	4.07	32.98
C-G	0.25	-0.20	0.55	1.44	-5.48	-1.62	-0.08	-0.71	3.31	1.59	3.48	38.79

G-C	-0.14	-0.18	0.1	0.26	-15.15	-1.31	0	0.41	3.34	0	1.7	33.92
C-G	0.14	-0.18	0.1	-0.26	-15.15	-1.3	0	0.54	3.38	0	1.72	37.99
G-C	-0.14	-0.18	0.1	0.26	-15.15	-1.29	0	0.41	3.34	0	1.7	33.93
A-T	0.03	-0.1	0.09	-0.04	-15.13	-1.87	-0.03	0.5	3.37	-0.01	1.71	37.13
A-T	0.03	-0.1	0.09	-0.04	-15.13	-1.88	0	0.45	3.36	0	1.71	35.96
A-T	0.03	-0.1	0.09	-0.04	-15.13	-1.88	-0.01	0.45	3.36	0	1.71	35.97
T-A	-0.03	-0.1	0.09	0.04	-15.13	-1.88	0	0.44	3.35	0	1.7	35.67
T-A	-0.03	-0.1	0.09	0.04	-15.13	-1.87	0	0.45	3.36	0	1.71	35.96
A-T	0.03	-0.1	0.09	-0.04	-15.13	-1.87	0	0.47	3.36	0	1.71	36.25
A-T	0.03	-0.1	0.09	-0.04	-15.13	-1.88	0	0.45	3.36	0	1.71	35.96
T-A	-0.03	-0.1	0.09	0.04	-15.13	-1.88	0	0.44	3.35	0	1.7	35.67
3' A-T	0.03	-0.1	0.09	-0.04	-15.13	-1.88	0	0.47	3.36	0	1.71	36.26

Single molecule burst selection:

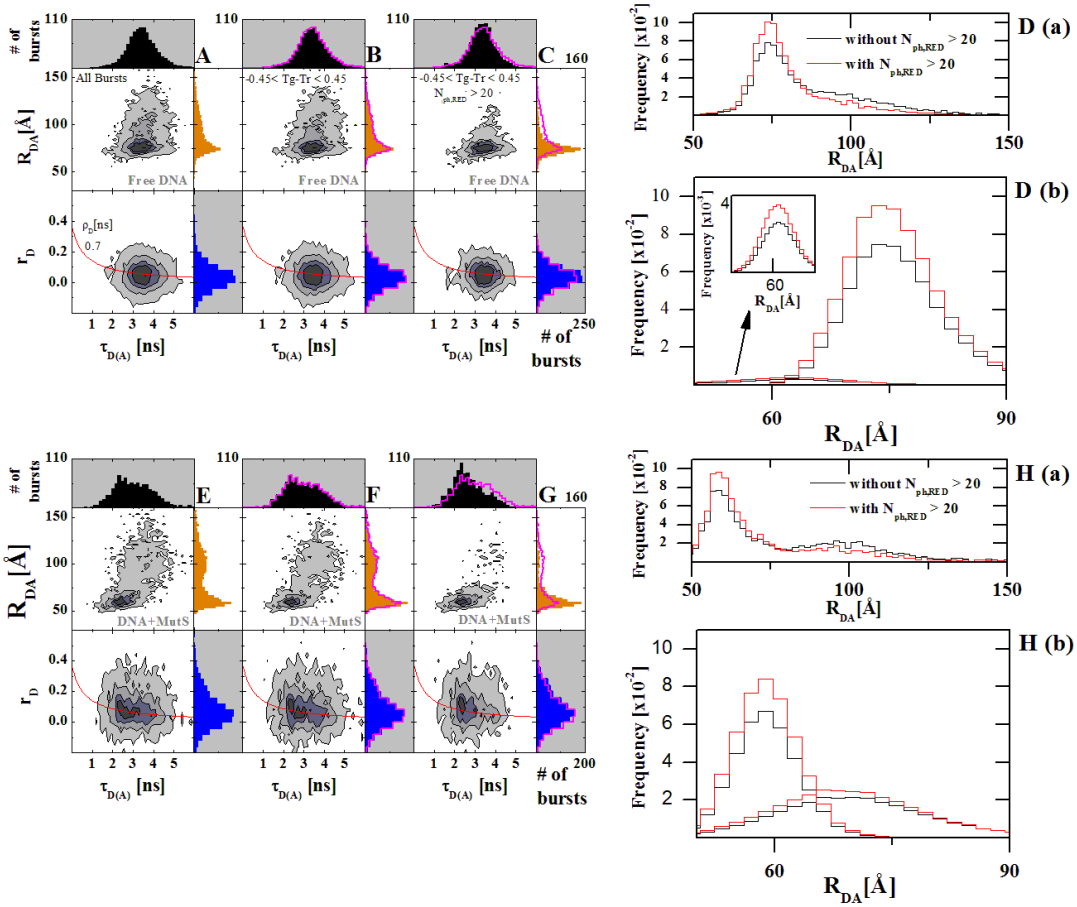

Fig. A. 1: Two dimensional frequency histogram of the burst selection of the smMFD measurements, where frequency increases from white to black. R_{DA} represents the donor-acceptor (DA) distance and was calculated based on the green and red fluorescence, corrected for background, detection efficiencies and crosstalk. $\tau_{D(A)}$ is the donor lifetime in the presence of acceptor. Panels A, B and C show 2D plots of R_{DA} vs. $\tau_{D(A)}$ (top) and r_D (donor anisotropy) vs. $\tau_{D(A)}$ (bottom) for the stepwise burst selection of the DNA-only measurements. Panel A shows the populations obtained for all bursts, panel B shows the populations obtained after $-0.45<T_g-T_r<0.45$ burst selection and panel C shows the resulting populations after $-0.45<T_g-T_r<0.45$ and $N_{ph,RED}>20$ burst selections. The pink population in B and C corresponds to the populations without burst selection. D (a) and D (b) show the detail of the populations in PDA before (black population) and after (red population) burst selection. Panels E, F and G show the same analysis for DNA+MutS measurements. H (a) and H (b) shows the detail of the populations in PDA before and after burst selection. The red curve was computed with the Perrin equation $r = r_0/(1+\tau/\rho)$, using a fundamental anisotropy r_0 of 0.37 and a mean correlation time of 1ns.

A burst selection was performed on the smMFD measurements. The selection step reduces the background (FRET-inactive species) and allows the analysis to be constrained to the FRET-active subpopulations[74]. Two selection steps were performed:

1. **$-0.45<T_g-T_r<0.45$**: here, the molecules with an event of acceptor photobleaching were excluded. The time difference T_g-T_r of the mean observation

time of all photons detected for the donor and acceptor channels within a single molecule fluorescence burst allows the identification and exclusion of photobleached molecules[74]. T_g and T_r represent the median time of fluorescence emission of both detection channels. Without photobleaching, T_g and T_r would be similar and thus T_g-$T_r \approx 0$ [74].

2. $\mathbf{N_{ph,RED}>2}$0: Bursts in the red channel with less than 20 photons were excluded from the analysis. This allows the exclusion of red bursts that are not originated by FRET, but by crosstalk from green donor signal into the red acceptor detection channel. This way, a significant amount of the donor-only species was removed from the analysis.

As can be seen from figure A.1, the performed burst selection does not change the position or the widths of the FRET populations, and can be thus used to significantly reduce the background and facilitate the analysis. Furthermore, the fitting of the anisotropy populations to the Perrin equation yielded a mean donor anisotropy r_D of 0.022 and a mean rotational correlation time ρ_D of 0.22ns for G:T alone, and a r_D of 0.062 and a ρ_D of 0.74ns for G:T+MutS. These values indicate that the donor-fluorophore in G:T is highly mobile and justifies the assumption of a κ^2 of 2/3 and the calculation of DA distances, based on a R_0 of 53.2Å.

Publications

"Binding orientations of MutS to mismatches monitored by single-molecule FRET" (manuscript in preparation)

Cristovao, M.[a], Sisamakis, E.[b], Seidel, C.A.M.[b], Rothwell, P.[b], Friedhoff, P.[a]

[a]Institute of Biochemistry, Justus-Liebig University, Giessen, Germany

[b]Institute of Molecular Physical Chemistry, Heinrich-Heine University, Düsseldorf, Germany

Poster presentations

2006 (September): 12th Single Molecule workshop, Picoquant, Berlin "Studies on Mismatch Repair Proteins, using single-cysteine variants"

2007 (April): Nacon VII Conference, Tapton Hall, University of Sheffield, Sheffield, England "The interaction of MutS with DNA"

2008 (June): Faseb Conference, Saxtons River, Vermont, USA "DNA bending by MutS, monitored down to the single molecule level"

Oral presentations

2006 (September): 1st Annual Marie Curie Meeting, University of Bristol, Bristol, England

2007 (March): 1st Offspring Meeting, Early Stage and Experienced Researchers Marie Curie Meeting, Giessen, Germany

2007 (September): Annual and Mid-term Marie Curie Meeting, Vilnius, Lithuania

2008 (April): 2st Offspring Meeting, Early Stage and Experienced Researchers Marie Curie Meeting, Newcastle, England

2008 (September): Final Marie Curie Meeting, Berlin, Germany

2008 (December): 3rd Marie Curie Workshop, "Single Molecule", Department of Biology, University of York, York, England